Calcium Carbonate Scale Deposition Kinetics on Stainless Steel Surfaces

Omoregbe Bello

Submitted in accordance with the requirement for the degree of

Doctor of Philosophy

The University of Leeds

School of Mechanical Engineering

Leeds, UK

January 2017

The candidate confirms that the work submitted is his own and that appropriate credit has been given where reference has been made to the work of others.

Acknowledgement

All glory and thanks to God for grace, strength and motivation for the successful completion of this research.

I would like to express my profound gratitude to Professor Anne Neville for her thorough supervision, guidance, encouragement and support. I am very grateful to Dr Thibaut Charpentier who has been very helpful and supportive throughout this project. Their motivation, insight, passion, encouragement and assistance throughout this project were the driving force for the success of this work.

I wish to express my gratitude to the University of Leeds, United Kingdom and Chevron technology company, Houston Texas, US, for their financial support and technical contributions. I also appreciate the members of my research group, the Institute of functional surfaces (iFs) especially the scale focus group for creating a friendly and challenging atmosphere. Thanks to friends like Doris, Leo, Ogbemi, Jide, McDonald, Lukman, Sikiru, Frederick, Obinna, Kelvin, Omotayo, Danny, Abi and Wassim for sharing their knowledge.

The administrative and technical supports of Fiona Slade, Ron Cellier, Jordan Thomas, Andrew O' Brien and Michael Huggan are deeply appreciated.

Special thanks and appreciation to my mother, siblings and every member of my family for the strong foundation and pillars upon which this success is built. Their prayers, the bond, the constant encouragement, support and love really made it possible.

My deepest appreciation to ***my beloved wife*** Patience Bello, for her perseverance, support and encouragement throughout this research, and also to my wonderful kids, Jasper, Jenkins and Janelle.

Abstract

Calcium carbonate scale is one of the most common inorganic scales which deposits on the surface of oil and gas production facilities. This causes significant loss of production and ultimately leads to shut down of production lines if not properly managed.

There has been a great amount of research on calcium carbonate deposition studies, but most of these studies have been on understanding calcium carbonate bulk precipitation process. However, little attention have been made on calcium carbonate surface deposition mechanism, which is the main challenge in mitigating scaling in oil and gas and desalination industries.

Understanding the mechanism of its formation at different environmental conditions and using a methodology that would reflect the field scenario will gives information required for a reliable predictive model.

This study investigated calcium carbonate surface build-up under flow conditions, across a wide range of saturation ratio (SR) at 25^{o}C and 70^{o}C respectively. Both bulk induction time (t_{ind}) and surface induction time, which is referred to as scaling time (t_s) were determined from capillary flow rig experiments.

Mineral scale surface fouling was monitored by a sensitive differential pressure technique with respect to build up of scale on the wall of the capillary cell resulting to change of pressure across the test capillary cell.

It was found that, two scaling regimes occur within the brine composition investigated. At SR < 80, surface fouling is controlled by nucleation and growth, while at SR > 80, is controlled by the adhesion of pre-precipitated crystals. This result was supported by the turbidity measurement and inductively coupled plasma mass spectrometry (ICP-MS) analysis.

The calcium carbonate growth rate determined by measuring the amount of scale deposited at the surface of the capillary cell by Inductively coupled plasma mass spectrometry analysis (ICP-MS) was smaller compared to the amount of scale predicted from Hagen Poiseuille (HP) equation, where the

growth rate is estimated from the pressure drop across the capillary cell as scale build up on the wall of the capillary cell. This was attributed to non-uniformity of the scale layer along the capillary cell which is omitted in the HP equation.

A semi empirical model has been developed from the experimental work, which can predict scale deposition growth rate over a period of time and as a function of deposition flux at a given temperature.

Table of Contents

List of Figures

List of Tables

Nomenclature

r_c: radius of critical nuclei (cm)

IP: activity product of free ions species

J: nucleation rate (cm^{-3} s^{-1})

h:height of the circular disc (cm)

ΔG_{cr}: free energy change for the critical cluster size formation (J $mole^{-1}$)

A: frequency constant (cm^{-3} s^{-1})

k: Boltzmann constant (J/K)

T: absolute temperature (K)

γ: Interfacial energy (mJ/m^2)

β: Shape factor

V_m: molecular volume (cm^3 $mole^{-1}$)

f(θ): correction factor

R: molar gas constant (J $mole^{-1}K^{-1}$)

SI: saturation index

SR : saturation ratio

K_a : activity based solubility product constant

t_{ind}: induction time (min)

t_s : scaling time (min)

t_n : time for system to reach steady state (min)

t_g: time for nuclei to reach a detectable size (min)

K_{sp}: Solubility product constant

B: slope of the plot log t_{ind} and $1/(\log SR)^2$

N_A: Avogadro number (mol^{-1})

W_a: work of the adhesion ($N\ m^{-1}$)

θ: contact angle (degs)

m: mass of solute deposited (g)

C: solute concentration (mol/l)

C^e: equilibrium saturation concentration (mol/l)

K_m: mass transfer coefficient (m/s)

K_r: reaction rate constant (mol/l/s)

V :flow velocity (m/min)

Q: volumetric flow rate (ml/min)

R_e: Reynolds number

L_e: entrance length (mm)

ρ: Density (Kg/m^3)

ΔG_w: Lifshitz van der Waal interaction component

ΔG_E: electrostatic double-layer component

ΔG_A: Lewis acid- based component

ΔG_B: Brownian motion component

ΔG_T: Total interaction energy

ΔP_i :Initial pressure drop before deposition (Psi)

ΔP_t: pressure drop at time t (Psi)

μ_i: Initial viscosity of brine (mPa.s)

μ_t: viscosity of brine at time t (mPa.s)

r_i : initial radius of the capillary cell (mm)

R: radius of capillary cell after deposition (mm)

t: scale deposition thickness (mm)

D: internal diameter of the capillary cell (mm)

L: Length of capillary cell (mm)

ppt_{Barite}: amount of barite (ml/kg)

x: mole fraction

$\gamma_{Ba^{2+}}$: activity coefficient of barium ion

$\gamma_{SO4^{2-}}$: activity coefficient of sulphate ion

SHMP: Sodium hexametaphosphate

P_o : Initial concentration of SHMP (mol/l)

P : Final concentration of SHMP (mol/l)

r_{CALG}: SHMP adsorption rate (L/molmin)

I : ionic strength (mol/l)

R^I : mole factor

S_f : solubility factor

LSI: Langelier's saturation index

pHs : pH of water saturated with $CaCO_3$

TDS: total dissolved solid

P_{ca} : negative logarithm of calcium ion concentration (mg/l)

P_{AlK}: bicarbonate alkalinity (mg/l)

SDI : Stiff-Davis index

ε : Chemical kinetics coefficient

α : Formation damage

W : total mass of wax deposited on pipe wall (g)

ρ_w : density of wax (kg/m^3)

A : pipe wall area (m^2)

D_T: internal diameter of test tube (m)

D_R : internal diameter of reference tube (m)

ΔP_T : pressure drop of the test tube (Psi)

ΔP_r : pressure drop of the reference tube (Psi)

n : material constant

W_r : Wax deposition rate (cm/min)

D_o : bare tube internal diameter (m)

q (t): volumetric flow rate as a function of time (ml/min)

W(t) : weight of deposit layer as a function of time (g)

l(t) : length of remaining liquid segment inside the tube at time t (m)

P_r : prandtl number

r_n : radius of the tube at different location(cm)

ΔV_i : volume of liquids (cm^3)

Δt_i : change in time (min)

P: capillary pressure (Psi)

CHAPTER 1. Introduction

1.1 Research background

The petroleum industry provides a major source of energy supply in the world economy .They play a vital role in creating jobs and development of nations. The petroleum industries are being faced with production challenges to meet the energy demand. In flow assurance these include corrosion, inorganic and organic scale deposits and formation of stable emulsions which affect crude oil flow. One possible way of addressing these problems is to understand the mechanism of scale formation at the surface of facilities.

This study focuses on the deposition of inorganic scale ($CaCO_3$) in oil and gas production facilities. $CaCO_3$ is one of the most common inorganic scales encountered in crude oil production. $CaCO_3$ scaling is triggered from pressure drop, which promotes dissolved CO_2 escaping from produced water, resulting in an increase in the water pH and the saturation index of the brine solution being exceeded[1, 2].

There are other inorganic scales such as $BaSO_4$ and $SrSO_4$ scales that occur as a result of injecting seawater into the reservoir, where the formation water meet and the two are incompatible [3-7]. The presence of these scales in an oilfield can cause under deposit corrosion, reduce corrosion and scale inhibitors efficiency, fouling of equipment, and ultimately lowering of production rates.

Scale prevention is important in oil and gas and desalination industries to ensure optimum production. Organic and inorganic scale precipitation and deposition have been studied and different predictive models have been developed over many years on scale precipitation processes such as residence time, induction time, nucleation and crystal growth. These models have been mainly based on thermodynamic parameters.

However, little attention be made on the effect of hydrodynamic parameters on inorganic scale surface deposition kinetics using a methodology that will reflect the field scenario and developing a model that can predict the scale thickness

growth rate over a period of time and as a function of saturation index, temperature and flow rate.

This study investigates the mechanism by which scale builds up on surface facilities and develops an empirical kinetic model such that at different conditions the rate of surface scale formation can be predicted.

A range of scales produced in an attempt to Enhance Oil Recovery (EOR) operations from offshore reservoirs are shown in Figure 1-1, where pressure is maintained by injecting sea water into the reservoir. This operation causes severe scaling in the reservoir as a result of the different water composition (formation water and injection water), which leads to the precipitation of barite, celestite and gypsum. These compounds slow down the flow in production tubing and equipment and also reduce the porosity of the surrounding rocks [8].

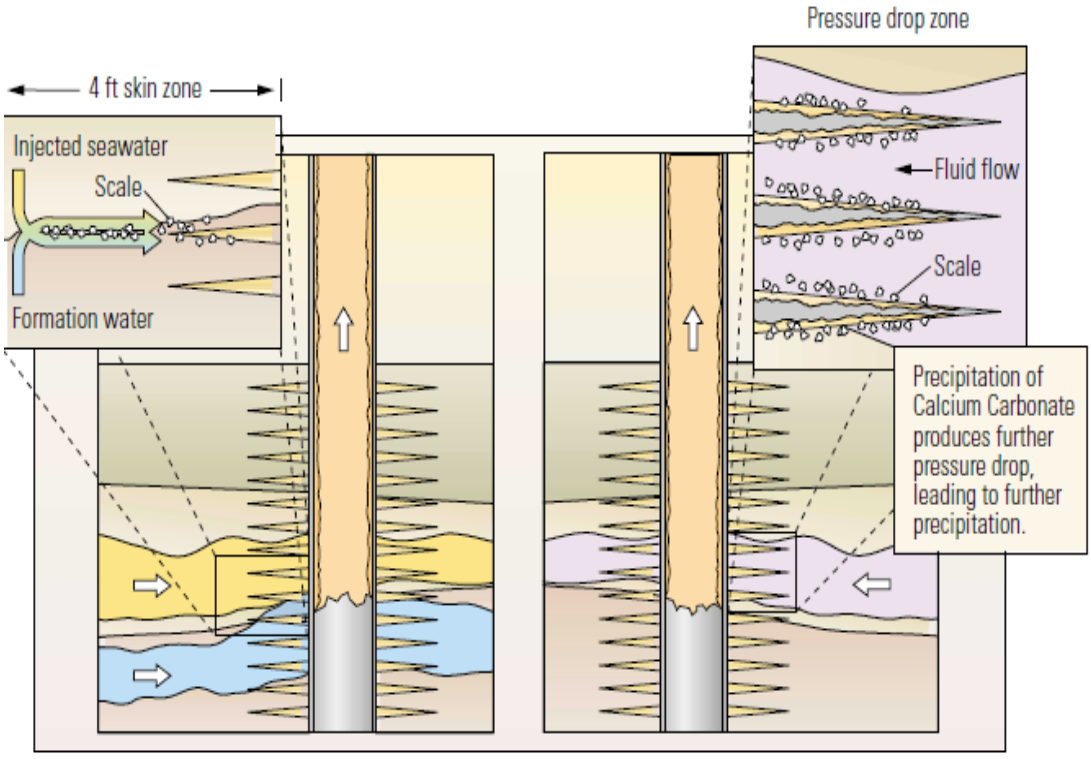

Figure 1-1. Scaling due to mixing of incompatible fluids (left) and auto scaling (right) [9]

$CaCO_3$ precipitation, unlike other types of sulphate scale, $BaSO_4$, $CaSO_4$, $SrSO_4$, usually appears in the upper section of the production tubing, which does not normally affect the actual formation, but it causes damage through filling of the production string and downstream by affecting the functionality of valves and safety equipment [10].

There are have been various methods used to mitigate inorganic scales, such as use of hydrochloric (HCl) acid wash and mechanical scraping (pigging). These methods are capital and labour intensive and not economically acceptable. They do not tend to often have long term mitigation. Scale inhibitors are often deployed to address the problem of scaling in crude oil production and desalination industries.

The use of scale inhibitors, polyphosphino carboxylic acid (PPCA), diethylenediamine Penta (methylene phosphonic acid) DETPMP and polyvinyl sulfonate (PVS) have been reported to have significant effect in preventing inorganic scale [11-15]. Shaw and Sorbie [16, 17] studied the performance of combined effect of phosphate and polymeric inhibitors on barium sulphate scale and compared the minimum inhibition concentration to that of the individual inhibitors. The combined inhibitor gave better performance in terms of inhibiting $BaSO_4$ scale at different dosage. Chen et al [18] and Mavredaki et al [19] studied the effect of DETPMP and PPCA on the induction time and crystal growth rate of surface scaling, the presences of these inhibitors, changes the morphology of calcite to at least a stable form (vaterite). However, these chemicals must be environmentally friendly (biodegradable and bioaccumulation) in order to avoid pollution of the environment.

Zhang et al [1] developed a kinetic and thermodynamic model to predict oilfield down hole carbonate scales profile by studying the impact of production parameters changes, such as increasing water cut, temperature using a tube blocking rig, but this model did not consider the uniformity of capillary tube in determining the scale thickness and the uncertainties of the saturation ratio of the brine with time.

There are various organic scale models developed by Wang et al [20, 21] and Lawal et al [22], where the thickness of asphaltene deposits across a long capillary tube

is determined as a function of the pressure build up across the capillary tube during asphaltene deposition, using Hagen Poiseuille flow equation. These models were based on the assumption that the asphaltene deposited is uniformly deposited along the capillary.

1.2 Objectives of research

The aim of the research is to develop the understanding of scale deposition on the surface of facilities and focuses on the kinetics of surface growth. The specific objectives are:

- To study the kinetics of calcium carbonate scale build-up on stainless steel surfaces under hydrodynamic conditions.

- To establish the influence of surface crystal growth and particle adhesion in different environments: flow regimes, saturation ratios and presence of particles in solution.

- To develop empirical models for predicting scale deposition growth rates under flow conditions.

Figure 1-2 (a and b), shows a cross section of a pipe and schematic diagram of bulk scaling and surface scale in a flow system. It also illustrates the two main locations that scale can form; as discrete particles in the bulk solution and at the surface as a compacted solid layer. This study investigates the relationship between bulk precipitation and surface deposition and how the deposit grows on the facility surfaces.

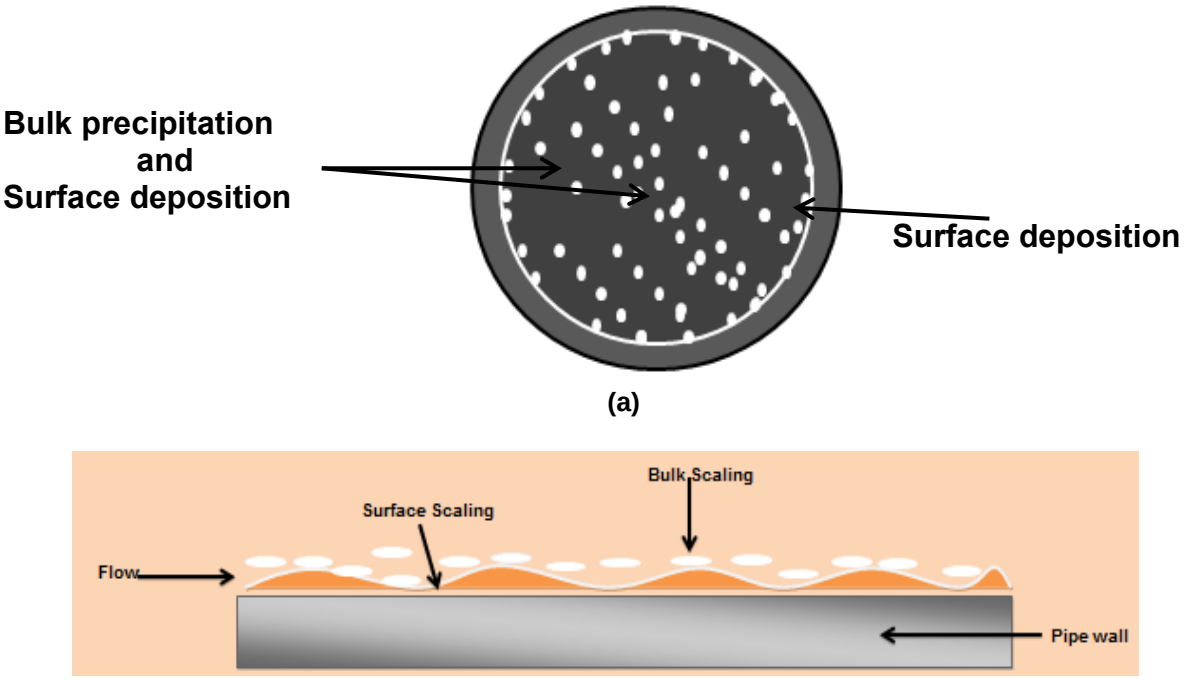

Figure 1-2 (a) Cross section of a pipe and (b) Schematic diagram of bulk scaling and surface scale in a flow system

The formation of scale on the surface of facilities has been of a major concern in the oil and gas industry. Understanding the mechanism of scale formation on the surface of facilities and predicting its growth rate over a period of time will provide better strategies for mitigating its occurrence in the field.

In this work, it is hypothesized that scale formation mechanisms can occur on the surface of facilities, either by

- Heterogeneous nucleation and crystallization processes at the surface of the facilities or

- Heterogeneous precipitation in the bulk solution and adhesion of pre-precipitated crystals from the bulk solution to the surface of the steel.

The methodologies used in the thesis enable these different modes of scale layer formation to be developed.

1.3 Thesis outline

Chapter one gives a brief overview of the scaling problem in oil and gas industry and the current preventive methods been used within the industries and the objectives of this study.

Chapter two provides the fundamental understanding of the scale formation, types of oilfield scale and the factors affecting scale formation and scale formation mechanisms and detailed preventative methods adopted in oil and gas industries. It also includes a review of some previous work carried out by various authors and scale deposition models.

Chapter three focuses on flow capillary rig commissioning, design, the working principle and the details of flow parameters in the capillary rig.

Chapter four provides the experimental methodology, surface and bulk analysis tests carried out, the equipment used and their working principles.

Chapter five shows the bulk analysis test results of calcium carbonate scale precipitation at different experimental conditions and the interpretation of the results.

Chapter six presents the results of calcium carbonate scale surface deposition studies at different temperatures, flow rates and saturation ratios. The results of different surface analysis techniques used for this work is also presented.

Chapter seven presents the analysed results, interpretation and discussion of calcium carbonate surface deposition kinetics in relation to nucleation theory, surface deposition mechanism and growth kinetics. The empirical models established in this work are also presented.

Chapter eight shows the conclusions of the work and knowledge achieved

Chapter nine provides the recommended future work for this study and references cited in this work.

CHAPTER 2. Scale formation literatures review

2.1 Fundamental of scale formation

Scale is defined as any hard insoluble salt deposit on the surface of materials in the presences of water; the type of scale present in the water body depends on the environment. Scales are formed due to the change in environmental conditions such as pressure, temperature and water chemistry. This can result in oilfield problems and they are expensive to control. The deposition of scale deposits on tubular surfaces reduces the fluid flow by reducing cross-sectional area and increasing surface roughness. Fluid flow within reservoirs is restricted due to blockage of pores as shown in Figure 2-1.

Figure 2-1. Image of scale deposition in a pipe [9]

Calcium carbonate and barium sulphate scale are the major types of scaling found in oilfield production wells and surface facilities. Carbonate and sulphate scale formation can slow down production by blockage of tubing and flow lines, and fouling of equipment [23, 24]. In order to control a potential scale problem, it is important to determine the amount of calcium carbonate and barium sulphate scale that will be deposited during oil and water production.

Scales are formed when brine contains dissolved solids at higher concentration than their equilibrium concentration, which results in high supersaturation of the solution due to change in concentration of ions in solution, temperature, pressure and pH [25]. Water formation associated with crude oil production contains a large concentration of chloride ion (Cl^-), sodium ion (Na^+), sulphate (SO_4^{2-}), bicarbonate (HCO_3^-), calcium ion (Ca^{2+}), magnesium (Mg^{2+}), barium (Ba^{2+}), potassium (K^+), and strontium (Sr^{2+}). Calcium carbonate ($CaCO_3$), calcium sulphate ($CaSO_4$) and barium sulphate ($BaSO_4$) are the most common scales found in crude oil production facilities. The precipitation of these inorganic scales can be influenced by temperature and pressure [26].

The degree of precipitation depends on the solution chemistry, the degree of saturation, variation in turbulence, pressure, flow velocity and presence of nucleating agent. The precipitation of inorganic scales increases with increasing supersaturation ratio, which is a function of temperature and pressure.

According to Kan and Tomson [27], a major component of scale and corrosion management is the ability to accurately predict the brine chemistry, pH and scaling tendency of production system.

2.2 Types of oilfield scales

The type of scale formed in the oilfield depends on the ions present in the environment. This can be classified according to their sensitivity to pH, some are not sensitive to pH ($CaSO_4$, $BaSO_4$, $SrSO_4$), but the carbonates of (dolomite, calcite and siderite) are very sensitive to pH. This makes their deposition rate difficult to predict because the solution pH influences their scaling tendencies [27].

2.2.1 Calcite

Calcite ($CaCO_3$) is the most common scale found in crude oil production and desalination industries. The earth contains about 12% by weight of calcite and closely related carbonates. Calcite is often formed when pressure drops from bottom hole to the surface.

Calcite scale formation is predominantly a consequence of the pressure drop during production. At a pressure below the bubble point, carbon dioxide is

remove [27]. There are other consequence of pressure drop; the solubility of calcite in sea water decreases with decreasing pressure. $CaCO_3$ is the major component of calcite crystals, but often some percentage of iron and magnesium carbonate co-exist.

Calcite formed naturally, mainly contains pure $CaCO_3$. The supersaturation of $CaCO_3$ can be determined using thermodynamic models and the brine chemistry analysis. $CaCO_3$ at high supersaturation will be in a metastable state in the solution. $CaCO_3$ will not precipitate in an unstable state. However, to predict if $CaCO_3$ will be a problem in a field, the kinetics of formation must be taken into consideration [28, 29].

The decomposition of calcium bicarbonate gives calcium carbonate, water and carbon dioxide, as shown in equation 2-1.

$$Ca(HCO_3)_2 \rightarrow CaCO_3 + H_2O + CO_2 \qquad 2\text{-}1$$

2.3 Calcium carbonate scale formation

Calcium carbonate ($CaCO_3$) is formed when there is a pressure drop in the reservoir, the pressure drops as a result of crude oil and water production from the reservoir leads to supersaturation of calcium carbonate precipitation [30, 31].

Calcium and carbonate ions form calcium carbonate scale that has low solubility and is likely to precipitate in water, irrespective of the concentration of the ions in the solution [18]. The presence of calcium carbonate in production wells can decrease the permeability in the near well area, which may create a problem in the production tubing [28].

The major driving force for calcium carbonate formation is supersaturation, which depends on the brine chemistry; this can be calculated using thermodynamic models and the brine chemistry analysis data. Calcium carbonate can be in a metastable state in solution at high supersaturation. In assessing whether calcium carbonate scaling will be a problem during crude oil production, the kinetic mechanism of its formation must be taken into consideration [32].

Calcium carbonate is relatively easy to treat due to it solubility in acid (HCl). CO_2 influences calcium carbonate formation during EOR, CO_2 injected into the reservoir generate a miscible solvent in situ through a mechanism similar to that of high-pressure gas, but their mechanism are different.

CO_2 at absolute pressure, extracts high molecular weight hydrocarbons from the oil and concentrate them at the CO_2-oil displacement front [33]. Carbonic acid formed from the dissolution of CO_2 in the formation water can dissolve carbonate rock, which increases the concentration of calcium in the brine solution resulting to the precipitation of calcium carbonate [34]. Jongwook et al [35] gave an equation to determine the CO_2 saturation injected into water-saturated sandstone as function of resistivity index(RI) as shown in equation 2-2.

$$S_{CO_2} = 1 - S_w = 1 - \left(\frac{R_o}{R}\right)^{\frac{1}{n}} \quad \text{2-2}$$

Where S_{CO_2} is the CO_2 saturation fraction, S_w water saturation, R is the true resistivity of the sample, R_o is the resistivity of the same rock filled water with water.

2.3.1 Calcium carbonate solution equilibria

The chemical equilibria of calcium carbonate in aqueous solution can be described as carbonic acid undergoing ionization reaction [36], and the ion pair formation and hydrolysis of calcium ions as shown in the following equations 2-3 to 2-6. When carbon dioxide comes in contact with water, it dissolves and forms carbonic acid.

$$CO_2\ (g) \rightleftarrows CO_2\ (aq) \quad \text{2-3}$$

$$CO_2(g) + H_2O \rightleftarrows H_2CO_3 \quad \text{2-4}$$

$$H_2CO_3 \rightleftarrows H_2CO_3^- + H^+ \quad \text{2-5}$$

$$HCO_3^- \rightleftarrows CO_3^- + H^+ \quad \text{2-6}$$

Calcium ions (Ca^{2+}) react with bicarbonate ions (HCO_3^-) to form calcium bicarbonate as shown in equations 2-7 to 2-9.

$$Ca^{2+} + HCO_3^- \rightleftarrows CaHCO_3 \quad (2\text{-}7)$$

$$Ca^{2+} + CO_3^{2-} \rightleftarrows CaCO_3 \quad (2\text{-}8)$$

$$Ca^{2+} + OH^- \rightleftarrows CaOH^+ \quad (2\text{-}9)$$

The precipitation of calcium carbonate is given according to equation 2-10.

$$Ca^{2+} + CO_3^{2-} \rightarrow CaCO_3 \quad (2\text{-}10)$$

By increasing the concentration of carbon dioxide, more calcium bicarbonate is formed. A decrease in carbon dioxide content in the system at equilibrium would result in the formation of calcium carbonate.

This shows that the solubility of calcium carbonate is greatly influenced by the amount of carbon dioxide in water. The amount of carbon dioxide that will dissolve in water is proportional to the CO_2 partial pressure (P_{CO2}) in the gas over the water, which is determined by the product of the mole fraction of CO_2 in the gas phase and the total pressure of the system [33]. Figure 2-2 show the effect of CO_2 partial pressure on the pH of water containing low amounts of dissolved minerals and on solubility of $CaCO_3$ in water.

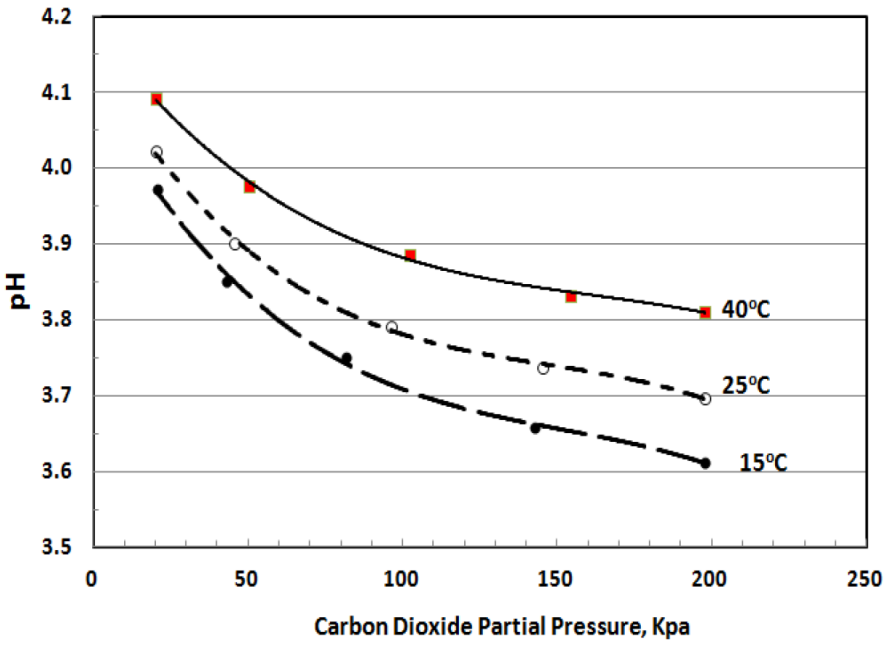

Figure 2-2. Effect of CO_2 partial pressure on pH of water [33]

2.3.2 Forms of calcium carbonate ($CaCO_3$ polymorphs)

Calcium carbonate occurs mainly in three anhydrous crystalline polymorphs. These are calcite, aragonite and vaterite [37-39] . Figure 2-3 to Figure 2-5 show the crystal images of calcium carbonate polymorphs and two hydrated crystal forms (hexahydrate and monohydrate). It also occurs as amorphous form. Calcite is the most stable form of calcium carbonate under room temperature; aragonite and vaterite are metastable in nature, but vaterite is usually on an unstable state [40].

The stabilization and crystallization of these polymorphs depends on the environmental conditions such as pH, brine chemistry (ionic medium, concentration of ions), the degree of supersaturation, and temperature [41].

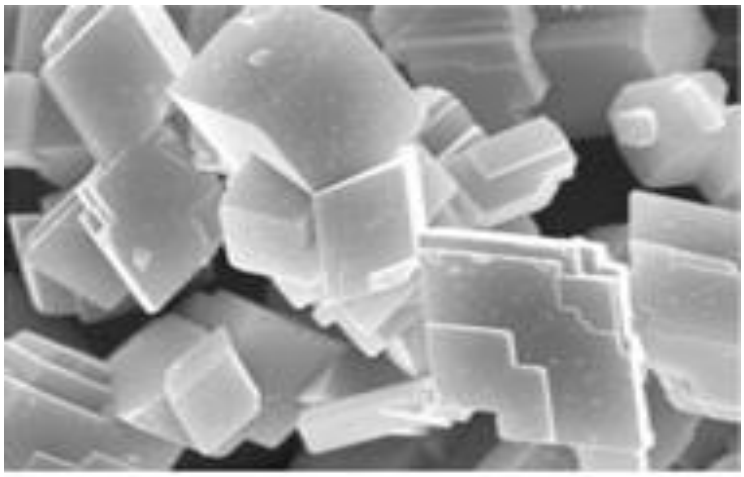

Figure 2-3. SEM image of calcite scale crystals [41]

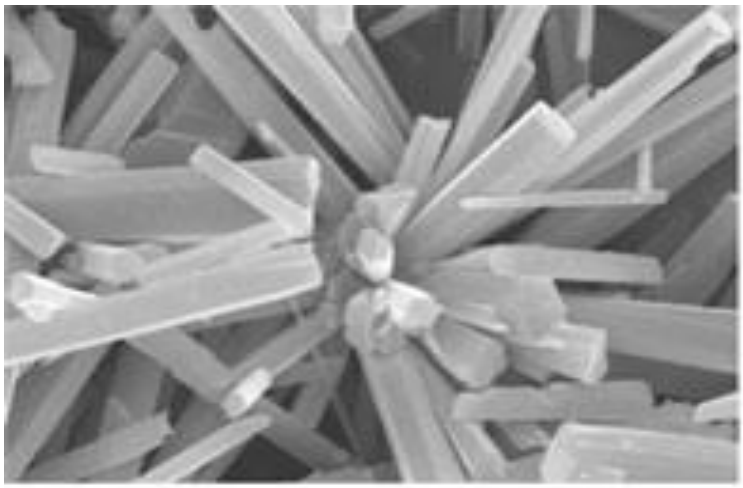

Figure 2-4. SEM image of aragonite scale crystals [41]

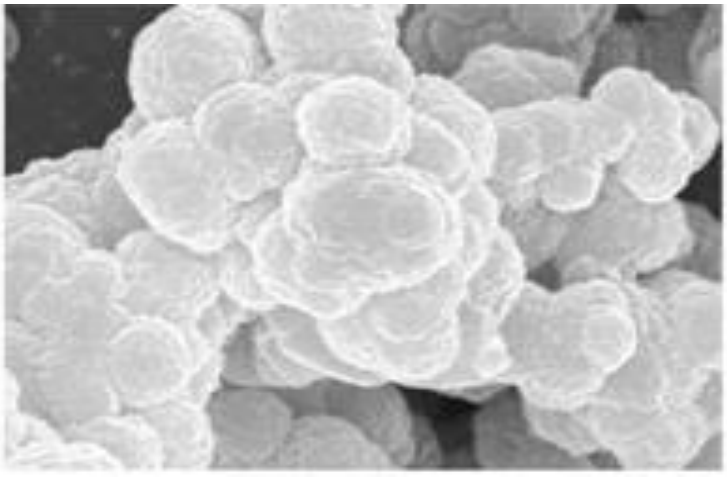

Figure 2-5. SEM image of vaterite scale crystals [41]

It has been reported [23, 42], that calcite is mainly a centred rhombohedral cell as shown in Figure 2-6. With aragonite as an orthorhombic crystalline form.

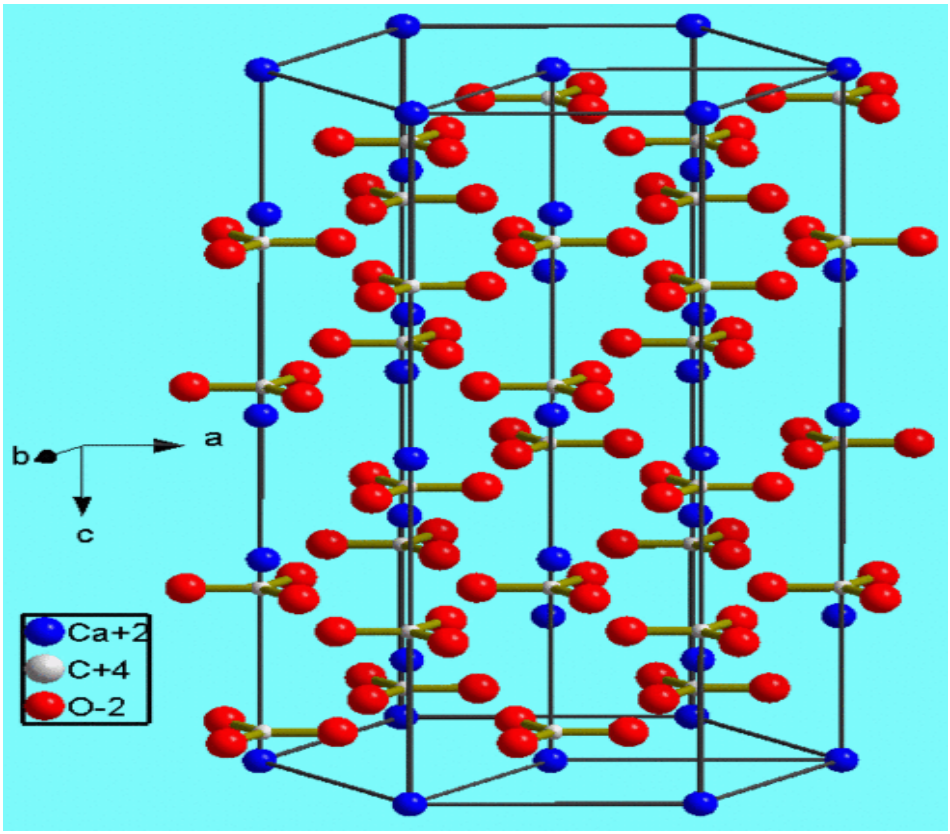

Figure 2-6. Crystalline structure of calcite [43]

Vaterite is readily converted to more stable calcite and aragonite structure [44]. The amorphous calcium carbonate and hexahydrate calcium carbonate are formed at high pressure.

Brankling et al [44], studied the formation of vaterite and its prevention. It was reported that the solubility of vaterite in water is much higher compared to the solubility of aragonite and calcite at this same temperature. However, during scale formation there is no driving tendency to vaterite precipitation and calcite is dominantly present. Previous research showed that vaterite could be formed from solution with high supersaturation. Table 2-1 shows the solubility constants of different calcium carbonate polymorphs at 25^{o}C.

Table 2-1. Solubility constants for the different calcium carbonate polymorphs at 25°C and in general form [45]

Polymorphs	K_{sp} at 25^{o}C	log K_{sp}
Amorphous $CaCO_3$	6.28	10< T<55^{o}C 6.1987+0.00053369t +0.0001096t^2
Hexahydrate $CaCO_3$	6.59	0< T <25^{o}C 0.1598 – 2011.1/T
Monohydrocalcite	7.15	15< T<50^{o}C 7.050 + 0.000159T^2
Vaterite	7.913 ± 0.020	0 < T < 90°C -172.1295 - 0.077993 T +3074.688 / T + 71.595 log T
Aragonite	8.336 ± 0.020	0 < T < 90°C -171.9773 - 0.07793 T +2903.293 / T + 71.595 log T
Calcite	8.480 ± 0.020	0 < T < 90°C -171.9065 – 0.077993 T +2839.319 / T + 71.595 log T

2.3.3 Barite

Barite, also known as barium sulphate ($BaSO_4$), is formed when two incompatible brines are mixed together during enhanced oil recovery processes when the pressure of the reservoir is maintained to keep the production volume of the field [46].

Barite scale occurs when either brines (formation water and sea water) from different oil wells are mixed or when there is flooding of high sulphate containing water mixed with the sea water flooding. When these brines are produced and it turns out one is high in barium and the other is high in sulphate, they mix at the bottom of the well, but it takes some time to mix completely [27].

The saturation index of barite can be high and the precipitation is faster, which can result in high supersaturation levels that might be difficult to control with inhibitors, irrespective of the inhibitor dosage. Barium sulphate has very low solubility, which makes it difficult to control. Barium ions combine with sulphate ions to form barium sulphate as shown in equation 2-11.

$$Ba^{2+} + SO_4^{2-} \rightarrow BaSO_4 \qquad 2\text{-}11$$

2.3.4 Calcium sulphate

The precipitation of calcium sulphate ($CaSO_4$) results from a mixture of incompatible waters during water flooding. It can also result from a pressure drop when production is from a reservoir where the brine is saturated with calcium sulphate or from temperature increases during the processing of the brine on the surface [27].

Calcium sulphate usually occurs in three forms, which differ by their water of crystallization. Anhydrite ($CaSO_4$) is the major form commonly found, gypsum ($CaSO_4.2H_2O$) is the most stable form of calcium sulphate from temperature of 40^oC to 90^oC and hemihydrate ($CaSO_4.1/2H_2O$) has high total dissolved solid content. The transition temperatures are dependent on the composition of brine solution.

2.3.5 Strontium sulphate

Strontium sulphate ($SrSO_4$) has a low solubility product constant of 3.2×10^{-7} at 25°C compared to calcium sulphates of solubility product constant of 9.1×10^{-6} at 25°C. It occurs as a result of the mixture of incompatible brines during water injection process.

Todd et al [47] investigated barium and strontium sulphate solid scale formation in rock pores and discovered permeability damage and scaling crystal morphology which was influenced by sulphate supersaturation and scaling ion concentration ratios in the brines. The permeability was dependent on the initial rock permeability.

2.3.6 Siderite

Iron carbonate is mainly referred to as corrosion product and not a mineral scales. However, there is interaction between $FeCO_3$ and $CaCO_3$ on carbon steel surfaces. $FeCO_3$ will precipitate first in solution [48]. It is observed that in the absence of corrosion, the ratio of Ca^{2+} to Fe^{2+} is approximately 100:1, due to the corresponding solubility product (K_{sp}) ratios [27]. Which are 2.8×10^{-9} and 3.2×10^{-11} respectively.

$FeCO_3$ can be protective depending on the environmental conditions. Protective $FeCO_3$ films can form in wet CO_2 systems provided that the pH and the dissolved $FeCO_3$ in the bulk solution are sufficiently high. The formation of $FeCO_3$ film is temperature dependent and a high supersaturation is needed to form a protective film [49] .

2.4 Chemical background of scale formation

Formation of scales is a product of instability in the bulk solution or solution chemistry of the scaling environments. One of the key indicators responsible for scale formation is the solubility of the solute in solution at given temperature [50, 51] . This factor is measured by the solubility product constant (K_{sp}).

2.4.1 Solubility product

Solubility is the amount of solute that will dissolve in a solvent at a particular temperature [52]. Salt is a substance formed by the reaction between positive and negative ions. The dissolution of salt in water (solvent) produces anions and

cations known as the solute molecules. The product of the ions produced from the salt is called the solubility product (K_{sp}). The solubility product constant is defined from equation 2-12 and 2-13

$$AB \leftrightharpoons A^+ + B^- \quad \text{2-12}$$

$$K_{sp} = [A^+][B^-] \quad \text{2-13}$$

Where $[A^+]$ and $[B^-]$ denotes the molar concentration (mol/dm^3) of the cation and anion in bulk solution respectively.

The solubility product is a measure of the amount in moles of ions present in a particular volume of solvent that can be in a system before precipitation [9]. The value of K_{sp} varies with solvent. The solubility product value determines the tendency for salt to dissolve in a solvent. High K_{sp} values mean more salt will be dissolved in the solvent, which means the salt is highly soluble.

The dissolution of salt in water can produce acidic, basic or neutral solution. pH has impact on the solubility product of some compounds. Calcium carbonate dissolves in water to produce Ca^{2+} and CO_3^{2-}. CO_3^{2-} attract a proton from water producing a basic solution. The equilibrium position shifts by favouring the formation of calcium carbonate ($CaCO_3$) from the reaction of Ca^{2+} and CO_3^{2-}.

2.5 Scale formation process

Scale formation results from the crystallisation of minerals from solution, which occurs in a series of steps as shown in Figure 2-7. The first step is the cationic (Ca^{2+}) and anionic (CO_3^{2-}) species colliding to form ion pairs in solution. The ionic pairs form micro-aggregates, which grow to become nucleation sites for crystallization.

These microcrystals agglomerate and grow into larger microcrystals and combined to form adherent macrocrystals, which continue to grow by adsorption of more scaling ions from the solution, thereby forming a scale film on a surface [53].

The scale formation process in Figure 2-7 occurs primarily in two steps, which are nucleation and crystal growth. Nucleation and crystal growth depend on

temperature and the degree of supersaturation, which is the driving force for scale formation.

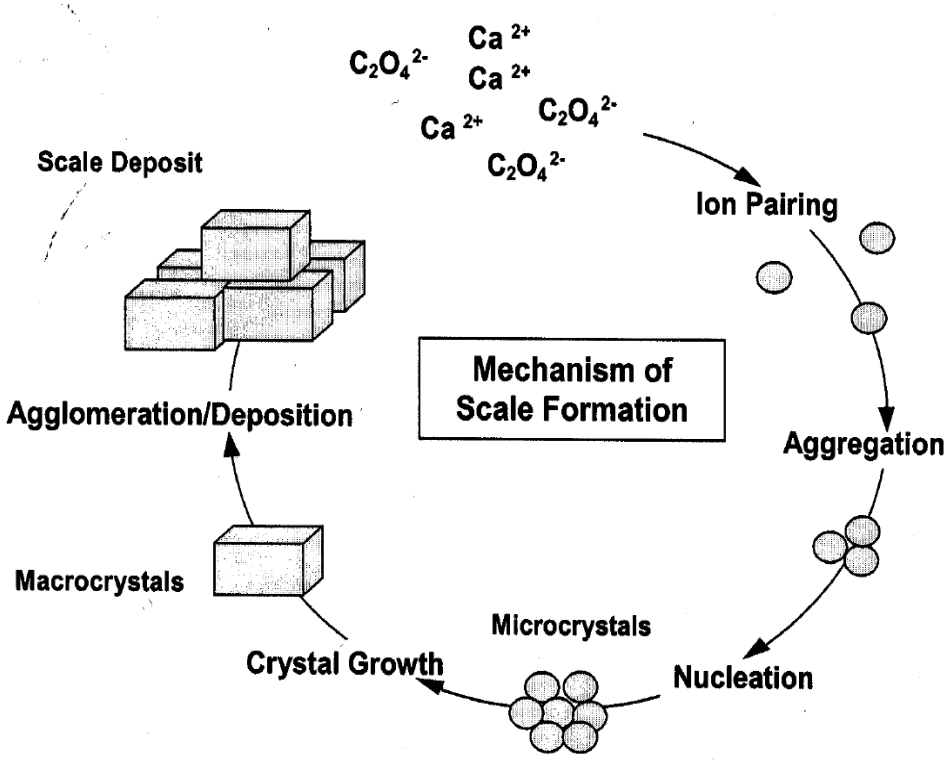

Figure 2-7: Scale formation process [53]

2.5.1 Chemical potential and supersaturation

The reactivity of chemical components in solution is measured by its chemical potential, which is determined by how the Gibbs free energy (ΔG) of the system changes when the number of moles or molecules of the reactant in the system changes at constant pressure and temperature [54].

The system tends to minimize its Gibbs free energy by lowering its chemical potential. The relationship between the Gibbs free energy and the chemical activity is given in the following equation 2-14.

$$\Delta G = -\frac{1}{2} RTIn\left(\frac{IP}{K_{sp}}\right) \qquad 2\text{-}14$$

Where R denotes the molar gas constant in $Jmol^{-1}K^{-1}$, T temperature in Kelvin (K), IP is the activity product of free ion activity $[Ca^{2+}]$ $[CO_3^{2-}]$ and K_{sp} is the solubility product constant.

The chemical potential of a system is pressure and temperature dependent. The solubility of a system is affected by the variation of chemical potential of the system, since the solubility of a system depends on the temperature [9].

In oil and gas wells, it is very important to take into consideration the pressure dependency due to high pressure being observed at the reservoir. The effectiveness of chemical process is determined by thermodynamic driving force, this driving force is represented by supersaturation. Supersaturation occurs when there is increase in concentration of dissolved anions (CO_3^{2-}) and cation (Ca^{2+}) to levels beyond their normal solubility limits in water [53].

Supersaturation is the driving force for scale formation; solutions can become supersaturated as a result of changes in temperature, pressure, pH or change in concentration of ions in solution. As the level of supersaturation increases the system becomes thermodynamically unstable and precipitation can occur. It should be noted that local conditions of supersaturation may occur causing scale deposit even when the bulk average brine composition remains the same.

The scaling tendency is determined by supersaturation ratio (SR) or supersaturation index (SI). The supersaturation ratio (SR) for calcium carbonate is defined as:

$$SR = \frac{[Ca^{2+}][{CO_3}^{2-}]}{K_{spCaCO_3}} \qquad 2\text{-}15$$

The activity based supersaturation ratio for ionic compounds for crystallisation theory is given by,

$$Sa = (\frac{IP}{K_a})^{1/v} \qquad 2\text{-}16$$

Where IP is the ionic activity product of the total number of cations and anions which dissociate in solution and K_a is the activity based solubility product of the salt [55]. Therefore, for calcium carbonate, the supersaturation ratio S= S_a is given as:

$$S = \frac{\sqrt{[Ca^{2+}] \times [{CO_3}^{2-}]}}{K_{sp}\ (CaCO_3)} \qquad 2\text{-}17$$

Supersaturation index is calculate from equation 2-18

$$SI = \log\left(\frac{IP}{K_{sp}}\right) \qquad 2\text{-}18$$

For scale formation to take place, there are three possibilities from the solution with thermodynamics [56].

● SR < 1, the solution is under saturated and the tendency for scaling is not thermodynamically feasible.

● SR= 1, the solution is at equilibrium, i.e. Scale formation and dissolution rate in the solution is the same.

● SR > 1, the solution is supersaturated and there is high tendency for scale formation.

2.5.2 Induction time

The induction time is the time between the occurrences of supersaturation to the formation of stable nuclei of the precipitating salt [28]. The induction period is greatly influence by the nature and degree of the supersaturation of the bulk solution, the level of agitation, viscosity of the solution and presences of impurities [57].

According to Ostvold et al [28] the measured induction time is longer than the estimated, since the nuclei have to grow to a size that can be detected experimentally. The induction time is determined from the equation 2-19

$$t_{ind} = t_n + t_g \qquad 2\text{-}19$$

Where t_{ind} denotes the induction time t_n denotes the time for the system to reach steady state and form the stable nuclei and t_g denotes the time before the nuclei have reached a detectable size.

pH can be used to monitor the start of scale precipitation, decrease in pH, increases the rate of precipitation of inorganic scales as shown in equation 2-20

$$Ca^{2+} + HCO_3^- \rightarrow CaCO_{3(s)} + H^+ \qquad 2\text{-}20$$

Ostvold et al [28], used a pH measurements as a basis to determine the induction time for $CaCO_3$ scales by making an assumption that the induction t_{ind}, is inversely proportional to the nucleation rate J as given in equation 2-21

$$t_{ind} \propto J^{-1} \qquad 2\text{-}21$$

But for a homogenous nucleation, the relationship between t_{ind} and SR is given by equation 2-22

$$logt_{ind} \propto \left[\frac{\gamma^3}{T^3(logSR)^2}\right] \qquad 2\text{-}22$$

Simplifying equation 2-22 and introducing constant of proportionality A, the relationship between (log t_{ind}) and (log SR)^2 using classical nucleation theory [57, 58] as shown in equation 2-23 and 2-24

$$\log(t_{ind}) = \left[A + \frac{B}{T^3(logSR)^2}\right] \qquad 2\text{-}23$$

$$B = \frac{\beta\gamma^3 Vm^2 NA\, f(\theta)}{(1.3R)^3} \qquad 2\text{-}24$$

where γ denotes the interfacial energy (mJ/m^2), between the solid phases forming the liquid, V_m denotes the molecular volume of crystals ($6.132x10^{-23}$ cm^3 for calcite) T the temperature (K), SR the saturation ratio, t_{ind} the induction time (s), A an empirical constant (dimensionless), R the molar gas constant (J/mol.K), N_A denotes the Avogadro's constant (mol^{-1}),$f(\theta)$ is a correction factor depending on the type of nucleation, β is a geometric factor of $\frac{16\pi}{3}$ for spherical shape crystal.

Studies [58-60], have shown a linear relationship between (log t_{ind}) and (log SR)$^{-2}$, although, most models assume homogeneous nucleation in static system, but in reality processes such as heterogeneous nucleation might be taking place in a flowing system [57].

A Study by Mavredaki and Neville[61] , shows that the induction time for nucleation process is an important function of supersaturation, that is, increase in supersaturation decrease the induction period for nucleation process. This relationship is shown in Figure 2-8.

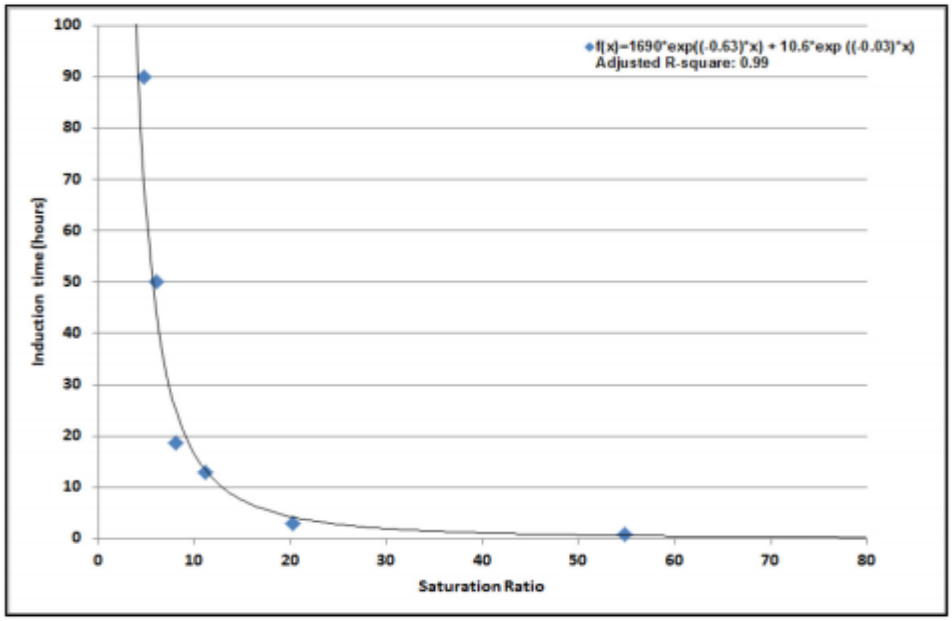

Figure 2-8: Induction time as a function of saturation ratio [61]

2.5.3 Nucleation

Nucleation occurs at nucleation sites of surfaces contacting the liquid or vapour suspended particles. The development of crystals occurs in solution after creation of ionic species, nuclei or seeds, which acts as sites for crystallization. Nucleation is a process that can occur spontaneously or be induced by external influence such as agitation, mechanical shock, pressure and friction within the solution [62]

One of the features of nucleation is the ability to form a metastability of the old phase. This process requires it to overcome the free energy barrier [63]. This is clear by considering the change free energy during the formation of the nucleus. The free energy for the bulk solution is less than that of the solvent phase, but this does not apply.

The surface molecules are lightly bound to their species compared to that of bulk solution, therefore their contribution to the free energy of the new phase is greater. Surface energy is the term use to describe the difference between the free energy of the bulk solution per molecules and that of the surface.

Nucleation is divided into two part, primary nucleation, where the formation of new crystals do not depend on the presence of pre-existing crystals and secondary nucleation, where the formation of new crystals is driven by the presence of existing crystals in the bulk solution. Figure 2-9 shows the schematic illustration of the two types of nucleation.

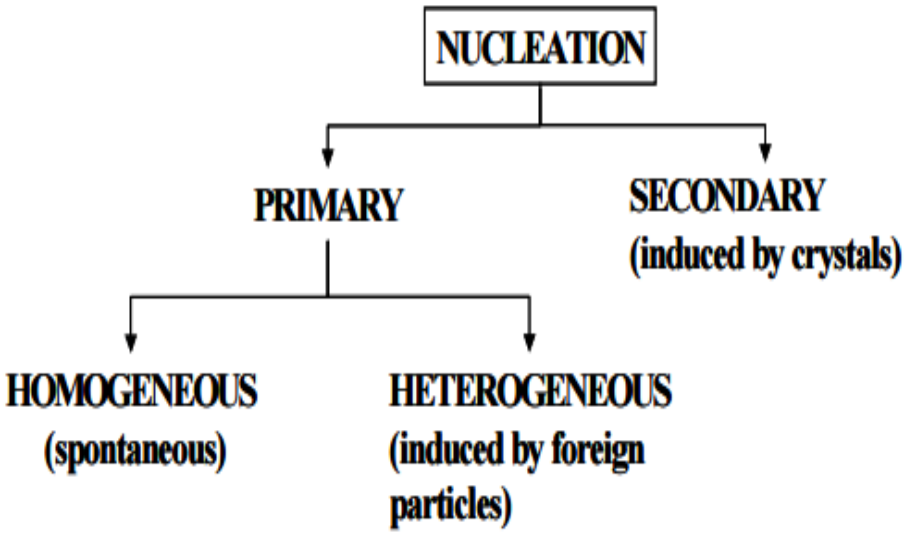

Figure 2-9: Types of nucleation [57]

2.5.4 Primary nucleation

Primary nucleation is the type of nucleation that occur, where the formation of new crystals is independent of the pre-existing crystals. This can occur spontaneously or induced by the presence of foreign particles in the solution. This type of nucleation process is referred to as homogenous and heterogeneous nucleation.

2.5.4.1 Homogenous nucleation

Homogenous nucleation is the formation of nuclei in the absences of any foreign materials. It is much more difficult in the interior of a uniform substance. Homogenous nucleation process is spontaneous and random, but it requires

superheating or super cooling of the medium [64]. The formation of interface at the boundaries of a new phase results from the creation of nucleus.

Figure 2-10 shows the nature of homogenous nucleation process for barium sulphate scale. Homogeneous nucleation occur at high supersaturation.

Studying the kinetics of homogeneous nucleation process is sometimes difficult due to the challenges in designing a system free of impurities and impurities presents in the system can accelerate the nucleation process [65, 66].

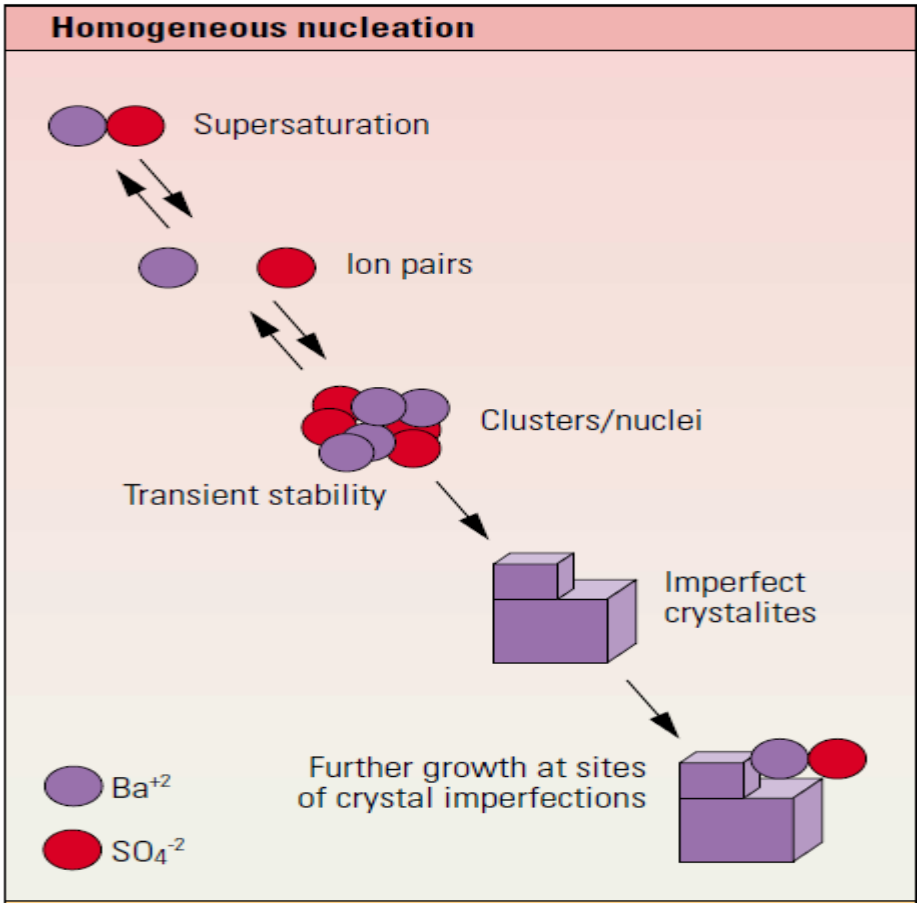

Figure 2-10: Homogenous nucleation [67]

The classical nucleation based on vapour condensation is used to describe the homogeneous nucleation process in terms free energy in relation to the variation to nucleus size as shown in Figure 2-11.

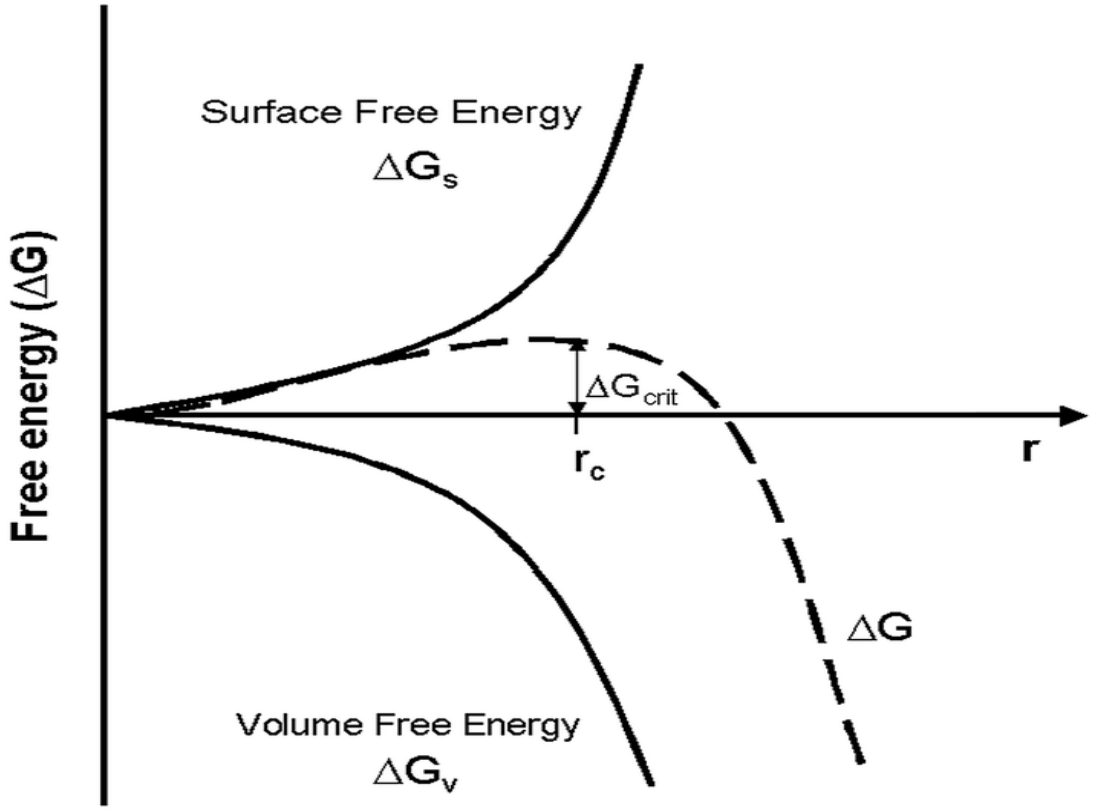

Figure 2-11: Free energy diagram for nucleation and critical nucleus [57]

The overall free energy changes in homogeneous nucleation process is given in 2-25 according to classical nucleation theory [57]

$$\Delta G = \Delta G_v + \Delta G_s \qquad 2\text{-}25$$

Where ΔG denotes the overall excess free energy between a small spherical particle of radius r and the solute in solution, ΔG_v denotes the free energy of transformation between the solution and large particle. ΔG_s denotes the energy related to the creation of new surface. ΔG_s and ΔG_v depend on r differently, with ΔG_v negative and ΔG_s positive.

The overall free energy of formation ΔG may reach a maximum ΔG_{crit} vaule. This maximum value is responsible for the formation of stable particles and corresponds to the critical size of a nucleus. The radius r_c of the critical nucleus corresponds to the minimum size at which a nucleus is stable.

The characteristics of a newly created crystalline lattice structure in a supersaturated solution depends on its size, it may either grow or dissolve. This depends on the following conditions [57].

- $r > r_c$, the particle will grow

- $r < r_c$, the particle will dissolve or evaporate due to insufficient energy to create its surface.

The nucleation rate J in terms of free energy for the critical cluster size ΔG_c is given as

$$J = A \exp\left(\frac{-\Delta G_c}{KT}\right) \quad 2\text{-}26$$

Where A denotes the experimental factor constant, ΔG_c denotes the free energy change for the critical cluster size, K Boltzmann constant, T temperature.

The free energy change for the critical cluster size ΔG_c is given as,

$$\Delta G_c = \frac{16\pi\gamma^3 v^2}{3(KTInSR)^2} \quad 2\text{-}27$$

Where ɣ denote the interfacial energy in mJ/m^2, v the molecular volume in cm^3 /mol and SR, saturation ratio.

2.5.4.2 Heterogeneous nucleation

Heterogeneous nucleation occurs when scale grows on pre-existing surface defects such as rough spots on the liquid-tubing surface [67, 68] as shown in Figure 2-12. It applies to the phase transformation between any two phases of solid, liquid or gas. Heterogeneous nucleation occurs more frequently than the homogenous nucleation.

It forms at pre-existing surfaces. Such surfaces have low effective surface energy, thereby decreasing the free energy needed for nucleation, which is equal to the product of homogenous nucleation and the function of the contact angle [57] as shown in equation 2-28.

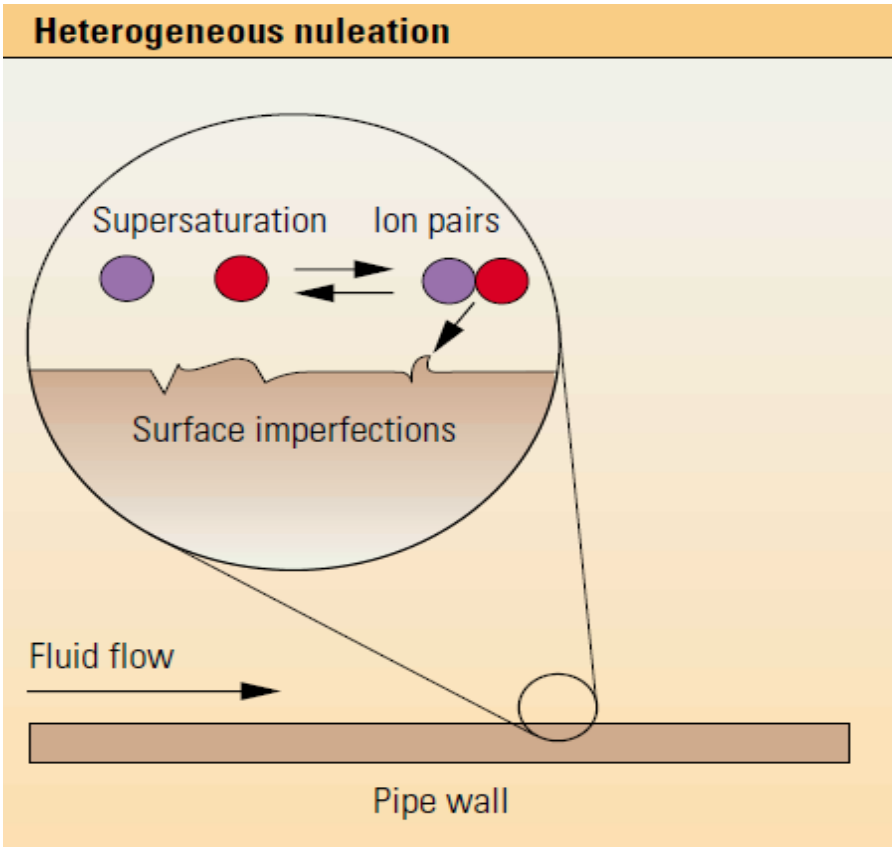

Figure 2-12: Heterogeneous nucleation[67]

In heterogeneous nucleation, the total energy changes for the formation of a critical nucleus ΔG_c must be less than the corresponding free energy change for homogeneous nucleation i.e.

$$\Delta G_{cHeterogeneous} = \emptyset \Delta G_{cHomogeneous} \qquad 2\text{-}28$$

Where Ø is between 0<Ø<1.

According to classical nucleation theory [28, 69], one of the factors controlling nucleation process is interfacial energy. Figure 2-13 shows the three interfacial energy phases during nucleation process (solid surface, liquid and crystalline deposit).

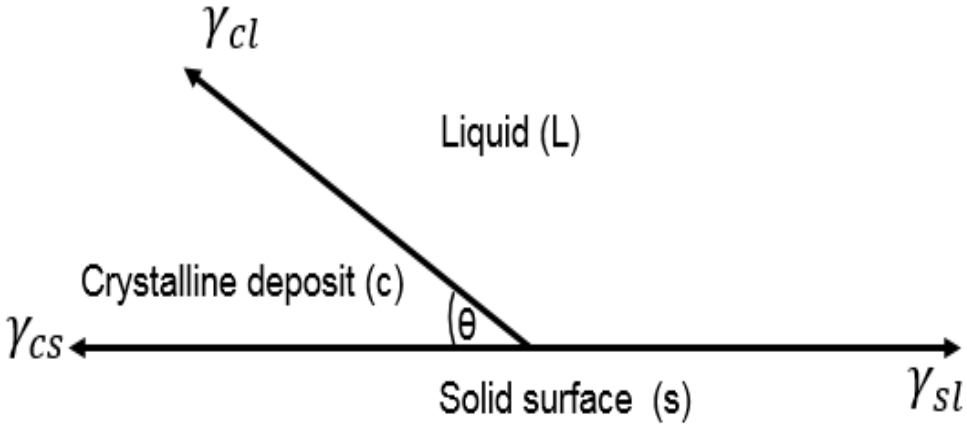

Figure 2-13: The interfacial energy at the boundaries between three phases [70]

Where $\boldsymbol{\gamma_{cl}}$ denotes the interfacial energy between solid crystalline phase and liquid, $\boldsymbol{\gamma_{sl}}$ denotes the interfacial energy between the foreign solid surface and the liquid, $\boldsymbol{\gamma_{cs}}$ denotes the solid crystalline phase and foreign solid surface and θ denotes the contact angle between the crystalline deposit and the foreign solid surface, which also referred to as the angle of wetting in liquid to solid surface.

The relationship between this three phases and contact angle is given by equation [70] 2-29 and 2-30

$$\gamma_{sl} = \gamma_{cs} + \gamma_{cl} cos\theta \qquad 2\text{-}29$$

$$cos\theta = \frac{\gamma_{sl} - \gamma_{cs}}{\gamma_{cl}} \qquad 2\text{-}30$$

2.5.5 Secondary nucleation

The nucleation process that occur due to the presence of pre-existing crystals of material being crystallized is termed secondary nucleation [71]. In solid phase, secondary nucleation process result from the presence of particles or crystals of the same substance. Secondary nucleation is quite different from primary nucleation (homogeneous and heterogeneous nucleation) process, as heterogeneous nucleation occur due to the presence of foreign interface.

Daudey et al [72] and Elodie et al [73] define two major mechanism of secondary nucleation in solution crystallization as a mechanical process and an activated process. In the mechanical process, secondary nuclei are formed by attrition which involves the disintegration of the crystals into two dissimilar parts. This process occurs at a very low saturation ratio. The activated process is sometimes referred to as surface nucleation. This process occurs at a certain level of supersaturation around the crystal or activating the nuclei in the bulk solution. Heidjen et al [74] differentiate the two secondary nucleation mechanisms as shown in Figure 2-14.

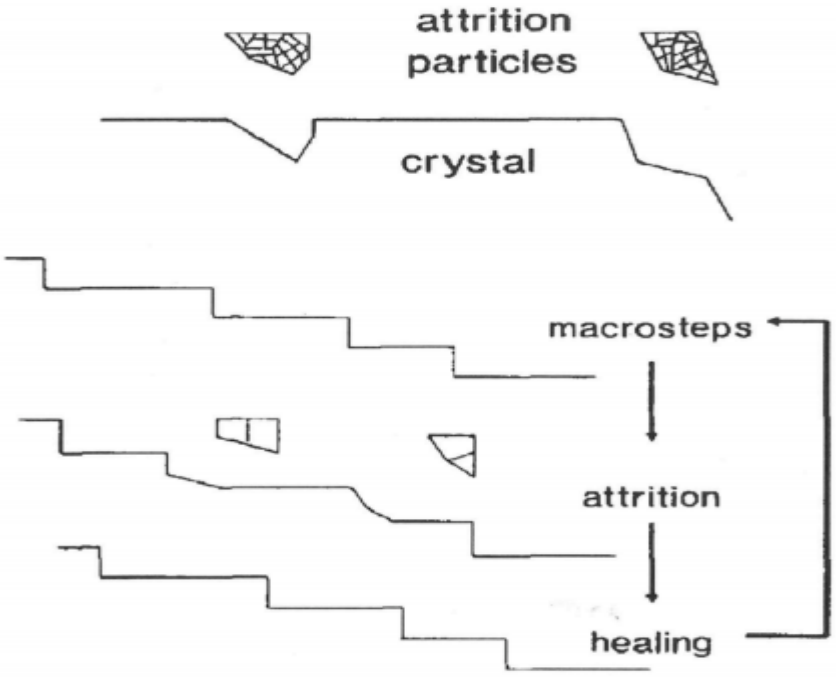

Figure 2-14 : Visualisation of the difference between mechanical breeding and surface breeding [74]

Clifford et al [75] suggested that solution-solid interface is the main source of secondary nucleation and identified supersaturation at the interface between the solution and growing crystals as the main parameter for secondary nucleation process.

2.5.6 Crystal growth

Crystal is a solid material whose constituent atoms, molecules or ions are arranged repeating pattern extending in all three dimensions. Crystal growth is a major stage of crystallization process, it consist of the addition of new atoms, ions or polymers stings into the characteristic arrangement of a crystalline. Once a stable nuclei is formed, whose particles is larger than the critical size, they start to grow into a visible crystal size [57].

Crystal growth is connected with its surface area and the free energy, a low surface energy and surface area promote crystal growth stability. Three key mechanism of crystal growth was proposed by researchers [57]. These are, surface energy theory, adsorption layer theory and diffusion theory.

Margrethe et al [9] reported that, in a supersaturated solution, unstable clusters of atoms develop local fluctuations in the equilibrium concentration. This can increase the tendency for these clusters to form seed crystals, these crystals grow by adsorbing ions, preferably at defects in the surface.

The crystals exhibit a reduction of free energy when expanding its surface due to critical size of the crystals, this favours the growth of a larger crystals. Crabtree et al [67] studied that, crystal growth also tends to initiate on a pre-existing fluid-boundary surface, called heterogeneous nucleation. That high degree of turbulence can speed up scale deposition

2.5.7 Crystal growth mechanism and theory

The following crystal growth mechanism and theory is discussed under the following headings.

2.5.7.1 Surface energy theory

Gibbs suggest that, the shape of a growing crystals has a minimum surface energy, and the total free energy of a crystal in equilibrium with its surrounding at constant temperature and pressure would be minimum for a given volume, assuming the volume free energy per unit volume is constant throughout the crystal [57].

Crystals developed an equilibrium shape when it is allowed to grow in a supersaturated medium. i.e. the development of the various faces must be in

such manner that, the entire crystal has minimum total surface free energy for specific volume [57].

According to Wuff [76], the equilibrium shape of a crystal is related to the free energies of the faces. It proposed that, crystal faces would grow at rates proportional to their respective surface energies and the total growth rate of a face should be inversely proportional to the lattice density of the respective lattice plane. Which implies that, high index faces grow faster than low index faces and the velocity of growth of a crystal face is measured by the outward rate of movement in a direction of the face.

2.5.7.2 Adsorption layer theory

The adsorption layer theory according to Volmer, assumed that crystal growth is a discontinues process, which is based on the existence of an absorbed layer of solute molecules or atom on a crystal face [57, 77]. The theory also suggested that when units of the crystallizing substance get to the crystal face, they do not integrate instantly into the crystal lattice. But lose its degree of freedom and migrate over the crystal face by surface diffusion, which is loosely adsorbed at the interface and a dynamic equilibrium is created between the layer and the bulk solution.

The adsorption layer is important in formation of the crystal growth and secondary nucleation. The adsorbed layer has a thickness layer not more than 10nm. Ions or molecules link into the lattice in the position where the greatest attractive force at the active centre, which is build stepwise under ideal condition and the ionic continue until the entire plane face is completed before a further layer can commence. A centre of crystallization is established on the plane surface [78]. This was suggested by Gibbs-Volmer as two-dimensional nucleus [76].

The rate of two-dimensional nucleation rate is expressed as:

$$J = B * exp\left(\frac{-\Delta G_{crit}}{KT}\right) \qquad 2\text{-}31$$

$$J = B * exp\left[-\frac{\pi h \gamma^2 v}{K^2 T^2 InSR}\right] \qquad 2\text{-}32$$

Where J denotes the two-dimensional nucleation rate, B denotes a constant define by equation 2-23, v molecular volume of nucleus(cm^3), r radius of the circular disc (cm), h height of the circular disc, γ, interfacial energy (mJ/m^2), K Boltzmann constant (J/K), T temperature (K)

2.5.7.3 Diffusion Theory

Noyes and Whitney considered that the deposition of solid on the face of a growing crystal is a diffusion process, and the process is controlled by the concentration difference at the solid surface and in the bulk of the solution [57]. This assumption was represented by equation 2-33

$$\frac{\partial m}{\partial t} = K_m A(C - C^e) \qquad 2\text{-}33$$

Where m denotes the mass of solute deposited at time t, A the surface area of crystal, C denotes solute concentration in the solution, C^e equilibrium saturation concentration, K_m mass transfer coefficient.

Berthoud and Valeton [79], modified equation 2-33 and assumed a two step process in the mass deposition. They suggested the processes as diffusion process, whereby the solute molecules are transported from the bulk solution of the fluid phase to the solid surface, followed by surface reaction where the solute molecules are integrated into the crystal lattice [57, 80]. These two processes are influence by concentration differences at the solid surface and the bulk solution as shown in equation 2-34 and 2-35 respectively.

Diffusion process $$\frac{\partial m}{\partial t} = K_d A(C - C^s) \qquad 2\text{-}34$$

Surface reaction $$\frac{\partial m}{\partial t} = K_r A(C_s - C^e) \qquad 2\text{-}35$$

Where K_d denotes the mass transfer coefficient, K_r rate constant for surface reaction, C_s solute concentration in the solution at the crystal interface.

Vekilov et al [63] illustrated the atomic processes occurring at a crystal surface. The surface consist of flat regions called terraces and raised partial layers called steps. The steps contains the kinks sites, which are very useful, since molecules that attach there are bonded to the other molecules than the ones attach to the terraces, which are more likely to attach strongly to the surface as shown in Figure 2-15.

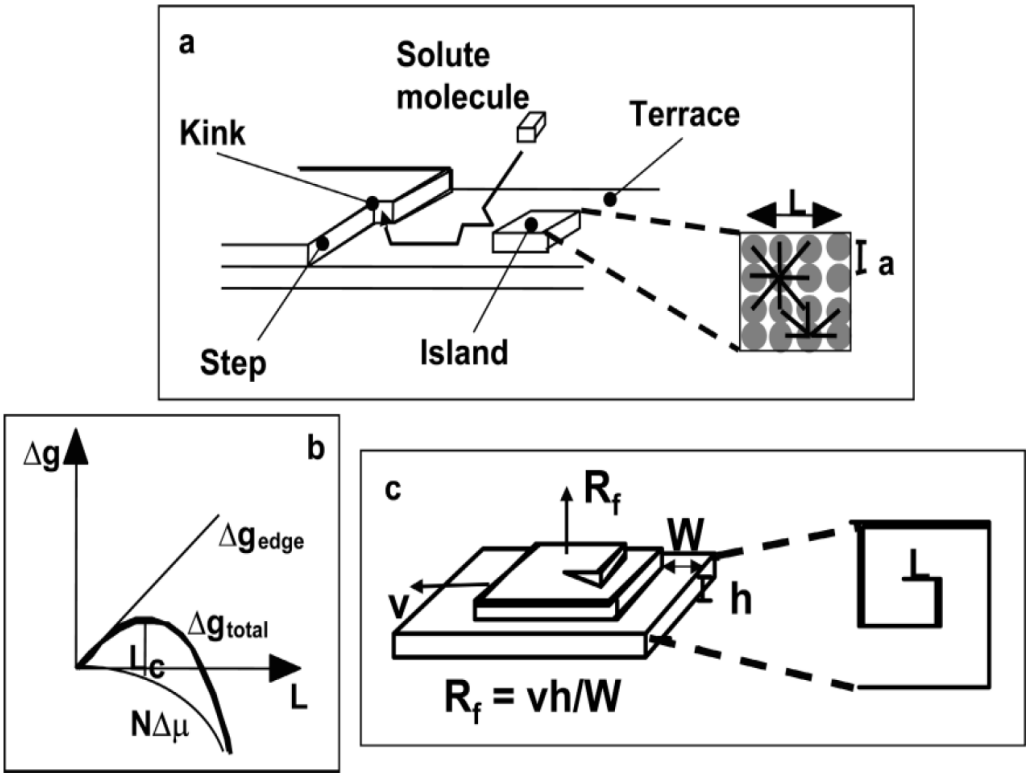

Figure 2-15: The kinetics of scale crystal growth [63]

(a) Illustration of the atomic processes during crystal growth. Solute molecules enter kinks either directly from solution or after adsorbing and diffusing across terraces. Island can nucleate on the terraces provided they overcome the free energy barrier to 2D nucleation illustrated in (b). (c) Shows the geometry of a dislocation hillock. The existence of a critical size leads to the formation of the spiral structure, since the new segment of the step cannot move until it reaches that size [63].

2.6 Adhesion

Surface scaling is a major challenge being faced in oil and gas and desalination industry, and one of the mechanism by which scale is form on the surface of facilities, is adhesion of pre-precipitated crystals.

Adhesion occurs when surfaces cling to one another by intermolecular forces such as valence forces. The scale crystals can attach to the wall of the substrate either by nucleated crystals being transported to the surface of the capillary cell or agglomerate in the bulk where they attach to the surface of the substrate. This process can occur through intermolecular forces such as Van der Waals force, electrostatic interaction and chemical bonding [81-84]. Adhesion is complex phenomenon as Physicists and Engineers define adhesion as the total force exerted when two adhered materials are separated [70, 85] .

According to Collins [86], the mechanism by which scale crystals deposit on the surface of facilities under flow conditions, depends on the size of the crystals, geometry of the substrate and the flow regime of the system.

In scaling, the question in relation to adhesion relates to how the scale crystals can attach to the surface of substrates. The key questions are:

- Do the nucleated crystals evolve from the flow and are they transported to the surface of the steel?
- Do the crystals form and agglomerate in the bulk and transport to the surface where they adhere?
- Which forces are responsible for the adhering of these crystals

Studies [85, 86], suggested that, pre-precipitated crystals from the bulk solution are transported to the surface of the substrates or wall of the pipe through the following mechanism.

- Transport due to inertial forces
- Brownian diffusion

- Eddy diffusion
- Deposition due to shear dispersion and forces
- Deposition resulting from gravity forces
- Particle motion resulting from electrostatic forces

However, these transport mechanisms depends on the flow regime, pipe geometry and the particle size. Figure 2-16 labelled 1, 2 and 3, show the interaction of crystals in bulk solution to the surface of substrates. For a pre-precipitated crystal to adhere to the surface of the substrate, it depends on the following conditions stated in Table 2-2

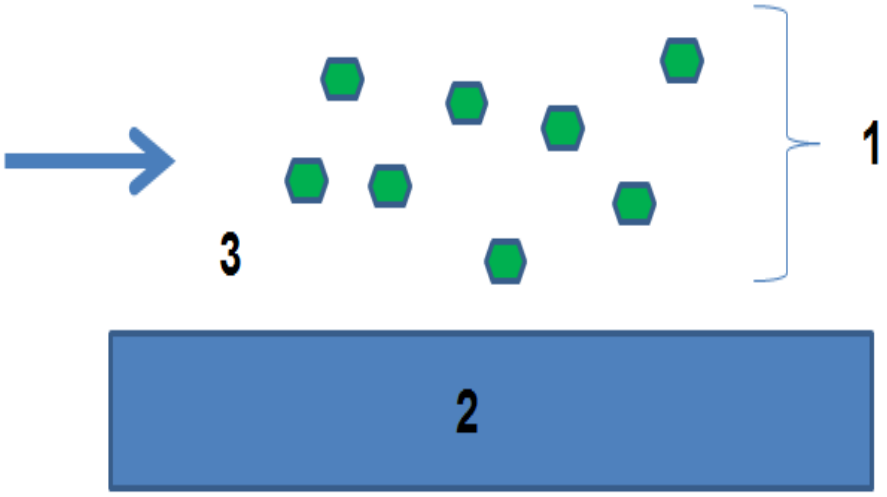

Figure 2-16: Interaction of crystals in bulk solution to the surface of a substrate

Table 2-2: Properties of crystals (1), substrate (2) and environment (3) that affect the adherence of crystals to the surface of substrates

Crystal properties(1)	Substrate Properties (2)	Environment (3)
Particle size and shape distribution	Surface roughness	Salinity
Concentration	Material type (charge, energy)	Temperature
Flow rate	Wettability	Flow regime
Surface charge		

The adherence of crystals to the surface of substrate does not occur instantly when particles gets to the surface due to the presences of energy barrier to deposition [86].

2.6.1 Surface energy and adhesion forces

The adhesion process is best described in terms of colloid chemistry, which is mainly associated with a fouling process. Adherence of scales to the surface of materials is governed by Derjaguin, Landau, Verwey and Overbeck (DLVO) theory [83]

The total interaction energy ΔG_T between a deposit and a metal surface is given as the sum of the individual interaction parameters [86] as shown in equation 2-36.

$$\Delta G_T = \Delta G_W + \Delta G_E + \Delta G_A + \Delta G_B \qquad 2\text{-}36$$

Where ΔG_w denotes the Lifshitz –van der Waals interaction component, ΔG_E, electrostatic double-layer component, ΔG_A, Lewis acid-base component, ΔG_B, Brownian motion component. Adhesion or deposition will take place when ΔG_T is negative.

The DLVO theory is the combined effect of Van der Waals and double layer force. The Van der Waals forces correspond to low strength interactions between molecules, atoms and crystals. The repulsion is due to the formation of an electrical double layer close to the surface when immersed in a liquid [86] Van der

Waals force comprises of different forces acting, this include dipole-dipole force, dipole–induced force and dispersion forces, the dispersion forces are always present.

The double layer force is associated with a surface in a liquid which may be charged by adsorption of charged molecules such as polyelectrolyte from the solution and is effected by the presences of the surrounding ions. This results in development of a wall surface potentials which will attract counter ions from the surrounding solution and repel surface charge balanced by opposite charged counter ions in the solution. In electric double layer, ions in the region closer to the wall surface are strongly bound to the surface [87].

A study by Malte [87] reported that increasing the distance of substrate surfaces, the ionic concentrations values of the solution changes. The layer of ions in rapid thermal motion is referred to as diffused electric double layer. Surface energy has been reported as one of the factors influencing the adherence of scale crystals to the surface of substrates [70, 88].

Surface energy is the energy required to build an area of a particular surface or the corresponding energy required by solid to attract or repel different substance. Surface energy is a key parameter in describing adhesion properties of any solid materials.

2.6.2 Measuring work of adhesion and surface energy

There are different methods of measuring work of adhesion, one of the method is by measuring the contact angle formed when a drop of liquid is applied to a solid surface [70]. Work of adhesion is the energy released in the process of wetting, it is a measure of the strength of the contact between two phases.

Recalling equation 2-29 and 2-30,Young established the relationship between surface free energies and contact angle [70] as stated.

$$\gamma_{sl} = \gamma_{cs} + \gamma_{cl}cos\theta \qquad 2\text{-}37$$

$$cos\theta = \frac{\gamma_{sl} - \gamma_{cs}}{\gamma_{cl}} \qquad 2\text{-}38$$

Where γ_{cl} denotes the interfacial energy between solid crystalline phase and liquid, γ_{sl} denotes the interfacial energy between the foreign solid surface and the liquid, γ_{cl} denotes the solid crystalline phase and foreign solid surface and θ denote the contact angle between the crystalline deposit and the foreign solid surface.

Dupre [70], define work of adhesion, using equation 2-39

$$W_a = \gamma_{sl}(1 + cos\theta) \qquad 2\text{-}39$$

Where γ_{sl} and θ are determined experimentally.

2.7 Factors affecting scale formation

Various operating factors can influence the formation of scale. It is well known that pH, temperature, operating pressure, flow velocity, degree of supersaturation and presence of other salts or interference ions in solution can influence scale formation [89].

2.7.1 Effect of pH

The pH of a solution determines the degree of alkalinity or acidity of the solution. pH is one of the major factors which influence the scale formation process. The pH of scale solution influences the saturation and precipitation. As the pH of a solution increases, the conversion of bicarbonate to carbonate also increases, hence the tendency for calcium carbonate formation.

Gomez [90], studied the influence of the initial pH and supersaturation on the induction times by carrying out a series of experiments at 25^{o}C, in 2.2dm^{3} capacity batch reactor, he observed that the pH decreases along the process. The crystallization produces a progressive local accumulation of protons near the crystal surface, which also reflected in the decrease of the pH in the bulk solution.

Andritsos and Karabelas [91], reported the effect of pH on calcium carbonate scale formation. The study showed that increasing the pH of solution leads to rapid deposition of calcium carbonate scale from 2mgcm^{-2} to 12mgcm^{-2}, after 2hours tests of experiment. And also between the pH of 8 and 8.8, there was no

spontaneous precipitation of calcium carbonate scale observed for up to 2hours of the run.

Prassad [53] study the dependency of solubility on pH. The study showed that, pH affects the formation of calcium carbonate by controlling the level of CO_3^{2-} present in the solution since both the carbonate and bicarbonate ionic pair of weak acid. The pH also have effect on the equilibrium of hydronium ion (H_3O^+). The effect of solubility dependency on pH is shown in Figure 2-17.

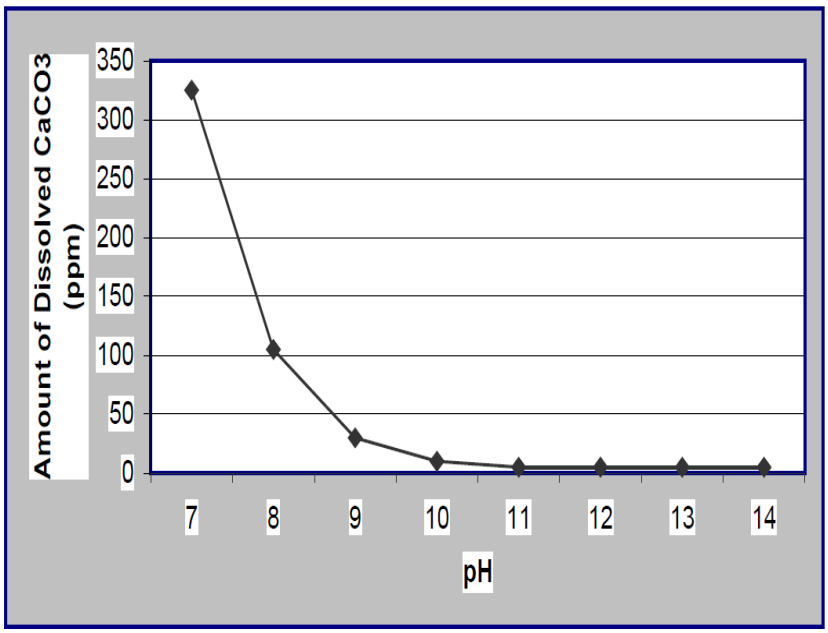

Figure 2-17: Solubility of calcium carbonate in pure water as a function of pH [53]

2.7.2 Effect of temperature

Temperature is one of the crystallization parameters that affects the degree of precipitation and supersaturation of inorganic scales [27, 89]. The kinetics of calcium carbonate scale increases with increasing temperatures and increases rapidly at a temperature above 60°C [92].

According to Troup et al [93], solubility of salts is a function of temperature and pressure, which means supersaturation can occur as a result of change in temperature and also the solubility of inorganic salts is either partially constant or increases with increased temperature. Nevertheless, for most alkaline scales, their solubility decreases with increase in temperature.

Todd et al [47], studied the effect of temperature on barium sulfate and strontium sulfate scale. In the study, they observed that the morphology of barium and strontium sulfate crystals changes by increasing the precipitation temperature from 20^{o}C to 70^{o}C. In the study, they concluded that crystals that precipitate at high temperature are less defect.

Temperature influences the crystallization behaviour of polymorphs. A study by Mitsutaka [94] showed that at a high temperature of 50^{o}C, the nucleation of aragonite, calcite and vaterite crystals was observed, but at lower of 25^{o}C fine particles of calcite and vaterite crystals were observed without the presence of aragonite crystals.

Young et al [95], show the effect of temperature on the morphology of calcium carbonate crystals. In the study, they observed that at 25^{o}C, spherical particles composed of vaterite and calcite crystals were present, whereas at a temperature of 60^{o}C, a needle-like particles composed of aragonite crystals were observed. They attributed the changes in the morphology of calcium carbonate scale to thermal vibration and effect of temperature on solubility of $CaCO_3$ scale. It was also observed by Feng et al [96], that temperature has an impact on the particle size of $CaCO_3$ scale deposition by influencing the pH of the solution. At a lower pH of the solution, large sizes of $CaCO_3$ were observed.

Muryanto et al [97], reported that there is a reduction in the amount of calcium carbonate scale deposited at lower temperature with high malic acid concentration. At higher temperature, the activation energy of the scaling ions or molecules increases, resulting in a faster reaction rate. This invariably increasing the deposition rate of calcium carbonate scale and it was also observed from their study that the morphology of calcium carbonate scale changes with increasing temperature.

Dyer et al [98], studied the effect of temperature and pressure on oilfield scale formation. The study report that, as the temperature increase, the scaling tendency of the carbonate scaling brine increased. The scaling tendency of sulphate scaling system decrease with increased temperature. Which they concluded that the effect of temperature on scaling tendency is more significant

than that of the pressure. Figure 2-18 shows the effect of temperature on the solubility of inorganic scales.

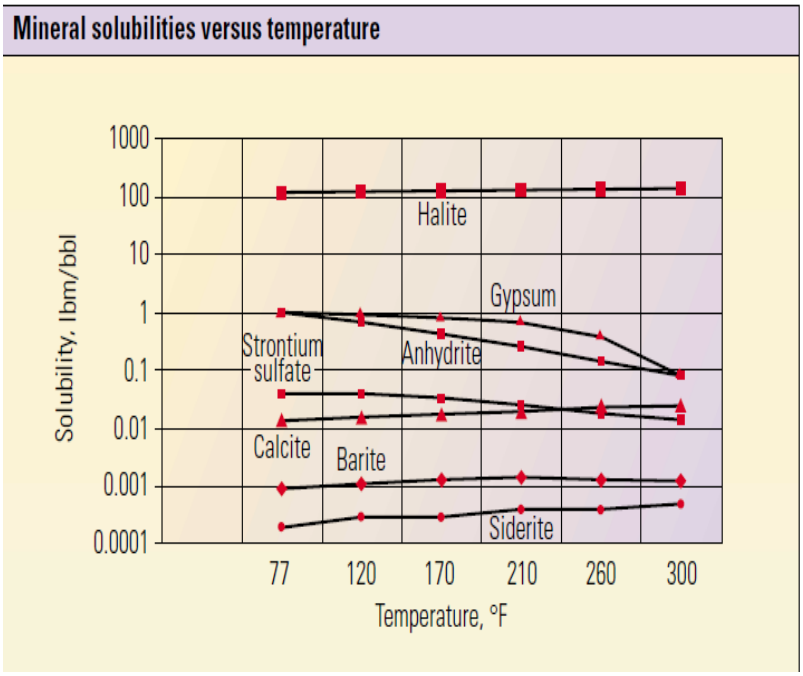

Figure 2-18: The effect of temperature on the solubility of inorganic scales [67]

2.7.3 Effects of operating pressure

Scaling usually occur when there is decrease in pressure of the formation water. Calcium carbonates precipitate from the produced water as the release of CO_2 causes an increase in pH and the degree of supersaturation of the carbonate solution [99].

According to Amer et al [100], at different operating pressure, clear water in the reservoir, mix with the reservoir brine which might result to scale precipitation. A decrease in pressure of the brine solution, leads to a lower solubility of the salt.

Pressure also affect the rate of permeability of scale. Increase in pressure, decreases the rate of permeability of scales. The reaction rate of the ionic species increases with increasing pressure. Figure 2-19 shows the predicted barium sulphate supersaturation as a function of pressure and temperature.

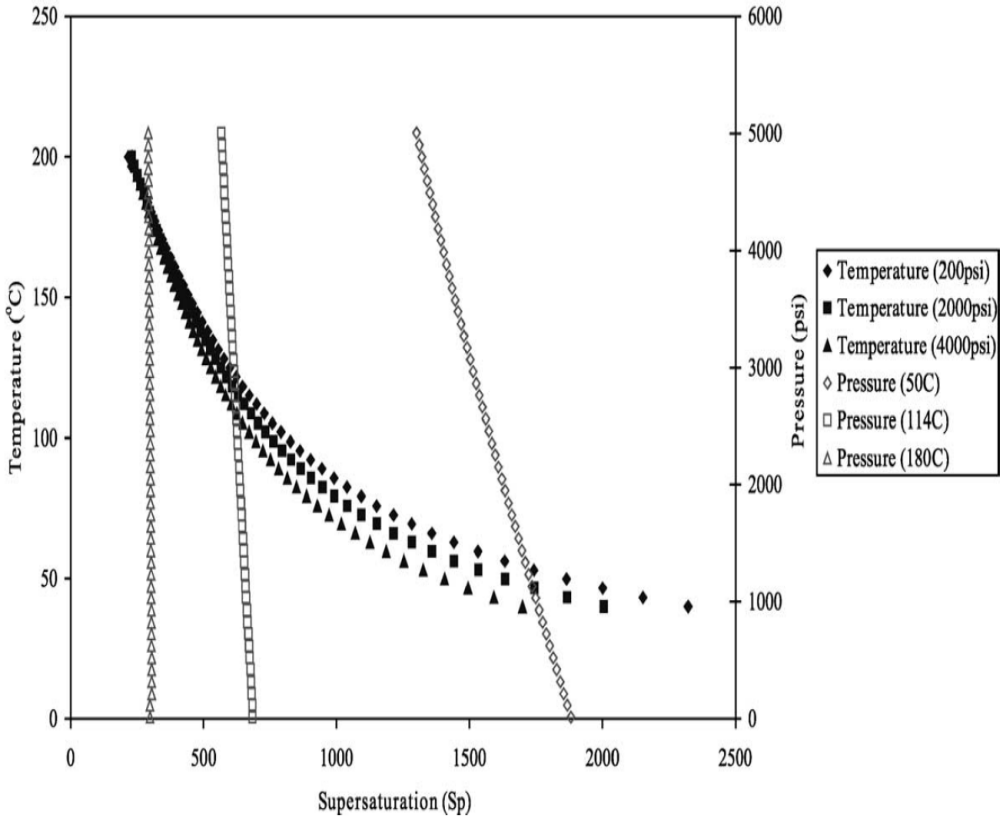

Figure 2-19: Predicted barium sulphate supersaturation as a function of pressure and temperature [100]

2.7.4 Effects of solution supersaturation

Supersaturation is one of the driving forces for crystallization [101, 102]. The degree of supersaturation determine the scaling tendency of oilfield brine. Scale formation occur when the solution brine attain the supersaturation level. Supersaturation also influences the crystal growth and agglomeration of scales, which affects the crystal size, amount of precipitate, particle morphology and polymorphism. Some of the effect of supersaturation on scale precipitation and deposition from literature is presented below.

A study by Mitsutaka [94] reported that the morphology of $CaCO_3$ is influenced by the concentration of the reactant solutions. And also in the study, they observed that the crystal size of $CaCO_3$ decreases with concentration. They attributed the change in crystal size to high nucleation rate resulting from high supersaturation. At high supersaturation, a metastable vaterite tends to crystallize and a stable calcite precipitate at low supersaturation. The amount of vaterite formed increases with solution concentration.

Moghadasi et al [103], observed in their study that increasing the supersaturation ratio of both barium and strontium sulphate scales produced an increased in the amount of scale formed and the morphology of the crystals changes with supersaturation.

Alsaiari et al [104] studied the interaction between ferrous iron and calcium iron in supersaturated solution of calcium carbonate scale in continuous stirred tank reactor. It was observed from their study that calcium ions greatly influence the solubility of iron carbonate, whereas the effect of ferrous iron in the solubility of calcium carbonate in the solution was not significant, this was attributed to the increased stability of complex ferrous iron formed in the presences of calcium. Different regions of variation of iron behaviour was distinguish as shown in Figure 2-20, R-1 represent the transition of solution from stable state to a metastable state, at this region no precipitation was observed, Region R-2 indicate the precipitation of iron with no precipitation of calcium, due to low solubility of iron. R-3 indicate the region where the precipitation was completely stopped, while R-4 show the region where both siderite and calcite precipitate spontaneously resulting from high supersaturation of both iron carbonate and calcium carbonate.

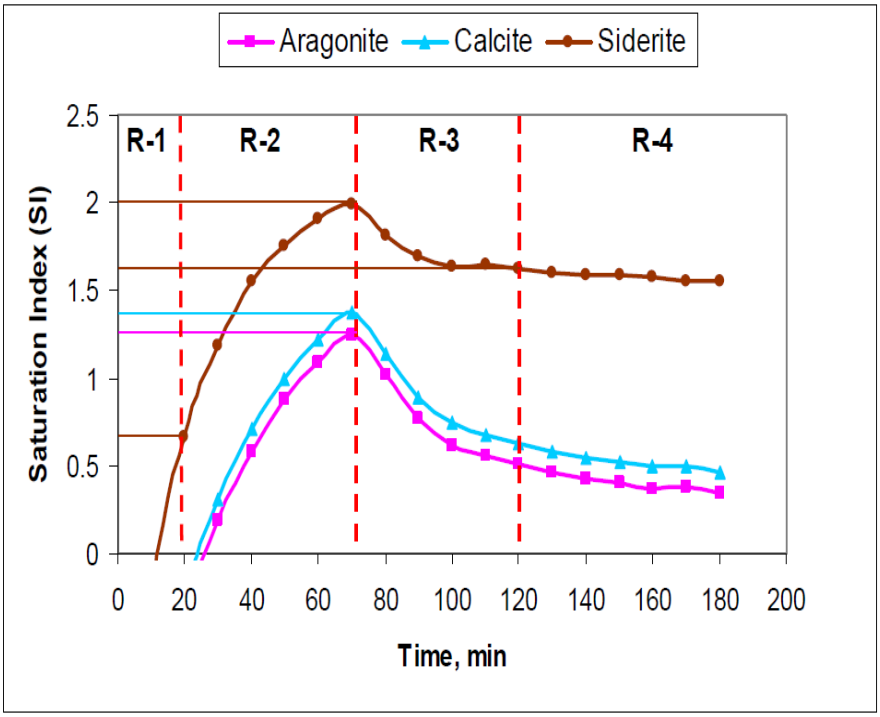

Figure 2-20: Change in saturation index (SI) with time [104]

2.7.5 Effect of flow velocity and hydrodynamic conditions

Studies [46, 101, 105] have shown that flow velocity, Reynolds number, shear stress, turbulence etc. affect the morphology of inorganic scale in a flow system. It is also reported that morphology of calcium carbonate polymorphs changes with residence time [106].

The work of Sutherland et al [46] shows that turbulence increases the likelihood of scale formation and also has an impact on the efficiency of scale Inhibitors. Zhang et al [1], observed that calcium carbonate scaling rate increase sharply with increased flow velocity, which become relatively stable when the velocity is above 0.5m/s, but above 0.7m/s, the calcium carbonate scaling rate drops, which may be due to shear forces resulting from high flow velocity.

According to Moghadasi et al [103], under dynamic flow conditions, the structure of the crystals formed are similar to that formed under static conditions, but the crystal faces change at high shear stress.

Hasson et al [80] studied the influence of hydrodynamics on the degree of $CaCO_3$ formation, comparing two flow systems. One consists of a supersaturated solution flowing as a falling film system and the other consist of a supersaturated solution in full pipe flow. The deposition and inhibition mechanism were different in both flow system, the inhibition of the film falling system was more effective compared to that the full pipe flow system; however the deposition rate was greater in the film falling system. The reason given was that, the supersaturation level for the full pipe flow system was constant, but high supersaturation level was observed in a significant portion of the falling film system which could create a spontaneous nucleation in the system forming colloids particles, these particles diffuse to the wall of the tube.

A study by Chen et al [107] showed that under hydrodynamic conditions, calcium carbonate polymorphs which was unstable at the initial stage of crystallization disappear and aragonite crystals were mainly present in the bulk solution. Muryanto et al [97] reported that the mass of $CaCO_3$ deposited increases with increased flow rate for both blank test and addition of malic acid under laminar flow conditions. They attributed this increase in mass of $CaCO_3$ to the rate of

reaction of the scaling ions in the bulk solution. High flow rate, increases the rate of precipitation and deposition of $CaCO_3$.

2.7.6 Effect of solution chemistry

The formation of carbonate and sulphate scale depends mainly on the solution composition and environmental factors. Solution chemistry has major influence on inorganic scale formation [108-110]. The composition of the ionic species in solution determines the degree of supersaturation. As the rate of scaling ions increases, the solution becomes more supersaturated depending on the environmental conditions such as temperature and pressure [26].

Maria et al [111] determined the rate of precipitation of barium and strontium sulphate from a supersaturated solutions, by considering three deep water operations fields with different scaling tendencies. The study shows that the rate of precipitation decreased at lower temperature and depended on the water chemistry of the field, in line with equation 2-40.

$$J \propto T^3 SR^2 \qquad 2\text{-}40$$

2.7.7 Effect of impurities

The presence of foreign minerals or ions have strong influence on inorganic scale formation [67, 112, 113]. The work by Karabelas [114] examined the effect of foreign particles scale formation. A small amount of particles affect the morphology of calcium carbonate, but it was concluded that colloidal particles such as SiO_2 has no influence on calcium carbonate formation.

Frota et al [26] stated that low concentration of metallic ions may affect nucleation and the crystal growth of calcium carbonate. Graham et al [8], investigated the impact of ferrous ions on the performance of scale inhibitors under calcium carbonate scaling using dynamic tube blocking rig. From its result, the presence of ferrous ion in the solution affect the performance of scale inhibitor by increasing the minimum inhibitor concentration (MIC). Which was more obvious in barium sulphate scale. The reason given as a result of this observation was that addition of small amount of dissolved ferrous ion changes the composition of the brine and the morphology of the scale crystals, invariably affecting the performance of scale inhibitors.

Chen et al [115] studied the influence of Mg^{2+} on the kinetics and crystals of polymorphs of calcium carbonate scale formation on metal surface. The study show that, the presence of Mg^{2+} have a greater effect on precipitation of calcium carbonate. They also observed that Mg^{2+} was incorporated into the deposit crystals and the ratio of Mg^{2+} in the deposits formed was proportional to the ratio Mg/Ca in the scale solution. In the study, the presence of Mg^{2+} enhance the transformation of Vaterite to calcite which adsorbs onto the surface of vaterite and calcite. This resulted to increase in the surface roughness. They attributed the changes in the morphology of $CaCO_3$ observed as a result of the poisoning of the growth sites of the crystals by Mg^{2+} which inhibit the growth rate of the deposit formed on the surface of the metal.

According to Nancollas et al [116], the presence of low amount of Mg^{2+} inhibit calcite growth with the formation of magnesium calcite. Increasing the concentration of Mg^{2+} leads to a rapid precipitation of aragonite, which affect the efficiency of scale inhibitors. Figure 2-21 shows the effect of Mg^{2+} in bulk solution on induction time of calcium carbonate scale.

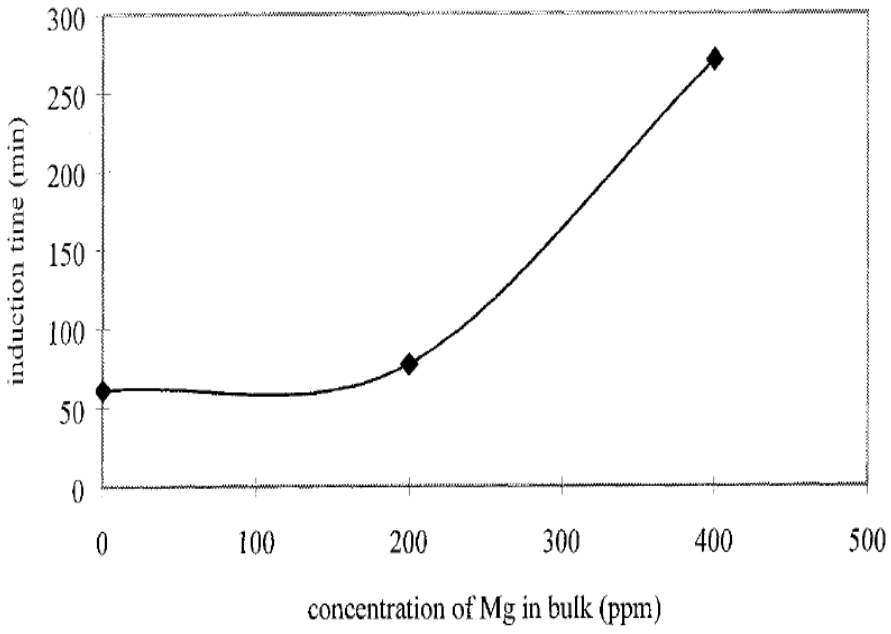

Figure 2-21: Effect of Mg^{2+} on the induction time of precipitates formed in the bulk solution[115]

2.7.8 Effect of surface roughness

The nature of deposited surface influence the formation of inorganic scales [19, 115, 117]. Most natural surfaces have each unit area of the substrate with finite number of nucleation sites. Nucleation depends on the number of active free sites, surface properties of material, such as corrosiveness, ionic charges and absorptivity, affect the formation of scales. However, if these surfaces have a low roughness area, the minimal number of contact point may likely reduce the possibility of adhesion by reducing the bodies contacts [118].

Eroini et al [119] studied the effect of modified substrate surface on inorganic scale prevention, using different substrates. The study showed that, isotropic superfinished surface, which is the only hydrophilic substrate in all the surfaces tested has the highest ability to inhibit calcium carbonate scale formation. This was attributed to its ability to generate a non-directional roughness profile, making the topography of the surface uniform.

Gunn [120] examined the effect of surface roughness on the nucleation and growth of calcium sulphate formation using heated stainless steel material. The study observed that, increasing the surface roughness of steel, increase the rate of nucleation of calcium sulphate scale.

2.7.9 Summary of scale formation literatures review

The formation of calcium carbonate scale in oil and gas and desalination industries has been studied extensively by various authors, using different techniques. These studies have investigates different environmental factors affecting the formation of calcium carbonate scale, such as temperature, pressure, pH, solution supersaturation, flow velocity, solution chemistry, presence of impurities and surface roughness. The influence of these factors on scale kinetics and induction time are not fully understood.

They have been challenges of reconciling the effects of these factors on bulk precipitation to surface deposition processes as majority of these studies focuses on effect of these factors on bulk precipitation processes. It has also been investigated that the kinetics of bulk precipitation process is different from that of surface deposition process [61, 119].

There are other challenges arising from the techniques being used in these studies as they do not reflect the field scenarios in terms experimental conditions and pipe geometry.

The effect of main driving force on scale formation, such as temperature, flow velocity and solution supersaturation on both bulk precipitation and surface deposition has not be study extensively.

2.8 Scale deposition kinetics studies and predictive models

Generally, the deposition of both organic and inorganic scales causes a lot of flow assurance problems in crude oil production. This section of this work focuses on the previous studies of scale deposition and predictive models from various authors.

2.8.1 Inorganic scale surface deposition kinetics studies and their predictive models

Scale prevention is important in oil and gas and desalination industries to ensure optimum production. Several models have been developed over the past years; these models concentrate mainly on the bulk scaling, little attempt has been made in reconciling the bulk precipitation data with surface deposition data.

The effect of hydrodynamic parameters such as shear stress, Reynolds number, flow velocity etc. on inorganic scales surface deposition kinetics has not be incorporated in the previous models. Here are the summary of some previous models.

Shipley et al [121] developed a semi empirical model to determine the effect of hydrate inhibitors on oilfield scale formation and inhibition from experimental solubility measurements of barite, calcite, halite and gypsum. The study, recommended the procedures to determine the effect of hydrate inhibition on mineral scale solubility at different experimental conditions such as temperature, ionic strength etc. Firstly determine the thermodynamic constant from equation 2-41.

$$pK_{BaSO_4} = -136035 + \frac{768041}{T(K)} + 48595 \times \log_{10}(T(K)) - (0.394 - 1.11910^{-4}T(℃) \times \frac{P(atm)}{500} \quad 2\text{-}41$$

The amount of barite (ppt_{Barite}) in mol/kg that will precipitate from a solution of unknown composition in hydrate inhibitor/water/ salt solution was determined from equation 2-42

$$ppt_{Barite} = \frac{[Ba^{2+}]_0 + [{SO_4}^{2-}]_0 - x}{2} \quad 2\text{-}42$$

$$x = \sqrt{([Ba^{2+}]_0 + [{SO_4}^{2-}]_0)^2 - 4([Ba^{2+}]_0 \left[{SO_4}^{2-}]_0 - \frac{{K^{Barite}}_{sp}}{\gamma_{Ba^{2+}}.\gamma_{SO_4{}^{2-}}.\gamma_{BaSO_4}}\right)} \quad 2\text{-}43$$

Where x denotes the mole fraction, $\gamma_{Ba^{2+}}$, $\gamma_{{SO_4}^{2-}}$, are the activity coefficients.

Hasson and Cornel [105] studied the kinetics of $CaCO_3$ precipitation in a continuous stirred tank vessel in the presence of sodium hexametaphosphate (SHMP) as shown in Figure 2-22. The study showed that the rate of SHMP adsorption on the precipitation of calcium carbonate crystals was inversely proportional to the square root of residence time. The following adsorption and residual supersaturation model was developed, as shown in equation 2-44 and 2-45 respectively.

$$r_{CALG} = \frac{P_o - P}{\tau} = Ap^n . \sqrt{\frac{9D_{EFF}}{\pi R^2 . \tau}} = const . \frac{P^n}{\tau^{0.5}} \quad 2\text{-}44$$

Where D_{EFF} denote the effective diffusivity (m^2/min), r_{CALG} SHMP adsorption rate (L/mol min), P_o and P initial and final concentration of SHMP (mol/l) τ is the residence time (min)

Residual supersaturation is given by equation 2-45,

$$[Ca^{2+}].[{CO_3}^{2-}] = 1.66\ x\ 10^4\ (P^{0.67}.\sqrt{\tau})^{0.65}\ (ppm\ as\ CaCO_3)^2 \quad 2\text{-}45$$

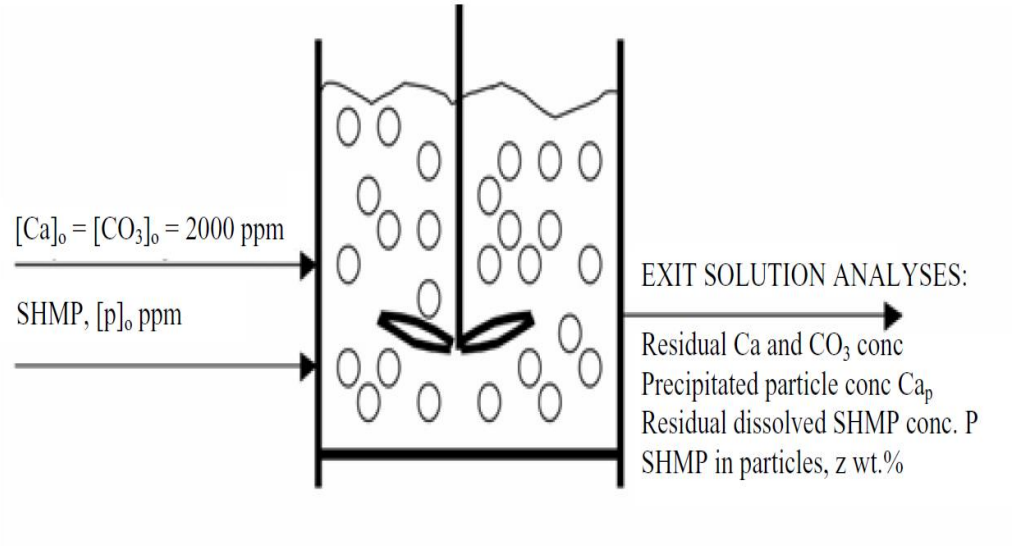

Figure 2-22: Schematic diagram of the continuous flow precipitation vessel [105]

Dyer et al [98], studied the effect of temperature and pressure on oilfield scale formation. The prediction model showed that an increase in temperature, increased the scaling tendency for carbonate scaling brine. However, an increase in temperature decreased the scaling tendency of sulphate scaling brine. It was concluded that pressure had little effect on both carbonate and sulphate scaling brines.

Alireza et al [122], developed a predictive model to evaluate $CaCO_3$ scale formation as a function of temperature, ionic strength, pH, calcium ion concentration, bicarbonate ion concentration and CO_2 mole fraction in a condition of CO_2 saturated water. The model work by determining the ionic strength from a correlation factors, followed by other experimental conditions based on equations 2-46 to 2-50.

$$In(K) = a + bI + cI^2 + dI^3 \qquad 2\text{-}46$$

Where $$a = A_1 + \frac{B_1}{T} + \frac{C_1}{T^2} + \frac{D_1}{T^3} \qquad 2\text{-}47$$

$$b = A_2 + \frac{B_2}{T} + \frac{C_2}{T^2} + \frac{D_2}{T^3} \qquad 2\text{-}48$$

$$c = A_3 + \frac{B_3}{T} + \frac{C_3}{T^2} + \frac{D_3}{T^3} \quad \text{2-49}$$

$$d = A_4 + \frac{B_4}{T} + \frac{C_4}{T^2} + \frac{D_4}{T^3} \quad \text{2-50}$$

Where A_1 to D_4 denotes tuned coefficient factors as a function of temperature and I is the ionic strength.

The R^I factor is determined from the solubility factor and mole fraction of CO_2,

$$R^I = \frac{C_{HCO3^-} \times 0.82}{x_{CO2} \times S_f} \quad \text{2-51}$$

$$pH = (0.4341)In(R^I) + 6.2964 \quad \text{2-52}$$

Abbe and Ajienka [123], predicted the scaling tendency of calcium carbonate from an oilfield brine, using a software program Scale-check. Their prediction was based on Stiff-Davis predictive model, which is established on the principle of saturation and pH of unsaturated water and the pH when saturated with calcium carbonate. The programme was able to predict scaling tendency of calcium carbonate to some extent, which could help in developing a preventive measure for calcium carbonate scaling under the environmental conditions investigated.

Langelier [124] compared the actual pH with the pHs when saturated with $CaCO_3$ as stated in equation 2-53.

$$LSI = pH - pHs \quad \text{2-53}$$

Where LSI is the Langelier's saturation index. The model is applied to non-oilfield brine. If the LSI is positive, the water has scale forming tendency and is likely to be relatively non-corrosive, but if LSI is negative, the water has no scaling tendency and likely to be corrosive. However, this model only considered the thermodynamic driving force of scale formation, whereas the amount of calcium carbonate scale that will precipitate at equilibrium was not considered.

Stiff and Davis [125, 126], developed a scale predictive model to improve on the limitation of Langelier saturation index as a function of the total dissolved solids (TDS). The model considered the pH of unsaturated and saturated water

containing calcium carbonate scale. This index is applied to oilfield brines, where the total dissolved solid (TDS) is greater than 5000 ppm, and the pH, is calculated from equation 2-54

$$pHs = P_{Ca^+} + P_{AIk} + K \quad \text{2-54}$$

Where K takes into account the influence of the higher overall concentration of ions in the water, P_{AIK} = bicarbonate [M] alkalinity (mg/l).

$$SDI = pH - P_{Ca} - P_{AIk} - K \quad \text{2-55}$$

Where $$P_{Ca} = -\log[Ca^{2+}] \quad \text{2-56}$$

K denotes a constant, whose value depends on the temperature and salt concentration. SDI denotes Stiff-Davis index, pH of water sample P_{ca} is the, negative logarithm of calcium ion concentration. P_{AIK}, the negative logarithm of total alkalinity.

If the SDI is positive, it indicates that the water has a scaling tendency and is likely to be relatively non-corrosive. If the SDI is negative, indicates that the water has no scaling tendency and is likely to be corrosive. The limitation to this model is that beyond a temperature of 90^{o}C, the value of constant K cannot be determined as the total dissolve solid limit is exceeded.

Vetter [127], studied the effect of different environmental factors such as temperature, pressure and brine composition on the precipitation of $BaSO_4$ formation. In the study, the time delay between initial precipitation and actual precipitation of $BaSO_4$ is inversely proportional to the magnitude of supersaturation. The deposition of barium sulphate is a function of pressure drop. This was concluded that the hydrodynamics, long residence time and the inclusion of hydrodynamic factors in a predictive model enhanced the prediction of $BaSO_4$ formation in oilfield.

Carageorgos et al [128] developed a laboratory technique for the determination of model coefficient from pressure measurements for sulfate scaling in the reservoir cores, as shown in Figure 2-23 . The model coefficients are the reaction rate constant and the formation-damage parameter showing the rock porosity due to the deposit of barium sulfate. This coefficients depends on temperature, brine concentration and the pore space structure of the rock.

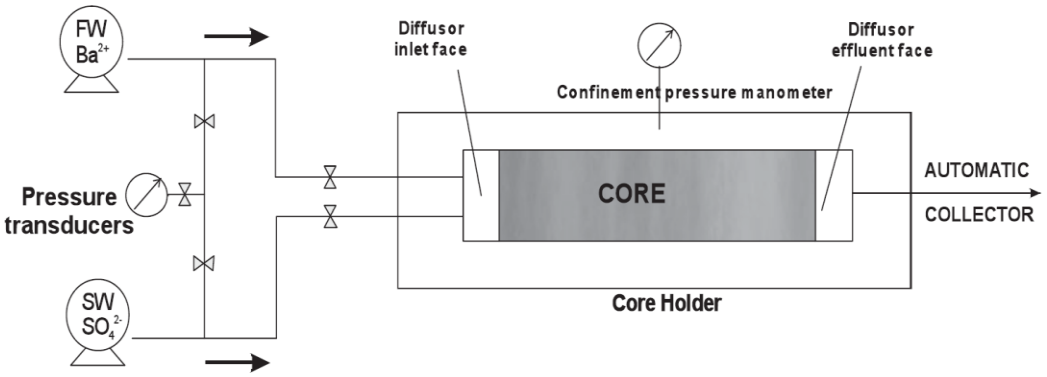

Figure 2-23. Experimental setup for commingled injection of incompatible waters [128]

From their study they proposed equation 2-57 and 2-58 to determine the [Ba^{2+}] and [$SO4^{2-}$] concentration profiles.

$$C_{Ba} = \frac{(1-\alpha)}{e^{-\varepsilon k(1-\alpha)x_D} - \alpha} \qquad 2\text{-}57$$

$$C_{SO_4} = \frac{(1-\alpha)}{1-\alpha e^{-\varepsilon k(1-\alpha)x_D}} \qquad 2\text{-}58$$

Where ε_k and α are the chemical kinetics and formation damage coefficients respectively.

Patrick et al [129], developed a prediction model for scaling conditions over life cycle of a gas well. The model results were able to determine the zones along a long wellbores which is more likely to have a scaling problems and the time duration for the scaling problem to occur, the model indicates an increase in supersaturation with reference to scaling ions as the fluids are produced.

Wright et al [130] predicted the scaling tendency of both sulfate and carbonate scaling of Glemis field. The model observed that the rate factors controlling the kinetics of calcium carbonated scale formation was determined and a preventive method was designed to prevent both sulfate and carbonate scaling in the field.

Mazzollni et al [131] used a computer model to predict the scaling tendency of $BaSO_4$. The model calculate the level of saturation of the aqueous phase for scaling minerals and the degree of precipitation to attain thermodynamic equilibrium.

Zhang et al [1] developed a kinetics and thermodynamic model using dynamic tube blocking rig for calcium carbonate scale prediction. The effect of temperature, pressure and flow velocity on calcium carbonate scale formation was determined. In the model, calcium carbonate deposition thickness rate was determine as a function of time. The effect of flow was significant in the estimated thickness rate at different experimental conditions. One of the limitation of this model, is that a long capillary tube were deployed as the scaling surface and effect of the uniformity of the scale layer was not considered.

Stamatakis et al [58] determined the induction time of calcium carbonate precipitation in porous rocks under flow conditions between temperature of 25^{o}C to 100^{o}C, using a radiotracer technique. The empirical model developed from the study, was based on classical nucleation theory which predicted the induction time of calcium carbonate scale under flow conditions as shown in equation 2-59.

$$logt_{ind}(\min) = \ 3.2 - \frac{3.0}{SI} - \frac{959.8}{T} + \frac{1849.9}{SI \ \times T} \qquad 2\text{-}59$$

Where t_{ind} denotes the induction time in (min), SI saturation index, T absolute temperature (K). From their study, it was reported that the equation can predict the induction time of calcium carbonate scale formation under a specific flow condition in the near well region and the induction time is proportional to the inverse of the saturation index and temperature.

Setta et al [108], studied the surface kinetics of calcium carbonate formation on austenitic stainless steel surface, using an in-situ flow rig and rotating cylinder electrode and developed an empirical model for calcium carbonate, within a wide range of supersaturation index. The model enables the prediction of the calcium carbonate thickness growth over a period of time. Figure 2-24 shows calcium carbonate scale deposition as a function of saturation index at 24^{o}C and 70^{o}C.

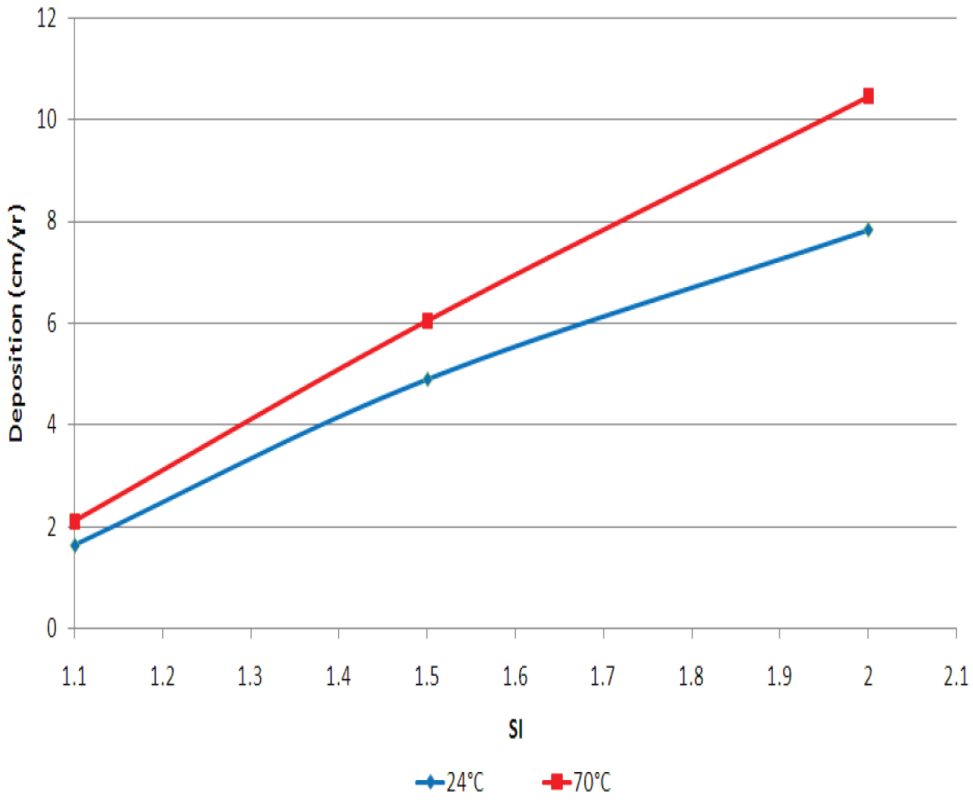

Figure 2-24: Calcium carbonate scale deposition in cm/year as a function of saturation index (SI) at 24°C and 70°C [108]

2.8.2 Asphaltene and wax deposition kinetics studies and their predictive models

The deposition of asphaltene and wax cause a lot of problem in crude oil production, extensive studies have been carried out in the past on wax and asphaltene deposition and different predictive models have been developed.

This models tends to prevent the deposition of asphaltene and wax in oilfield to some extent compared to that of inorganic scales such as $CaCO_3$. Here are some of the studies.

Kamran et al [132], used high-pressure deposition cell to measure the deposition of asphaltene from crude oil under real field conditions. The model developed from the study can predict the deposition of asphaltene in an oilfield under realistic field condition of temperature, pressure and shear stress.

Wang et al [133, 134] developed asphaltene deposition tool (ADEPT) that can predict the formation of asphaltene and determine the amount and profile of

asphaltene deposition in the oilfield. The tool is based on thermodynamic and deposition properties of asphaltene. The model was validated with data obtained from capillary deposition experiment data at different operating conditions for the same oil-precipitant mixture. The prediction of asphaltene deposition using the model was in agreement with results obtained experimentally from the study.

Lawal et al [22], studied the deposition of asphaltene in a glass capillary flow experimental set up. They monitored the deposition of asphaltene by capturing the image of the asphaltene deposition along the capillary tube and measuring the pressure drop across the capillary. They developed a predictive model that could determine the deposition thickness as a function of pressure drop along the capillary tube. The model was based on Hagen-poiseuille equation, as shown in following equation 2-60 to 2-63.

$$\frac{(\Delta P_t) r^4}{\mu_t} = \frac{(\Delta P_i) {r_i}^4}{\mu_i} \qquad 2\text{-}60$$

Where ΔP_i and ΔP_t denotes the initial pressure drop before deposition and at time t, the pressure drop along the capillary (Psi). μ_i and μ_t are the initial viscosity of the brine and average viscosity at time t respectively in (Ns/m^2), r_i and r are the original capillary tube radius and effective radius after deposition respectively in (m).

Simplifying equation 2-60 by neglecting the effect of viscosity since $\mu_i \approx \mu_t$

Equation 2-60 becomes

$$r_t = r_i \left(\frac{(\Delta P_i)}{(\Delta P_t)}\right)^{1/4} \qquad 2\text{-}61$$

The hydrodynamic thickness (e_t) is given by the equation 2-62,

$$r_t = r_i - e_t \qquad 2\text{-}62$$

From equation 2-62 and 2-63

$$e_t = r_i \left(1 - \left(\frac{\Delta P_i}{\Delta P_T}\right)^{1/4}\right) \qquad 2\text{-}63$$

Equation 2-63 is valid when $e_t \ll r_i$

Hsu and Brubaker [135], developed model to predict wax deposition from waxy crude production lines. The model can predict the deposition of wax along a cold flowlines and the potential wax problem. The model considered both the molecular diffusion and shear stress effect on wax deposition.

From the model, the wax deposition rate on pipe wall due to molecular diffusion is given by equation 2-64

$$\frac{dW}{dt} = \rho_w AD_m \frac{dC}{dr} = \rho_w A \left(\frac{k_m}{\mu}\right) \frac{dC}{dT} \frac{dT}{dr} \qquad 2\text{-}64$$

Where W denotes the total wax mass deposited on pipe wall, t denotes the time, k_m is constant, ρ_w denotes density of the deposited wax, μ is fluid viscosity, D_m is the molecular diffusion coefficient of the precipitated wax, A is the pipe wall area available for wax deposition, $A = \pi DL$, $\frac{dC}{dr}$ is the radial concentration gradient of the precipitated wax, $\frac{dC}{dT}$ is the concentration gradient of the precipitated wax with respect to temperature. $\frac{dT}{dr}$ is the radial temperature gradient.

Hsu and Santamaria [136] developed a laboratory test method to measure wax deposition of waxy live crudes under turbulent flow conditions. The equipment consist of high pressure turbulent flow loop, the system is made of two tube units (test tube and reference tube). The test tube is designed to monitor the wax deposition from the oil, while the reference tube is used for measurement of wax deposition thickness. From their studies, they determined the wax deposition thickness using the equation 2-65 and 2-66 for both laminar and turbulent flow respectively.

The internal diameter of test tube (ID) during wax deposition process is given by equation 2-65

$$D_T(inch) = \frac{0.402}{\left(\frac{\Delta P_T}{\Delta P_R}\right)^{\left(\frac{1}{3n+1}\right)}} \qquad 2\text{-}65$$

For turbulent flow,

$$D_T(inch) = \frac{0.402}{\left(\frac{\Delta P_T}{\Delta P_R}\right)^{\left(\frac{1}{4+0.75n}\right)}} \quad \text{2-66}$$

Where 0.402 is the internal diameter (ID) of the reference tube, ΔP_T and ΔP_R are the pressure drop across the test tube and reference tube during wax deposition, n is the material constant.

They also went further to determine the cumulative wax deposition rate (W_r) from equation 2-67

$$W_r = 381 \frac{{D_o}^2 - {D_T}^2}{D_T(t - t_o)} \quad \text{2-67}$$

Where, D_o is the bare tube ID (inch) of test tube, D_T is the effective tube ID (inch) of test tube, t is the time during wax deposition and t_o is the starting time.

Wang and Buckley [21], estimate thickness of deposit layer from displacement test. Where the amount of asphaltene deposits on the capillary tube is removed by nitrogen gas at high pressure. From their studies, the thickness of asphaltene deposits were determined from equation 2-68 and 2-69 for both evenly and non-evenly distributed deposits along a capillary tube.

For evenly distributed deposit along the tube,

$$q(t) = \frac{(P - P_c)\pi r^4}{8\mu l(t)} \quad \text{2-68}$$

The weight of deposit layer as a function of time,

$$W(t) = \pi r^2 \rho L \left\{1 - \left[1 - \frac{Pr^2}{4\mu L^2}\right]^2\right\} \quad \text{2-69}$$

where q(t) denotes the volume flow rate at the outlet end at time t, and l(t) denotes the length of the remaining liquid segment inside the tube at time t, Pr denotes the prandtl number, L length of the tube, ρ denotes the density of the liquid, the weight of deposit displaced is measured using a non-destructive technique (N_2 and glycerol probe), the value of q(t) and l(t) is calculated from W(t), using the relationship between liquid density and the effective radius r. The thickness of

deposit layer is obtained from the difference between r and the original radius of the tube r_o.

For unevenly distributed deposit layer, deposit thickness at different capillary locations was calculated from equation 2-70 and 2-71

$$r_n = \left[\frac{8\mu C_{1(\Delta V_n)^2}}{\pi^2 P \Delta t_n}\right]^{1/6} \quad \text{2-70}$$

$$r_i = \left[\frac{8\mu C_{1(\Delta V_i)^2}}{\pi^2 \Delta t_i} \left(P - \frac{8\mu C_1 \Delta V_i}{\pi^2 \Delta t_i} \sum_{j=i+1}^{n} \frac{\Delta V_j}{{r_j}^2}\right)^{-1}\right]^{1/6} \quad \text{2-71}$$

Where i = 1, 2… n-1, C_1 is coefficient, which is $1.45033\ x\ 10^{17}$, P is the capillary pressure, ΔV_i denotes the volume of liquid, Δt_i denotes the time.

2.8.3 Summary of scale surface deposition kinetics studies and predictive models

Organic and inorganic scale precipitation and deposition have been studied and different predictive models have been developed over many years on scale precipitation process such as residence time, induction time, nucleation and crystal growth. These models have been mainly based on thermodynamics parameters. However, little attention has be made on the effect of hydrodynamic parameters on inorganic scale surface deposition kinetics. The use of a methodology that will reflects the field scenario has been a challenge in most models.

Developing a model that can predict the scale thickness growth rate over a period of time and as a function of saturation ratio, temperature and flow velocity has been limited.

The models developed by Kurup et al [133] and Lawal et al [22] to determine the uniformity of surface layer across the capillary as a function of differential pressure and to determine the scale thickness growth will be investigated. Subsequently a detailed empirical model that can predict the thickness growth rate of both inorganic and organic scales in the field as a function of deposition flux will be developed.

A different technique of estimating the amount of deposit present in the capillary after the deposition test will be established. The results obtained will be compared with the asphaltene models.

2.9 Scale formation in a pipe flow system and fluid mechanics principles

The main cause of scaling in any system is the change in the environmental conditions such as temperature and pressure, which affect the degree of saturation of the system. Considering the scenario of $CaCO_3$ scale formation from a supersaturated solution under turbulent flow regime in pipe system, in this system, the gaseous phase is not in contact [80].

According to Hasson et al [105] at high supersaturation ratio, there is depletion in the bulk solution due to scale formation and the mean supersaturation ratio in the bulk is uniform along the pipe. And also there is a possibility of $CaCO_3$ precipitation occurring in the bulk and at the surface of the pipe wall.

The formation of scale is favoured by pipe wall surface, depending on the wettability and surface energy. Hasson proposes two rate determine steps in the pipe flow system, firstly, diffusion of all ionic species towards the scale- water interface and surface reaction of the ionic species [137] and $CaCO_3$ crystals as shown in Figure 2-25.

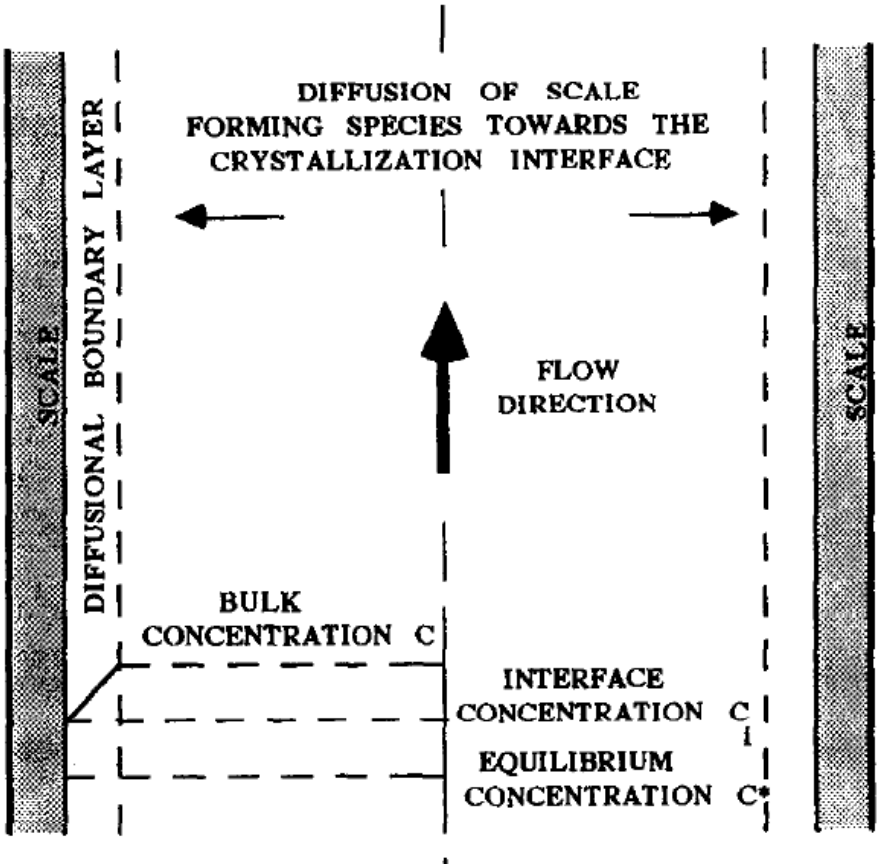

Figure 2-25:Scale formation process in a pipe flow system [80]

To effectively study the kinetics of scale deposition in a pipe flow system, there must be detail understanding of the principle of fluid mechanics in a pipe flow system. The nature of flow in fluid mechanics is generally grouped into two flow regimes, which are laminar and turbulent flow regime, but there is a region between this two flow boundaries called transitional flow. In this study, there will be more emphasis on the laminar flow regime as it affects the capillary flow rig.

2.9.1 Pressure loss in laminar flow

The pressure loss in laminar flow is given by equations 2-72 to 2-75 .

Driving force due to pressure = Pressure drop x Area

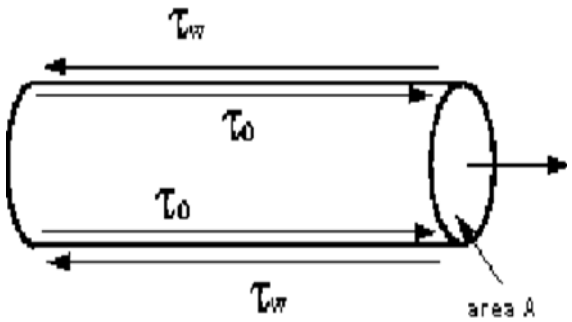

Figure 2-26: Pressure loss in laminar flow [138]

$$F = \frac{\Delta P \pi d^2}{4} \quad \text{2-72}$$

Retarding force due to stress by the wall = $\tau_w \pi d l$ 2-73

At equilibrium, driving force = retarding force,

$$\frac{\Delta P \pi d^2}{4} = \tau_w \pi d l \quad \text{2-74}$$

$$\Delta P = \frac{\tau_w 4 l}{d} \quad \text{2-75}$$

At equilibrium, the shearing forces on a cylinder = pressure force as shown in Figure 2-27**.**

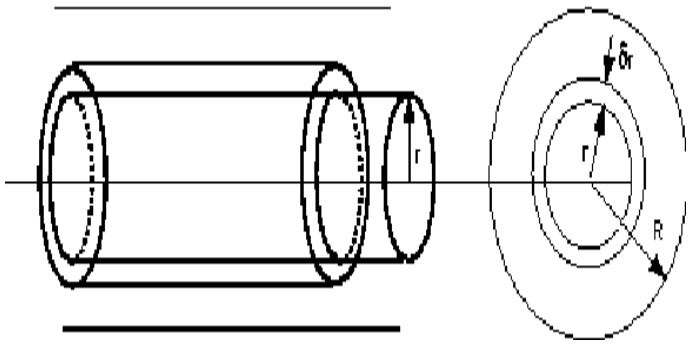

Figure 2-27: Shearing forces on a cylinder [138]

$$2\tau\pi r l = \Delta P \pi r^2 \quad \text{2-76}$$

$$\tau = \frac{\Delta P r}{2l} \quad \text{2-77}$$

Where τ_w denotes the wall shear stress, l denotes the length of the pipe, d denotes the diameter of the pipe, r denotes the radius of the pipe, ΔP denotes the pressure loss.

2.9.2 Hagen-Poiseuille's law

The flow along a pipe is driven by a pressure difference, the viscosity acts to retard the passage of the fluid along the pipe through the no-slip condition at the wall. The flow rate is given by equation 2-78.

$$Q = \frac{\pi D^4 \Delta P}{128 \mu l} \qquad 2\text{-}78$$

From equation 2-78 above, the flow rate,

- Increases when D is increased
- Increases when ΔP is increased
- Decreases when μ is increased
- Decreased when l is increased

However, the limitations of Hagen-poiseuille flow equation with respect to capillary flow rig in determining the amount of deposit on the surface of substrate are highlighted in chapter 3 of this work.

2.9.3 Dynamic tube blocking rig

The dynamic tube blocking rig (DTB) is one of the most efficient techniques to study inorganic scale deposition kinetics as it operates at field condition of temperature and pressure.

Various studies [10, 139-141], used the dynamic tube blocking rig for scale inhibitors efficiency ranking under different environmental conditions by examining the scale inhibitors ability to prevent scale adherence and growth within a tubing coil. The dynamic tube blocking rig (DTB) examines the growth of $CaCO_3$ and blockage of micro bore metal cell by measuring the differential pressure as a

function of time across the sample cell, which result from scale build up in the material. DTB takes into account the adherence of the scale to pipe work to a certain extent, the rig operates under laminar flow condition.

The schematic diagram of a conventional DTB is shown in Figure 2-28.

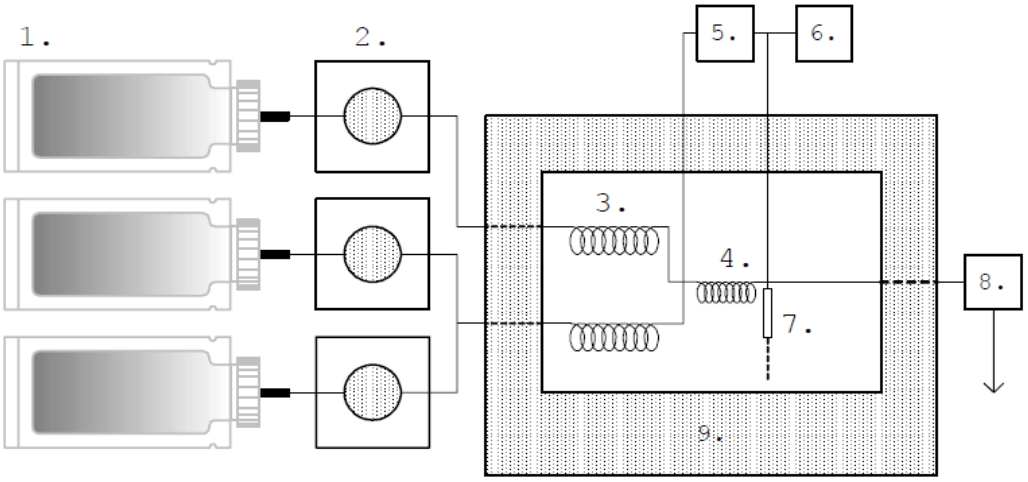

1. Collapsible bottles
2. Pumps + switching valves
3. Pre-heating coils
4. Capillary scaling coil
5. Diff. P transducer
6. Abs. P transducer
7. Thermocouple
8. Back-pressure regulator
9. Oven

Figure 2-28: A simplified diagram of anaerobic dynamic tube-blocking rig [142]

Here are some studies, using the conventional dynamic tube blocking rig.

Xuan et al [143] , studied the effect of scale inhibitors on the induction time, nucleation and growth stages of scale formation. They combined both polymer based inhibitors and phosphoric based scale inhibitor and compared the results obtained from dynamic tube blocking test and static jar test to the results they obtained from ultrasonic technique. The ultrasonic technique gave better understanding of scale inhibitor mechanism. The study observed that, the combined scale inhibitor showed better performance in the static jar test than the dynamic test. The scale inhibitors showed great performance at certain inhibitor concentration. The minimum inhibitor concentration of each of the inhibitors were determined at different dosage. Some of the data generated from their studies is shown in Figure 2-29.

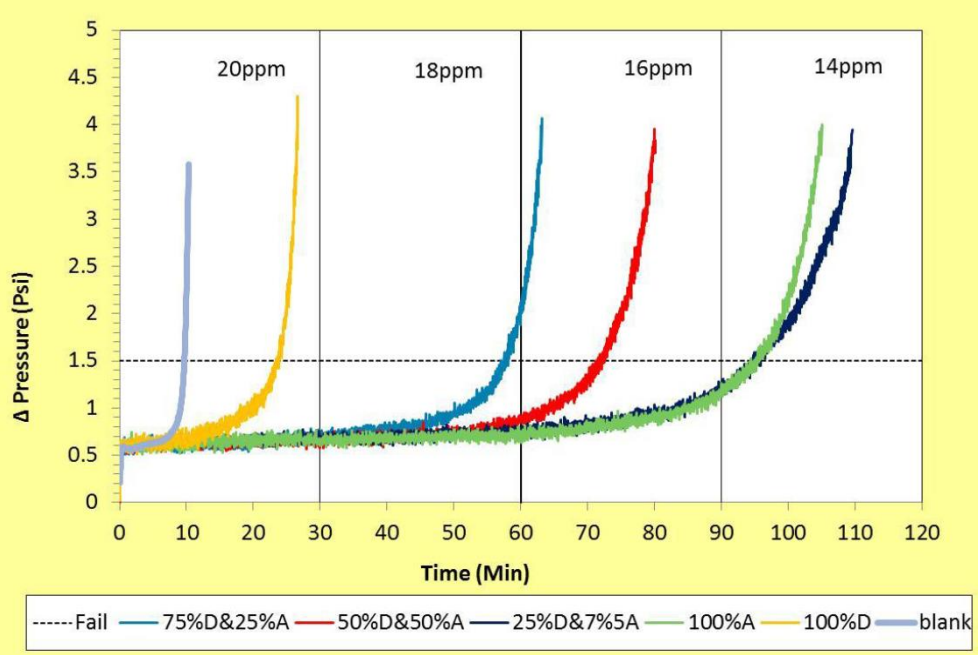

Figure 2-29 : Dynamic loop test with FW:SW 50:50 at 70ºC [143]

Graham et a l[144], studied the impact of ferrous ions on scale inhibitors performance using the dynamic tube blocking. They reported that, the presences of ferrous ions affect the minimum inhibitor concentration of scale inhibitors when tested with $CaCO_3$ scale, which have more impact when tested with $BaSO_4$ scale.

Graham and McMahon [145], studied the effect of scale inhibitor performance against bulk and surface scale nucleation and growth by the addition of film forming corrosion inhibitors. They reported that the presence of film forming corrosion inhibitors has the ability to reduce scale adhesion and tube blockage, but has no impact on degree of scale precipitation in the bulk.

Dong et al [112], investigated the performance of scale inhibitor in water containing high levels of dissolved iron by comparing the results obtained from the DTB and static jar test. It was reported that modified phosphate inhibitors (RSI-1 and RSI-2) show great performance compared to the conventional scale inhibitors (PPCA, DTPMP) at different inhibitor dosage as shown in Figure 2-30.

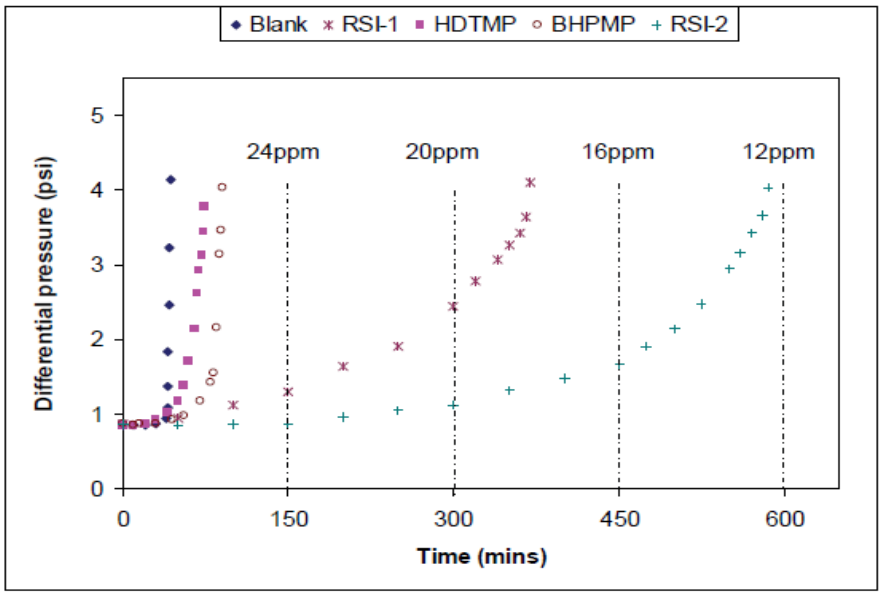

Figure 2-30: The performance of selected inhibitors in dynamic tube blocking tests in the presence of 100ppm Fe^{2+} [112]

Graham and Williams [140], design a HT/HP stirred reactor test rig to conduct calcium carbonate scale deposition kinetics, in order to overcome the limitation of the DTB. From their design, the HT/HP stirred reactor rig can be used to study calcium carbonate scale kinetics at high temperature and pressure over long residence time, similar to the field conditions. Some of the data obtained from their study is shown in Figure 2-31.

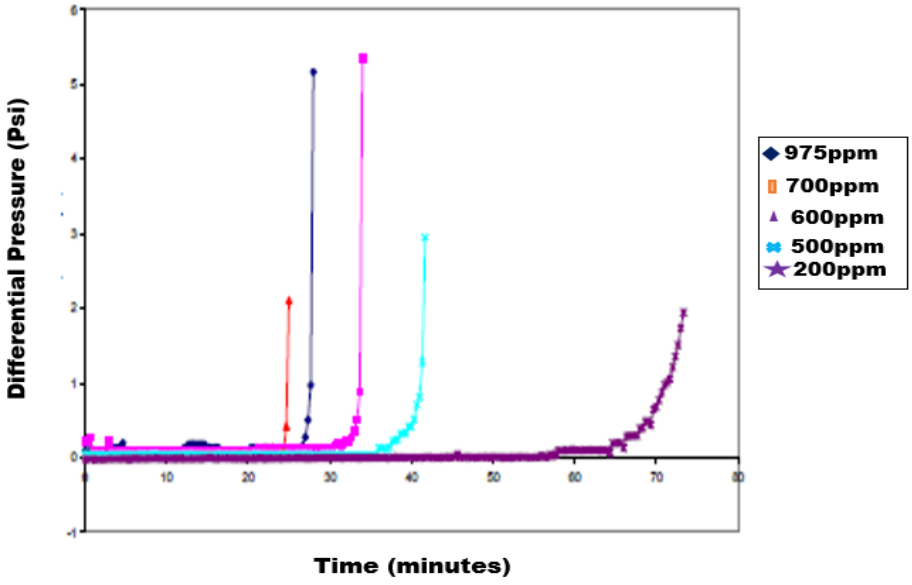

Figure 2-31: The effect of bicarbonate concentration on blank scaling time [140]

Bazin et al [10], compared the effectiveness of using DTB for minimum inhibitor concentration determination at different flow rates and capillary geometry. It was reported that, DTB technique is influenced by change in flow rates and capillary geometry. The data obtained from their study at different inhibitor concentration and flow rates is shown in Figure 2-32.

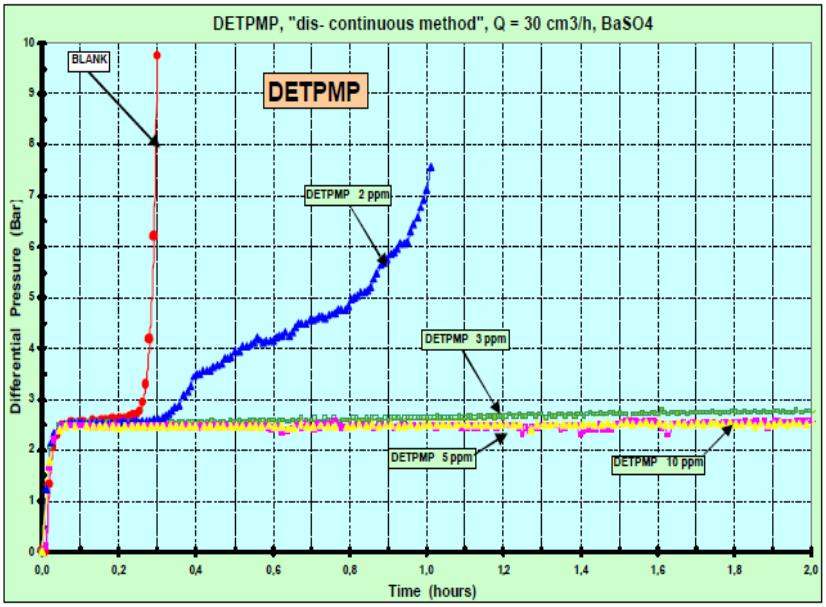

Figure 2-32: DETPMP performance on $BaSO_4$, inhibitor injected step by step (L=7.5m;ID=0.5mm;Q=30cm^3/h;T=90°C) [10]

However, none of this studies design a sample cell capillary tube, which shows a replicate of pipe flow lines experience in the oilfield, instead they used a micro-bore tubing coil for their studies. Using the conversional dynamic tube blocking rig to study the deposition of scales and to develop an empirical model that can predict scale formation maybe challenging. This is because the technique is mainly designed for ranking and showing the effectiveness of scale inhibitors. The technique also used a long capillary tube between 1-2m, which make it difficult to determine the amount of deposit present in the capillary tube. This difficulty is due to unevenly distribution of the deposited scales and saturation ratio changes with time along the capillary.

Therefore it is worthwhile to design a technique with short capillary, which is more reliable in determining the actual deposit present in the capillary and the saturation ratio of the flowing brine. With the short capillary, it can be assumed that the saturation ratio is constant due to the short resident time.

The sample cell capillary made of stainless steel, is used to study calcium carbonate scale surface deposition kinetics under dynamic flow conditions. This will reflect the field operational conditions.

Chapter 3 of this report will give details of this rig design and various experimental parameters that can be determined from this rig.

CHAPTER 3. Capillary rig development and commissioning

3.1 Introduction

This chapter provides the detailed design of already commissioned capillary rig for the surface deposition tests. The capillary flow rig was modified to accommodate changes needed for this study and also for optimum performance of the scaling time determination. The design changes made for the capillary flow rig are:

- Change of scaling surface from capillary coil of 1-2m to a capillary cell of 10mm length.
- Change of pipe geometry from 3mm to 1mm (mixing capillary), to have a fully developed flow from the mixing point to the capillary cell.
- High resolution pressure transducer installed on the capillary flow rig for differential pressure measurement. This enable a low pressure drop variation to be detected by the pressure transducer.
- Design of bulk and surface analysis sections of the capillary flow rig.
- Design of the surface analysis test coupon.

The capillary flow rig descriptions is split into three sections with respect to the experimental test conducted. These are:

- The capillary flow rig description for surface deposition test.
- Capillary flow rig description of bulk precipitation test (turbidity measurement and inductively coupled plasma test)
- Capillary flow description for scanning electron microscope (SEM) and X-ray diffraction (XRD) test.

3.2 Capillary flow rig description for surface deposition test

Dynamic tube-blocking rigs are widely used for the study of scaling phenomena and in particular for the ranking of scale inhibitors [98, 143, 146, 147]. A typical experiment involves measurements of the differential pressure across a small diameter bore tubing of approximately 1-2m length [10, 98, 142, 148]. If the experiment is properly designed, the time for the pressure across the cell to increase gives a measure of the scaling time, which is the time for the differential pressure to deviate from 0Psi, such technique is often used to assess the efficiency of scale inhibitors before being deployed in the production lines.

The drawback of this techniques is that the saturation ratio will drop across the capillary cell and it is therefore difficult to use the methodology to develop a robust kinetic models where the experimental conditions need to remain constant.

In this work, a capillary flow rig is developed to resolve this issues and study $CaCO_3$ surface deposition kinetics. Figure 3-1 show the modified rig, which enables the examination of the growth and blockage of the micro bore metal cell (a very short cell where the conditions can be considered constant across the capillary cell) by measuring the differential pressure as a function of time across the capillary sample cell.

These results from scale build up in the capillary cell and from the differential pressure (ΔP) versus time gives an understanding of the growth kinetics. The brine solutions are pumped with two reciprocating pumps (Gilson pumps type, 100SC) which drive the cation and anion brine solutions into two separate coils made of stainless steel, immersed in a heated water bath. This raises the solution temperature to the desired test temperature before arriving at the mixing section.

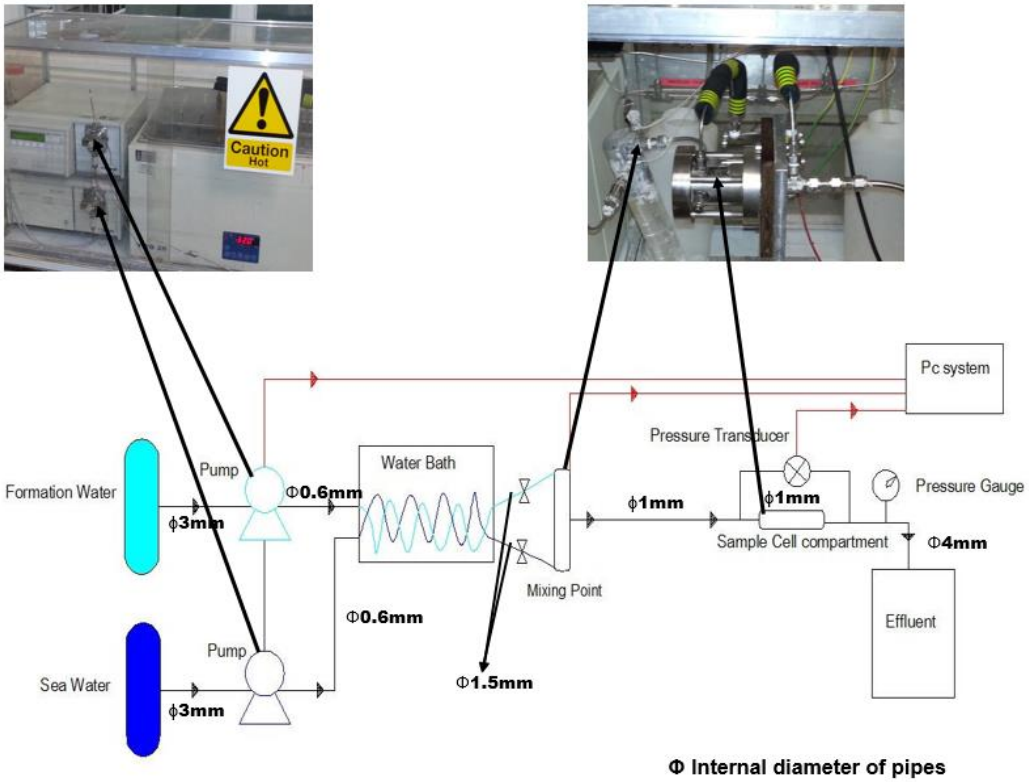

Figure 3-1: Schematic diagram of the capillary tube blocking rig

The test cell can be located any distance from the mixing section as shown in Figure 3-2, this distance can be changed to alter the time the mixed solution to reach the working section, such that the brine solution precipitation can be controlled to either have precipitated crystals or not in the bulk solution as it flow through the working capillary section.

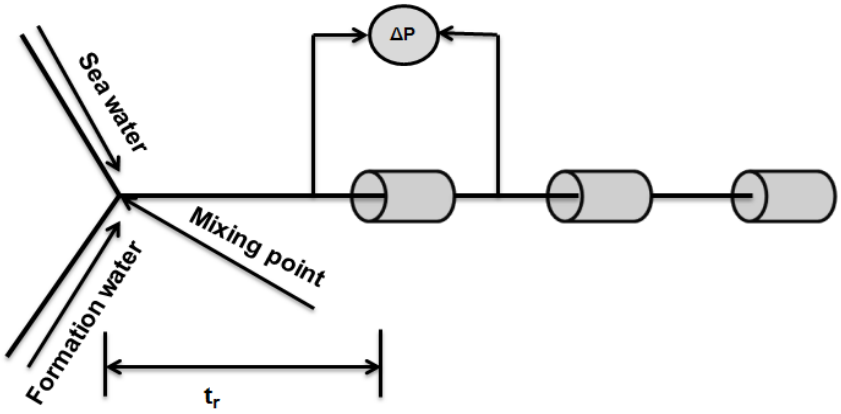

Figure 3-2: Schematic diagram of capillary rig showing the mixing part and capillary cell

The combined solution which has a saturation ratio value greater than 1 passes through a capillary test cell, made of stainless steel (316L) of internal diameter 1mm, length 10mm and scale crystal nucleate and grows on the surface of the capillary cell. The saturation ratio can be assumed constant along its length due to it short residence time (0.1sec, 0.05sec and 0.03sec for 5ml/min, 10ml/min and 15ml/min respectively).The formation of scale is monitored by measuring the differential pressure across the capillary cell. The differential pressure transducer (PX80D0-30-5T from Omega, 0-30Psi).

The pressure is maintained by a pressure gauge regulator leading to the effluent. When the stainless steel capillary cell blocks, the automatic pumps shut-down and the differential pressure and solution temperature as a function of time are logged by the computer which contain a LabVIEW data acquisition system.

The pressure increase is measured continuously throughout the experiment. At the end of each test, the rig is cleaned with a cleaning solution of (50% Sodium hydroxide NaOH g/L and 50% Ethylene-diamine-acetic acid EDTA g/L) at a pH of 10 for 30 minutes followed by distilled water for two hours.

3.3 Capillary flow rig description for bulk analysis test

The turbidity measurements and the inductively coupled plasma (ICP) test was carried out by creating a two way control valve on the capillary pipe before the capillary cell as shown in Figure 3-3. As such the amount of mixed brine collected can be controlled by setting the volumetric flow rate from the pump.

The flow rate was set for 10ml/min for the turbidity test. At every minutes, 10ml of brine solution were taken for the first five minutes, this was later increased to every 10minutes. For the ICP test, 1ml of the brine was measure and added to 9ml of quenching solution, using micropipette. The details of the turbidity measurements and inductively coupled plasma test is shown in chapter 4 of this work.

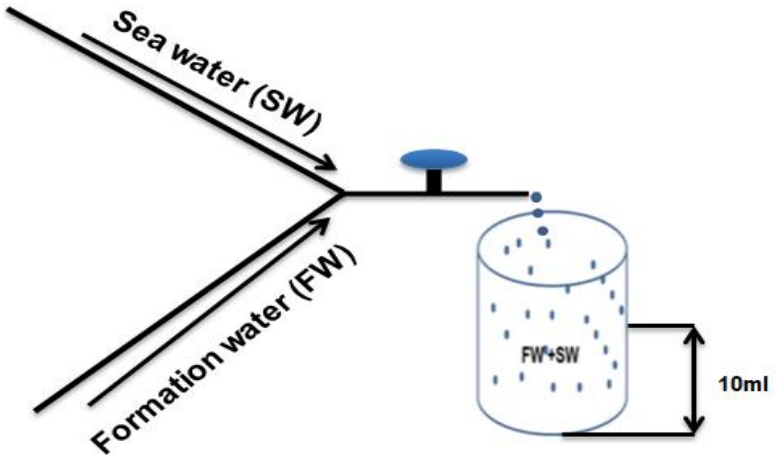

Figure 3-3: Capillary rig showing the bulk analysis section

3.4 Capillary flow rig description for scanning electron microscope and X-ray diffraction test

The capillary flow rig was fitted with capillary tube compartment after the capillary cell. A flat stainless steel coupon was inserted into a stainless steel extension tube fitted on the capillary flow rig, where deposition took place for scanning electron microscopy (SEM) and X-ray diffraction (XRD) observation. At the end of each deposition test, the stainless steel coupon

3.4.1 Capillary tube and stainless steel extension tube design

Figure 3-4 and Figure 3-5 show the schematic diagram of the capillary cell and the stainless steel extension tube for surface analysis test. From the capillary rig design, it is difficult to carry out in-situ surface analysis of the calcium carbonate scale deposited on the capillary cell during the test. However, for this study, a non-destructive technique is used to carry out the surface analysis test without any damage to the surface scale and the substrate.

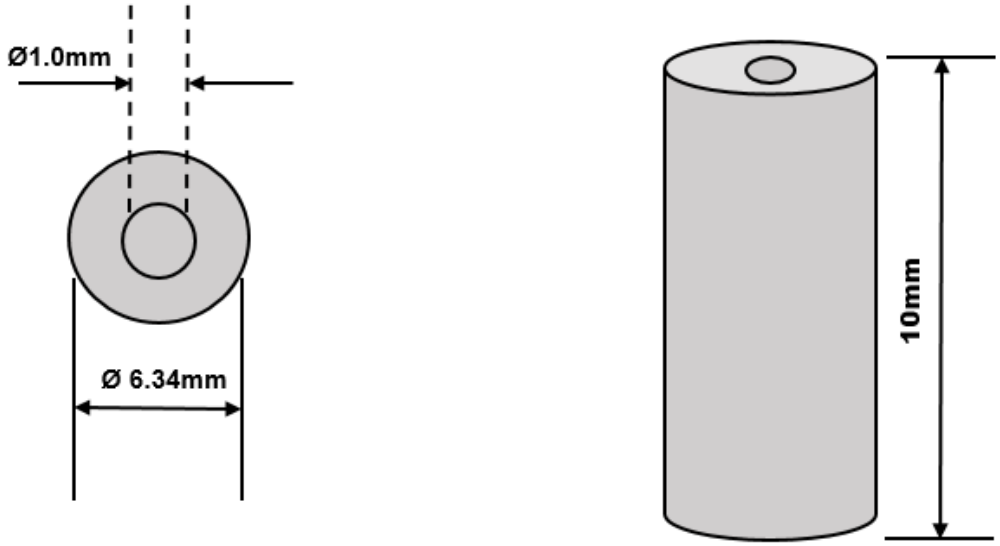

Figure 3-4: Schematic diagram of the capillary cell

The stainless steel coupon (316L) is 4.4mm in width and length 25mm, the extension tube is of length 35mm and internal diameter of 4.6mm. This is done before the deposition test is carried out, the flat coupon is cleaned with acetone solvent to dissolve any interfering chemical substance or material on the surface followed by distilled water and dried before inserting into the extension tube. At the end of the test, the scaled coupon is dried and taken for surface analysis test.

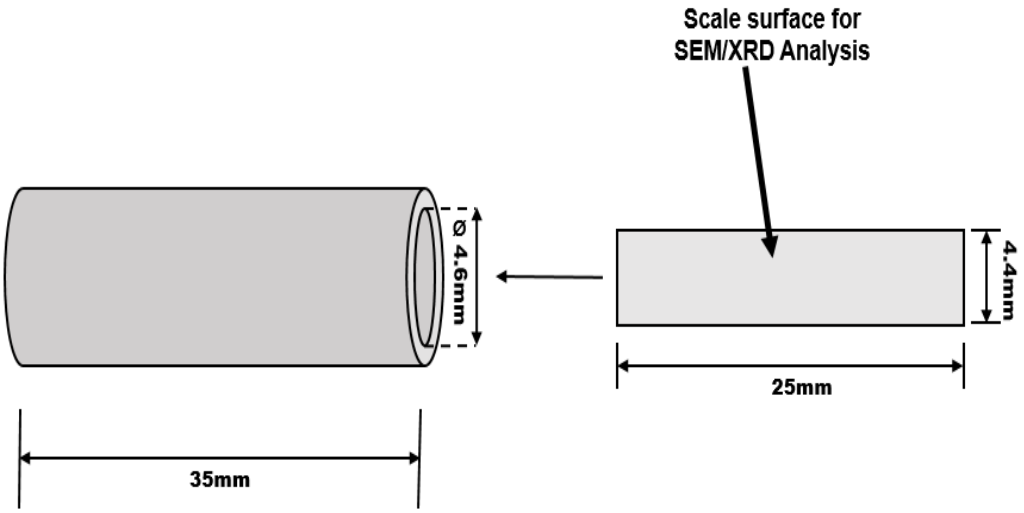

Figure 3-5: Schematic diagram of the stainless steel extension tube and flat coupon for surface analysis

However, it is difficult to know which scale deposition mechanism is occurring when scale build up in the capillary cell under flow conditions, the following three scale deposition mechanism is being suggested:

- ❖ Crystallization process,
- ❖ Adhesion process,
- ❖ Mixed regime.

The experimental methodology for this work will provide answers to these key questions.

3.5 Capillary rig design and modification

In the design and modification of the capillary rig, various pipe flow parameters were considered.

1. The entrance effect
2. The residence time (mixing section and the capillary cell)
3. Reynolds number

3.5.1 Entrance effect

Hagen Poiseuille flow equation shows that increasing the flow velocity should increase the differential pressure as shown in equation 3-1.One of the factor to be considered to make this assumption possible is to determine the entrance length.

$$Q = \frac{\pi D^4 \Delta P}{128 \mu l} \qquad 3\text{-}1$$

To ensure the flow is fully developed, the capillary length after mixing must be greater than the entrance length, and the internal diameter of the capillary before the capillary cell must be the same. This was calculated using the relationship between the Reynolds number (R_e), internal diameter (D) and the entrance length

(L_e) as shown in equation 3-2 [149] for laminar flow regime. Figure 3-6 shows a schematic diagram of developing flow and fully developed flow.

$$\frac{L_e}{D} = 0.06R_e \qquad 3\text{-}2$$

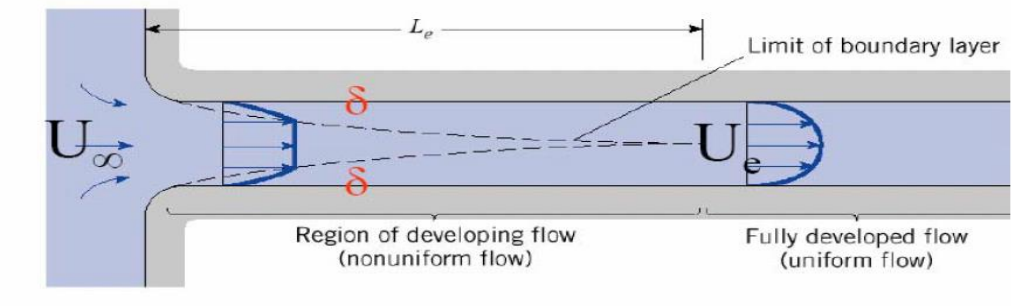

Figure 3-6: Pipe flow system showing a region of developing flow and fully developed flow [149].

The entrance length L_e calculated from different flow rates at fluid viscosity of 8.94×10^{-4} mPa.s and 4.06×10^{-4}mPa.s [150] for 25°C and 70°C respectively is shown in Table 3-1

Table 3-1: Entrance length of the capillary mixing section

Flow rate (ml/min)	Entrance length L_e (mm)	
	25°C	**70°C**
5	7.11	15.66
10	14.23	31.32
15	21.34	46.98
20	28.46	62.64
25	35.57	78.29
30	42.69	93.96

However, for sake of clarity and consistency of the interpretation of differential pressure (ΔP) data obtained from the capillary rig, all values were normalised to

0 Psi as the starting differential pressure for each experiments. In reality from the experimental results, ΔP values changes with flow rate.

3.5.2 Residence time (mixing section and the capillary cell)

The residence time for the fluid to travel through the capillary after mixing, before it gets to the capillary cell. And also the residence time within the capillary cell to effluent were calculated from equation 3-3. Table 3-2 shows the residence time of the brine at different flow rates.

$$Residence\ time\ \tau = \frac{Volume\ of\ the\ system\ (V)}{Volumetric\ flow\ rate\ (Q)} \qquad 3\text{-}3$$

The volume of the system V (mm^3) =$\pi r^2 l$, where r denotes the internal radius of the capillary (mm) and l denotes the length of the capillary (mm). Q denotes the volumetric flow rate (ml/min).

Table 3-2: Capillary residence time at different flow rates

Flow rate (ml/min)	Residence time (s)	
	Capillary cell **L= 10mm, ID = 1mm**	**Mixing section** **L= 80mm, ID = 1mm**
5	0.1	2.18
10	0.05	1.08
15	0.03	0.72
20	0.025	0.54
25	0.019	0.43
30	0.015	0.36

3.5.3 Reynolds number

The Reynolds number at different flow rate was calculated from equation 3-4, in order to determine the flow regime of the fluid entering the mixing section and the capillary cell. The Reynolds number at different temperatures and flow rates is shown in Table 3-3

$$Reynolds\ number\ R_e = \frac{\rho VD}{\mu} \quad \text{3-4}$$

Where ρ denotes the density of fluid (kg/m^3), V flow velocity (m/s), D internal diameter of the capillary (m), μ denotes the viscosity of the fluid (Ns/m^2).

Table 3-3: Reynolds number at different flow rates

Flow rate (ml/min)	Reynolds Number R_e Capillary cell, ID = 1mm		Reynolds Number R_e Mixing section, ID = 1.6mm	
	25ºC	70ºC	25ºC	70ºC
5	117	261	74	163
10	237	522	148	327
15	356	783	222	489
20	474	1044	297	653
25	593	1305	371	816
30	712	1566	445	979

3.6 Hagen Poiseuille (HP) flow prediction

Recalling the Hagen Poiseuille flow equations for laminar flow condition shown in equation 3-1, assume a uniform flow, the flow rate is a function of the diameter D, pressure drop ΔP, viscosity of fluid μ and the capillary length L.

$$Q = \frac{\pi D^4 \Delta P}{128 \mu l} \quad \text{3-5}$$

The following are assumptions of Hagen Poiseuille flow equations for laminar flow regime.

- The flow is constant through the capillary,
- The fluid is incompressible and Newtonian,
- The flow is laminar through a pipe of constant cross-section,
- No acceleration of fluid in the pipe,
- The flow must be fully developed

In a study by Wang et al [20, 21] and Lawal et al [22], they used the pressure drop across the capillary tube during asphaltene deposition as a measure of thickness of asphaltene deposited across the capillary cell. The thickness of asphaltene deposited was determined from equation 3-6 to 3-9. For a constant flow rate,

$$\frac{(\Delta P_T) r^4}{\mu_T} = \frac{(\Delta P_i) R^4}{\mu_i} \qquad 3\text{-}6$$

Where Q denotes the flow velocity (m^3/s), D the internal diameter of the capillary (m), ΔP the pressure drop along the capillary (Psi), μ the viscosity (NS/m^2), l the length of the capillary (m), ΔP_i and ΔP_T are initial pressure drop before deposition and at time T, the pressure drop along the capillary. μ_i and μ_T are the original viscosity of the brine and average viscosity at time T respectively, R and r are the original capillary tube radius and effective radius after deposition respectively. The schematic diagram of the scaling process is illustrated in Figure 3-7

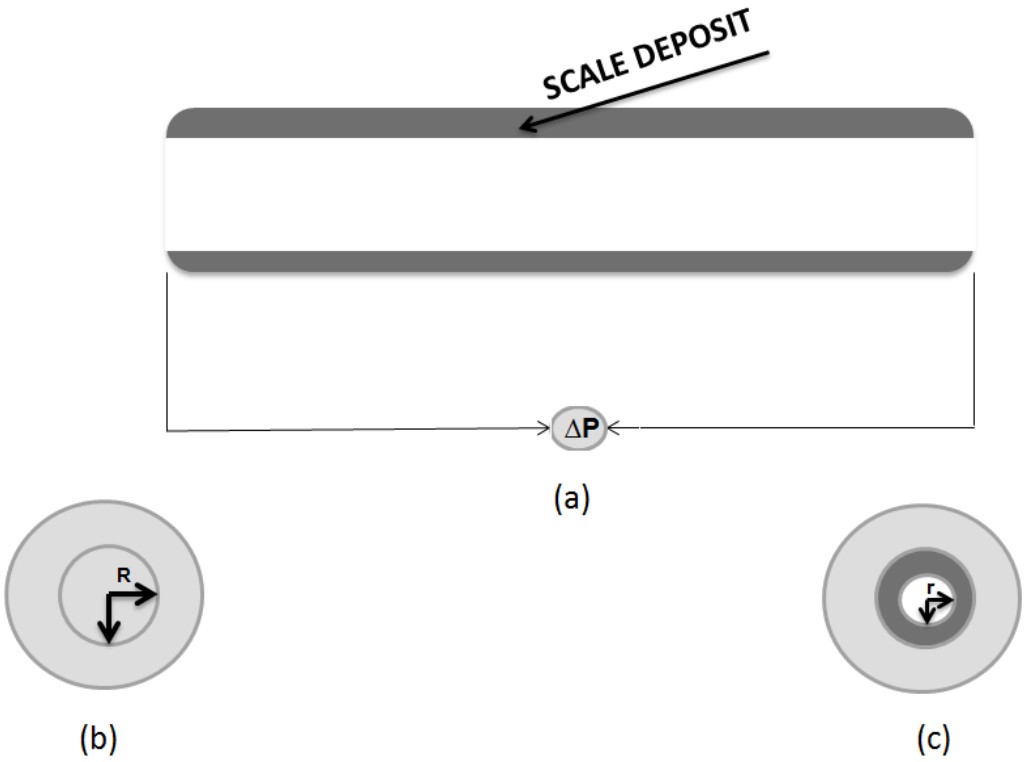

Figure 3-7:(a) Scale deposited uniformly on a capillary tube (b) and (c) Cross section of capillary tube before and after deposition

Simplifying equation 3-6 by neglecting the effect of viscosity change since $\mu_i \approx \mu_T$ [22]

Therefore equation 3-6 becomes.

$$r = R\left(\frac{(\Delta P_i)}{(\Delta P_T)}\right)^{1/4} \quad 3\text{-}7$$

The scale deposition thickness (t) is given by the equation 3-9,

$$t = R - r \quad 3\text{-}8$$

From equation 3-7 and 3-8

$$t = R\left(1 - \left(\frac{\Delta P_i}{\Delta P_T}\right)^{1/4}\right) \quad 3\text{-}9$$

However, in this study, the pressure was used to determine or monitor where to stop the test, and at the end of the test, the deposited scale on the surface of the

capillary cell were dissolve and measured by Inductively coupled plasma Mass Spectrometry (ICP-MS). It was also assumed that the initial pressure drop at the beginning of the experiment is not significant compared to the cut off pressure (5Psi) as the amount of $CaCO_3$ scale measured before the scaling time (t_s) is less than 5% of the amount of scale at t_s, which is the time the differential pressure deviate from 0 Psi as shown in Figure 3-8. The value of t_s varies depending on the experimental conditions and the sensitivity of the pressure transducers. The values of t_s determined at different tests are shown in Figure 3-9 and Figure 3-10 for SR 5, 5ml/min and SR 11, 10ml/min at 25^{o}C respectively. The repeatability of the t_s values from the two plots is shown with the error bars in Figure 3-11 determined from the average t_s values of the repeated tests.

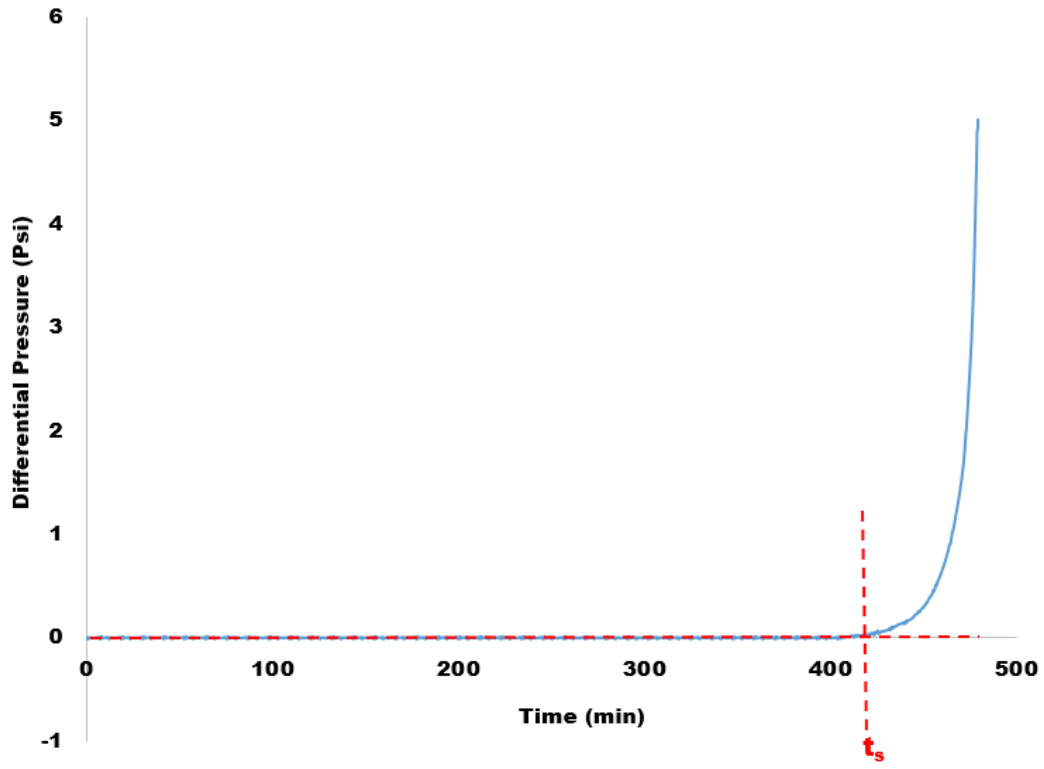

Figure 3-8: Differential pressure as a function of time

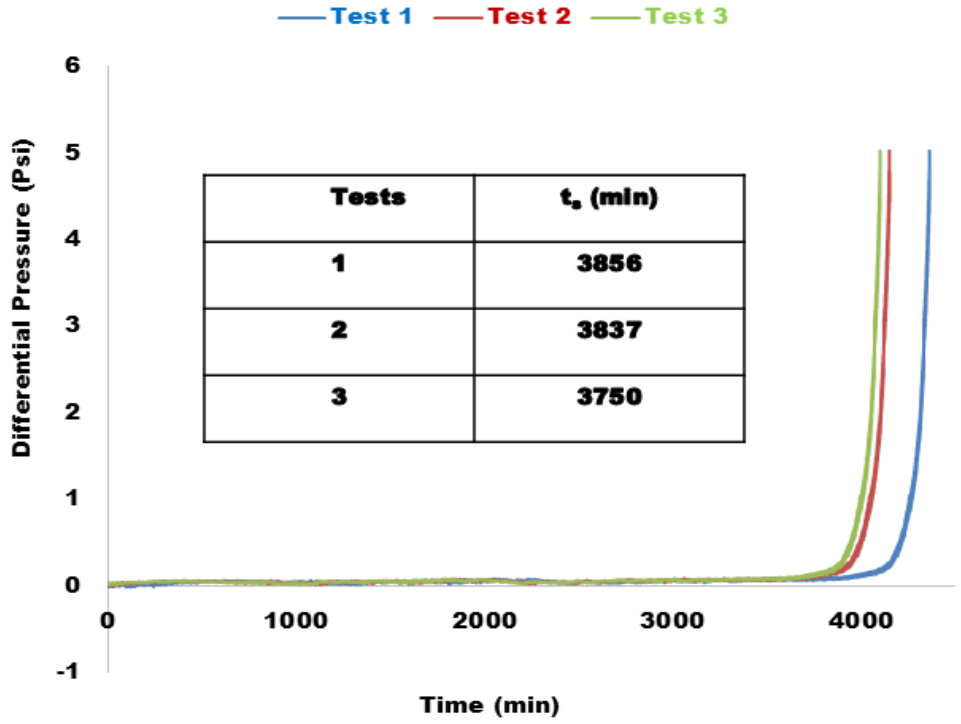

Figure 3-9: Repeatability test for SR 5, 5ml/min at 25ºC

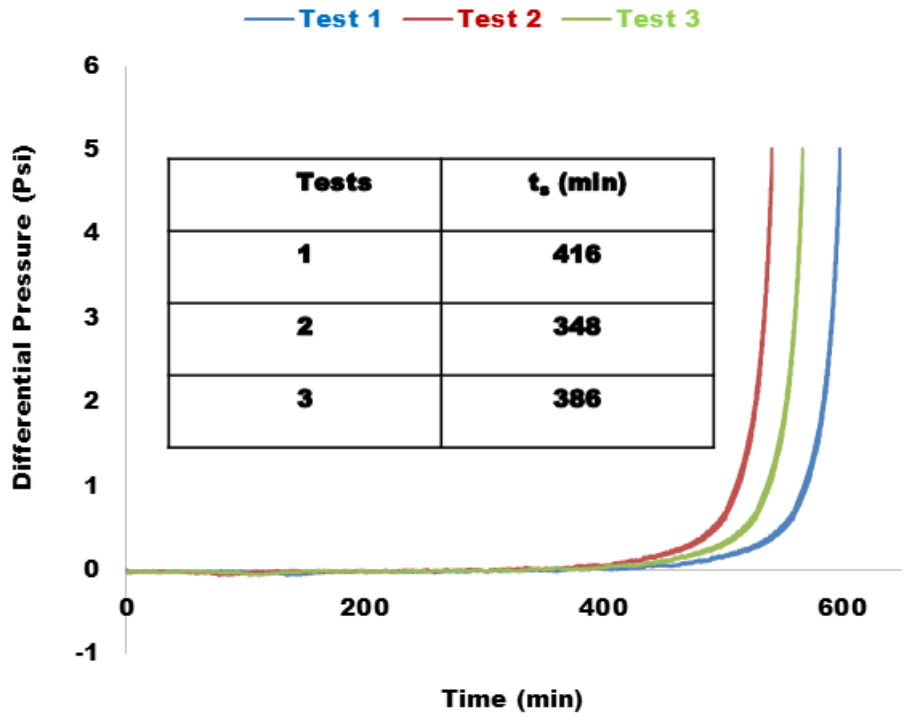

Figure 3-10: Repeatability test for SR 11, 10ml/min at 25ºC

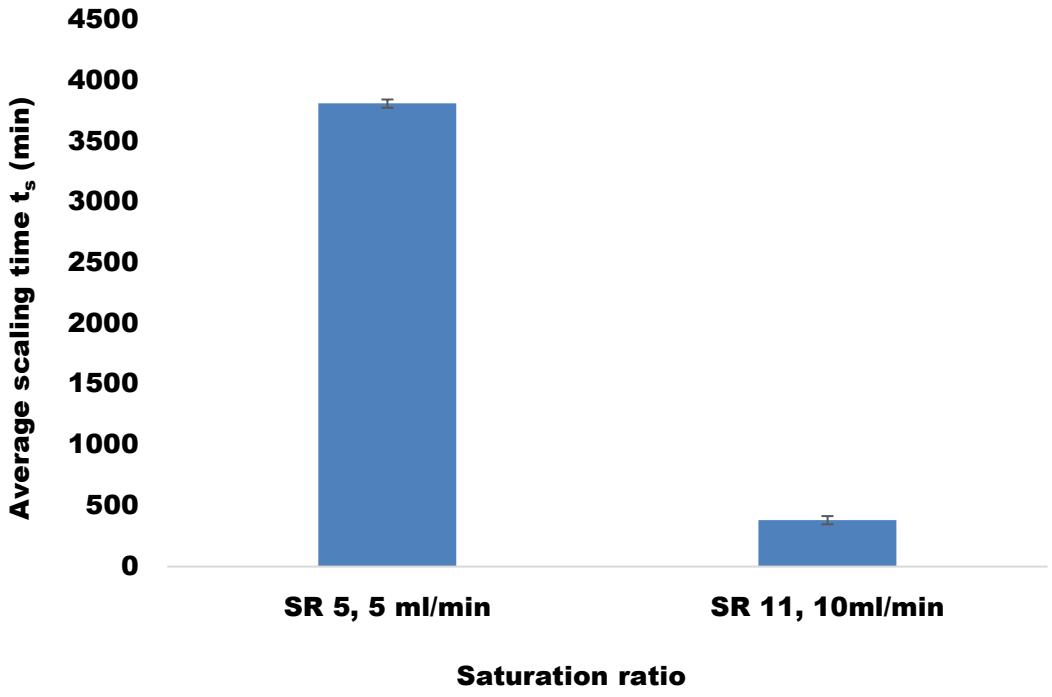

Figure 3-11: Repeatability test for SR 5,5ml/min and SR 11, 10ml/min at 25ºC

It was also assumed that the growth rate is linear and from t_s, a rapid pressure increase indicating fast deposition rate (scale on substrate and scale on scale), at that point the capillary cell is plugged and the effect of flow rate or pressure is almost irrelevant with respect to deposition rate.

3.7 Limitations of Hagen Poiseuille flow equation measurement with reference to capillary tube blocking rig

Hagen Poiseuille flow equation as a measure of scale deposition thickness growth rate may not give accurate results due to the following limitations.

- The scale layer is not uniform, which is more obvious in long capillaries.
- HP assumption estimate high deposition growth rate compared to ICP-MS measurement as shown in Figure 3-13 to Figure 3-15.
- The effect of surface roughness, interfacial energy, wettability is not considered in HP flow equation.

3.8 Determination of scale deposition growth rate

To determine the amount of calcium carbonate deposited on the capillary cell, the following method was adopted initially.

- ❖ To use the HP flow equation to estimate thickness of calcium carbonate on surface of the capillary cell.

- ❖ Measurements were taken for a clean capillary cell at different diameter and the HP values does not link.

- ❖ It was decided that a better way was to set the differential pressure at 5Psi then estimate the growth rate.

The growth rate of calcium carbonate build-up on capillary surface were calculated as the ratio of the amount of calcium carbonate scale deposited (measured by ICP-MS) to the change in onset pressure increase until it reaches a pressure of 5Psi.ie. (time it takes for the differential pressure to get to 5Psi and the scaling time) as shown in Figure 3-12.

The growth rate in mg/min was converted to cm/sec by assuming a uniform deposition of calcite along the capillary tube as shown in equation 3-10 to 3-12.

Mass of scale deposited m $= \rho \times v$ 3-10

Assuming a density of calcite $\rho = 2.711 g/cm^3$

The volume of hollow cylinder V $= \pi h(R^2 - r^2)$ (cm^3) 3-11

Scale deposition thickness $t = R - r$ 3-12

Where R denotes the radius of the capillary cell before deposition and r radius of the capillary cell after deposition (cm).

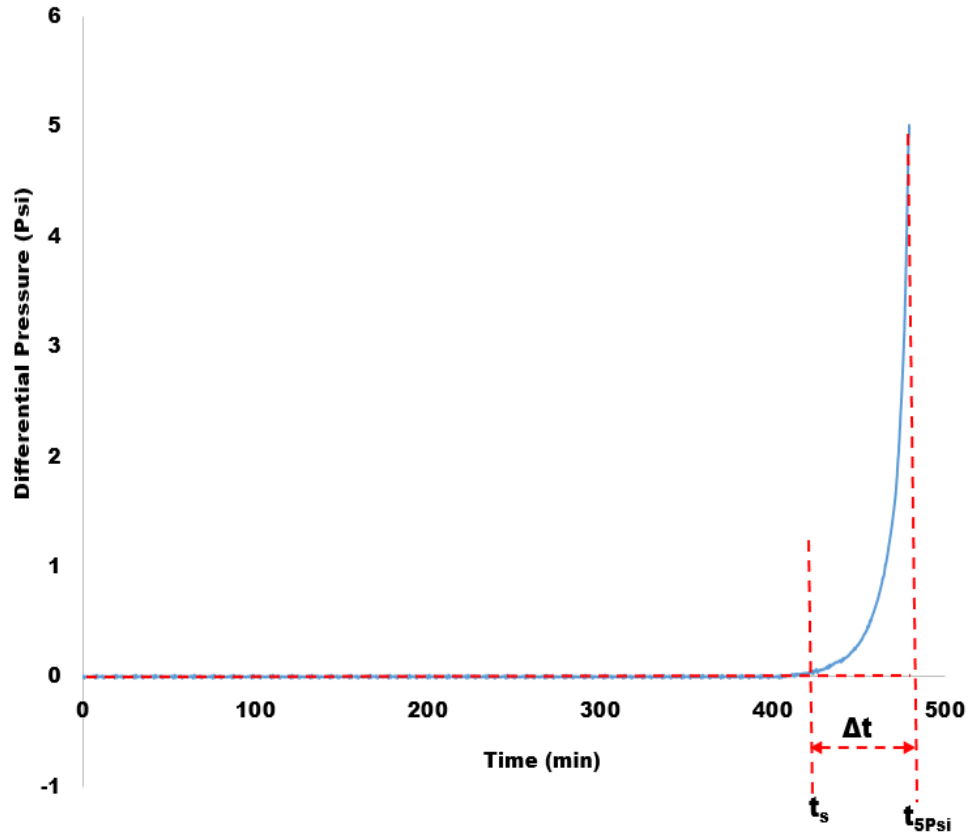

Figure 3-12: Differential pressure as a function of time

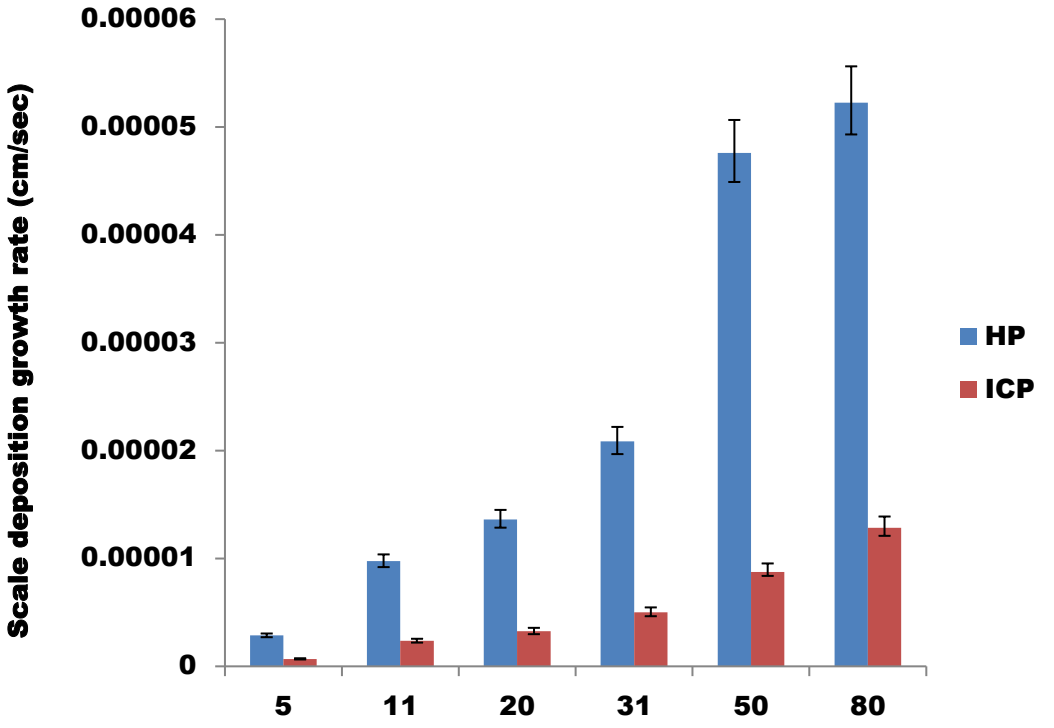

Figure 3-13: Scale deposition growth rate as a function of saturation ratio at 5ml/min and 25°C

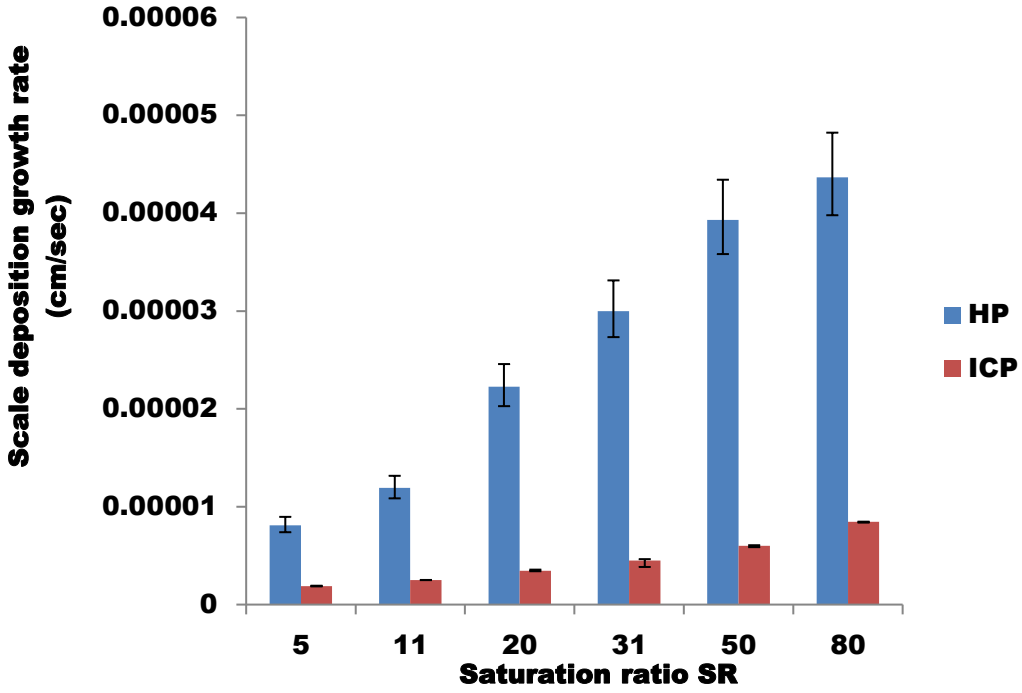

Figure 3-14: Scale deposition growth rate as a function of saturation ratio at 5ml/min and 70°C

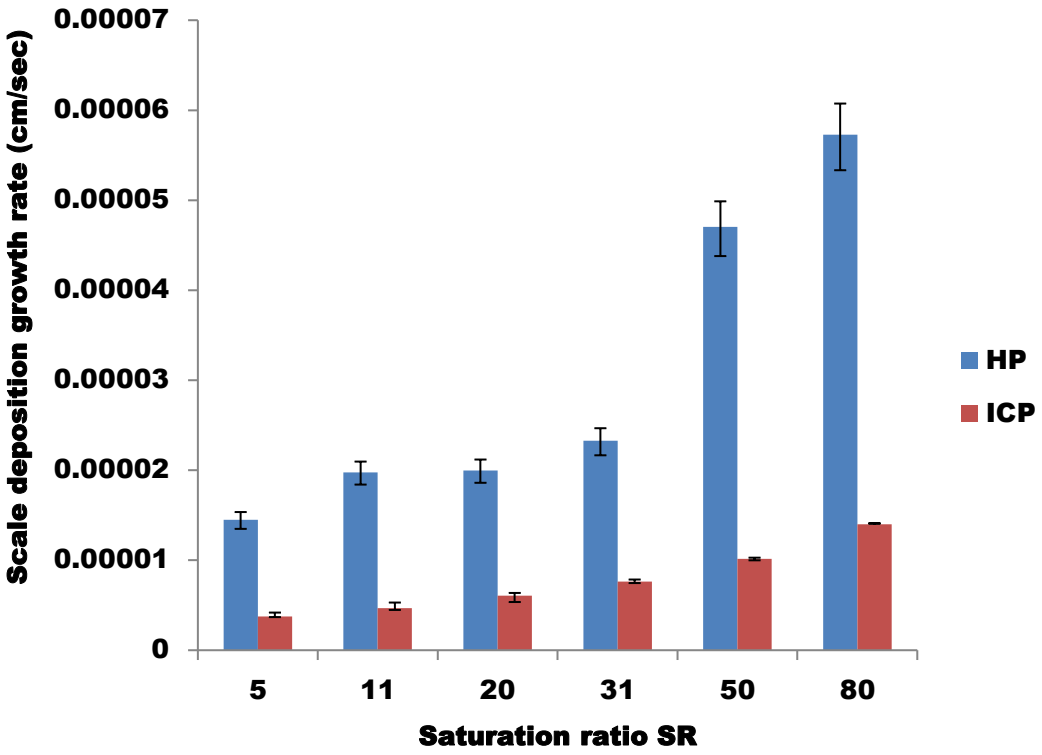

Figure 3-15: Scale deposition growth rate as a function of saturation ratio at 15ml/min and 70°C

3.9 Summary

Chapter 3, gives the capillary rig design overview and shows the modification and specification of the capillary rig to achieve the aims and objectives of the study. It also show that Hagen Poiseuille flow equation has some limitations in terms of estimating calcium carbonate deposition thickness growth rate.

It is therefore important to determine the amount of calcium carbonate deposited on the surface of the capillary cell by dissolving the scale and measure by ICP-MS technique.

The fluid flow parameters determined, enable us to work within a certain flow conditions and to understand the fluid mechanics of the capillary rig.

The data generated from the capillary flow rig shows a good repeatability and accuracy of the technique as shown in Figure 3-11. The next chapters of this thesis present the experimental methodology and details of apparatus used to carry out the bulk and surface analysis test on stainless steel sample inserted into the capillary flow rig.

CHAPTER 4. Experimental procedure and methodology

4.1 Introduction

This chapter presents a description of the apparatus used during the experiments namely, the bulk and surface analysis techniques used to study $CaCO_3$ scale surface deposition kinetics. It also provides the understanding of the materials and reagents used for the preparation of the synthetic brine solutions, and scale software used for the calculation of the saturation ratio of the brine solutions at different temperatures.

4.2 Experimental conditions

Experiments were run at 25^{o}C and 70^{o}C, at different flow rates (5, 10, 15, 20 and 30 ml/min). The brine ratio was 50 vol% formation water: 50% vol sea water. The capillary cell is made of stainless steel 316L (ID 1mm, length 10mm). This material was chosen to prevent corrosion products e.g. ($FeCO_3$) being formed from carbon steel and to focus on the kinetics of $CaCO_3$ surface deposition in the capillary flow rig. The composition of the stainless material is shown in Table 4-1

Table 4-1: Composition of stainless steel (316L) *[151]*

Element	Composition (Weight %)
Carbon (C)	0.03
Manganese (M_n)	2.00
Silicon (Si)	1.00
Chromium (Cr)	16.0 – 18.0
Nickel (Ni)	10.0 – 14.0
Phosphorus (P)	0.045
Sulphur (S)	0.03
Molybdenum (M_o)	2.0 – 3.0
Nitrogen (N)	0.10

4.3 Brine preparation

Formation water containing calcium ions (Ca^{2+}) and sea water containing carbonate ion (CO_3^{2-}) were used for the experiments. The reagents used for the preparation of these brines were sodium bicarbonate ($NaHCO_3$), sodium chloride (NaCl) and calcium chloride dihydrate ($CaCl_2.2H_2O$) which are all at different concentrations, depending on the saturation ratio to be achieved. The experiments were run at two different temperatures of 25°C and 70°C at 50:50 mixing ratio by varying the brine composition, but keeping the temperature constant for each saturation ratio.

The saturation ratio of these brines was calculated using the Scale SoftPitzer (Version 4.0). This software takes into account the co-precipitations that might occur in complex brines. Saturation ratio is calculated generally using equation 4-1.

$$SR = \frac{[Ca^{2+}][CO_{3^{2-}}]}{K_{sp_{CaCO_3}}} \qquad 4\text{-}1$$

Where $[Ca^{2+}]$ denotes the concentration of calcium ion, $[CO_3^{2-}]$ denotes the concentration of carbonate ion, K_{sp} denotes the solubility product constant of calcium carbonate. The scale software is programmed to predict the scaling tendency of mineral scales common in oil and gas production, The program calculates the effect of temperature (T), pressure (p), total dissolved solid (TDS), ion pairing and composition on activity coefficients [152-154]. The saturation ratio of the brines covers a region where there is low scaling regime to a region of high scaling regime as show in Table 4-2 and Table 4-3.

Table 4-2: Brine composition at 25ºC

Brine (mg/l)	Na^+	Cl^-	Ca^{2+}	HCO_3^-
Formation water	29381	28135	1250,2000,2950, 3600,4000,5000, 7500, 10000	-
Sea water	10666	18822	-	1850,4000,4800, 6000,8500, 10500, 15200, 18000
Saturation Ratio SR (50:50) mixed			SR 5, 11, 20, 31, 50, 80, 200, 398	SR 5, 11, 20, 31, 50 ,80, 200, 398

Table 4-3: Brine composition at 70ºC

Brine (mg/l)	Na^+	Cl^-	Ca^{2+}	HCO_3^-
Formation water	29381	28135	600,1000,1450 ,1800, 2000,2500, 3300, 5000	-
Sea water	10666	18822	-	850,1800,2000,2600, 3700, 4500, 8000, 10500
Saturation Ratio SR (50:50) mixed			SR 5, 11, 20, 31, 50, 80, 200, 398	SR 5, 11, 20, 31, 50, 80, 200, 398

4.4 Test method

Physical and chemical analyses were carried out, to enable the chemical characteristics of calcium carbonate scale to be determined. A schematic outline of the test methods is shown in Figure 4-1.

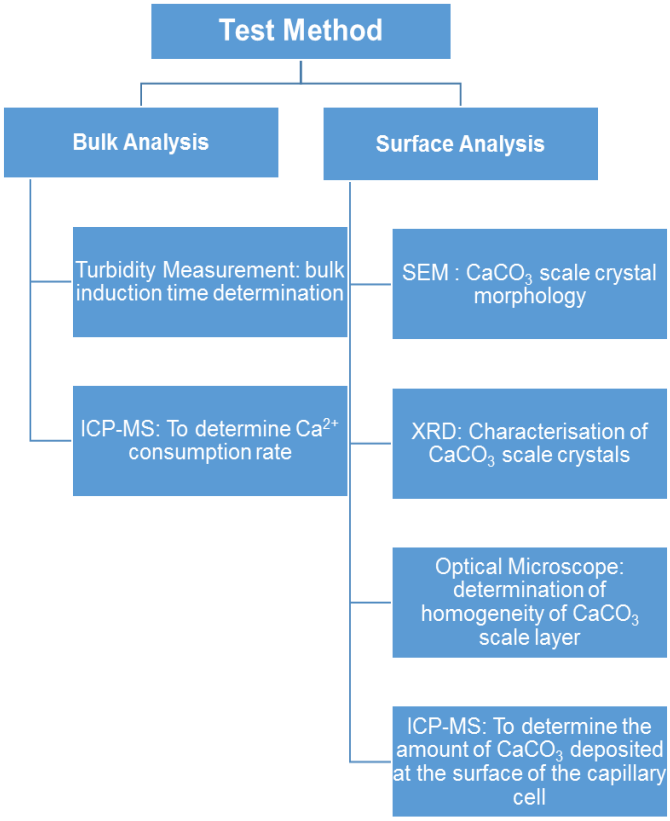

Figure 4-1: Schematic diagram of the bulk analysis test

4.4.1 Bulk analysis test

The experimental bulk measurements were conducted using different techniques. These techniques include turbidity measurement and inductively coupled plasma mass spectrometry (ICP-MS) measurement. This was carried out to support the surface analysis tests.

4.4.2 Inductively Coupled Plasma Mass Spectrometry (ICP-MS) measurement

The Inductively Coupled Plasma Mass Spectrometry (ICP-MS) is an analytical technique used for the determination of elements in a solution. It has high capability in detecting elements or ions and converts the atoms of the elements in the sample ions. These ions are detected and separated by the mass

spectrometer [155] . After each test, the capillary test samples were dissolved in 10% acetic acid and the amount of calcium carbonate deposited on the surface of the capillary cell was determined by ICP-MS. While for the bulk solution, the ICP measurements were carried out by preparing a quenching (KCl/PVS) solution of 11.42g of potassium chloride and 2g of polyvinyl sulfonate (PVS) scale inhibitor in 2 litres of distilled water. The solution was then adjusted with 10%HCl and concentrated NaOH solution to a pH value between 8 and 8.5. The sample tests were prepared by taking 1ml of the test brine with a micropipette into 9ml of the quenching solution (KCl/PVS) kept in test tube. The sample solutions were analysed for Ca^{2+}. The summary of the test protocol is given below. Figure 4-2 shows the ICP-MS apparatus used for the analysis.

4.4.3 Capillary cell preparation and solution sampling for ICP-MS analysis (bulk precipitation)

- Capillary cell samples were rinsed thoroughly with distilled water, followed by drying in an oven for 1 hour before experiments.

- Quenching solution was prepared by dissolving 11.42g of potassium chloride (KCl) and 2g of polyvinyl sulfonate (PVS) scale inhibitor in 2 litres of distilled water. PVS solution stabilise the sample and prevent further precipitation, KCl solution act as an ionisation suppressant for Atomic absorption determination of ions.

- The Quenching solution was adjusted with 10% HCl and concentrated NaOH solution to a pH value between 8 and 8.5.

- 1ml of brine solution containing formation water and sea water (FW+SW) is placed in a test tube containing 9ml quenching solution (PVS/KCl), using Eppendorf pipette, the test tube is shake thoroughly to ensure complete mixing.

- Brine solution is analysed by ICP for Calcium ion (Ca^{2+}).

4.4.4 Capillary cell preparation and solution sampling for ICP-MS analysis (surface deposition)

- Capillary cell samples were placed in 10% acetic acid solution (CH_3COOH) to determine the amount of $CaCO_3$ deposited on the surface of the capillary cell.

- Capillary cell samples were kept for 24 to 48hours in a test bottle, to completely dissolve the scale on the surface of the samples before sampling.

- 10ml of the sample solution was measured using Eppendorf pipette of 10ml, extreme care is taken to avoid impurities and test tubes are cap securely.

- Brine solution in 10ml test tube were analysed by ICP for Calcium ion (Ca^{2+}).

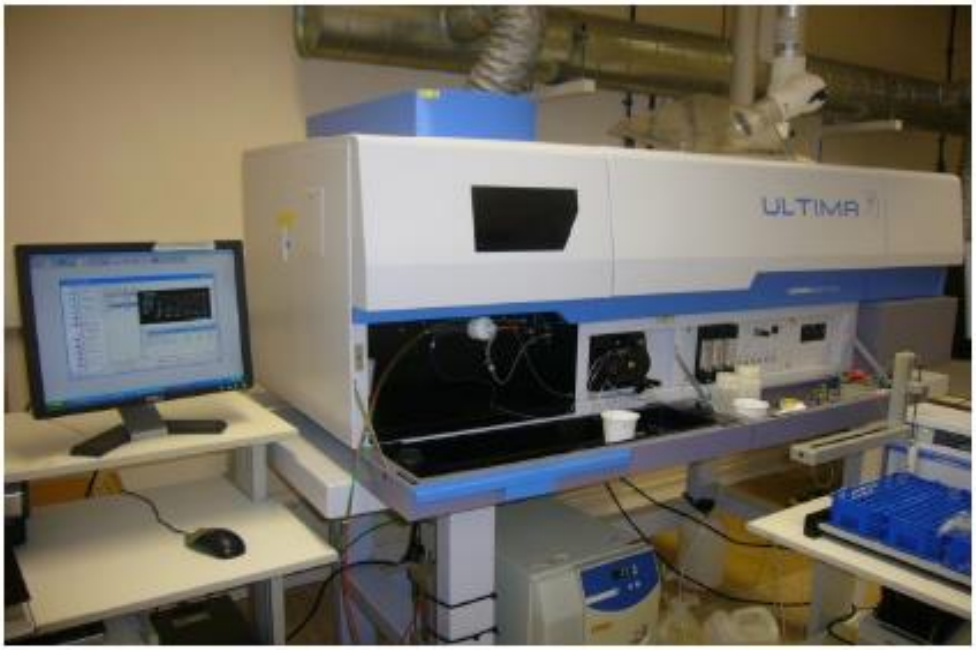

Figure 4-2 :Inductively Coupled Plasma (ICP) *[156]*

4.4.5 Turbidity measurement

Turbidity is a principal physical characteristic of the brine dispersion and is an expression of the optical property that causes light to be scattered and absorbed by particles and molecules, rather than transmitted in straight lines through a water sample [157].

The bulk induction times for $CaCO_3$ scale to form after mixing from the capillary flow rig, were determined through turbidity measurements on the collected fluids from the flow rig. Figure 4-3 shows a typical turbidity curve, showing three regimes, I denotes the induction time, where the first observable change in the turbidity of the bulk solution is observed, G is the crystal growth stage, where there is sharp increase in turbidity and P is the plateau stage, where there is no further precipitation or increase in turbidity.

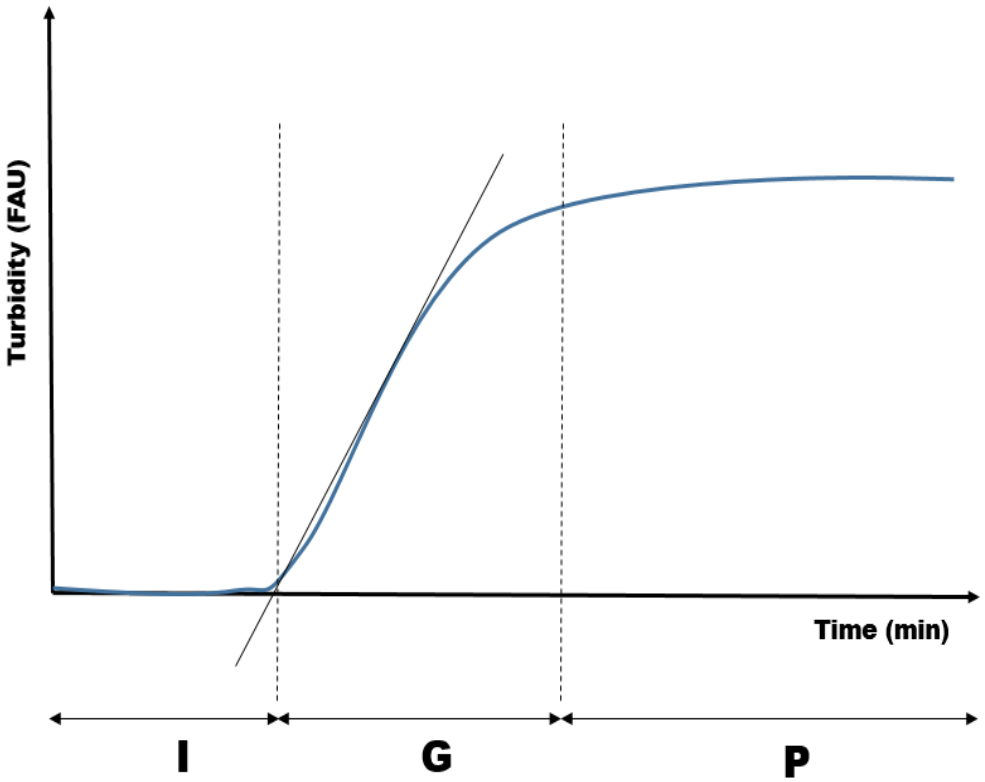

Figure 4-3: Typical turbidity curve

Every minute, a turbidity measurement was taken for the first five minutes, further increased to every 10minutes at a constant flow rate of 10ml/min for 25°C and 70°C respectively for all saturation ratios. The method used for this experiment

is a direct method which measures the attenuation (that is reduction in strength) of light as it passes through a sample column of water. Figure 4-4 shows the HACH colorimeter DR/890 model used for this study

Figure 4-4: HACH colorimeter DR/890 turbidity meter *[158]*

4.4.6 Surface analysis test

Flat stainless steel coupon was inserted into the capillary rig, where the calcium carbonate scale deposition took place. This was analysed by Scanning Electron Microscopy (SEM) and X-Ray Diffraction (XRD) observation, to enable the morphology and polymorphs of calcium carbonate crystals to be determined. Details design of the stainless steel extension tube and the flat coupon is mention in chapter 4. Optical Microscope was used to determine the homogeneity of the scale layers on the surface of a cross section of the capillary cell.

4.4.7 Scanning Electron Microscope (SEM) observation

A SEM was used to characterise the surface scale crystal deposited on the stainless steel coupon. The SEM model (EVO MA15) was used for the analysis. This SEM model is used for material analysis across a broader range of sample dimensions. It has a wide range of application vary from surface integration, forensics and failure analysis. Electron beam was focused on the scan samples and the equipment deliver images with information about the samples morphology, topography and composition of the scale deposited on the surface of the stainless steel coupon. The EVO MA15, has a maximum specimen height of 145mm, stage movement X,Y of 125mm, maximum specimen diameter of 250mm and maximum stage carrying capacity of 2kg [159]. The surface analysis

test was carried out in vacuum mode at a pressure of $3.5\ X\ 10^{-5} mbar$ at voltage of 10KV and working distance of 8mm. The magnification used was from 100x to 2000x. The SEM systems is shown in Figure 4-5.

Figure 4-5: Zeiss EVO MA15 SEM *[159]*

4.4.8 X-Ray Diffraction (XRD) observation

The morphology and crystalline species of calcium carbonate scale deposited on the surfaces of the stainless steel coupon were analysed using a Philip Pan Alytical X' pert PRO diffractometer. This equipment is used to analyse single or multiphase scale crystals. The high score plus software is used to acquire the data and analyse the sample using a build in data bank. The assembly that makes up of the sample holder, detector arm and the associated gearing is shown in Figure 4-6. This instrument is powered by a Philip PW3040/60X-ray generator and fitted with an X'celerator detector. The diffraction data is acquired by exposing the samples to CU-K_α X-ray radiation, which has a wavelength (λ) of 1.5418A^o, The X-rays are generated from a Cu anode supplied with 40KV and a current of 40mA [160]. X-ray on the crystal is diffracted in a pattern characteristics of the structure. Materials have different distinct diffraction patterns, compounds are identified by using a database of diffractions patterns and the purity of samples is also determine from it diffraction patterns [161]. The

diffraction pattern is used to determine and retrieve the lattices parameters of the crystal structures.

Figure 4-6: Philip Pan Alytical Pert PRO MPD *[160]*

4.4.9 Optical Microscope

The homogeneity of the calcium carbonate scale layer on the surface of a cross section of the capillary cell were analysed using Leica DM 6000M Optical microscope. It operates with a motorized Z-drive, motorized nosepiece turret and motorized stage. The motorized stages, operates as an integral part of the system and respond to magnifications changes [162]. Figure 4-7 shows the optical microscope used for this study.

Figure 4-7: Leica DM 6000M Optical microscope *[162]*

4.5 Summary

The equipment and techniques used for the bulk and surface analyses of calcium carbonate scale are presented in this chapter. The bulk analysis techniques used enable the understanding of the bulk precipitation process and also the amount of deposited scales can be determined or quantified using ICP-MS techniques.

The surface analysis techniques help in the understanding of the nature, particle size and homogeneity of calcium carbonate crystals formed on the surface of the substrate.

The next chapters provide the results obtained from the capillary rig and various bulk and surface analysis technique used in this study and their interpretation in terms of scale precipitation and deposition kinetics.

CHAPTER 5. Bulk precipitation study of calcium carbonate ($CaCO_3$) scale: Influence of saturation ratio

5.1 Introduction

This chapter presents the bulk scaling analysis obtained from the experimental work to support the surface deposition tests. The first section shows the results of the turbidity measurements and the second section shows the results of the Inductively Coupled Plasma Mass Spectrometry (ICP-MS) analysis.

Turbidity is an indication of the crystal formation of calcium carbonate scale in the bulk solution and enables measurement of the induction time of calcium carbonate precipitation. ICP-MS, enables the rate of consumption of calcium ions in the bulk solution to be determined from which the amount of calcium carbonate scale deposited on the surface of the capillary cell can be determined. The ICP-MS measurement enables the mass balance of the calcium ions consumed during scale formation to be completed and be reconciled with the ionic content of the effluent after the deposition test.

5.2 Calcium carbonate turbidity measurement at 25^{o}C and 70^{o}C

Turbidity measurement helps in the understanding of the inorganic scale precipitation process; the induction time of calcium carbonate scale can be determined. As described in Chapter 3, Figure 4-3 of this thesis, the typical turbidity curve shows three different regions of the scale precipitation process.

There is a region where the turbidity is zero; at this point there are no crystals in the bulk solution, which is referred to as the induction period. The region of rapid growth and finally the region where there is no further precipitation of scaling ions, at this point the turbidity curve attains a plateau region or equilibrium [143]. In this study for the bulk analysis, our emphasis is on the initial stage of the crystallization process and, as such, the induction time and scaling regime with respect to the scale mechanism are established.

Figure 5-1a and Figure 5-2a show the turbidity measurement of calcium carbonate scale at 25^{o}C and 70^{o}C under a laminar flow regime, while Figure 5-1b and Figure 5-2b , show the high resolution of the turbidity measurement for the

first five minutes of calcium carbonate precipitation indicated with red dotted lines.

The turbidity measurements were taken at one minute intervals for the first five minutes of calcium carbonate precipitation as shown in Figure 5-1b and Figure 5-2b respectively, and further extended to every 10 minutes to capture the later stages of calcium carbonate precipitation as shown in Figure 5-1a and Figure 5-2a respectively. The nucleation process for high saturation ratios 200 and 398 was rapid as expected. This is due to high ionic concentration of the brine solution and there was no induction time recorded. This is in agreement with studies at high concentration, representing rapid precipitation of calcium carbonate scale [115, 163-165].

The precipitation rate of calcium carbonate scale increases with increasing temperature. The solubility of $CaCO_3$ decreases with increasing temperature and also the kinetics of the scale process are enhanced. This implies that, for SR > 80, the induction time is less than the residence time ($t_{ind} < t_r$) and so there are crystals present in the bulk solution when it passes the capillary. The residence time in the flow rig at a flow rate of 10ml/min is 1.08s, which is the time for the fluid to travel from the mixing point to the working section.

The precipitation rate for lower saturation values (SR < 80) was slow compared to high saturation ratio (SR > 80). Induction times of 5, 4, 3, 2, 1 and < 1 min were obtained for SR 5, SR 11, SR 20, SR 31, SR 50 and SR 80 respectively at 25^{o}C and induction times of 4, 3, 2, 1, <1 and < 1 mins was recorded for SR 5, SR 11, SR 20, SR 31, SR 50 and SR 80 at 70^{o}C respectively.

These results show that, at lower saturation ratio (SR < 80) there are no crystals present in the bulk solution at the capillary, since the induction time is greater than the residence time ($t_{ind} > t_r$).

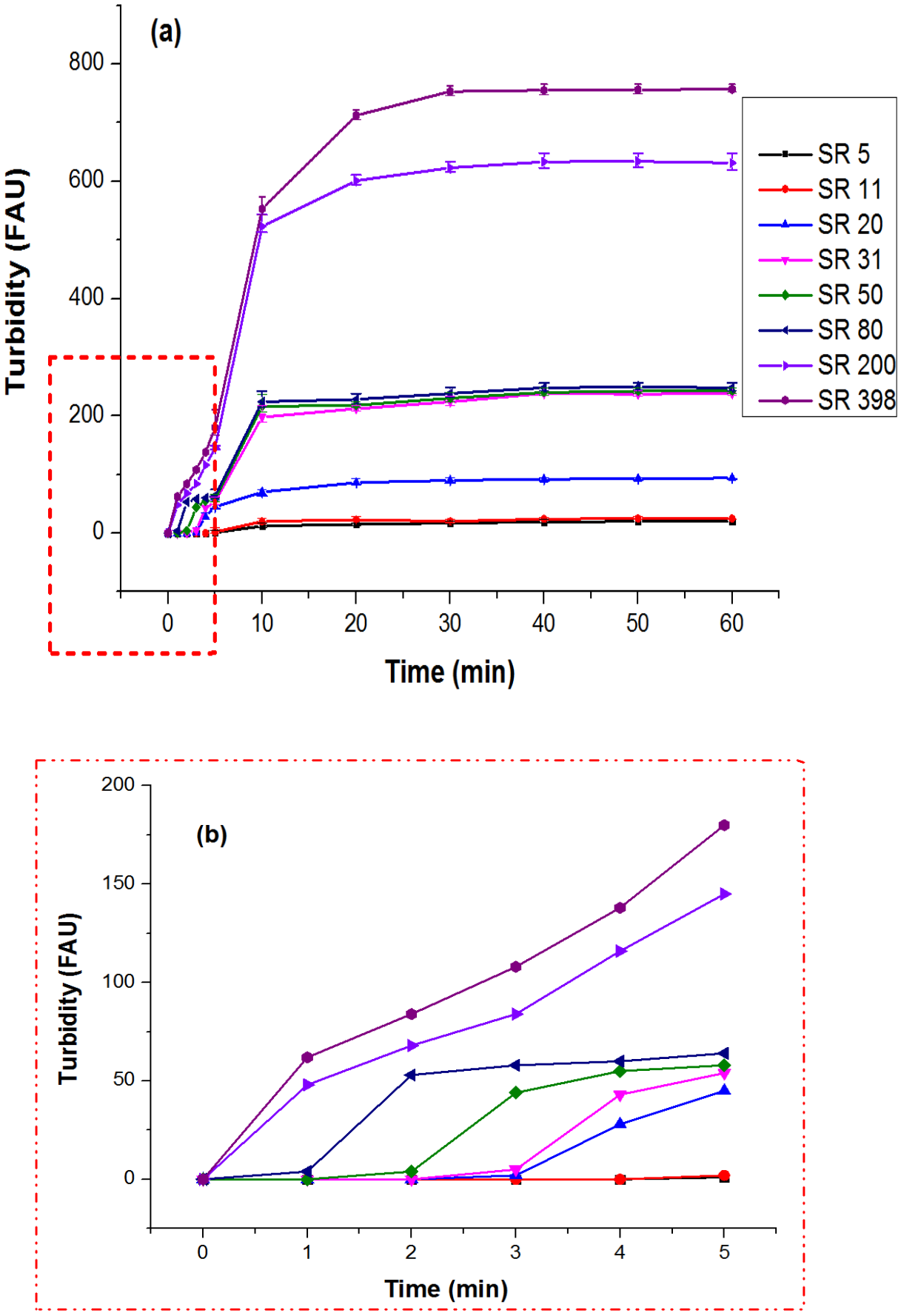

Figure 5-1 (a & b): $CaCO_3$ scale turbidity measurement at 25°C

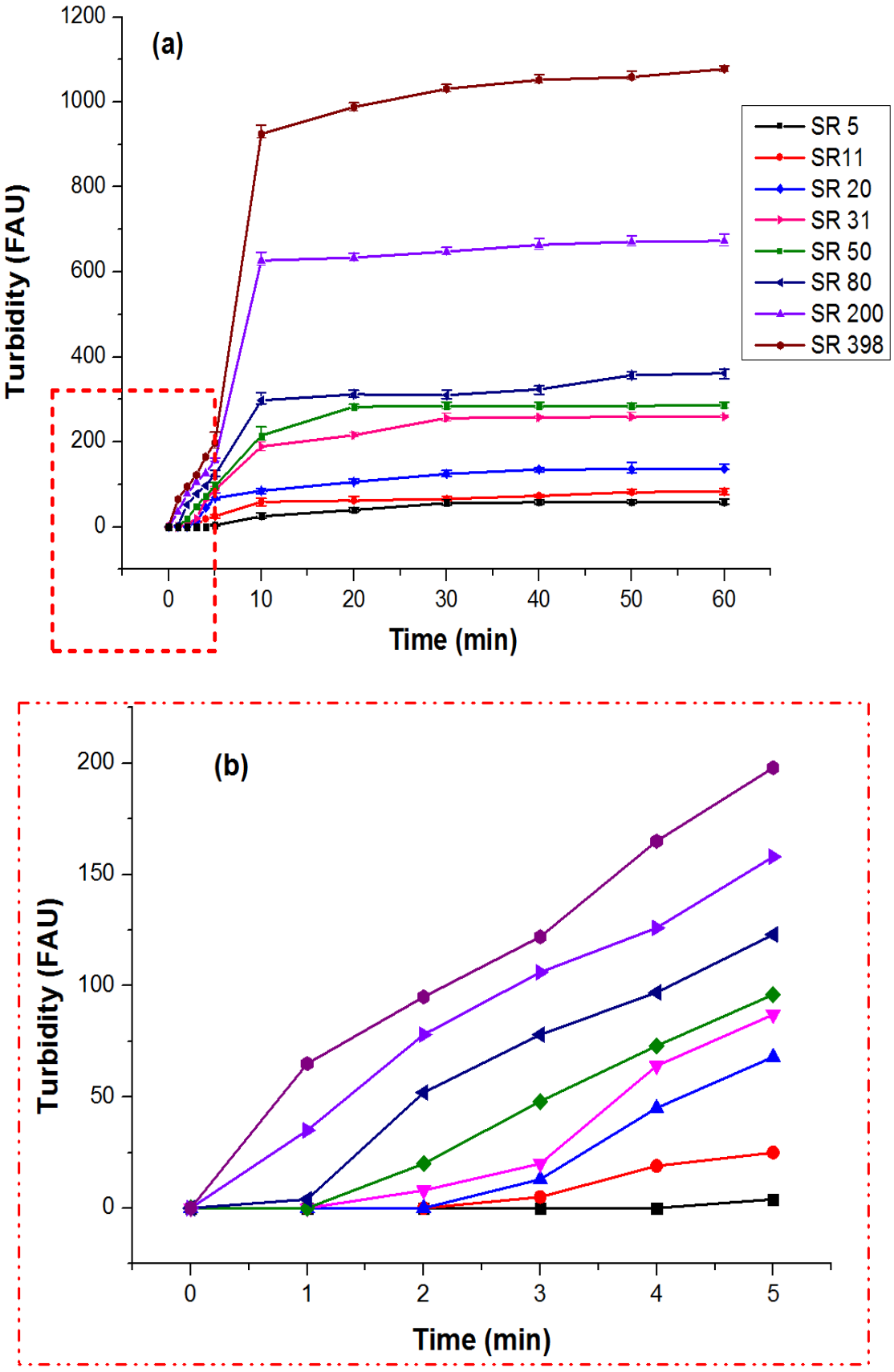

Figure 5-2 (a & b): $CaCO_3$ scale turbidity measurement at 70ºC

A study by Stamatakis et al [58] which determined the induction time of calcium carbonate scale formation under dynamic flow conditions. It was reported that at SR > 80, the induction time becomes independent of the temperature, but depends on the initial degree of the solution saturation ratio. At very high degrees of supersaturation, the process is dominated by solution concentration.

The turbidity curves suggest we can create two Scenarios within the brine composition investigated; That is, a region where the SR > 80, the scale mechanism is predominantly heterogeneous nucleation and adhesion, while the region where the SR < 80, is dominated by crystallization process. This hypothesis will be validated by results obtained in the surface deposition study presented in chapter 7.

5.3 Inductively Coupled Plasma Mass Spectrometry (ICP-MS) measurement at 25^{o}C and 70^{o}C

The rate of consumption of ionic species (Ca^{2+}, CO_3^{2-}) in the bulk solution gives an understanding of the precipitation rate of calcium carbonate scale ($CaCO_3$). In this study, the rate of consumption of calcium ions (Ca^{2+}) in the bulk solution was determined at different saturation ratios and temperatures.

Figure 5-3 and Figure 5-4 show the calcium ion concentration consumption rate in bulk solution at 25^{o}C and 70^{o}C for all the saturation values. At 25^{o}C, the calcium ion (Ca^{2+}) concentration drops rapidly from 1250, 2000, 2950, 3600, 4000, 5000, 7500 and 10000mg/l to,875, 1035, 1643, 2021, 2053, 2226, 4024, 7036mg/l for saturation values of 5, 11, 20, 31, 50, 80, 200 and 398 respectively, for the first few minutes, followed by a gradual decrease in calcium ion (Ca^{2+}) concentration. There were no further reaction or precipitation of calcium ion after 30 minutes. This corresponds to the plateau stage of the turbidity curve, while the initial part of the rapid precipitation or consumption rate corresponds to the growth stage of calcium carbonate as shown in the typical turbidity curve.

At 70^{o}C, calcium ion (Ca^{2+}) concentration drops more rapidly compared to the condition at 25^{o}C, as calcium ion concentration drops from 600, 1000, 1450, 1800, 2000, 2500, 3300 and 5000mg/l to 589,785, 840, 945,1020, 1950, 2025, 2636mg/l for saturation values of 5, 11, 20, 31, 50, 80, 200 and 398 respectively.

After 20 minutes when there was no further precipitation. As such the calcium ion (Ca^{2+}) concentration was constant until the end of the one hour experiment.

The calcium ion (Ca^{2+}) concentration plateaux appear faster at 70°C compared to 25°C due to the effect of temperature on the rate of precipitation or formation of calcium carbonate scale ($CaCO_3$). The rate of formation of calcium carbonate scale increases with temperature and also higher saturation values enhance crystal formation in the bulk solution, which could increase the tendency for scaling process through heterogeneous nucleation.

There is a possibility of the nucleation process taking place instantaneously as most of the calcium ion consumption takes place at the early stage of crystallization [108]. This indicate the formation of nuclei at the same time, followed by growth of nuclei thereafter. Until there is no further reaction showing that all the calcium ion (Ca^{2+}) in the bulk solution is fully consumed by the carbonate ion (CO_3^{2-}) in the solution, as shown in the plateau stage in Figure 5-3 and Figure 5-4.

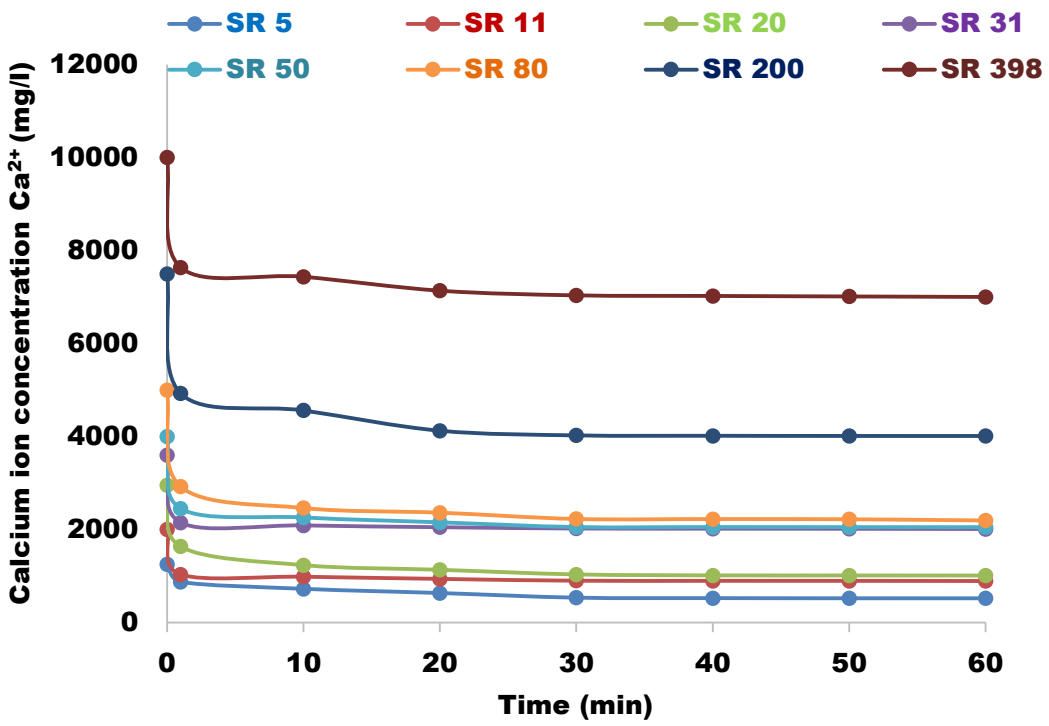

Figure 5-3: Calcium ion concentration [Ca^{2+}] as a function of time determined by ICP at 25°C

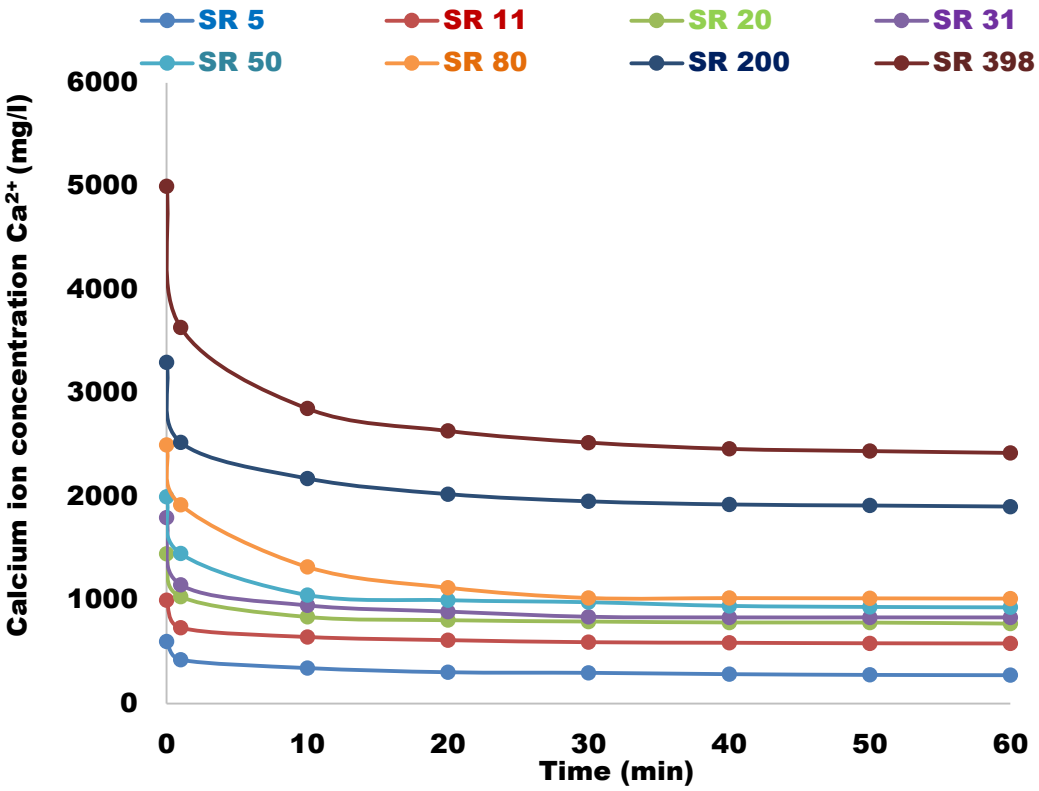

Figure 5-4: Calcium ion concentration [Ca^{2+}] as a function of time determined by ICP at 70°C

5.4 Summary

The bulk analyses studies enable us to create two scenarios within the brine composition values investigated.ie. At saturation ratio SR >80, there is no induction time recorded. As such for the times that represent the residence time from the mixing point to the capillary in the flow rig described in chapter 3. The mechanism of scale is likely to be dominated by mixed regime of heterogeneous nucleation and adhesion.

At saturation values SR < 80, the induction times recorded showed that there will be no crystals in the bulk solution as it passes the capillary. The induction time is greater than the residence time ($t_{ind} > t_r$). The scale mechanism is likely to be a crystallization process.

This two scenarios will be validated, based on the results obtained in the surface deposition study presented in chapter 7.

CHAPTER 6. Calcium carbonate scale surface deposition kinetics

6.1 Introduction

The main focus of this study is to determine the kinetics of *surface* scaling under hydrodynamic conditions. This chapter shows the raw experimental results obtained from the capillary flow rig with respect to the effect of flow rate, degree of supersaturation and temperature on calcium carbonate scale ($CaCO_3$) deposition. The results obtained from various surface analysis techniques are also presented.

6.1.1 The effect of flow rate on calcium carbonate surface deposition kinetics at 25ºC

Flow rate is one of the driving forces for calcium carbonate scale precipitation and deposition. Increasing the flow rate promotes scale precipitation by increasing the motion of scaling ions in the bulk solution, which invariably increases the tendency for calcium ions (Ca^{2+}) and carbonate ions (CO_3^{2-}) to react or form clusters after the induction time. Figure 6-1 to Figure 6-8, show differential pressure as a function of time at different flow rates for SR values of 5, 11, 20, 31, 50, 200 and 398.

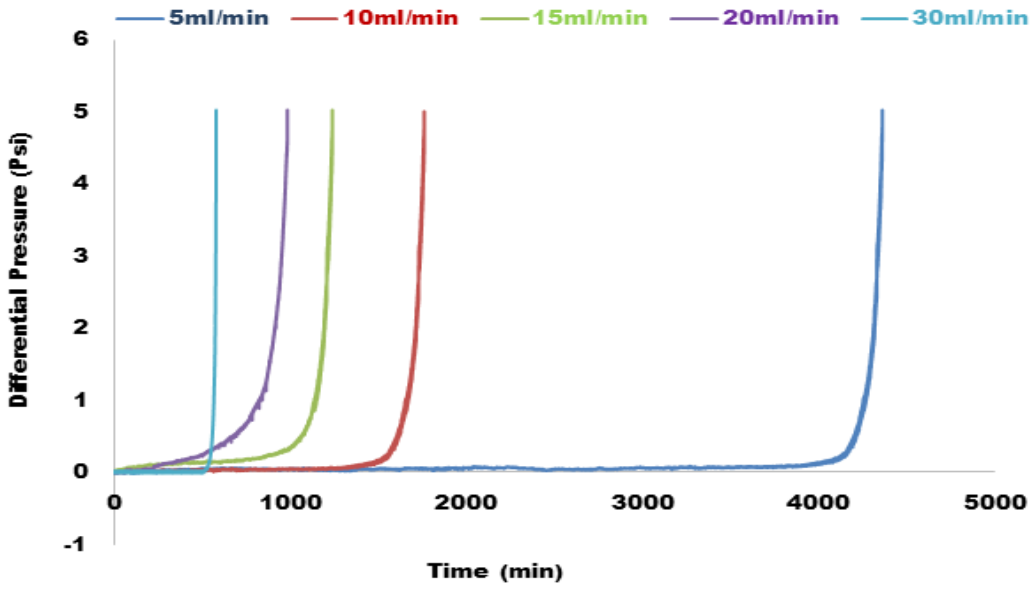

Figure 6-1. Differential pressure as a function of time for saturation ratio 5, 25ºC at different flow rates

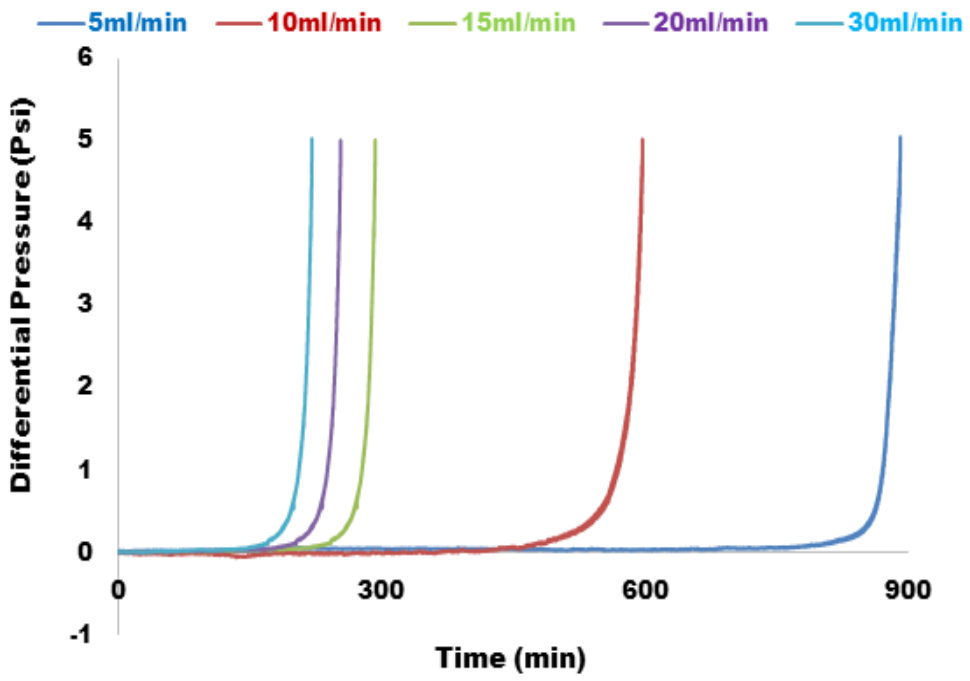

Figure 6-2: Differential pressure as a function of time for saturation ratio 11, 25°C at different flow rates

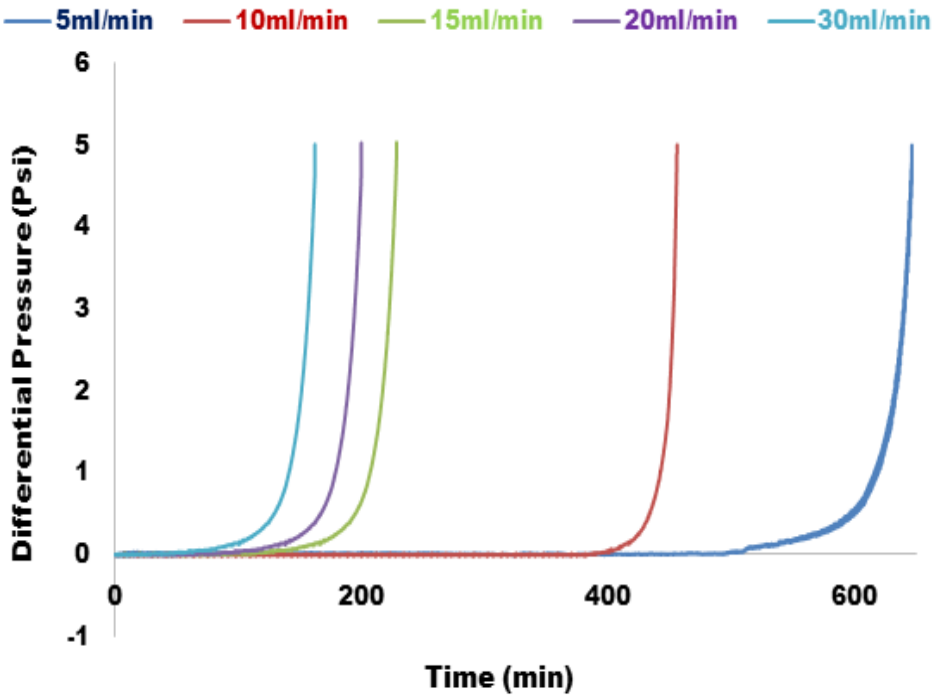

Figure 6-3: Differential pressure as a function of time for saturation ratio 20, 25°C at different flow rates

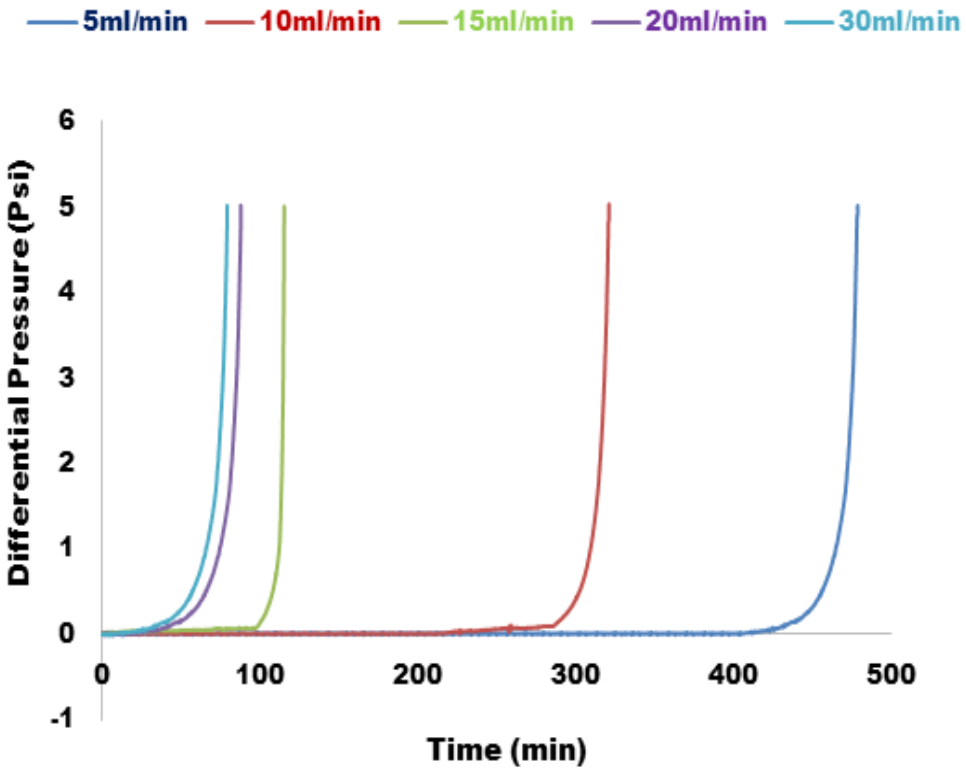

Figure 6-4: Differential pressure as a function of time for saturation ratio 31, 25°C at different flow rates

From the results, it is clear that calcium carbonate scale deposition rate increases with flow rate. At low flow rates of 5ml/min for SR 5, it takes about 4362 minutes (72.7hours) for the differential pressure to get to 5Psi, however, when the flow rate is increase to 30ml/min, it takes 581.9minutes (9.7 hours) to get to 5Psi. The result observed also shows that the differential pressure value remains the same until after 4120mins, when there was a rapid precipitation and deposition of calcium carbonate scale on the surface of the capillary cell, resulting to a sharp increase in the differential pressure.

A similar trend is observed for other flow rates and saturation values as shown in Table 6-1.

Table 6-1: Calcium carbonate scale deposition time for SR 5, 5ml/min at 25ºC

Flow rate (ml/min)	Deposition time (5Psi) (hours)
5	72.7
10	29.4
15	20.6
20	16.4
30	9.7

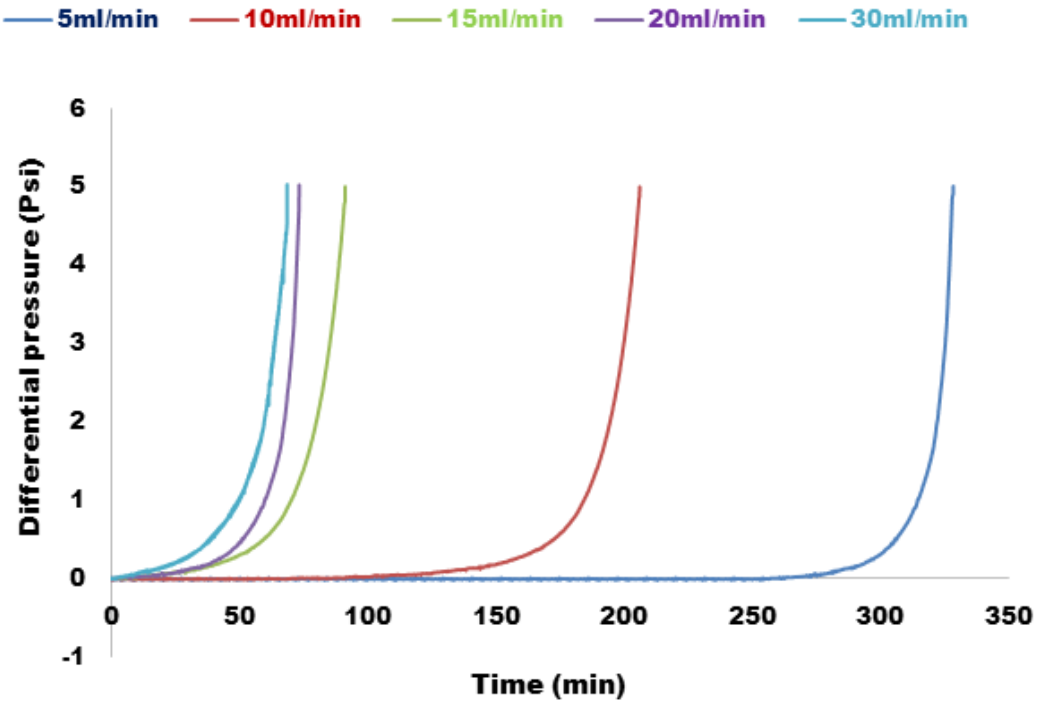

Figure 6-5: Differential pressure as a function of time for saturation ratio 50, 25ºC at different flow rates

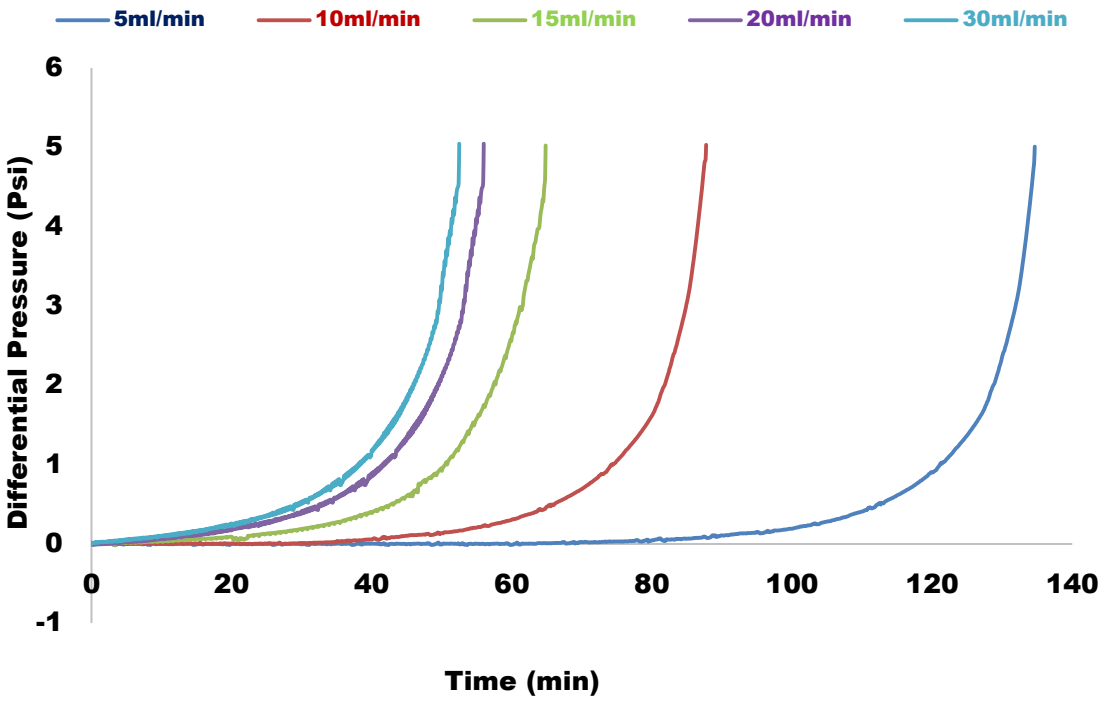

Figure 6-6: Differential pressure as a function of time for saturation ratio 80, 25ºC at different flow rates

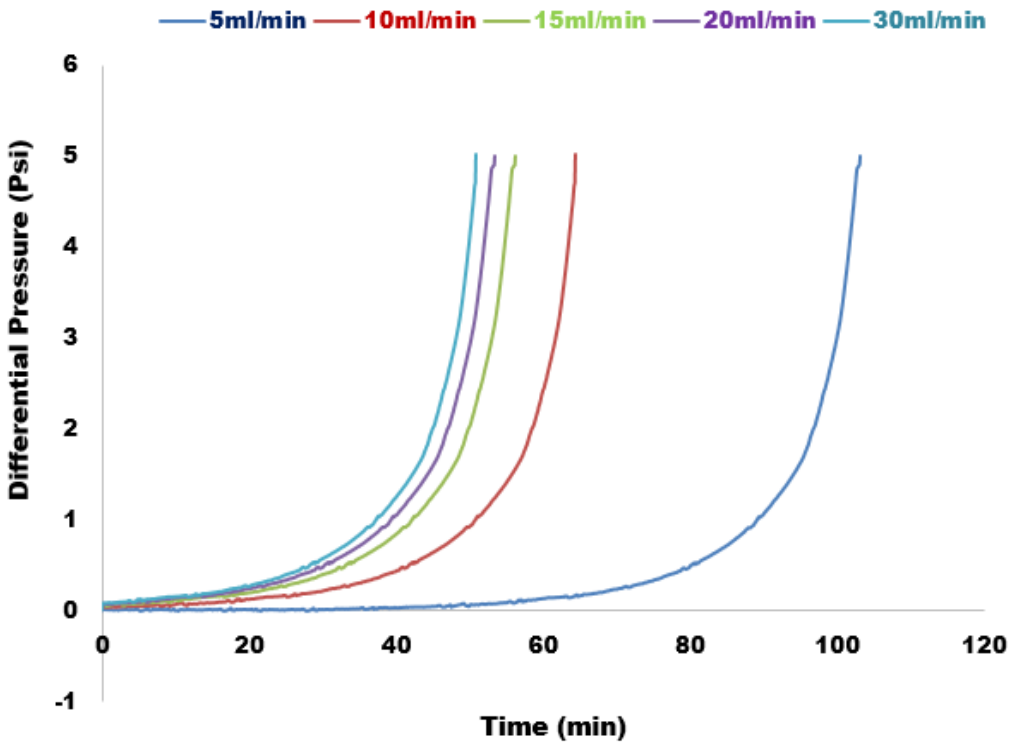

Figure 6-7: Differential pressure as a function of time for saturation ratio 200, 25ºC at different flow rates

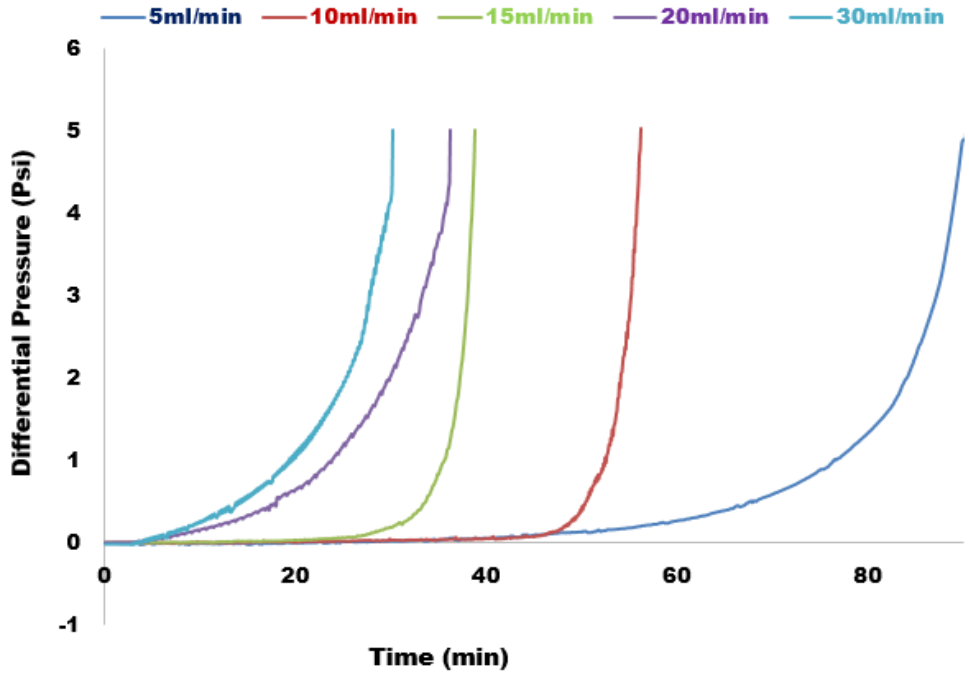

Figure 6-8: Differential pressure as a function of time for saturation ratio 398, 25°C at different flow rates

6.1.2 The effect of flow rates on calcium carbonate surface deposition kinetics at 70°C

Figure 6-9 to Figure 6-16, show the effect of flow rate on calcium carbonate ($CaCO_3$) scale surface deposition rate at temperature 70°C, for SR 5, 11, 20, 31, 50, 80 and 200 and 398 respectively. The rate of calcium carbonate scale deposition was rapid as the deposition time decreased with flow rate for all brine compositions investigated, which is similar to what was observed at 25°C.

However, the temperature enhanced the deposition kinetics as in the case of SR 5 at 25°C, the deposition time was 4362 minutes compared to SR 5 at 70°C of deposition time 1001minutes.

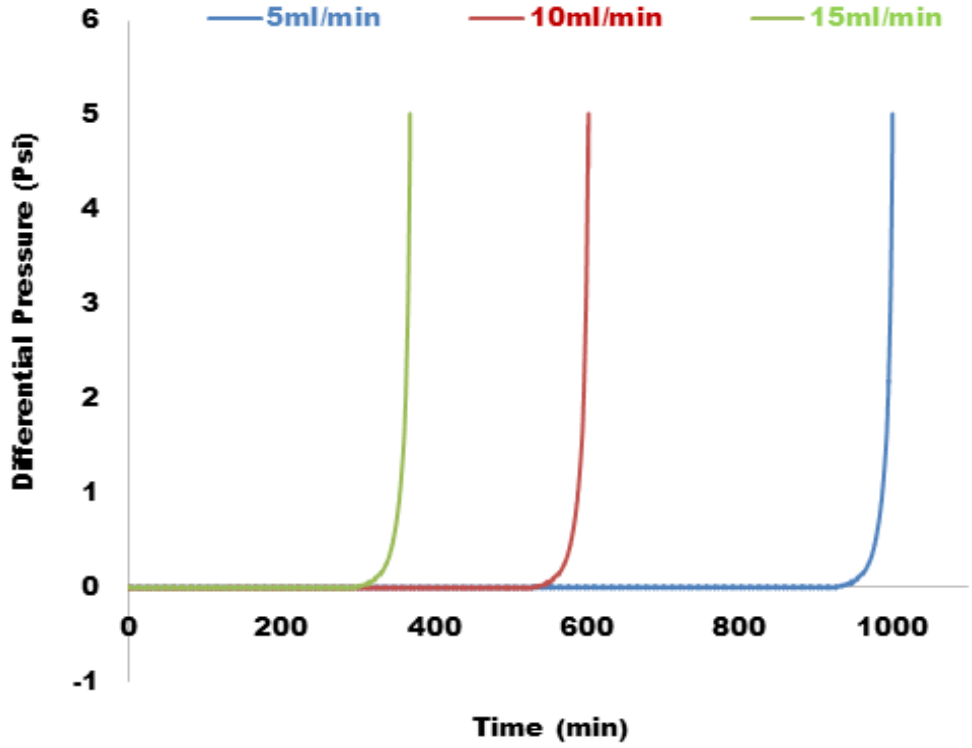

Figure 6-9: Differential pressure as a function of time for saturation ratio 5, 70°C at different flow rates

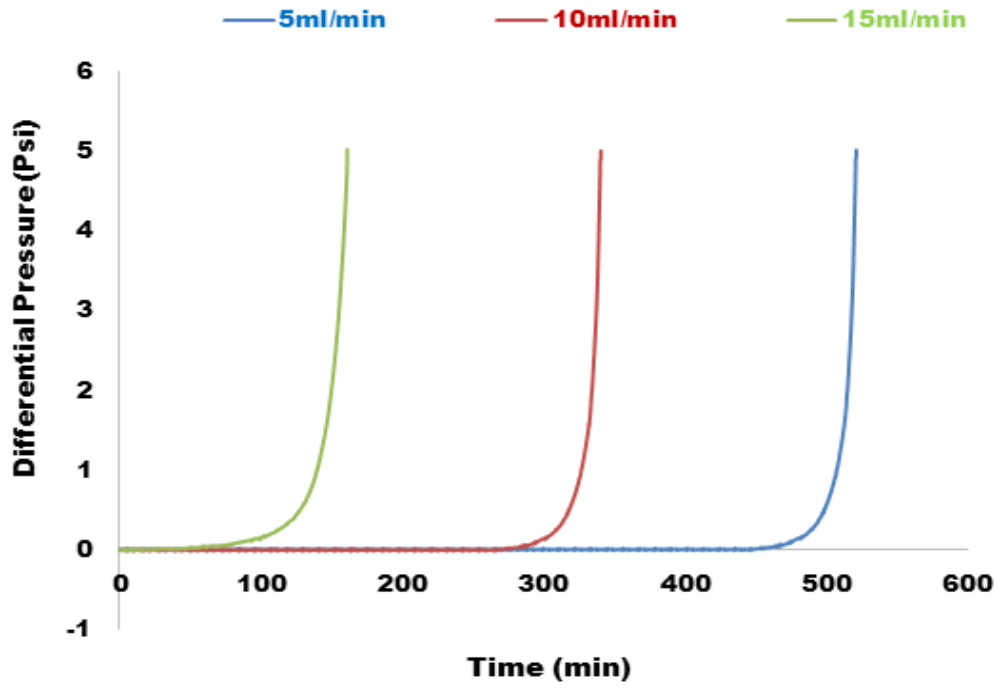

Figure 6-10: Differential pressure as a function of time for saturation ratio 11, 70°C at different flow rates

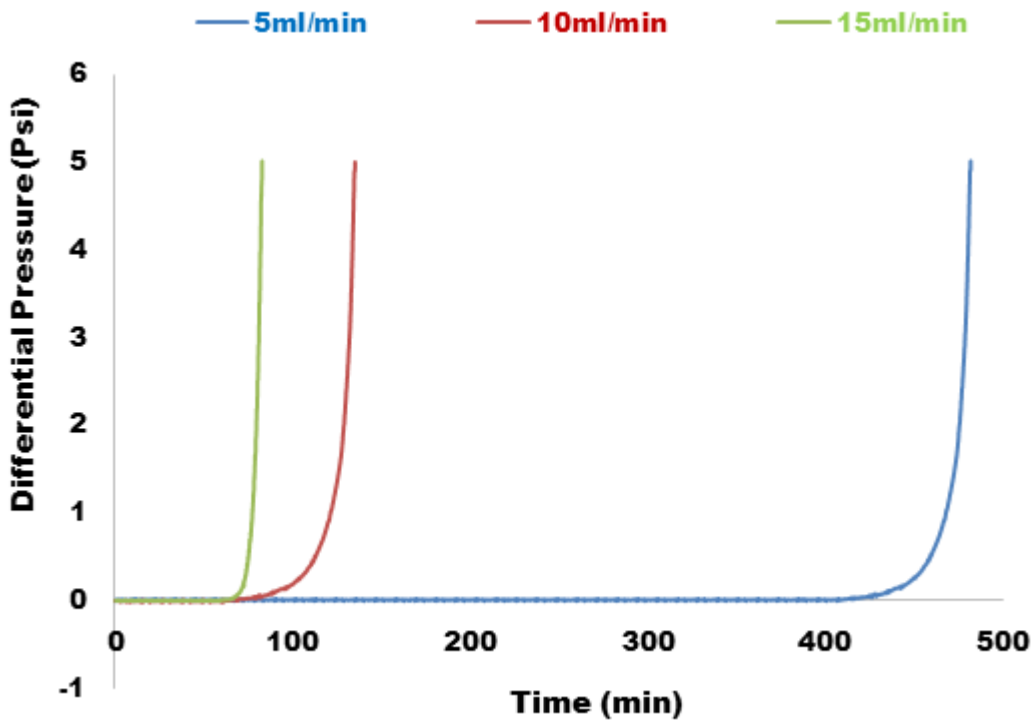

Figure 6-11: Differential pressure as a function of time for saturation ratio 20, 70°C at different flow rates

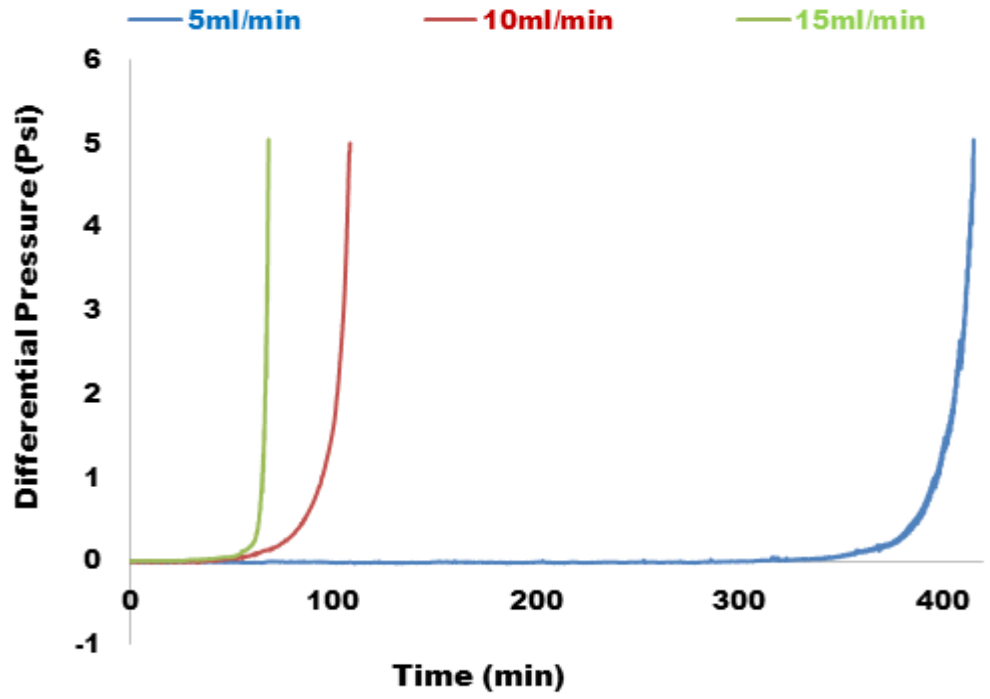

Figure 6-12: Differential pressure as a function of time for saturation ratio 31, 70°C at different flow rates

The results clearly show that, even at the same saturation ratio, temperature has a great influence on the deposition time of calcium carbonate scale. A similar trend was observed for all the saturation values investigated.

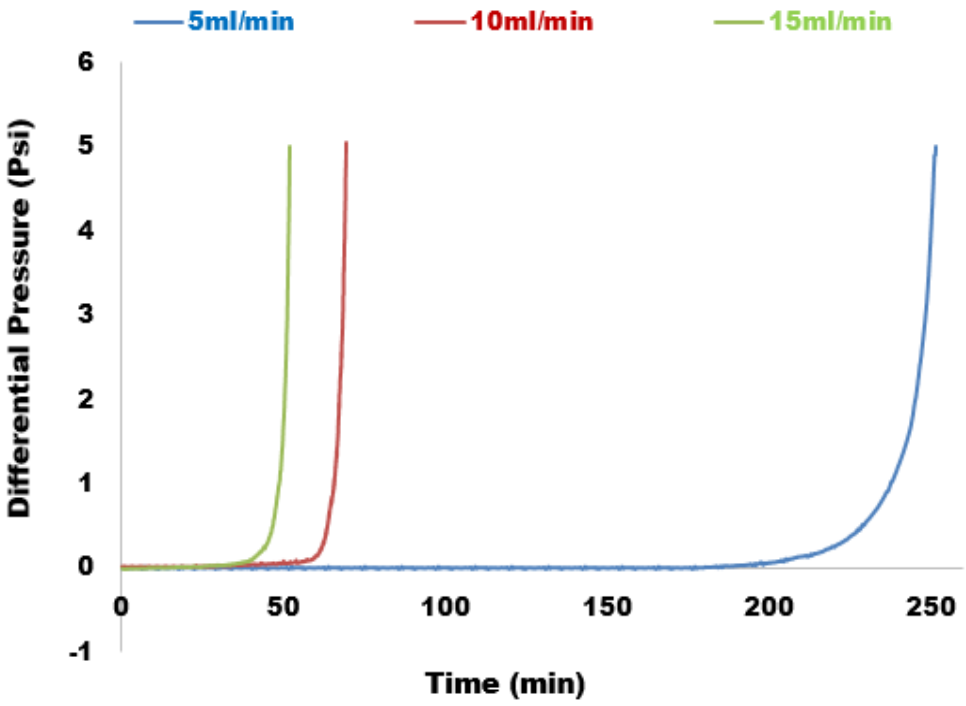

Figure 6-13: Differential pressure as a function of time for saturation ratio 50, 70^{o}C at different flow rates

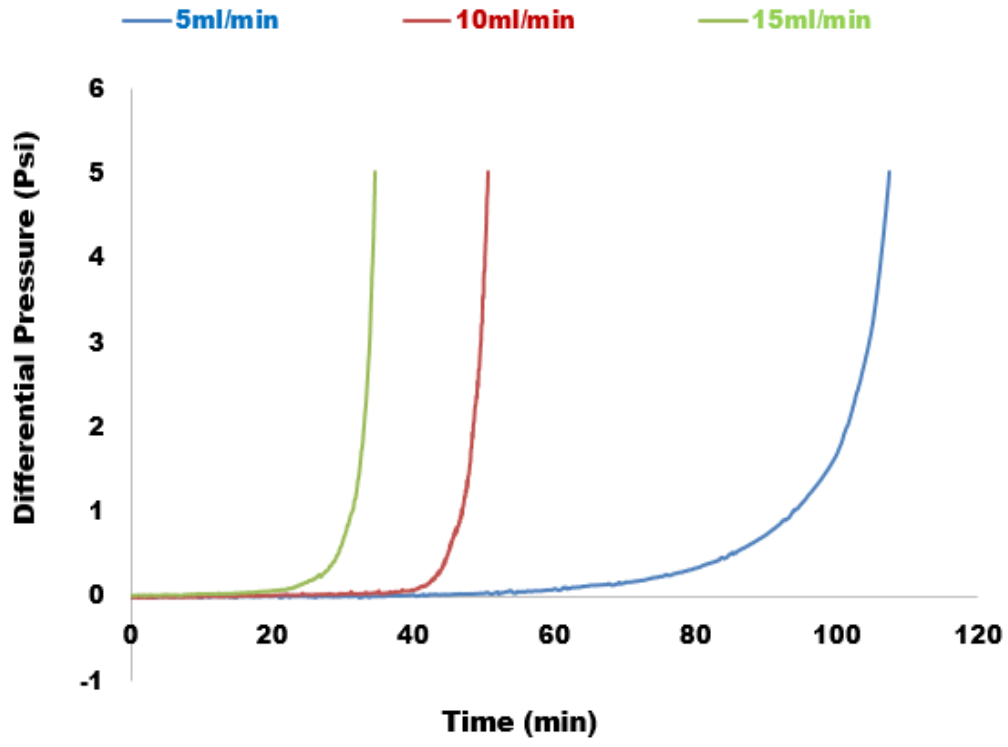

Figure 6-14: Differential pressure as a function of time for saturation ratio 80, 70°C at different flow rates

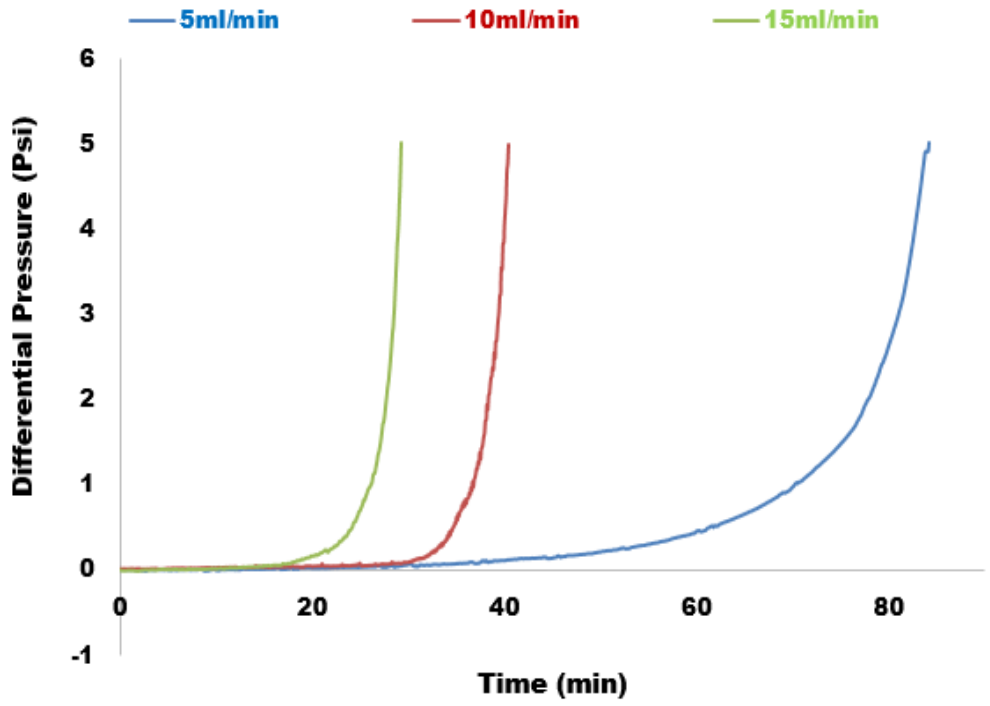

Figure 6-15: Differential pressure as a function of time for saturation ratio 200, 70°C at different flow rates

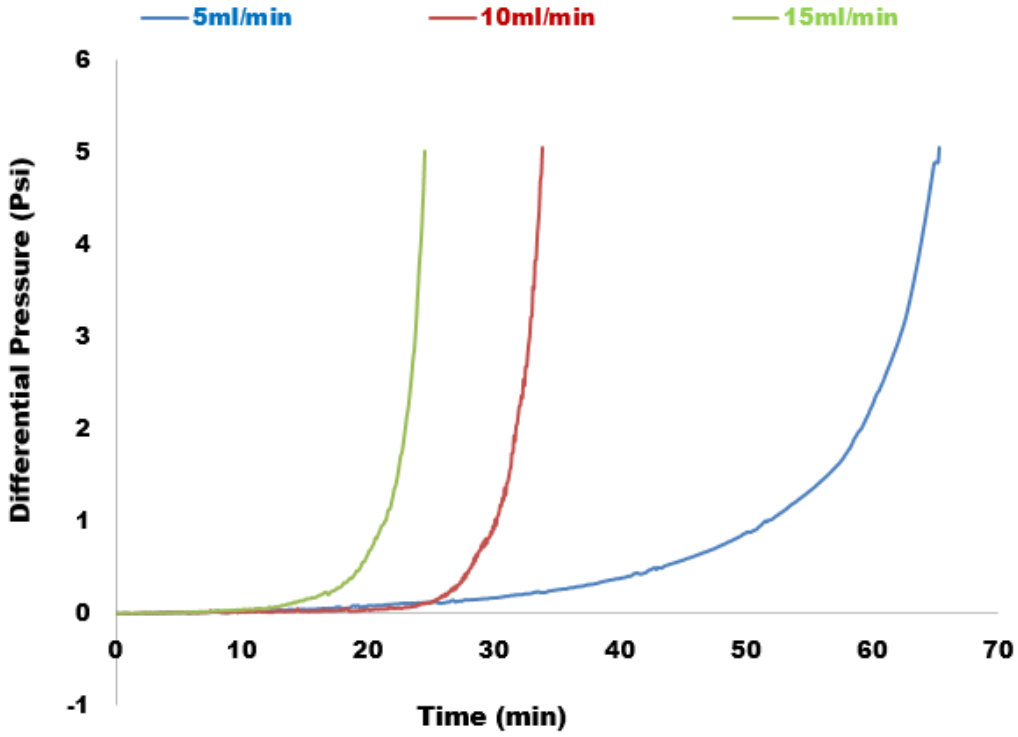

Figure 6-16: Differential pressure as a function of time for saturation ratio 398, 70°C at different flow rates.

The analysis of this data generated from the capillary flow rig and the discussions in relation to nucleation theory, calcium carbonate surface kinetics mechanisms and the growth kinetics are presented in chapter 7 of this thesis to reflect the aims and objectives of the study.

6.2 Scanning Electron Microscope (SEM) observations

The scanning electron microscope was used to support calcium carbonate scale surface deposition results obtained from the capillary rig and bulk analysis results. This technique helps to determine the shape and size of calcium carbonate ($CaCO_3$) scale crystals as they transit from one form to another due to experimental conditions. It is observed from Figure 6-17 to Figure 6-20, that the degree of supersaturation influences the morphology of scale crystals [166-168] and also flow rate changes the morphology of calcium carbonate scale [80, 101].

The SEM images shown in Figure 6-17 to Figure 6-20, indicate that the morphology of calcium carbonate scale crystals changes with flow rate. It is also well known from other studies [78, 169], that apart from degree of supersaturation

and flow rates, there are other factors which could influence the morphology and particle size of calcium carbonate scale crystals such as temperature, pH, ionic concentration of Ca^{2+} and CO_3^{2-} and presence of additives.

At flow rate of 10ml/min, the crystals are predominantly cubic crystals, which are mainly calcite and no traces of aragonite or vaterite crystals. However, calcite crystals became larger at high flow rate of 15ml/min with more aragonite crystals observed for SR 31, compared to a flow rate of 10ml/min which is completely dominated with calcite crystals. A similar trend is observed for SR 50 at 25^{o}C and 70^{o}C respectively.

The SEM image observed is due to high supersaturation value and temperature which enhance the kinetics of the calcium carbonate scale precipitation. There was no presence of vaterite crystals in both conditions. This may be due to the unstable nature of vaterite crystals at high supersaturated solution.

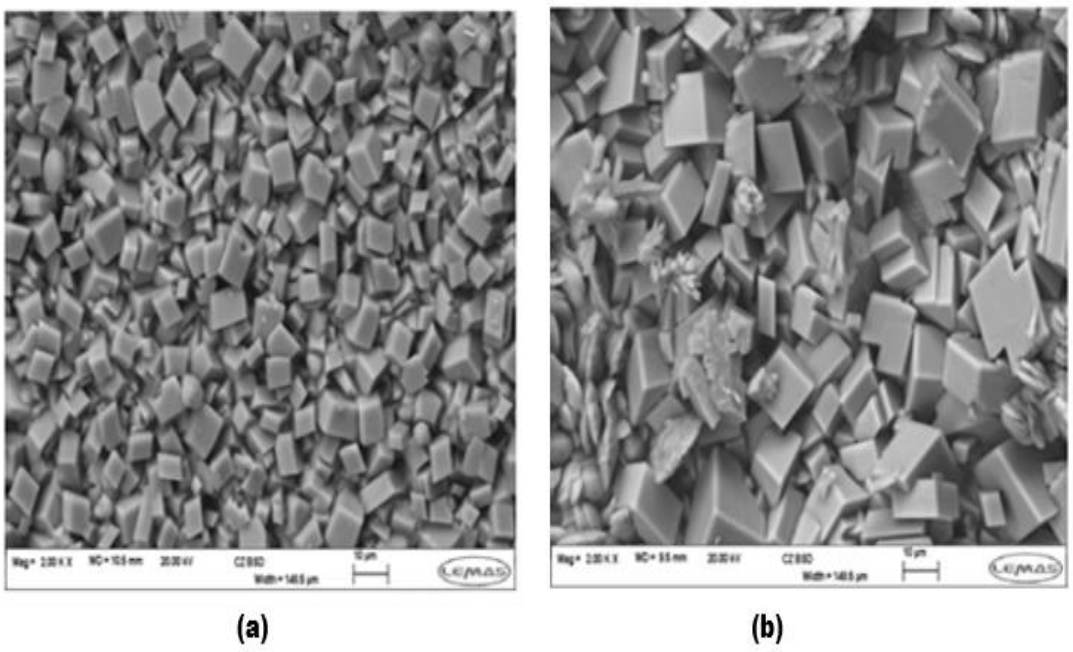

Figure 6-17 : **SEM image of calcium carbonate crystals at SR 31, 25^{o}C for (a) 10ml/min and (b) 15ml/min**

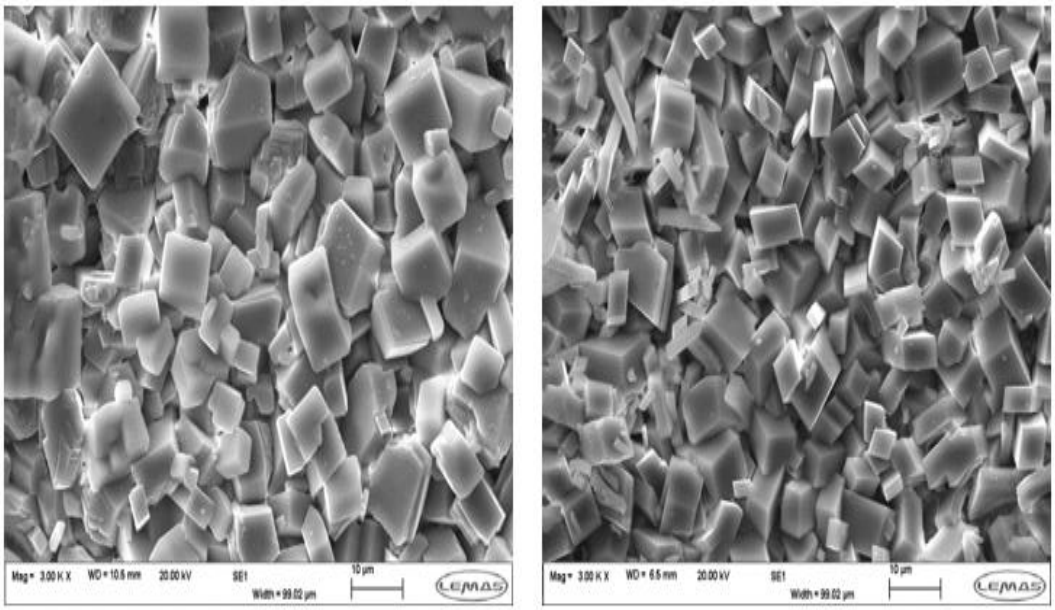

(a) (b)

Figure 6-18: **SEM image of calcium carbonate crystals at SR 50, 25^{o}C for (a) 10ml/min and (b) 15ml/min**

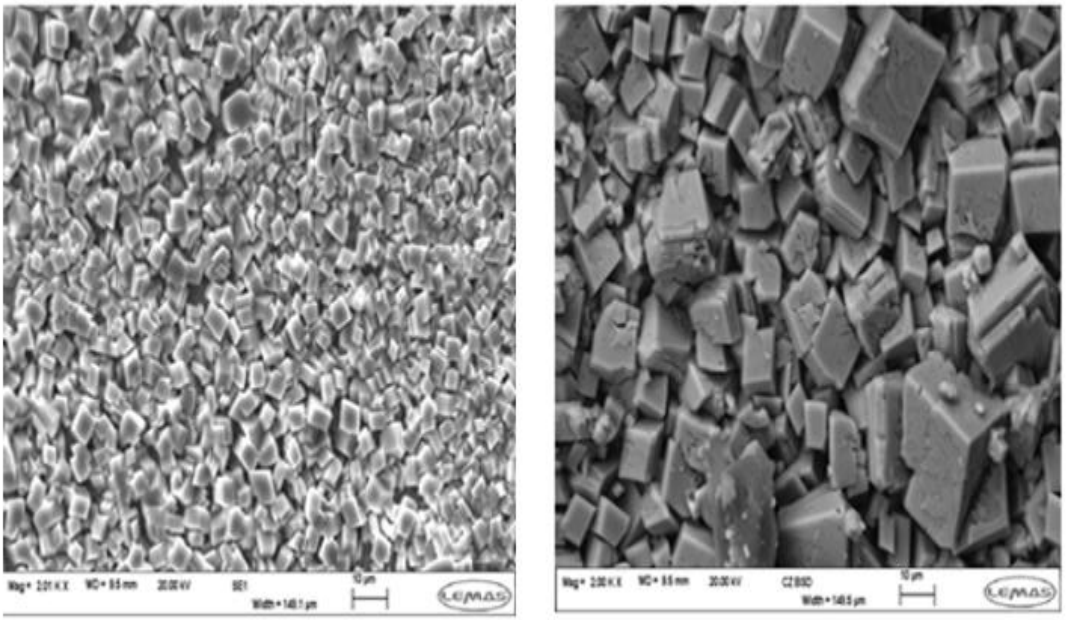

(a) (b)

Figure 6-19: SEM image of calcium carbonate crystals at SR 31, 70^{o}C for (a) 10ml/min and (b) 15ml/min

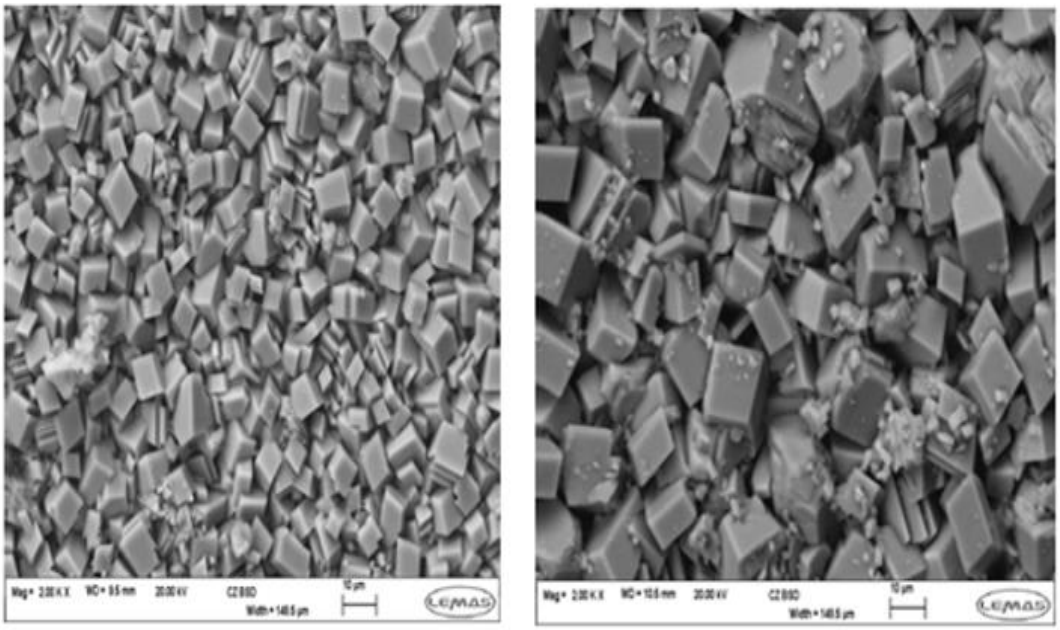

(a) (b)

Figure 6-20: SEM image of calcium carbonate crystals at SR 50, 70ºC for (a) 10ml/min and (b) 15ml/min

6.3 X-ray Diffraction (XRD) Measurements

Figure 6-21 and Figure 6-22 show the X-ray diffraction pattern for saturation ratio of 31 and 50 at 25ºC for flow rates of 10ml/min and 15ml/min respectively. From the results, A denotes aragonite crystals and C denotes calcite crystals. It is observed from the results that, at flow rate of 10ml/min, the crystals are dominated by calcite crystals, but as the flow increases to 15ml/min, the morphology changes with traces of aragonite crystals present on the surface of the stainless steel.

The highest peak obtained at about 29.5º is assigned to calcite, with 51.2º is assigned to aragonite. The few traces of aragonite observed at 25ºC for both flow rates are due to the effect of low temperature on aragonite stability [170], as calcite crystals are more stable at low temperature.

Studies [171, 172], have shown that, at high saturation ratio, a spontaneous formation of calcium carbonate scale crystals clusters on the stainless steel surface is increased due to high precipitation of calcium carbonate scale at high saturation values. In terms of the morphology changes, flow rate has more influence on the morphology of calcium carbonate ($CaCO_3$) scale crystals than

saturation ratio. This is demonstrate in Figure 6-22, the morphologies are similar at both SR 31 and SR 50 and calcite crystals are dominant. The presence of vaterite crystal is not visible, suggesting that, the initial stage of crystallization of calcium carbonate scale is characterized by instability of vaterite and aragonite crystals under flow conditions [18] . These results also show that vaterite crystals are the least stable calcium carbonate polymorphs.

Studies [78, 147, 166, 169] suggested that, the presence of additive such as scale inhibitors, calcium hydroxide $Ca(OH)_2$ could favour the formation of vaterite crystals.

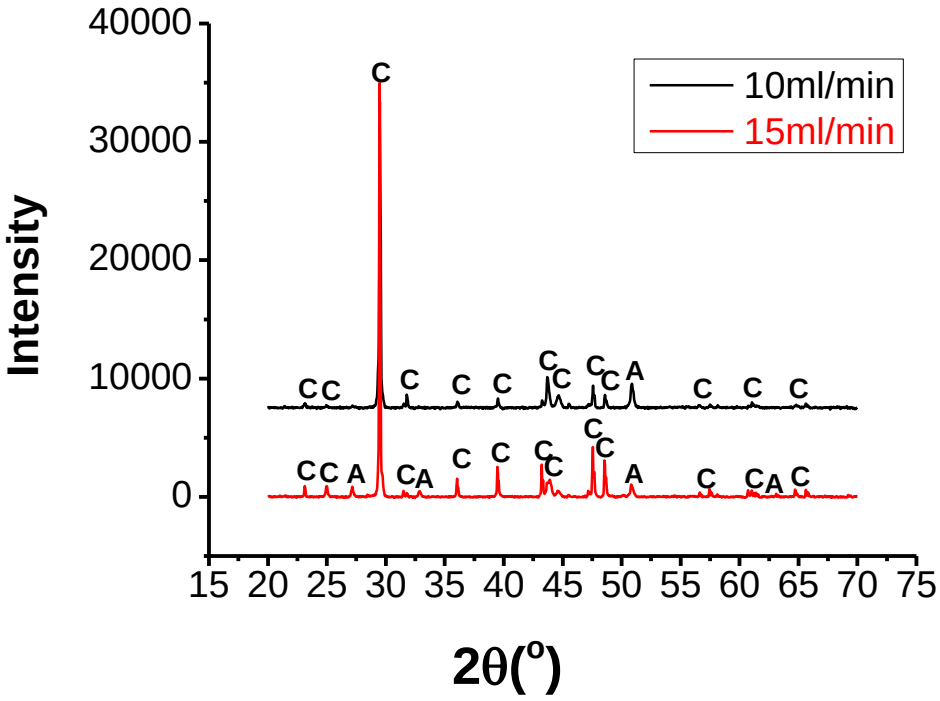

Figure 6-21: **XRD diffraction pattern for calcium carbonate ($CaCO_3$) scale crystals for SR 50 and 25ºC at flow rates 10ml/min and 15ml/min**

A Study by Chen and Neville [115], suggested that, the presences of impurities such as Mg^{2+} speed up the transition of vaterite to calcite crystals formed on substrate surface, that the amount of Mg^{2+} present in the bulk solution determines the proportion of vaterite transition to calcite.

The results observed from the SEM and XRD, suggested that the presence of high proportion of calcite crystals on the surface of the stainless steel maybe due

to the stability of calcite crystals at low temperature and high supersaturation and also the absence of additives or impurities and scale inhibitors in the bulk solution.

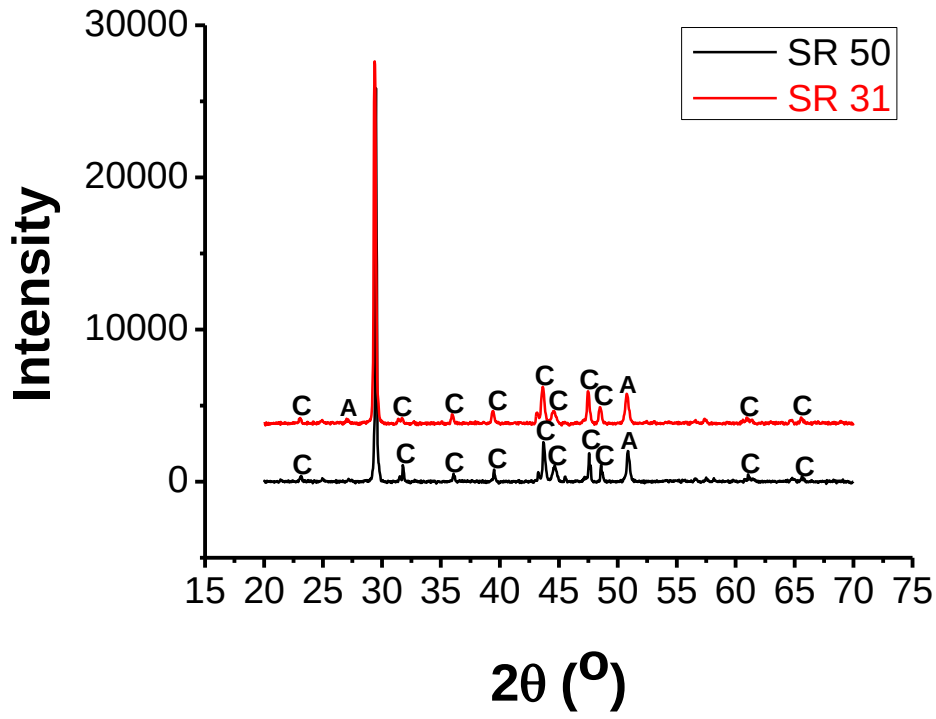

Figure 6-22: XRD diffraction pattern for calcium carbonate scale ($CaCO_3$) crystals at 25°C, 10ml/min for SR 31 and SR 50

6.4 Optical Microscope Images

In an attempt to determine the homogeneity of calcium carbonate crystals deposited on the capillary cell and to reconcile it with the assumption that the scale crystals along the capillary cell is not uniform, optical microscopy observation was carried out.

The optical microscope observations show that, irrespective of the experimental conditions, the calcium carbonate scale crystals layers were not uniform along the capillary cell, which may be more obvious in long capillary tube as in the case of dynamic tube blocking rig, where a long capillary coil of length 1 to 2m is used as the scaling surface.

Figure 6-23 (a-d) show the cross sections of the microscope image observation at different experimental conditions. The microscope image observation show

that the deposition rate of calcium carbonate ($CaCO_3$) scale increases with differential pressure for saturation ratio of 11 as expected. At differential pressure of 5Psi, the amount of calcium carbonate scale deposited on the surface of the capillary cell is higher compared to that at 1Psi.

The optical microscope observations show that, irrespective of the experimental conditions, the calcium carbonate scale crystals layers were not uniform along the capillary cell, which may be more obvious in long capillary tube as in the case of dynamic tube blocking rig, where a long capillary coil of length 1 to 2m is used as the scaling surface.

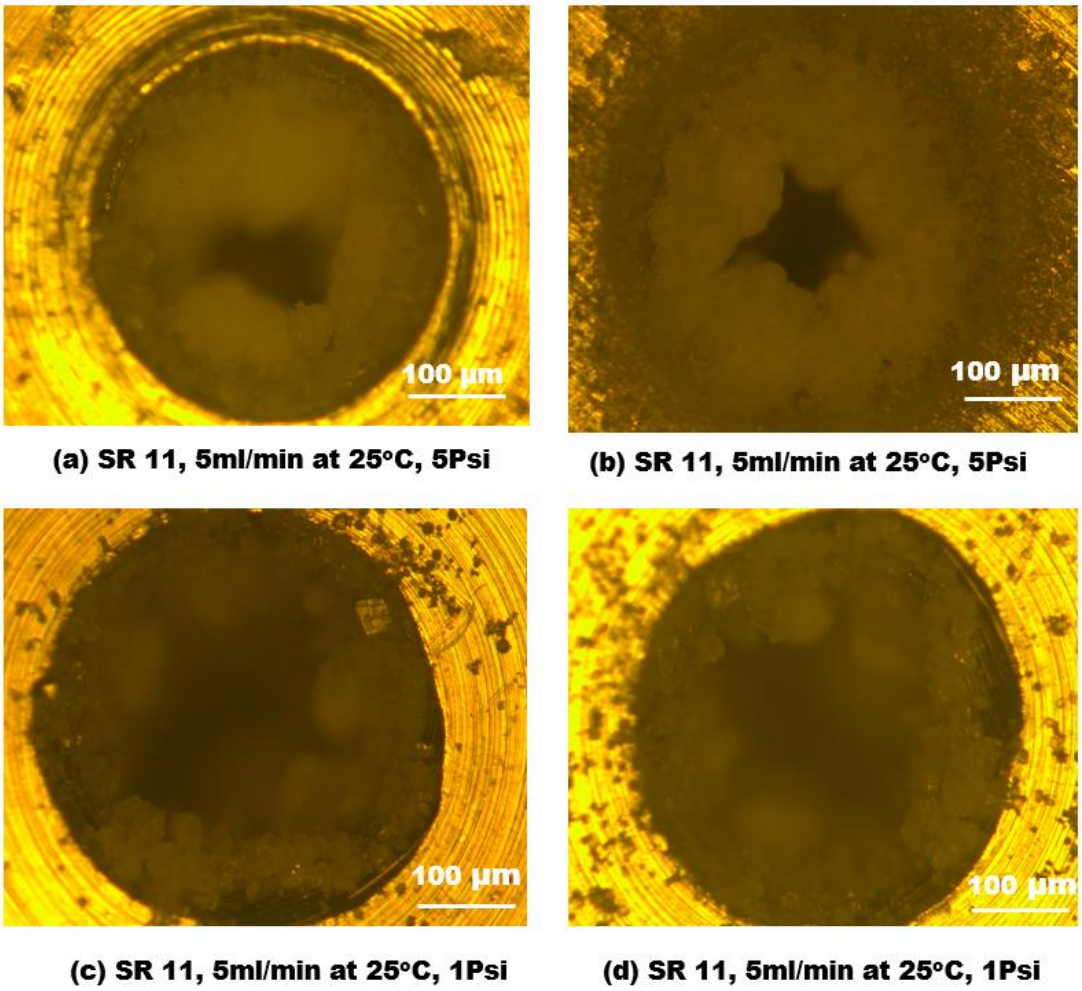

Figure 6-23: Cross sections of optical microscope images at different conditions

6.5 Scaling time and saturation ratio at 25°C and 70°C

The scaling time (t_s), is the time at which the differential pressure deviate from 0 Psi as shown previously in chapter 3 and Figure 6-24. The scaling time (t_s) is similar to the bulk induction time (t_{ind}) for bulk scaling process. Relating the scaling time to saturation ratio gives the understanding of the surface scaling mechanism under flow conditions.

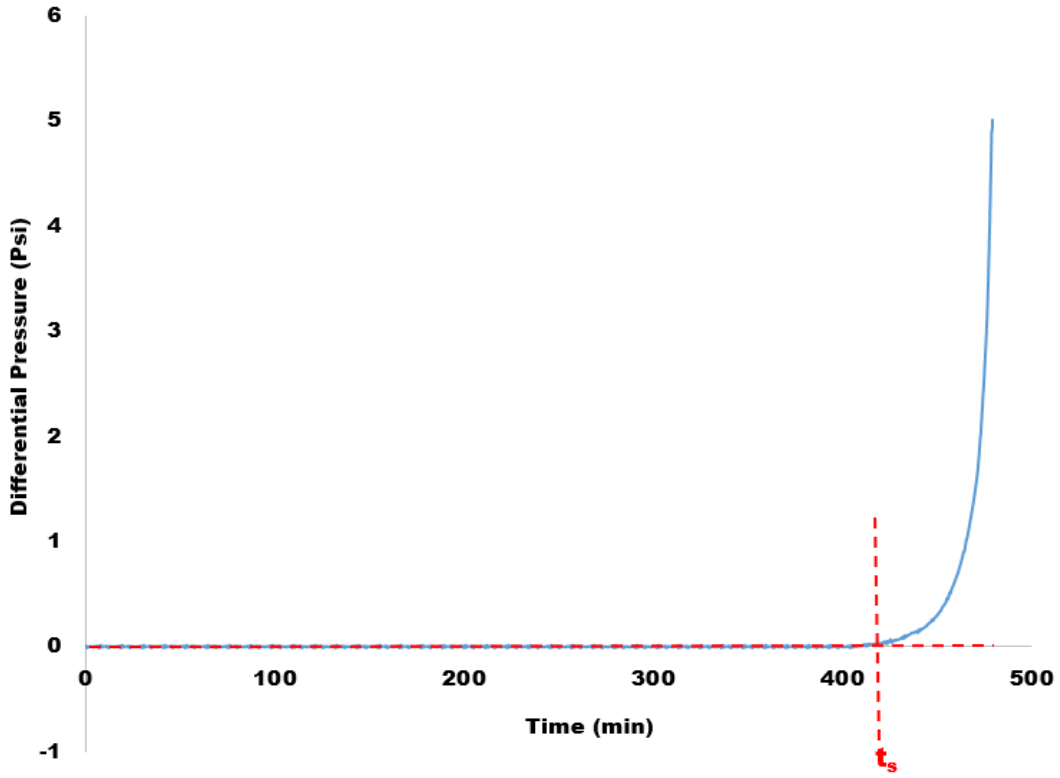

Figure 6-24: Scaling time (t_s) determination

Figure 6-25 and Figure 6-26 shows the relationship between scaling time (t_s) and saturation ratio (SR) for 25°C and 70°C respectively. From the results, it is observed that the scaling time (t_s), is inversely proportional to saturation ratio at different flow rate and temperature. Increased saturation value and flow rate, decrease the scaling time. This observation is in agreement with reported studies [58, 61, 119, 173].

The scaling time is greatly influenced by the degree of supersaturation, flow rate and temperature [58]. Brine with saturation value of 5 has the highest scaling time

of 4120 minutes compared to brine with saturation value of 398 with the lowest scaling time of 61 minutes for 5ml/min and 25°C as shown in Figure 6-25.

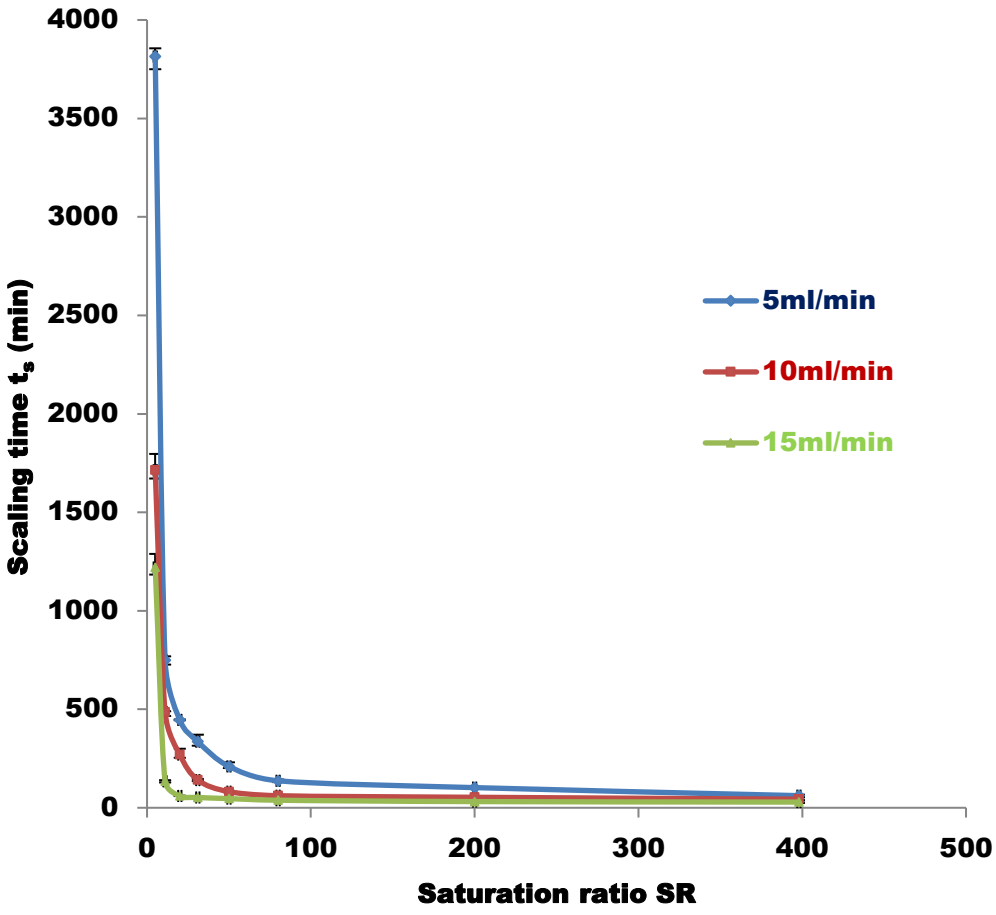

Figure 6-25: Relationship between scaling time t_s and saturation ratio at 25°C

The long scaling time observed at lower saturation ratio, is due to low ionic compositions of the bulk solution, which invariably slow down the nucleation process. At low flow rate, the formation of nuclei is slow resulting from decrease in mass transfer of scaling ions (Ca^{2+}, CO_3^{2-}) in the bulk solution. The motion of scaling ions in the solution determines the collision or reaction rate, which is more rapid at moderate flow rates as observed for a flow rates of 10ml/min and 15ml/min respectively.

At 70°C, the nucleation process was rapid compared to that of low temperature of 25°C. This is because, an increase in temperature increases the kinetic energy of the solution, which in turn increases the reaction rate of calcium ion (Ca^{2+}) and

bicarbonate ion (CO_3^{2-}) leading to rapid formation of calcium carbonate scale, even at the same saturation value. Temperature was the dominant parameter in the scaling process at SR 5 at both 25°C and 70°C (Figure 6-25 and Figure 6-26) where the highest scaling times are 4120minutes and 964minutes respectively.

A similar trends is observed for all flow rates and saturation values investigated in this study. These results clearly shows that the degree of supersaturation and flow rate has great influence on the rate of surface deposition, in agreement with the bulk analysis results.

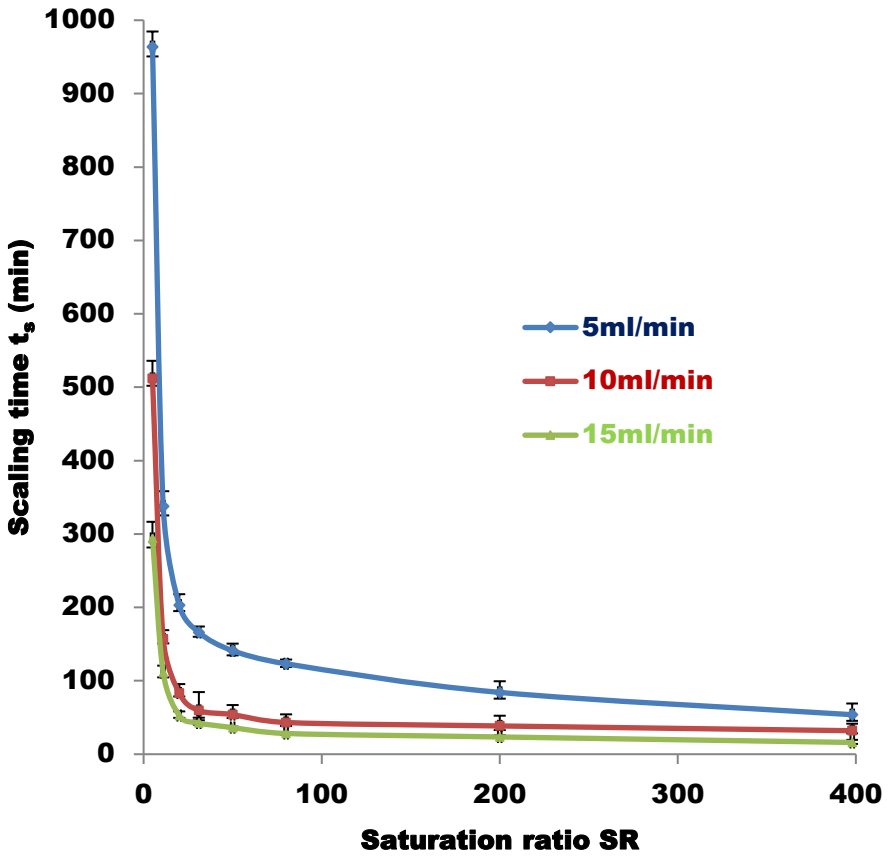

Figure 6-26: Relationship between scaling time t_s and saturation ratio at 70°C

6.6 Summary

The key parameters influencing the precipitation and deposition of calcium carbonate scale ($CaCO_3$) was clearly demonstrated from the raw results obtained.

The effect of flow rate on calcium carbonate scale deposition rate is due to the collision or motion of scaling ions in the bulk solution. The collisions of ions increases as the flow rate is increased, invariably leading to rapid formation of calcium carbonate scale. On the other hand, the adherence of this scale to the surface of the capillary cell is depended on different factors such as interfacial tension, wettability, surface roughness, flow regime etc. Details of these factors will be discussed in chapter 7.

The flow rate also affects the morphology of calcium carbonate scale crystals. Calcite crystals were more prominent at low flow rates, while traces of aragonite crystals were observed as the flow rate increased.

The optical microscope observations shows that the calcium carbonate crystals were not uniform along the capillary cell, which might be the reason for the difference in the amount of calcium carbonate scale determine by ICP-MS measurement and Hagen Poiseuille flow assumptions.

Temperature and degree of supersaturation has also shown a great influence on the deposition rate of calcium carbonate ($CaCO_3$) scale as their effect was significant in calcium carbonate scale deposition time obtained at different experimental conditions investigated.

Chapter 7 provides the detailed analysis of the raw results obtained from this chapter and discussions in relation to nucleation theory, calcium carbonate ($CaCO_3$) scale surface deposition mechanism, growth kinetics and empirical models established in this work.

CHAPTER 7. Discussion

7.1 Introduction

Calcium carbonate ($CaCO_3$) scale is one of the most widely studied inorganic scale types; different mechanisms and prediction models of its formation have been proposed by researchers over the years, but there are some challenges in terms of understanding its formation mechanisms under flow conditions. Having a reliable model that can predict its formation as a function of time and other environmental conditions is a real and timely challenge.

Understanding both *bulk* and *surface* scaling processes of calcium carbonate scale deposition could enable reliable strategies for mitigating its formation in the field to be developed. The previous two chapters of this work showed the results obtained from the capillary flow rig experiments in relation to both surface and bulk scaling processes for different environmental conditions.

This chapter presents the analysed results from chapter 5 and 6 and a discussion of calcium carbonate scale surface deposition mechanisms in relation to nucleation theory, surface deposition mechanisms, growth kinetics and $CaCO_3$ empirical models established for predicting surface scaling processes.

This chapter is split into the following key points.

- Nucleation theory
- Adhesion and crystallization mechanisms
- Determination of classical nucleation theory parameters
- $CaCO_3$ scale deposition growth kinetics
- $CaCO_3$ surface empirical models

7.2 $CaCO_3$ scale surface deposition mechanism

The mechanisms by which calcium carbonate ($CaCO_3$) scale can form on the surface of the capillary cell in relation to the results obtained from the capillary rig experiment, nucleation theory and scaling time (t_s) are analysed and discussed in this chapter.

Chapters 5 and 6 showed the results of how various factors such as temperature, flow rate and degree of supersaturation influence the bulk precipitation and surface deposition of calcium carbonate ($CaCO_3$) scale.

The scaling time (t_s) is similar to the bulk induction time (t_{ind}) for bulk scaling processes. It is defined as the time the differential pressure deviates from 0 Psi as presented in chapter 6, Figure 6-24. It is assumed that at t_s there is no scale build-up on the capillary cell surface as such the onset differential pressure remain the same. A period after t_s, there is rapid increase in differential pressure indicating the period of accelerated nucleation and growth of $CaCO_3$ crystals.

Relating t_s to SR can give the understanding of the *surface* scaling mechanisms under flow conditions. Consequently the constants that describe the nucleation theory can be determined from the relationship between (log t_s) and (log SR)^2 [57, 58] as shown in equation 7-1 and 7-2.

$$\log(t_s) = \left[A + \frac{B}{T^3(logSR)^2}\right] \qquad 7\text{-}1$$

$$B=\frac{\beta\gamma^3 Vm^2 NA\, f(\theta)}{(1.3R)^3} \qquad 7\text{-}2$$

From equation 7-1 and 7-2 [57], the main parameters governing the rate of nucleation are, temperature, saturation ratio and interfacial energy

Where γ denotes the interfacial energy (mN/m), V_m is the molecular volume of crystals ($6.132x10^{-23}$ cm^3 for calcite), T the temperature (K), SR the saturation ratio, t_s the scaling time (s), A an empirical constant (dimensionless), R the molar gas constant (J/mol.K), N_A denotes the Avogadro's constant (mol^{-1}),$f(\theta)$ is a correction factor depending on the type of nucleation, β is a geometric factor of $\frac{16\pi}{3}$ for spherical shape crystal.

The induction period has often been used as a quantitative method for assessing the nucleation process, but it is sometimes challenging in getting an accurate measurement in some chemical substances due to its complexity, techniques and the influence of some external factors. This work focuses on a *surface* scaling process in relation to saturation ratio, flow rate and temperature.

7.3 Adhesion and crystallization mechanism

The deposition of calcium carbonate ($CaCO_3$) scale on the surface of the capillary cell can occur either by adhesion of pre-precipitated scale or a heterogeneous nucleation (surface crystallization process).This two processes can occur simultaneously within a given range of brine saturation ratios.

Adhesion occurs when surfaces have an affinity to one another by intermolecular forces such as valence forces. The scale crystals can attach to the wall of the capillary cell either by nucleated crystals being transported to the surface of the capillary cell or by agglomerating in the bulk where they attach to the surface of the capillary cell. This process can occur through intermolecular forces such as Van der Waals force, electrostatic interaction and chemical bonding [81-83, 174, 175]. Adhesion of the crystals to the surface of the capillary cell is dependent on the nature of the crystals, substrate (capillary cell) and the experimental conditions or the environment.

A schematic diagram of the adhesion process is shown in Figure 7-1.

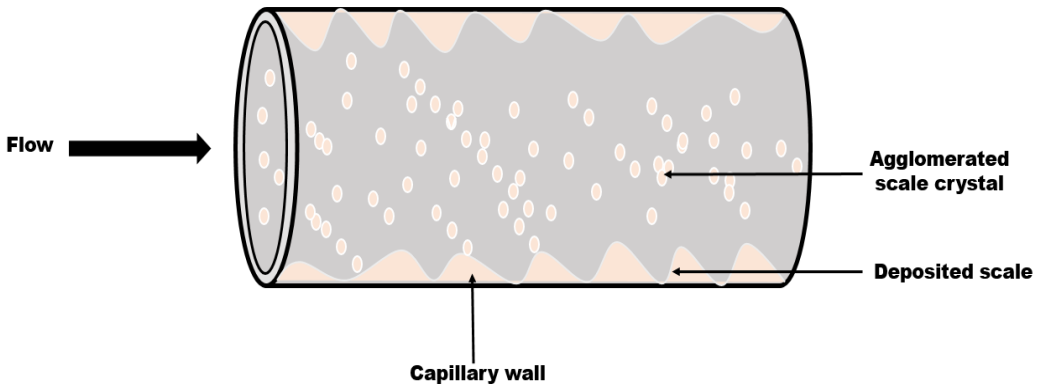

Figure 7-1: Scale deposited on the wall of capillary cell by heterogeneous nucleation and adhesion

The surface roughness of the capillary cell, wettability, contact angle and the interfacial energy are the main parameters that determine the stability or adherence of calcium carbonate scale crystals to the wall of the capillary cell. However, there are other factors which influence adhesion processes such as flow rate, temperature and solution concentration [99, 176, 177].

The other principal mechanism by which the scale layer can form is by crystallization at the surface, where the crystals are surface nucleated and grow directly from the scaling ions in the bulk solution as shown in the schematic diagram in Figure 7-2.

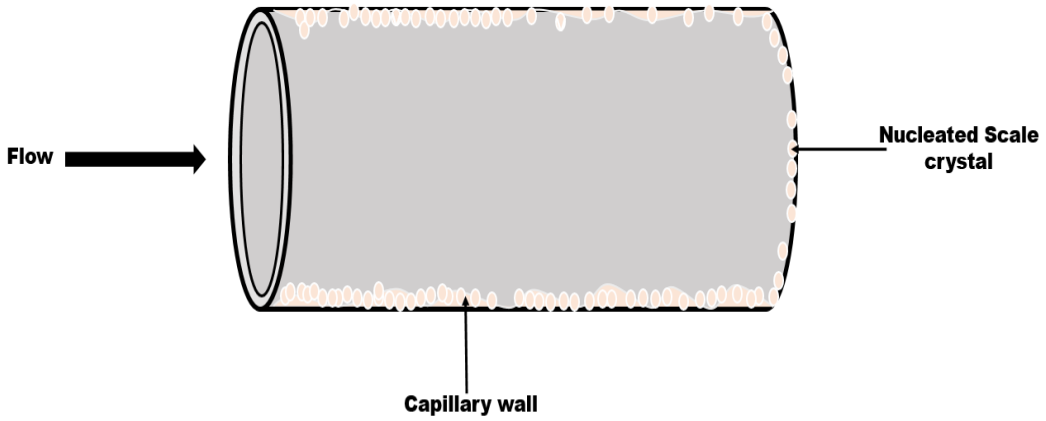

Figure 7-2: Scale deposited on the wall of the capillary cell by crystallization process

In this study, the interfacial energy of the crystals to the surface of the capillary cell was determined from the relationship between log t_s and $(\log SR)^{-2}$ for heterogeneous nucleation process (crystallization process) show in Figure 7-5 and Figure 7-6 for 25^{o}C and 70^{o}C respectively.

Calcium carbonate scale deposition rate was greatly influenced by flow rate as shown in chapter 6, where the deposition time decreased with increased flow rate. It should however be noted that the streamline forces resulting from increased flow rate did not have significant impact on the adherence of the crystals to the walls of the capillary cell rather it increased the mass transfer of the scaling ions (Ca^{2+}, CO_3^{2-}) leading to rapid formation of calcium carbonate scale. This observation could be due to the flow regime (laminar flow) used in this work.

In the case of turbulent flow, studies [1, 10, 56] have shown that, the scaling tendency may be slow. This is due to high streamline forces resulting from increased flow rate, invariably affecting the adherence of crystals to the walls of the capillary cell and also, the number of nuclei formed on a substrate surface per unit area is increased with increased flow rate, indicating that, at high flow rate, nucleation time is reduced [93].

Flow rate also influences the shear stress, increasing the flow rate, resulting in high shear stress. High shear stress changes the kinetics of a flow system. This increases the scale formation rate due to rapid agglomeration and deposition of scale on the surface of the capillary cell. The wall shear stress of the capillary cell are 0.76, 1.5, 2.3, 3.03, and 4.55N/m^2 corresponding to a flow rates of (5, 10, 15, 20 and 30ml/min), even at high shear stress, the surface fouling is dominant over the removal of scale.

The $CaCO_3$ scale deposition rate at saturation value greater than 80, (SR > 80) increase rapidly with flow rate, resulting to a decrease in capillary cell blocking time. This is in the agreement with the work of Bazin et al [10], where a dynamic tube blocking rig was used to evaluate the efficiency of different mineral scale inhibitors. The capillary cell blocking time was a lot faster at higher saturation values and flow rates. This is due to the effect of high supersaturation on calcium carbonate scale deposition rate as the kinetics mechanism at this condition maybe due to heterogeneous nucleation and adhesion of pre-precipitate crystals.

However, the force of interaction of the scale crystals to the wall of the capillary cell is greatly influenced by the concentration of the scaling ions in the bulk solution (Ca^{2+} , CO_3^{2-}), which accounts for the electric potential of the crystal surface and the capillary surface [178]. This is clearly demonstrated at high saturation ratio (SR > 80).

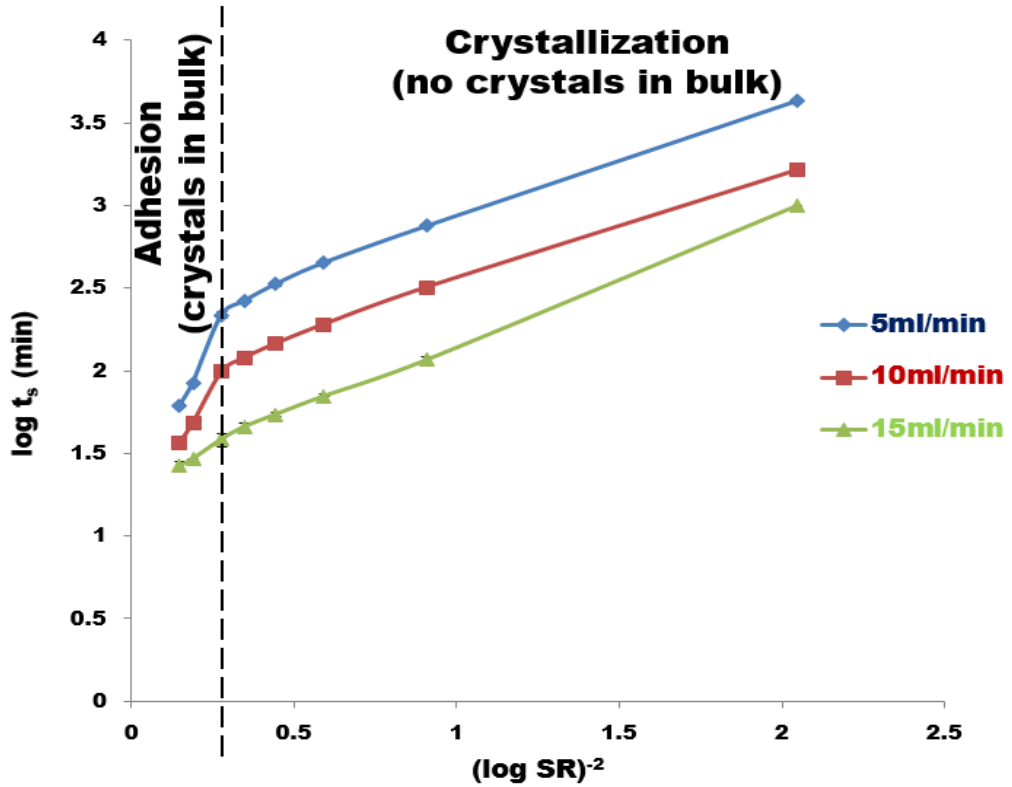

Figure 7-3: Relationship between log t_s and $(\log SR)^{-2}$ at 25°C

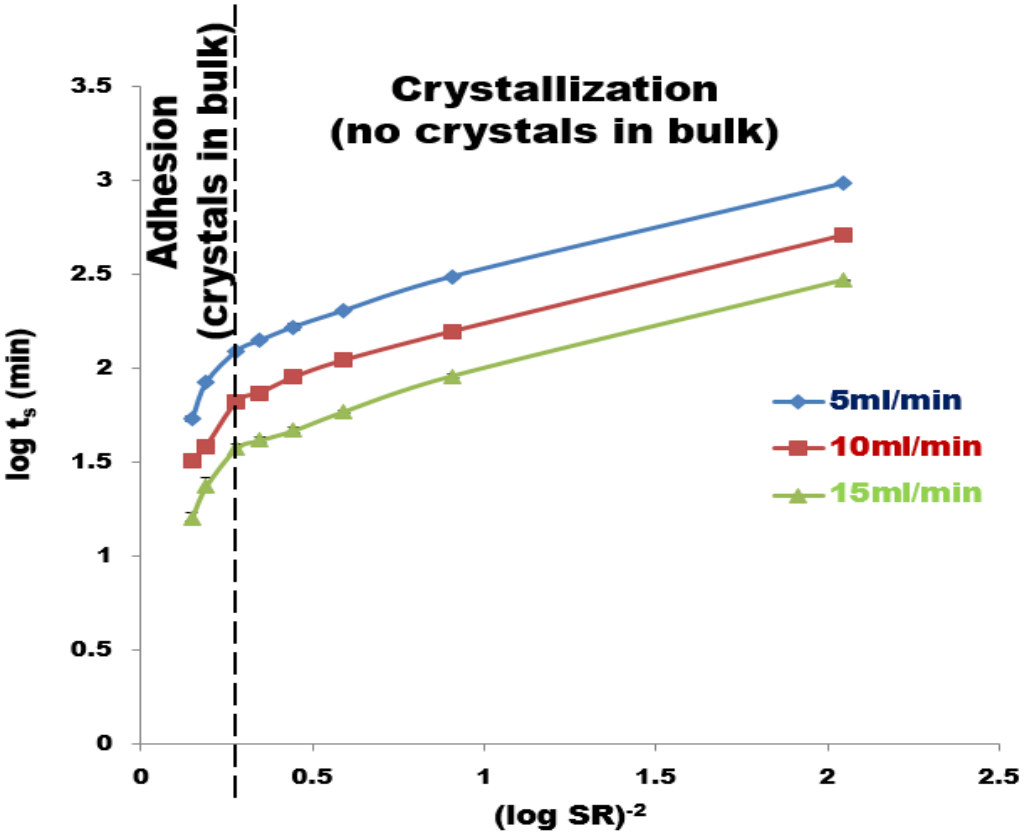

Figure 7-4: Relationship between log t_s and $(\log SR)^{-2}$ at 70°C

Supersaturation is the driving force for crystallization, according to classical nucleation theory [57], the main parameters governing the rate of nucleation are, temperature, saturation ratio and interfacial energy as shown in equation 7-1 and 7-2. The effects of saturation ratio and temperature on calcium carbonate scale nucleation processes were presented in chapter 6.

From this work, the relationship between this factors were established to determine the boundary between the processes that occurs within the brine composition investigated as shown in Figure 7-3 and Figure 7-4 for 25^{o}C and 70^{o}C respectively. This boundary is based on the fact that crystals were or were not seen in the bulk solution as stated previous in the bulk analysis study.

Figure 7-3 and Figure 7-4 show the relationship between log t_s and (log SR)$^{-2}$ at 25^{o}C and 70^{o}C respectively, from the results, the surface scaling kinetic mechanism were substantiated within the saturation ratios investigated.

It is observed that, there is a linear relationship between log t_s and (log SR)$^{-2}$ at lower saturation values (SR < 80), indicating heterogeneous nucleation which is purely crystallization process. In this mechanism, the nucleation process is driven by presence of foreign material and nucleation occurs at the nucleation site. The scaling time of this brines were quite slow due to the chemical composition or ionic strength of the bulk solution.

However, at high saturation values (SR > 80), calcium carbonate scale is form due to heterogeneous nucleation and adhesion. This is indicated at the left hand section of Figure 7-3 and Figure 7-4. The scaling process is driven by mass transport of nucleated crystals or agglomerated crystals in the bulk solution to the surface of the capillary cell where they adhere and grow.

This process is influenced by the concentration of the scaling ions in the bulk solution as a result, the surface charge density is affected by the ionic strength of the scaling ions in the bulk solution. As such, at high concentration of scaling ions (Ca^{2+}, CO_3^{2-}), the force of interaction between calcium carbonate scale crystals and the surface of the capillary cell is increased [176].

A study by Sohnel and Mullin [59], suggested that, there is linear relationship between log t_s and (log SR)$^{-2}$ at constant temperature for variety of substances,

however the linear relationship is within a defined range of saturation values. That is, there is a level of supersaturation where two nucleation mechanism occurs within the relationship as in the case of calcium carbonate scale ($CaCO_3$), where the plot of log t_s versus $(\log SR)^{-2}$ is separated into two part, with each curve having a gradient.

This two mechanisms were reported as homogeneous and heterogeneous nucleation. In this work, the plot of log t_s versus $(\log SR)^{-2}$ is separated into two section with the left part is predominantly heterogeneous nucleation and adhesion, while the right part is predominantly heterogeneous nucleation and growth (crystallization process). This is in agreement with bulk analysis test results obtained in chapter 5 of this work.

Similar trends occur for both temperatures (25^{o}C and 70^{o}C). This clearly show that at constant temperature, there is a linear relationship between log t_s and $(\log SR)^{-2}$, which is in agreement with other studies [28, 58, 59, 179].

7.3.1 Determination of parameters that define nucleation theory

Prediction of calcium carbonate scale formation is often based on thermodynamic prediction models. The bulk induction time is used as key parameters for scaling tendency of inorganic scales.

However, there are studies [28, 58, 63, 180, 181], where emphasis is on bulk induction time with respect to the saturation ratio in establishing a predictive models for calcium carbonate scale deposition process.

Surface scaling is the main challenge affecting the integrity of facilities in oil and gas and desalination industries. Understanding the mechanism of *surface* scaling processes and determining the parameters that influence the deposition of calcium carbonate scale on the surface of the facilities under flow conditions, can give a reliable predictive models for *surface* scaling deposition processes.

The results obtained from the relationship between scaling time (t_s) and saturation ratio (SR) from chapter 6 was analysed and fitted into nucleation theory equation, as such the parameters that describe the nucleation theory was determined from crystallization process plot shown in Figure 7-5 and Figure 7-6 for 25^{o}C and 70^{o}C respectively.

Rearranging equation 7-1

$$\log t_s = A + B \times T^{-3}(\log SR)^{-2} \qquad 7\text{-}3$$

The calculated parameters for nucleation theory and the interfacial energy at different flow rates for 25°C and 70°C respectively are summarised in Table 7-1 and Table 7-2 respectively.

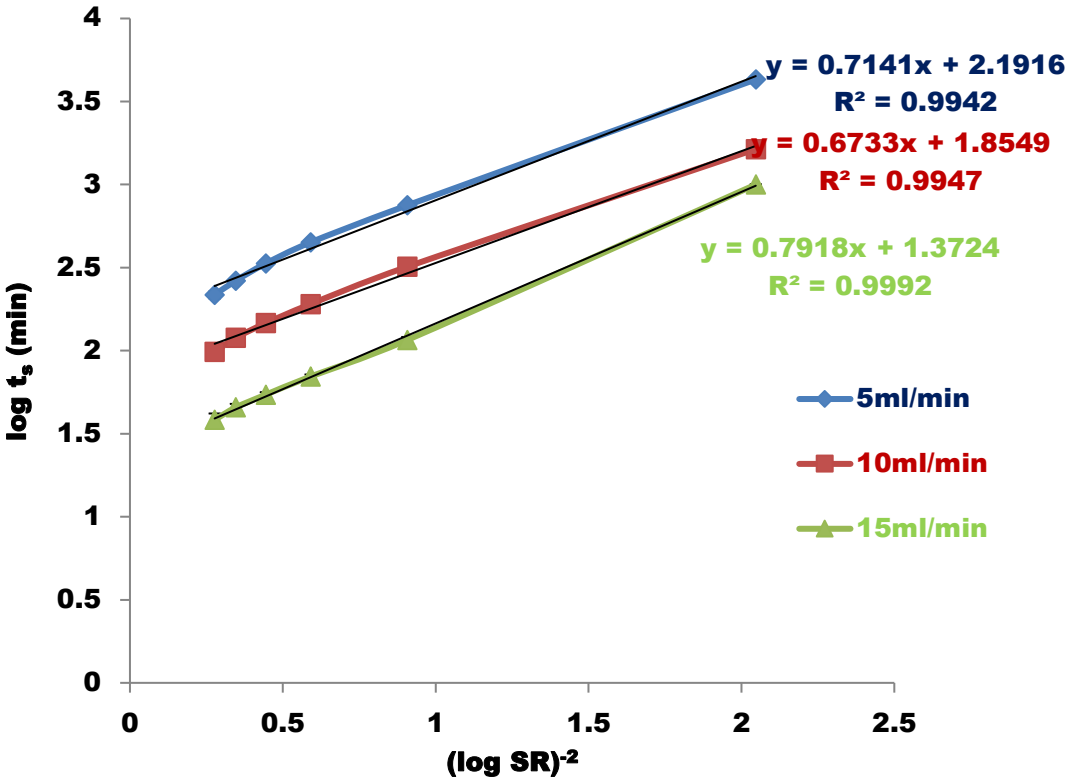

Figure 7-5: Relationship between log t_s and (log SR)$^{-2}$ at 25°C for heterogeneous nucleation (crystallization process)

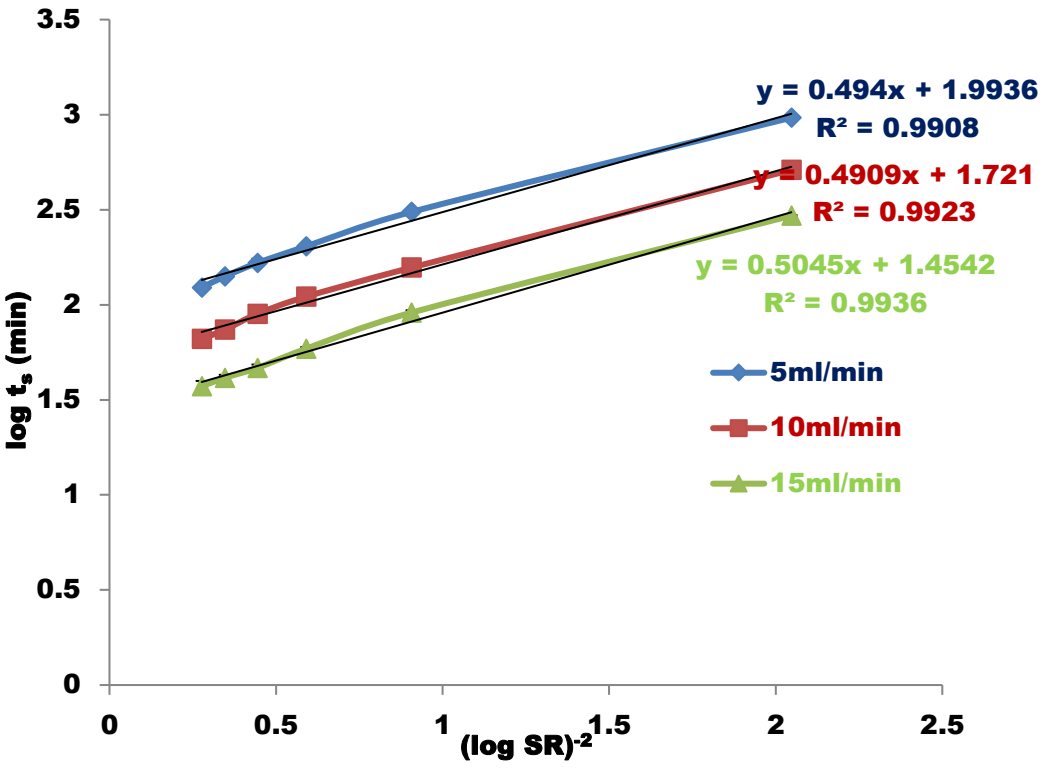

Figure 7-6: Relationship between log t_s and $(\log SR)^{-2}$ at 70°C for heterogeneous nucleation (crystallization process)

The interfacial energy values obtained for $CaCO_3$ at 25°C range from 0.038 to 0.040 mJ/m^2 compared to values between 25 to 83 mJ/m^2 obtained from previous studies [65, 69, 182, 183]. The difference in the interfacial energy values obtained could be due to the differences in techniques used for this study, the experimental conditions, the nature of crystals formed and heterogeneous nucleation process taking place. However saturation ratio varies, as most studies focused on bulk induction time from bulk scaling processes.

Spanos and Koutsoukos [182], reported in their study that very low interfacial energy values is attributed to heterogeneous nucleation process, while high interfacial energy relate to invalid hypothesis on data analysis. This hypothesis was also supported by study [69]. They estimated the interfacial energy for different calcium carbonate scale polymorphs, as each polymorphs have different interfacial energy values due to their crystalline structures.

Table 7-1: Crystallization parameters based on nucleation theory values at 25°C

Flow rate (ml/min)	A	B	γ (mJ/m^2)	R^2
5	2.1916	1.89×10^7	0.0387	0.9942
10	1.8549	1.78×10^7	0.0380	0.9947
15	1.3724	2.1×10^7	0.0400	0.9992

Table 7-2: Crystallization parameters based on nucleation theory values at 70°C

Flow rate (ml/min)	A	B	γ (mJ/m^2)	R^2
5	1.9936	1.99×10^7	0.0453	0.9908
10	1.7210	1.98×10^7	0.0452	0.9947
15	1.4542	2.04×10^7	0.0456	0.9992

The empirical relationship between log (t_s) and (log SR)$^{-2}$ were established with the values of constants A and B is determined from the intercepts and gradient of Figure 7-5 and Figure 7-6.

For flow rate of 5ml/min at 25°C, $\log(t_s) = 2.1916 + \frac{1.8\times 10^7}{T^3(logSR)^2}$ 7-4

For flow rate of 5ml/min at 70°C , $\log(t_s) = 1.9936 + \frac{1.99\times 10^7}{T^3(logSR)^2}$ 7-5

The empirical relationship shown in equation 7-4 and 7-5 is a step towards developing a semi empirical model for predicting surface scaling time of calcium carbonate scale within the environmental conditions considered in this work.

Having a predictive model for both *surface* and *bulk* induction time under flow condition and across a wide range of saturation ratios, could give more reliable strategists for preventing or mitigating scale deposition and precipitation on the surface of facilities. However, caution should be exercised when applying this models to system of high turbulent regime, temperature and water salinity as the empirical relationship may not be valid. These conditions may affects the adherence of scale crystals.

7.4 Calcium carbonate ($CaCO_3$) scale deposition growth kinetics

Calcium carbonate scale precipitation and deposition mechanism have been studied over the years using different techniques such as quartz crystal microbalance (QCM), rotary cylinder electrode (RCE), static bulk jar test, and dynamic tube blocking rig etc.[108, 148, 171, 184-186].These studies were based on determination of the growth kinetics through bulk analysis, gravimetric measurement of weight gain and/or also in-situ measurement in the case of QCM.

The QCM techniques is efficient at investigating the early stages of $CaCO_3$ deposition on the surface of substrate, the static bulk jar test and dynamic tube blocking rig is often used for ranking of inhibitors, while the rotary cylinder electrode is used for $CaCO_3$ scale study under flow conditions.

However, these techniques have some challenges with respect to understanding the initial stage and later stages of calcium carbonate scale deposition growth kinetics across a wide range of supersaturation values, temperature, pressures and flow rates. It is therefore important to use a technique that can give a better understanding of calcium carbonate scale growth kinetics. And also will that will reflect the field conditions, for a more efficient and reliable method of estimating growth rate.

This section of this work presents the analysed results and discussions of calcium carbonate scale growth rate obtained at different experimental conditions. This is one of the key aspect of this work and steps towards establishing an empirical model for predicting calcium carbonate scale deposition growth rate across a wide range of saturation ratios.

Recalling from chapter 3, Figure 3-12. Calcium carbonate scale deposition growth rate (G_R) were determined from the ratio of the amount of $CaCO_3$ scale measured by ICP-MS measurement (M_C) to the difference in the deposition time (t_{5Psi}) and scaling time (t_s) as shown in Figure 7-7 and equation 7-6.

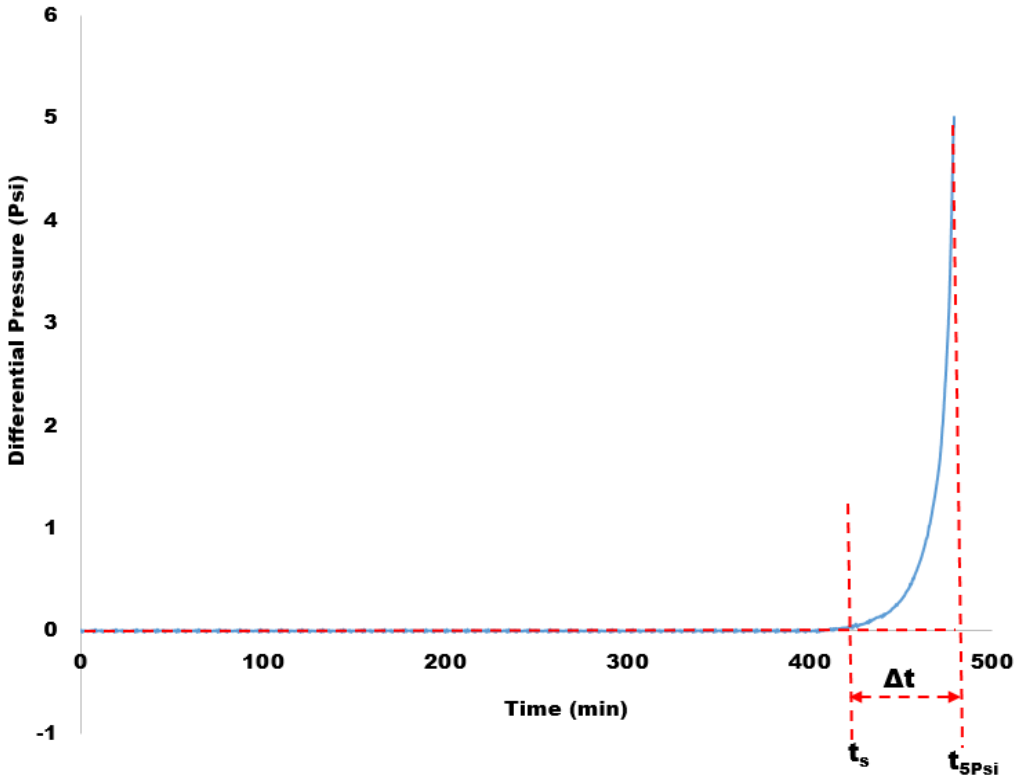

Figure 7-7: Determination of $CaCO_3$ scale growth rate

The amount of calcium carbonate scale ($CaCO_3$) deposited were converted to $CaCO_3$ scale deposition thickness by assuming a uniform deposition of scale crystal along the capillary cell and the crystal deposited as calcite, as previously mention in chapter 3.

$$\text{Scale deposition growth rate } (G_R) = \frac{\text{scale deposition thickness (cm)}}{(T_{5Psi} - t_s)} \qquad 7\text{-}6$$

7.5 Calcium carbonate ($CaCO_3$) scale deposition growth kinetics at 25°C and 70°C

The average growth rate of calcium carbonate scale as a function of saturation ratio at different flow rates is shown in Figure 7-8 to Figure 7-11 for 25°C and 70°C respectively. The average growth rate increase sharply with increased saturation ratio for (SR <80) as expected for both temperatures [187]. For saturation ratios (SR> 80), the average growth rates were not affected by increased saturation ratio, rather forms a plateau which correspond to the mechanism observed at high saturation ratios (SR>80) for the plot of log t_s versus $(\log SR)^{-2}$ shown in previous section of this work.

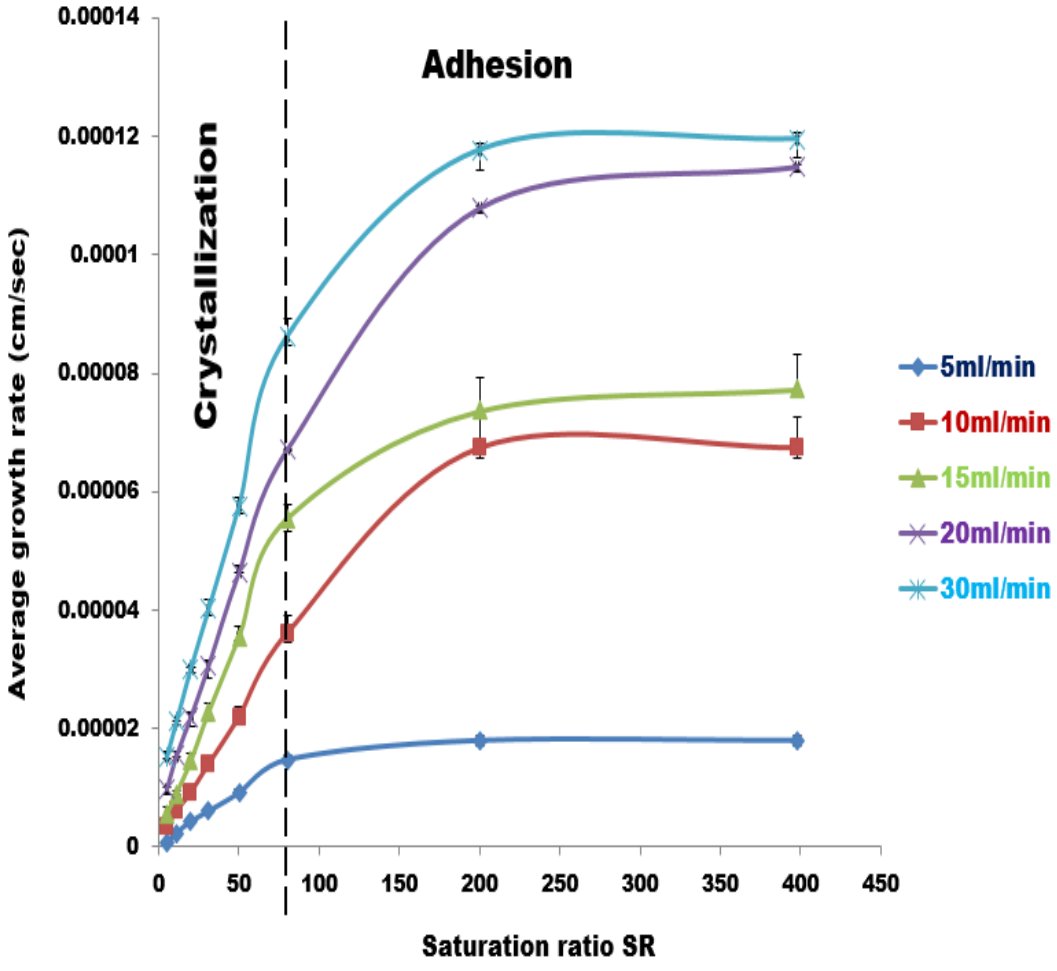

Figure 7-8: The average growth rate as a function of saturation ratio at 25°C

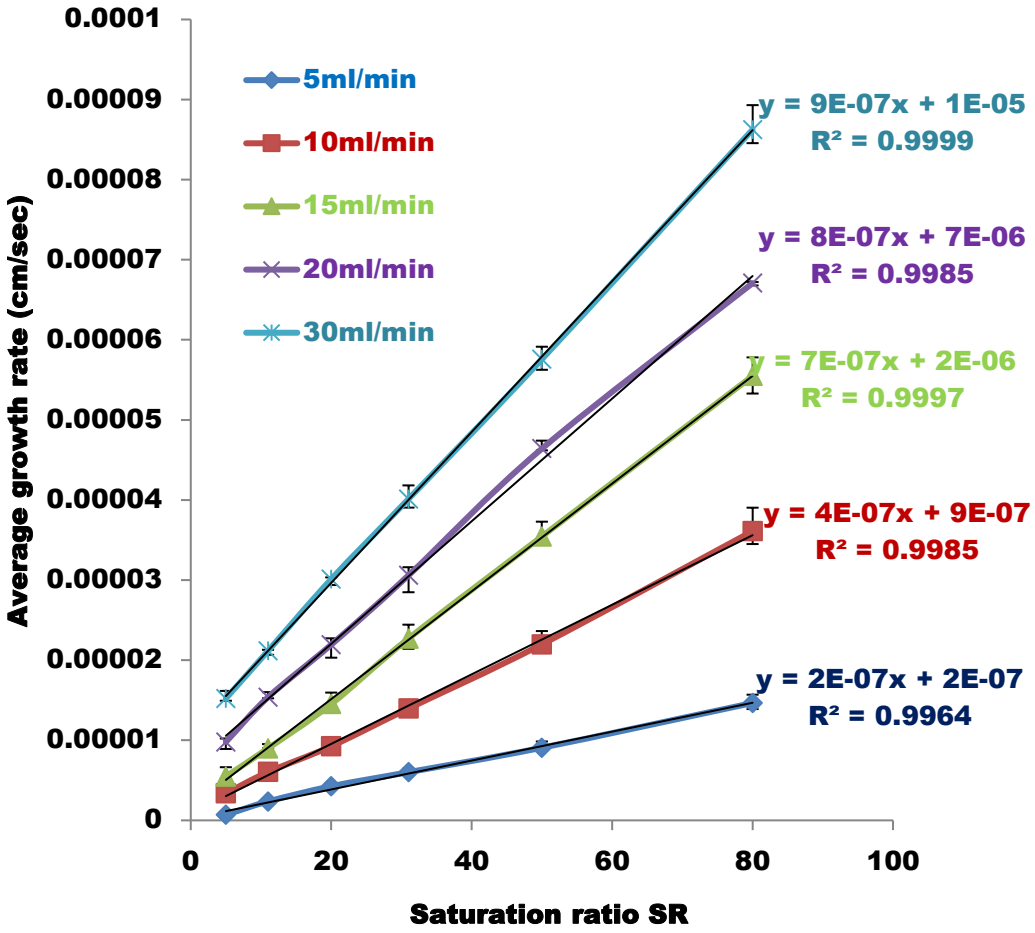

Figure 7-9: The average growth rate as a function of saturation ratio at 25ºC

The plots shows clearly that two different scale deposition mechanism were observed in the brine composition investigated. At saturation ratios (SR < 80), the scale is form due to crystallization process as the formation of calcium carbonate scale crystals is driven by the degree of the ionic strength and the motion of scaling ions (Ca^{2+}, CO_3^{2-}) in the bulk solution. The deposition time decrease with increased saturation ratio and flow rate, which invariably result to increase in average growth rate observed.

The trend is different for saturation ratios (SR >80) as the scale mechanism is predominantly adhesion of pre-precipitated crystals from the bulk solution. The agglomerated crystals in the bulk solution are transported to the surface of the capillary cell where they adhere and grow, which result to plugging of the capillary cell bore, as such increasing the flow rate and the ionic strength or concentration of the bulk solution, do not have significant effect on the average growth rate.

The average growth of calcium carbonate scale at 70ºC, 5ml/min is (1.89×10^{-6} cm/sec or 0.6mm/year), much higher compared to the average growth rate of calcium carbonate scale at 25ºC, 5ml/min (6.87×10^{-7} cm/sec or 0.22mm/year) for saturation ratio of 5 as expected. This is due to the effect of temperature on the rate of precipitation and deposition of calcium carbonate scale. Similar trends is observed in other conditions investigated.

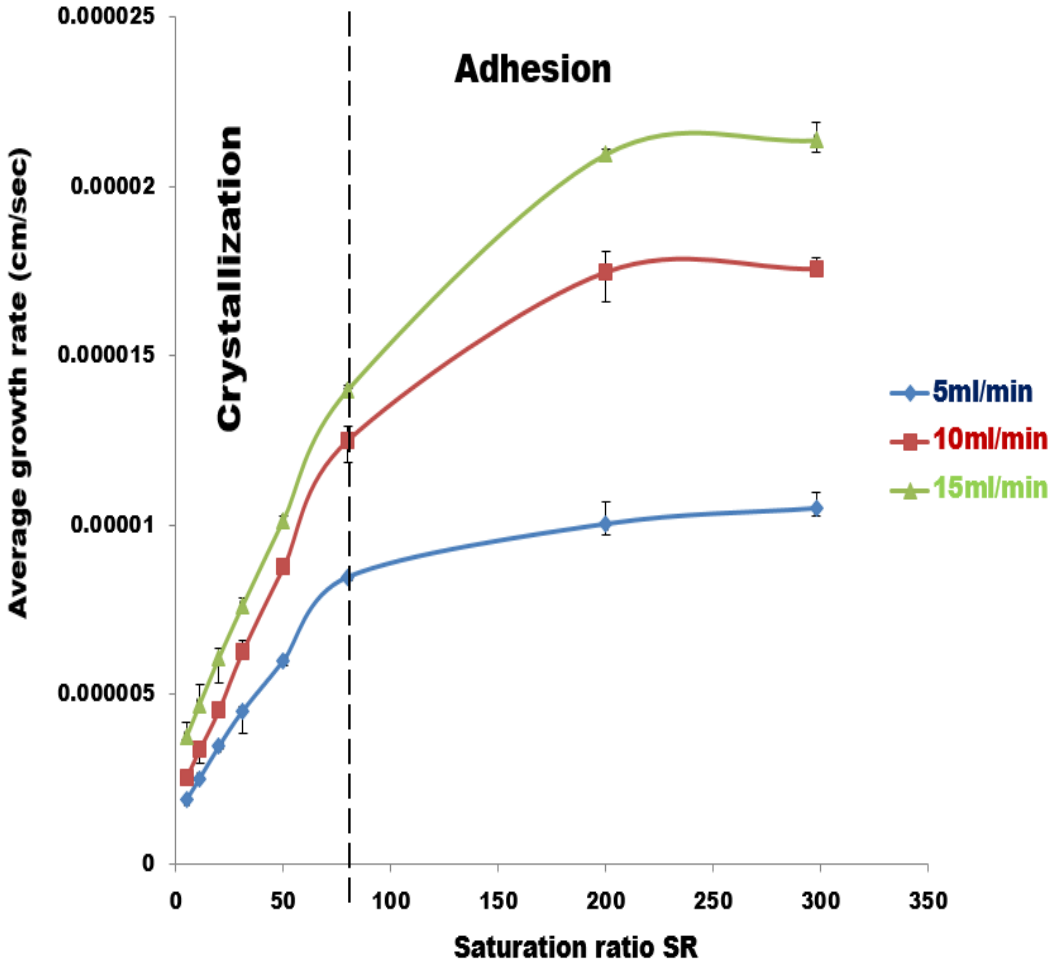

Figure 7-10: The average growth rate as a function of saturation ratio at 70ºC

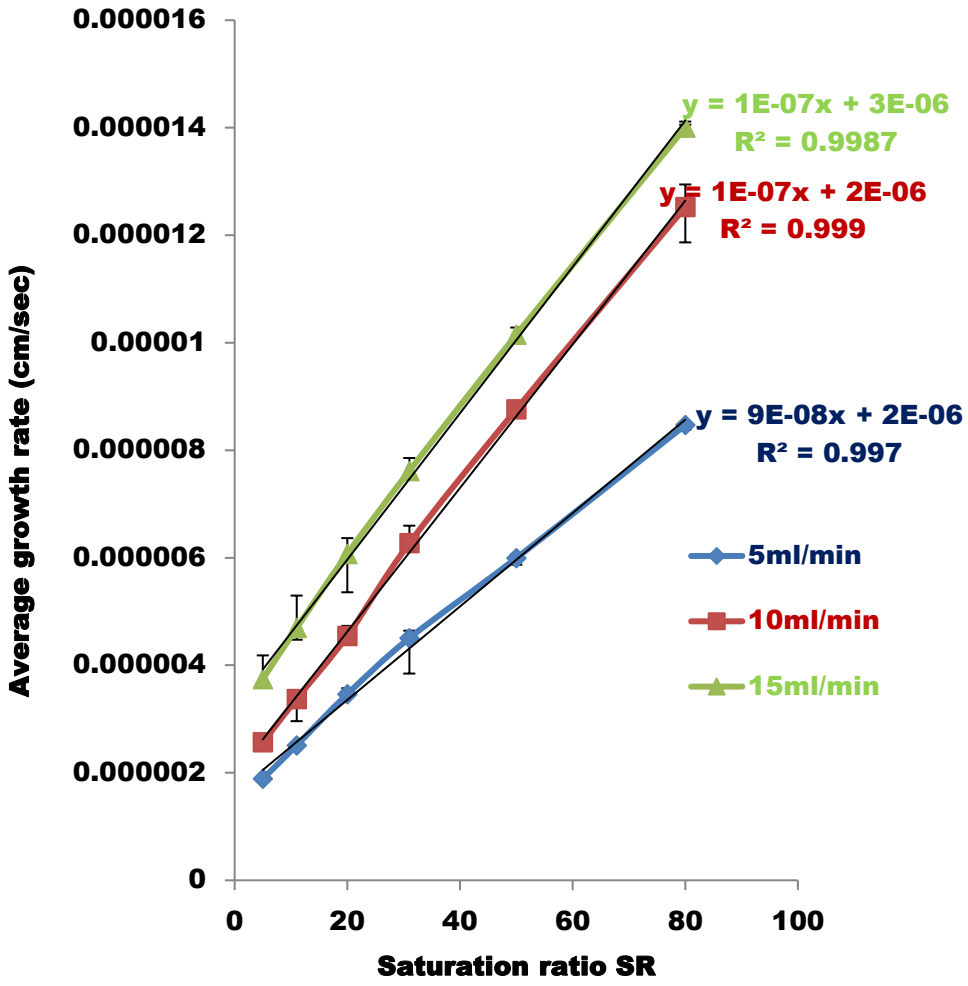

Figure 7-11: The average growth rate as a function of saturation ratio at 70ºC

The growth rate obtained from this work range from 6.87×10^{-7} cm/sec to 1.29×10^{-5} cm/sec for $CaCO_3$ test conducted at 25ºC. This is in close agreement with the growth rate obtained by Tai et al [188] where crystal growth rate of calcite was investigated as a function of ionic strength using a fluidized-bed crystallizer. Tai's study obtained growth trend between 4.2×10^{-7} cm/sec to 7.2×10^{-7} cm/sec for $CaCO_3$ at 25ºC. The study reported that the growth rate of calcite is greatly influenced by the concentration of calcium ion, carbonate ion and the fluid dynamics of the system. A linear relationship between the growth rate of calcite and the saturation ratio was obtained. The crystal growth process was said to be controlled by surface integration [188].

Growth rate values of 3×10^{-7} cm/sec to 9×10^{-7} cm/sec was also obtained by Weijden et al [189] for $CaCO_3$ at 25°C. The study reported that the growth rate of calcium carbonate scale increased with ionic strength of bulk solution and that linear growth rate of calcite is a function of the degree of the scaling ions (Ca^{2+} and CO_3^{2-}) in the bulk solution.

Table 7-3, shows the comparison of calcium carbonate scale deposition growth rate obtained from this work and other literatures values.

Table 7-3: Comparison of calcium carbonate scale deposition growth rate with literatures values

Techniques	Study	Sources	Deposition growth rate (cm/sec)
Capillary flow rig	$CaCO_3$ at 25°C	This study	6.87×10^{-7} to 1.29×10^{-5}
Fluidized-bed crystallizer	$CaCO_3$ at 25°C	Tai et al[188]	4.2×10^{-7} to 7.2×10^{-7}
Chemostat system	$CaCO_3$ at 25°C	Weijden et al[189]	3×10^{-7} to 9×10^{-7}

The results obtained from their study is similar to what is observed from this work, as the growth rate of calcium carbonate scale increase with increased saturation ratio for (SR <80) and the average growth rate has a linear relationship with saturation ratio for both temperatures and flow rates [6, 190].

The results obtained from this work, are highly reproducible as the coefficient of determination (R^2) for each of the conditions is approximately 1 as shown in Table 7-4 and Table 7-5 for 25°C and 70°C respectively.

The average growth rate of calcium carbonate scale deposited can be determined as a function of saturation ratio from the linear equations shown in Table 7-4 and Table 7-5. Where y denotes the average growth rate, x denotes the saturation ratio. That is, at a particular flow rate and temperature, the average growth rate of $CaCO_3$ can be predicted as a function of saturation ratio.

The average growth rate of calcium carbonate scale increased in proportion to the degree of supersaturation as expected, estimating the growth rate of calcium carbonate scale within the experimental conditions from this work can give an understanding of the growth kinetics mechanism and strategy of mitigating its occurrence in the field.

However, having a single scale predictive empirical model which considered the effect of flow rates into the existing empirical equations in Table 7-4 and Table 7-5, can give more reliable prediction of average growth rate of calcium carbonate scale as saturation ratio and flow rate are the main driving force for scale deposition.

The next section of this work focused on the prediction of calcium carbonate scale growth rate as a function of deposition flux (saturation ratio and flow rate) at different temperature. Also the discussions of empirical models established in relation to field conditions and literatures is presented.

Table 7-4: Fitted equation on the experimental data at different flow rates for 25ºC

Flow rate (ml/min)	Fitted equation	Coefficient of determination R^2
5	$Y = 9 \times 10^{-7}x + 1 \times 10^{-5}$	0.9999
10	$Y = 8 \times 10^{-7}x + 7 \times 10^{-6}$	0.9985
15	$Y = 7 \times 10^{-7}x + 2 \times 10^{-6}$	0.9999
20	$Y = 4 \times 10^{-7}x + 9 \times 10^{-7}$	0.9985
30	$Y = 2 \times 10^{-7}x + 2 \times 10^{-7}$	0.9964

Table 7-5: Fitted equation on the experimental data at different flow rates for 70°C

Flow rate (ml/min)	Fitted equation	Coefficient of determination R^2
5	$Y = 1 \times 10^{-7}x + 3 \times 10^{-6}$	0.9987
10	$Y = 1 \times 10^{-7}x + 2 \times 10^{-6}$	0.999
15	$Y = 9 \times 10^{-8}x + 2 \times 10^{-6}$	0.997

7.6 Calcium carbonate scale deposition kinetics empirical model

Scale prevention is important in oil and gas industries to ensure optimum production. Organic and inorganic scale precipitation and deposition have been studied and different predictive models have been developed over many years on scale precipitation process such as residence time, induction time, nucleation and crystal growth.

These models have been mainly based on thermodynamics parameters. However, little attention has be made on the effect of hydrodynamic parameters on inorganic scale surface deposition kinetics. The use of a methodology that will reflects the field scenario has been a challenge in most models.

To have a robust empirical model, both the thermodynamic parameters and hydrodynamic parameters needs to be considered as this can give better understanding of scale growth kinetics and also help in establishing a reliable strategist for predicting the scaling rate of both organic and inorganic scales in the field.

Researchers have often used pressure build up as method for assessing the deposition of scales across a capillary tube, and based their prediction models on the thickness of scales across the capillary tube due to the pressure build up on the wall of the capillary [1].

Work by Wang et al [20, 21] and Lawal et al [22] as stated previously in chapter 3, determined the thickness of asphaltene deposits across a long capillary tube as a function of the pressure build up across the capillary tube during asphaltene deposition, using Hagen Poiseuille flow equation shown in equation 7-7 and 7-8.

$$Q = \frac{\pi D^4 \Delta P}{128 \mu l} \quad 7\text{-}7$$

$$\frac{(\Delta P_T) r^4}{\mu_T} = \frac{(\Delta P_i) R^4}{\mu_i} \quad 7\text{-}8$$

Where Q denotes the flow velocity (m^3/s), D the internal diameter of the capillary (m), ΔP the pressure drop along the capillary (Psi), μ the viscosity (NS/m^2), l the length of the capillary (m), ΔP_i and ΔP_t are initial pressure drop before deposition and at time T, the pressure drop along the capillary, μ_i and μ_T are the original viscosity of the brine and average viscosity at time T respectively, R and r are the original capillary tube radius and effective radius after deposition respectively.

The scale deposition thickness was related to the initial radius of the tube and 1/4th of the power of the ratio of the initial pressure drop to the pressure drop with time as shown in equation 7-9. Detailed derivation of equation 7-9 is shown in chapter 3 of this work.

$$t = R\left(1 - \left(\frac{\Delta P_i}{\Delta P_T}\right)^{1/4}\right) \quad 7\text{-}9$$

Nevertheless, equation 7-9 assumed a uniformly deposited scale along the capillary tube, the optical microscopy image observations in chapter 6 showed that calcium carbonate scale deposited on the surface of the capillary cell were not uniform at different experimental conditions.

In this work, to ascertain the actual amount of deposit/scale present on the capillary cell, scale deposited on the surface of the capillary was dissolved and measured by ICP. This method gives a reliable results to use in a predictive empirical model.

Calcium carbonate scale growth rate determined by ICP-MS measurement were compared with the growth rate determined using Hagen Poiseuille flow equation

as shown previously in chapter 3, Figure 3-13 to Figure 3-15 for 25^{o}C and 70^{o}C respectively, by calculating the actual differential pressure of the capillary rig at different flow rates.

The growth rate determined by dissolving the scale and measured by ICP-MS were much smaller compared to the growth rate determined from Hagen Poiseuille flow prediction. This either due to non-uniformity of scale layer along capillary cell or the capillary cell is plugged with scale at some point along the capillary, resulting to plugged flow, which contradict the Hagen Poiseuille flow assumption of uniform deposition and a constant flow rate.

This was in agreement with the work of Wang et al [20], where they compared the amount of asphaltene deposited from pressure drop (Hagen Poiseuille flow prediction) and the amount of asphaltene recovered from the capillary tube after deposition test, using a capillary tube blocking rig. The amount of deposits were recovered by displacement test, which involve the use of N_2 gas at high pressure. From their results, the scale thickness growth rate determined by amount of deposits recovered after deposition test were small compared to the scale thickness growth rate calculated from Hagen Poiseuille flow assumption. They attributed this to the viscosity nature of asphaltene or the plugging of the capillary tube [20]

The average deposition thickness growth rate determine from this study, the same order of magnitude as the one determine by Kurup et al [191] as shown in

Table 7-6.

The deposition thickness growth rate of calcium carbonate scale from this work were higher compared to the deposition thickness growth rate of asphaltene as expected. This may be due to the solubility nature of calcium carbonate scale and the viscosity nature of asphaltene. Similar trend occurs in all saturation ratio and flow rates for both temperature of 25^{o}C and 70^{o}C respectively.

Table 7-6: Comparison of calcium carbonate scale deposit thickness growth rate and asphaltene deposit thickness growth rate

Scales	Sources	Deposit thickness growth rate (cm/sec)
$CaCO_3$	SR5, 5ml/min, 25°C	6.9×10^{-7}
Asphaltene	Kurup et al [191]	1.0×10^{-7}
		1.0×10^{-7}
	Hassi Messaoud [191]	2.0×10^{-7}
	Marrat [191]	2.5×10^{-7}

7.7 The empirical relationship between deposition growth rate and deposition flux

This study aimed at understanding the scale deposition kinetics mechanism and using a robust empirical model to predict scale deposition growth rate under hydrodynamic conditions and relating it to the influence of factors such as degree of supersaturation, flow rate and temperature.

However, bringing this relationship into a mathematical equations or empirical models can give understanding of predicting both organic and inorganic scales deposition growth rate under flow conditions.

This empirical models, considered both thermodynamic parameters and flow rates across a wide range of calcium carbonate scale saturation ratios, using a robust technique that could be related to field scenarios.

The empirical model takes into account the challenges of dynamic tube blocking rig, which is often used for inhibitor efficiency testing and the technique use a long capillary tube between (1-2m) as the scaling surface. There is a high tendency for the saturation ratio of the brine to change across the capillary tube and also the homogeneity of the scale crystal layer is also of a major concerns as the scale layer may not be uniform across the capillary tube.

Studies [1, 21, 22, 133] based their models on the data generated from pressure measurement as a function of other parameters such as time, temperature, solution chemistry etc. therefore, using this technique in generating data for empirical models, may not give accurate prediction of both organic and inorganic scales in the field.

In the empirical models established from this work, the short capillary cell and ICP-MS technique used can give more accurate and reliable data for formulating a empirical models as the residence time for the fluid to travel through the capillary cell is very short and as such, the saturation ratio is assumed to be constant across the capillary cell.

The data generated from the capillary rig is highly reproducible and reliable as the coefficient of determination (R^2) is approximately 1.

7.7.1 The empirical relationship between deposition growth rate and deposition flux at 25ºC and 70ºC

Figure 7-12 shows the empirical relationship between the average growth rate of calcium carbonate scale and deposition flux at 25ºC and 70ºC respectively. It is observed that the trend of calcium carbonate scale growth rate as function of the deposition flux is linear for both temperature with high coefficient of determination of approximately 1.

The data generated from this work were analysed using other equation fittings such as quadratic, polynomial, logarithm etc. These equation fittings gives coefficient of determination (R^2) of less than 0.8. The best fit of the data was linear relationship.

It is observed from Figure 7-12 that calcium carbonate scale deposition growth rate increase with increased deposition flux for 25ºC and 70ºC respectively as expected. The concentration of the bulk solution increase the rate of precipitation and deposition of calcium carbonate scale, which invariably increased the scaling tendency or reaction affinity of the scaling ions (Ca^{2+}, CO_3^{2-}) in the bulk solution. On the other hand, the motion or the collision of the scaling ions is driven by the flow rate of the system, resulting to diffusion or mass transport of ionic species to the surface of the capillary cell where they deposit and grow.

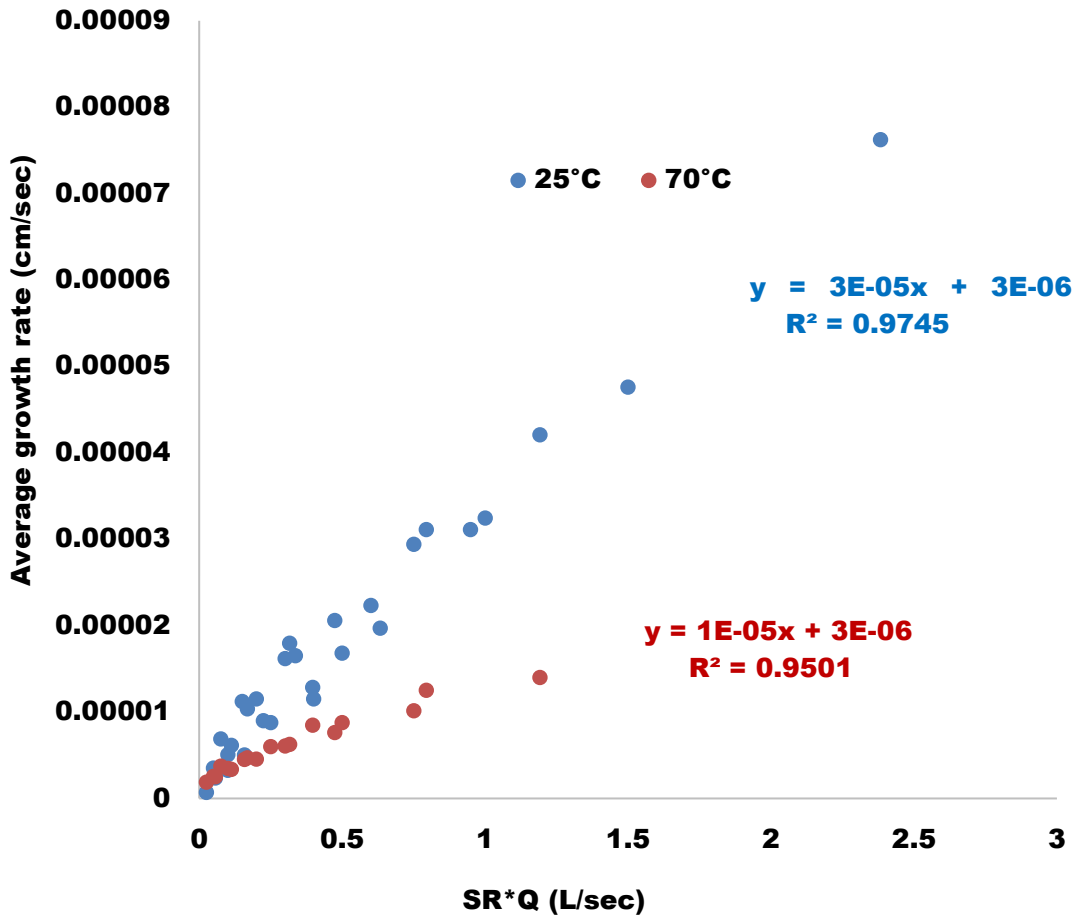

Figure 7-12: Scale deposition growth rate as a function of deposition flux at 25ºC and 70ºC

This is in agreement with the work of Hasson et al [80], which proposes two rate determine steps of calcium carbonate scale deposition in pipe flow system. Firstly, diffusion of the scaling ions in the bulk solution to $CaCO_3$ scale and water interface, followed by surface reaction of the ionic species. This is supported by Berthoud [192]. The two processes are controlled by concentration gradient of the scaling ions in the bulk solution.

The agglomeration of calcium carbonate scale crystals in the bulk solution increase with respect to the level of the ionic concentration and degree of flow in the capillary rig. This was clearly observed when deposition thickness growth rate of calcium carbonate scale increase with increased deposition flux.

It can be said that, two rate determining steps controlled the scaling process within the brine composition investigated in this work, that is, mass transport of ionic species to the surface of the capillary cell and surface reaction of the ionic species. However, mass transport process is likely to dominate the nucleation and growth process of $CaCO_3$ crystals as a result of linear relationship between the average growth rate and deposition flux observed in Figure 7-12.

Calcium carbonate scale thickness growth rate can be determined from the empirical relationship in Figure 7-12 for 25^{o}C and 70^{o}C respectively. Where Y denotes calcium carbonate scale thickness growth rate in cm/sec, x denotes the deposition flux (L/sec), which is a function of saturation ratio and flow rate.

This empirical relationship is expected to be valid within the brine composition, laminar flow regime and temperature investigated in this study.

However, caution should be exercised when applying this models to system of high turbulent regime, temperature and water salinity as the empirical relationship may not be valid. These conditions may affects the adherence of scale crystals.

7.8 Summary

This chapter presents the critical analysis, interpretation of the raw results from the differential pressure versus time curve in relation to scaling time (t_s). The discussions in relation to calcium carbonate *surface* deposition mechanisms, growth rate as a function of deposition flux and empirical models established from this work were also presented.

The results obtained show that, the scaling time is dependent on the following factors; degree of supersaturation, temperature and interfacial energy.

The interfacial energy values obtained from the capillary rig experiment is low compared to what is obtained from other studies, which may be attributed to the experimental condition used, the nature of the calcium carbonate crystals and the techniques used in this work. However, other studies have also relate the low interfacial energy values to heterogeneous nucleation process taking place as most studies assumed homogeneous nucleation process.

The plot of log t_s versus $(\log SR)^{-2}$ show that two scale kinetic mechanism occur within the saturation ratios investigated, that is, at high saturation values (SR >80), the scale mechanism is predominantly adhesion and heterogeneous nucleation, while at saturation values (SR < 80), the scale mechanism is predominantly crystallization process. This is in agreement with calcium carbonate scale growth kinetics and the bulk precipitation studies.

The plot of log t_s and $(\log SR)^{-2}$ for crystallization process show a linear relationship. The constants that describe nucleation theory were determined from the plot to establish an empirical predictive models for scaling time determination at constant temperature, similar to induction time predictive model from studies [58, 59], for bulk scaling processes at temperature of 25^{o}C and 70^{o}C respectively.

The average deposition thickness growth rate of calcium carbonate scale increase with increased deposition flux for 25^{o}C and 70^{o}C respectively. That is, $CaCO_3$ scale deposition thickness growth rate is strongly influenced by the ionic strength or degree of the supersaturation and flow rate.

There is linear relationship between the deposition thickness growth rate of calcium carbonate scale and saturation ratio for SR < 80 as expected and the coefficient of determination (R^2) is approximately 1.

Empirical kinetic model have been developed from the data generated from this work, which show a linear relationship between average deposition thickness growth rate of $CaCO_3$ scale and deposition flux for 25^{o}C and 70^{o}C respectively. The empirical model can be used to predict the deposition thickness growth rate of scales across a wide range of saturation ratios at specific temperature over a period of time.

The empirical relationship between $CaCO_3$ scale deposition thickness growth rate and the deposition flux can give an understanding of the $CaCO_3$ surface deposition kinetics growth rate and how the growth rate is influenced by the deposition flux and temperature. Also the scaling mechanism is likely to be dominated by mass transport of the ionic species.

The deposition thickness growth rate of $CaCO_3$ scale determined from this work is in the same order of magnitude compared to the asphaltene deposit thickness growth rate obtained from the work of Kurup et al [191].

CHAPTER 8. Conclusions

8.1 Conclusions

This chapter summarises the different findings arising from this work, which focuses on developing the understanding of calcium carbonate scale deposition on the surface of facilities and the kinetics of surface growth. This chapter is divided into distinct sections. This include conclusions relating to factors influencing the deposition and precipitation of $CaCO_3$.Conclusions reached in relation to $CaCO_3$ surface deposition mechanisms, growth kinetics and empirical models developed.

8.2 Factors influencing the formation and precipitation of $CaCO_3$

This study has shown that flow rates, degree of supersaturation and temperature has great influence on the $CaCO_3$ scale deposition in terms of their induction time, residence time, change in morphology, sizes and shapes of crystals, thickness of scale and amount of scale deposited. The conclusion arising from the effect of this factors on calcium carbonate scale deposition is divided into each individual headings.

8.2.1 Effect of flow rate on $CaCO_3$ scale deposition

- The effect of flow rates on the deposition and precipitation of calcium carbonate scale was significant. This was obvious in the deposition time obtained from various conditions. The deposition time of calcium carbonate scale was quite short for higher flow rates compared to low flow rates. This was attributed to the motion of scaling ions in the bulk solution which enhanced the reaction rate or the affinity for the scaling ions to react or form clusters after induction.

- The effect of flow rate to the adherence of calcium carbonate crystals to the walls of the capillary cell was not significant as the flow rate was increased. This was due to low shear stress associated with laminar flow regime.

- The morphology, sizes, shapes of calcium carbonate crystals changes with flow rates as calcite crystals were prominent at low flow rates. However, at high flow rates, calcite and aragonite were present at the surface as observed in the scanning electron microscope (SEM) and X-ray diffraction (XRD) results. $CaCO_3$ scale crystals layer were not uniform irrespective of the flow conditions.

- It is demonstrated from this work that, flow rates are of paramount important in calcium carbonate scale deposition kinetics studies and one of the key driving force for crystallization.

8.2.2 Effect of saturation ratio on $CaCO_3$ scale deposition

- The level of supersaturation influences the deposition process of calcium carbonate scale as shown from this work. The deposition time of calcium carbonate scale increases at low concentration of scaling ions in the bulk solution or saturation ratio. Also scaling time is inversely proportional to the saturation ratio.

- The influence of degree of supersaturation on calcium carbonate scale crystals and morphology was not quite obvious compared to the impact of flow rate. However the level of supersaturation was a key driving force for precipitation and deposition of calcium carbonate as the nucleation process was rapid at high saturation ratios and no induction time was recorded at this level (SR > 80).

8.2.3 Effect of temperature on $CaCO_3$ deposition

- This work has demonstrated that temperature is one of the key driving force for crystallization. The scaling tendency of calcium carbonate scale increases with increase in temperature.

- The influence of temperature on the precipitation and deposition of calcium carbonate scale is due to the solubility of calcium carbonate scale

at high temperature, thus the solubility of $CaCO_3$ decreases with increased temperature.

- The chemical potentials of the scaling ions (Ca^{2+} CO_3^{2-}) in the bulk solution increases with temperature, this influence the nucleation and growth rate of $CaCO_3$. Even at the same saturation ratio of 5, calcium carbonate deposition rate was more rapid at 70^{o}C compared to 25^{o}C

8.3 $CaCO_3$ surface deposition kinetics mechanism

The mechanisms occurring when scale build up in the capillary cell under hydrodynamic conditions has be substantiated in relation to scaling time and saturation ratio. The data generated from this work was fitted into classical nucleation theory to establish an empirical relationship between scaling time and saturation ratio at different temperatures and flow rates. The results obtained were in agreement with other studies, who focus mainly on bulk scaling process.

- Two scale deposition mechanism occur within the brine composition investigated. First, at saturation ratio SR > 80, there is was no induction time recorded. As such there was no crystals in bulk solution and the induction time was less than the residence time. The mechanism of scale was heterogeneous nucleation and adhesion.

- At saturation ratio SR < 80, the induction times recorded showed that there were no calcium carbonate crystals in the bulk solution as it flowed through the capillary, the induction time is greater than the residence time. The scale mechanism is heterogeneous nucleation or purely crystallization process.

- The interfacial energy values obtained from the capillary rig experiment is quite low compared to what is obtained from other studies, which may be attributed to the experimental conditions used, the nature of the calcium carbonate crystals and the techniques used in this work. However, other studies have also related the low interfacial energy values to the heterogeneous nucleation process taking place as most studies assumed homogeneous nucleation process.

- Empirical models have been established for predicting scaling time as a function of saturation ratios, flow rate and temperature. These models will helps in the understanding of calcium carbonate scale deposition in the field within the laminar flow regime. The empirical models showed a linear relationship between logarithm of scaling (log t_s) and logarithm square of saturation ratio (log SR)$^{-2}$ for crystallization process.

8.3.1 $CaCO_3$ scale growth kinetics

The use of Hagen Poiseuille flow assumption as means of estimating the deposition thickness of scale from differential pressure measurement across a long capillary tube may not give a reliable scale predictive models due to non-uniformity of the scale layer along the capillary tube.

- The use of short capillary cell and dissolving the scale deposited on the surface of the capillary cell and measured the amount of scale by ICP-MS gave more reliable scale deposition thickness rate and invariably good predictive models.

- The average deposition thickness growth rate of calcium carbonate scale increased with increase in deposition flux. Calcium carbonate scale deposition thickness growth rate is strongly influenced by the degree of the supersaturation, flow rate and temperature.

- Calcium carbonate deposition thickness growth shows a linear relationship with the deposition flux at saturation ratios (SR < 80) with high coefficient of determination (R^2) approximately 1

- An empirical kinetics models has been developed from the data generated from this work, which shows a linear relationship between average deposition thickness growth rate of calcium carbonate scale and deposition flux for 25^{o}C and 70^{o}C respectively. The empirical model can be used to predict the deposition thickness growth rate of scales across a wide range of saturation ratios at specific temperature over a period of time in the field.

- The empirical relationship between calcium carbonate scale deposition thickness growth rate and the deposition flux gives an understanding of the calcium carbonate scale surface deposition kinetics growth rate and how the growth rate is influence by the deposition flux and temperature.

- The deposition thickness growth rate of calcium carbonate scale determine from this work is in the same order of magnitude compared to the Asphaltene deposit thickness growth rate obtained from the work of Kurup et al [191] in their Asphaltene deposition study.

This work has a great impact in both the industry and academia, as most studies focus on bulk scaling processes as the major challenge facing oil and gas and desalination industries. Different predictive models based on thermodynamic parameters have been developed.

Findings from this work have shown that understanding both the mechanism of both bulk scaling and surface scaling processes and using a technique which reflect the field scenario by considering the effect of hydrodynamics will give a reliable strategy of mitigating scale formation in the field.

The empirical models developed from this work is expected to be valid at saturation ratio less than 80 (SR < 80), within a temperature of 25^{o}C and 70^{o}C and flow rates between 5ml/min to 30ml/min. The semi empirical models is a framework for a more detailed models to be developed and it needs further verifications and validations with respect to industrial applications. As such there can be an improvement from average deposition growth rate to deposition growth rate.

CHAPTER 9. Future work

The capillary flow rig used for this study, provided highly reproducible data and a robust technique for studying scale precipitation and deposition process under hydrodynamic conditions. The findings from this work have helped in the understanding of mechanism of scale deposition at the surface of facilities and development of a robust empirical models for predicting scale deposition growth rate. This work has developed a detailed frame work of studying the kinetics of inorganics scales under hydrodynamic conditions. Hence, the following recommendation is suggested on how to build on this frame work.

9.1 Hydrodynamic and in-situ study

The capillary flow rig can be upgraded for turbulent flow regime as the scale kinetics for turbulent flow regime may be different due to impact of shear stress on the walls of the capillary cell and the flow regime may also have effect on the residence and induction time of the flowing brine, which invariably might change the kinetic mechanism

Developing a techniques where the scaling process can be observed inline or in-situ by using a glass capillary cell and camera system and also inline turbidity can be measured by using a turbidity probe for bulk precipitation study.

Designing a carbon steel (X65) capillary cell to understand how the corrosion product ($FeCO_3$) will affect the deposition of inorganic scales under different experimental condition and also to have true reflection of pipe system been deployed in the oil and gas industries and their crude oil transportation pipe lines.

9.2 Inhibitor efficiency study

Conventional inhibitors such as PPCA, PVS, and DETPMP at different dosage, will enable the understanding of the mechanism of these inhibitors under hydrodynamic conditions and their ranking in terms of minimum inhibitor concentration (MIC). This will also help in the understanding and development of a robust empirical models where the effect of inhibitors can be considered and as such a scale mitigation strategies road map can be developed.

Introduction of green scale inhibitors to investigate its effectiveness on the early stage of crystallization process as such the induction period can be determined and surface analysis techniques can be used to observe the shape, sizes and the polymorphs of the crystals formed on the surface of the capillary. The efficiency of the green scale inhibitors will be compared with that of the conventional scale inhibitors using the capillary flow rig

Developing experimental technique, where a complex inorganic brine will be used to reflect the field scenarios of temperature, water chemistry etc. this will help in the understanding of the scale mechanism and the data generated can be correlated with the field data.

References

1. Zhang, Y. and Rod, F., *Laboratory Determination of Calcium Carbonate Scaling Rates for Oilfield Wellbore Environments*, in *International Symposium on Oilfield Scale* 2001, Society of Petroleum Engineers Inc.: Aberdeen, United Kingdom.
2. Zahedzadeh, M., Karambeigi, M.S., Roayaei, E., Emadi, M.A., Radmehr, M., Gholamianpour, H., Ashoori, S., and Shokrollahzadeh, S., *Comprehensive management of mineral scale deposition in carbonate oil fields – A case study.* Chemical Engineering Research and Design, 2014. 92(11): p. 2264-2272.
3. Bezerra, M.C.M., Khalil, C.N., and Rosario, F.F., *Barium and Strontium Sulfate Scale Formation Due to Incompatible Water in the Namorado Fields Campos Basin, Brazil*, in *SPE Latin America Petroleum Engineering Conference*1990, 1990: Rio de Janeiro, Brazil.
4. Jordan, M.M., Collins, I.R., and Mackay, E.J., *Low Sulfate Seawater Injection for Barium Sulfate Scale Control: A Life-of-Field Solution to a Complex Challenge.* SPE Production & Operations, 2008. 23(2): p. 192-209.
5. Baraka-Lokmane, S. and Hurtevent, C., *Chemical incompatibilities between formation water and injection sea water; comparison between modeling and site observations in fields operated by TOTAL*, in *Abu Dhabi International Petroleum Conference and Exhibition*2012, Society of Petroleum Engineers: Abu Dhabi, UAE.
6. Garside, J., Gaska, C., and Mullin, J.W., *Crystal growth rate studies with potassium sulphate in a fluidized bed crystallizer.* Journal of Crystal growth, 1972. 13–14: p. 510-516.
7. Al Nasser, W.N. and Al Salhi, F.H., *Kinetics determination of calcium carbonate precipitation behavior by inline techniques.* Powder Technology, 2015. 270, Part B: p. 548-560.
8. Stalker, R., Graham, G.M., and Simpson, C., *The Impact of Inorganic Scale Deposits and Their Removal on General CO2 Corrosion Rates and Corrosion Inhibitor Performance*, in *SPE International Symposium on*

Oilfield Corrosion 2004, Society of Petroleum Engineers: Aberdeen, United Kingdom.

9. Margrethe Nergaard, C.G., *An Introduction to scaling, causes, problems and solution.* NTNU - Institutt for petroleumstekenologi og anvendt, 2010.
10. Bazin, B., Kohler, N., and Zaitoun, A., *Some Insights Into the Tube Blocking Test Method To Evaluate the Efficiency of Mineral Scale Inhibitors*, in *SPE Annual Technical Conference and Exhibition* 2005, Society of Petroleum Engineers: Dallas, Texas.
11. Gill, J.S., *Development of Scale Inhibitors*, 1996, NACE International.
12. Duccini, Y., Dufour, A., Harm, W.M., Sanders, T.W., and Weinstein, B., *High performance oilfield scale inhibitors*, 1997, NACE International.
13. Hinrichsen, C.J., *Preventing Scale Deposition in Oil Production Facilities: An Industry Review*, 1998, NACE International.
14. Ibrahim, J.M., Sorbie, K., and Boak, L.S., *Coupled Adsorption/Precipitation Experiments: 1. Static Results*, 2012, Society of Petroleum Engineers.
15. Graham, G.M., Boak, L.S., and Hobden, C.M., *Examination of the Effect of Generically Different Scale Inhibitor Species (PPCA and DETPMP) on the Adherence and Growth of Barium Sulphate Scale on Metal Surfaces*, 2001, Society of Petroleum Engineers.
16. Shaw, S.S., Sorbie, K., and Boak, L.S., *The Effects of Barium Sulfate Saturation Ratio, Calcium, and Magnesium on the Inhibition Efficiency: Part II Polymeric Scale Inhibitors.* 2012.
17. Shaw, S.S. and Sorbie, K.S., *Synergistic Properties of Phosphonate and Polymeric Scale Inhibitor Blends for Barium Sulphate Scale Inhibition*, NACE International.
18. Chen, T., Neville, A., Sorbie, K.S., and Zhong, Z., *Using Synchrotron Radiation Wide-Angle X-Ray Scattering (WAXS) To Study the Inhibition Effect of DiEthyleneTriaminePenta (MethylenePhosphonic Acid) (DETPMP) on $CaCO_3$ Scale Formation*, in *SPE International Oilfield Scale Symposium*2006, Society of Petroleum Engineers: Aberdeen, UK.
19. Mavredaki, E., Neville, A., and Sorbie, K.S., *Study of BaSO4 Formation Kinetics and Inhibition Effect of Polyphosphino-Carboxylic Acid (PPCA) on Barite Formation with Synchrotron X-Ray Diffraction (SXRD)*, in *SPE*

*International Oilfield Scale Conference*2008, Society of Petroleum Engineers: Aberdeen, UK.

20. Jianxin Wang, J.S.B., And Jefferson L. Creek, *Asphaltene Deposition on Metallic Surfaces.* Journal of Dispersion Science and Technology, 2004. 25: p. 287 - 298.
21. Buckley, J. and Wang, J., *Estimate thickness of deposit layer from displacement test.* 2010.
22. Lawal, K.A., Crawshaw, J.P., S.Boek, E., and Vesovic, V., *Experiemntal investigation of asphaltene deposition in capillary flow.* Energy & Fuels, 2012.
23. Al Nasser, W.N. and Al Salhi, F.H., *Scaling and aggregation kinetics determination of calcium carbonate using inline technique.* Chemical Engineering Science, 2013. 86: p. 70-77.
24. Al Nasser, W.N., Pitt, K., Hounslow, M.J., and Salman, A.D., *Monitoring of aggregation and scaling of calcium carbonate in the presence of ultrasound irradiation using focused beam reflectance measurement.* Powder Technology, 2013. 238: p. 151-160.
25. Kohler, N., Courbin, G., and Ropital, F., *Static and Dynamic Evaluation of Calcium Carbonate Scale Formation and Inhibition*, in *SPE European Formation Damage Conference*2001, Society of Petroleum Engineers Inc.: The Hague, Netherlands.
26. Frota, T.M.P., Silva, D.R., Aguiar, J.R., Anjos, R.B., and Silva, I.K.V., *Assessment of scale formation in the column of an oil and natural gas producing well: A case study.* Brazillian Journal of petroleum and gas, 2013. 7(No 1).
27. Kan, A. and Tomson, M., *Scale Prediction for Oil and Gas Production.* SPE Journal, 2012. 17(2): p. pp. 362-378.
28. Østvold, T. and Randhol, P., *Kinetics of $CaCO_3$ Scale Formation. The Influence of Temperature, Supersaturation and Ionic Composition*, in *International Symposium on Oilfield Scale* 2001, Society of Petroleum Engineers Inc.: Aberdeen, United Kingdom.
29. Mitrouli, S.T., Kostoglou, M., and Karabelas, A.J., *Calcium carbonate scaling of desalination membranes: Assessment of scaling parameters*

from dead-end filtration experiments. Journal of Membrane Science, 2016. 510: p. 293-305.

30. Li, Z., Valladares Linares, R., Bucs, S., Aubry, C., Ghaffour, N., Vrouwenvelder, J.S., and Amy, G., *Calcium carbonate scaling in seawater desalination by ammonia–carbon dioxide forward osmosis: Mechanism and implications.* Journal of Membrane Science, 2015. 481: p. 36-43.
31. Al Omari, M.M.H., Rashid, I.S., Qinna, N.A., Jaber, A.M., and Badwan, A.A., *Chapter Two - Calcium Carbonate*, in *Profiles of Drug Substances, Excipients and Related Methodology*, G.B. Harry, Editor. 2016, Academic Press. p. 31-132.
32. Kamari, A., Gharagheizi, F., Bahadori, A., and Mohammadi, A.H., *Determination of the equilibrated calcium carbonate (calcite) scaling in aqueous phase using a reliable approach.* Journal of the Taiwan Institute of Chemical Engineers, 2014. 45(4): p. 1307-1313.
33. Mahmoud, M. and Elgawad, K.A., *Effect of CO_2 Flooding During EOR Process on the Rock Petrophysical and Electrical Properties*, in *North Africa Technical Conference & Exhibition*2013, Society of Petroleum Engineers: InterContinental Citystar,Cairo, Egypt.
34. Kim, J.W., Xue, Z., and Matsuoka, T., *Experimental Study on CO_2 Monitoring and Saturation with Combined P-wave Velocity and Resistivity*, in *International Oil and Gas Conference and Exhibition in China*2010, Society of Petroleum Engineers: Beijing, China.
35. Mcelhiney, J.E., Sydansk, R.D., Lintelmann, K.A., Benzel, W.M., and Davidson, K.B., *Determination of In-Situ Precipitation of Barium Sulphate During Coreflooding*, in *International Symposium on Oilfield Scale*2001, Copyright 2001, Society of Petroleum Engineers Inc.: Aberdeen, United Kingdom.
36. Michael, E.Q.P., *An Introduction to the Chemistry of the Sea.* 1998: p. 431.
37. Popescu, M.-A., Isopescu, R., Matei, C., Fagarasan, G., and Plesu, V., *Thermal decomposition of calcium carbonate polymorphs precipitated in the presence of ammonia and alkylamines.* Advanced Powder Technology, 2014. 25(2): p. 500-507.
38. Chen, H., Qing, C., Zheng, J., Liu, Y., and Wu, G., *Synthesis of calcium carbonate using extract components of croaker gill as morphology and*

polymorph adjust control agent. Materials Science and Engineering: C, 2016. 63: p. 485-488.

39. Islam, K.N., Bakar, M.Z.B.A., Noordin, M.M., Hussein, M.Z.B., Rahman, N.S.B.A., and Ali, M.E., *Characterisation of calcium carbonate and its polymorphs from cockle shells (Anadara granosa).* Powder Technology, 2011. 213(1–3): p. 188-191.
40. Sarkar, A. and Mahapatra, S., *Mechanism of unusual polymorphs transformations in calcium carbonate: Dissolution-recrystallization vs additive-mediated nucleation.* Chemical Science, 2012. 124: p. 1399-1404.
41. Amjad, Z. and Zuhl, R.W., *Kinetic and Morphological Investigation on the Precipitation of Calcium Carbonate in the Presence of Inhibitors*, 2006, NACE International.
42. Tong, H., Ma, W., Wang, L., Wan, P., Hu, J., and Cao, L., *Control over the crystal phase, shape, size and aggregation of calcium carbonate via a l-aspartic acid inducing process.* Biomaterials, 2004. 25(17): p. 3923-3929.
43. *Crystalline structure of Calcite*. Available from: http://en.wikipedia.org/wiki/Calcite.
44. Brankling, D., Bayman, M., and Jenvey, N., *Formation and Control of the Vaterite Scale Polymorph of Calcium Carbonate in the Galley Field Development*, in *International Symposium on Oilfield Scale*2001, Copyright 2001, Society of Petroleum Engineers Inc.: Aberdeen, United Kingdom.
45. Nehrke, G., *Calcite precipitation from aqueous solution: transformation from vaterite and role of solution stoichiometry*, 2007, Utrecht Universit. p. 27-40.
46. Johnston, C., Taylor, W., and Sutherland, L., *The Influence of Turbulence (or Hydrodynamic Effects) on Barium Sulphate Scale Formation and Inhibitor Performance*, in *2013 SPE International Symposium on Oilfield Chemistry*2013, 2013, Society of Petroleum Engineers: The Woodlands, TX, USA.
47. Todd, A.C. and Yuan, M.D., *Barium and Strontium Sulfate Solid-Solution Scale Formation at Elevated Temperatures.* SPE Production Engineering, 1992. 7(1): p. 85-92.

48. Alsaiari, H.A., Kan, A., and Tomson, M., *Effect of Calcium and Iron (II) Ions on the Precipitation of Calcium Carbonate and Ferrous Carbonate.* SPE Journal, 2010. 15(2): p. pp. 294-300.
49. Dugstad, A., *Mechanism of Protective Film Formation During CO2 Corrosion of Carbon Steel*, 1998, NACE International.
50. Tong, Y., Wang, Z., Yang, E., Pan, B., Jiang, J., Dang, L., and Wei, H., *Determination and correlation of solubility and solution thermodynamics of ethenzamide in different pure solvents.* Fluid Phase Equilibria, 2016. 427: p. 549-556.
51. Malwade, C.R. and Christensen, L.P., *Simple multipurpose apparatus for solubility measurement of solid solutes in liquids.* Education for Chemical Engineers, 2016. 16: p. 29-38.
52. Nancollas, G.H. and Reddy, M.M., *The Kinetics of Crystallization of Scale-Forming Minerals.* Society of Petroleum Engineers Journal, 1974. 14(2): p. 117-126.
53. Y.Duggirala, P., *Formation of Calcium Carbonate Scale and Control Strategies in Continuous Digeters.* Pulp and Paper Research, Nalco Company, 2007.
54. Dalas, E. and Koutsoukos, P.G., *The effect of magnetic fields on calcium carbonate scale formation.* Journal of Crystal growth, 1989. 96(4): p. 802-806.
55. Amjad, Z., *Scale Inhibition in Desalination Applications: An Overview*, 1996, NACE International.
56. Chen, T., Neville, A., Sorbie, K., and Zhong, Z., *In-Situ Monitoring The Inhibiting Effect Of Detpmp On Caco3 Scale Formation By Synchrotronx-Ray Diffraction*, 2007, NACE International.
57. Mullin, J.W., *Crystallization*, 2001, Butterworth-Heinemann.
58. Stamatakis, E., Stubos, A., Palyvos, J., Chatzichristos, C., and Muller, J., *An improved predictive correlation for the induction time of $CaCO_3$ scale formation during flow in porous media.* Journal of Colloid and Interface Science, 2005: p. 7-13.
59. Söhnel, O. and Mullin, J.W., *Interpretation of crystallization induction periods.* Journal of Colloid and Interface Science, 1988. 123(1): p. 43-50.

60. He, S., Kan, A.T., and Tomson, M.B., *Mathematical Inhibitor Model for Barium Sulfate Scale Control.* Langmuir, 1996. 12(7): p. 1901-1905.
61. Mavredaki, E. and Neville, A., *Prediction and evaluation of calcium carbonate deposition at surfaces*, 2014, Society of Petroleum Engineers.
62. Baraka-Lokmane, S., Charpentier, T.V.J., Hurtevent, C., Ordonez-Varela, J.-R., Neville, A., Olsen, J.H., Bache, O., Eroini, V., Ellingsen, J.A., and Moeller Nielsen, F., *Evaluation of Anti-fouling Surfaces for Prevention of Mineral Scaling in Sub-Surface Safety Valves*, 2014, Society of Petroleum Engineers.
63. Yoreo, J.J.D. and Vekilov, P.G., *Principles of Crytsal Nucleation and Growth*, in *Principle of Crystal Nucleation and Growth*2003: Department of Chemical and Biomolecular Engineering. p. 58-77.
64. Kügler, R.T., Beißert, K., and Kind, M., *On heterogeneous nucleation during the precipitation of barium sulfate.* Chemical Engineering Research and Design, 2016. 114: p. 30-38.
65. Söhnel, O. and Mullin, J.W., *A method for the determination of precipitation induction periods.* Journal of Crystal growth, 1978. 44(4): p. 377-382.
66. Kashchiev, D., *Chapter 11 - 11 Nucleation rate*, in *Nucleation*. 2000, Butterworth-Heinemann: Oxford. p. 174-177.
67. Crabtree, M., Eslinger, D., Fletcher, P., Miller, M., Johnson, A., and King, G., *Fighting Scale - Removal and prevention.* Oilfield Review, 1999: p. 30-45.
68. Ruckenstein, E., Berim, G.O., and Narsimhan, G., *A novel approach to the theory of homogeneous and heterogeneous nucleation.* Advances in Colloid and Interface Science, 2015. 215: p. 13-27.
69. Söhnel, O. and Mullin, J.W., *Precipitation of calcium carbonate.* Journal of Crystal growth, 1982. 60(2): p. 239-250.
70. Baldan, A., *Adhesion phenomena in bonded joints.* International Journal of Adhesion and Adhesives, 2012. 38: p. 95-116.
71. Garside, J. and Larson, M.A., *Direct observation of secondary nuclei production.* Journal of Crystal growth, 1978. 43(6): p. 694-704.

72. Daudey, P.J., Van Rosmalen, G.M., and De Jong, E.J., *Secondary nucleation kinetcs of ammonium sulfate in a CMSMPR crystallizer.* Journal of Crystal growth, 1990. 99(1–4, Part 2): p. 1076-1081.
73. Verdurand, E., Bebon, C., Colson, D., Klein, J.P., Blandin, A.F., and Bossoutrot, J.M., *Secondary nucleation and growth of organic crystals in industrial crystallization.* Journal of Crystal growth, 2005. 275(1–2): p. 1363-1367.
74. Van Der Heijden, A.E.D.M., Van Der Eerden, J.P., and Van Rosmalen, G.M., *The secondary nucleation rate: a physical model.* Chemical Engineering Science, 1994. 49(18): p. 3103-3113.
75. Tai, C.Y., Wu, J.-F., and Rousseau, R.W., *Interfacial supersaturation, secondary nucleation, and crystal growth.* Journal of Crystal growth, 1992. 116(3–4): p. 294-306.
76. Feigelson, R.S., *1 - Crystal Growth through the Ages: A Historical Perspective A2 - Nishinaga, Tatau*, in *Handbook of Crystal Growth (Second Edition)*. 2015, Elsevier: Boston. p. 1-83.
77. Zawala, J., Kosior, D., and Malysa, K., *Formation and influence of the dynamic adsorption layer on kinetics of the rising bubble collisions with solution/gas and solution/solid interfaces.* Advances in Colloid and Interface Science, 2015. 222: p. 765-778.
78. Cizer, O., Van Balen, K., Elsen, J., and Van Gemert, D., *Crystal morphology of precipitated calcite crystals from accelerated carbonation of lime binders.* ACEME08, 2008: p. pp.149-158.
79. Sinha, A.P. and Parameswar, D., *Mass Transport Principle and Operation*, 2012, PHI Learning private limited: New Delhi. p. 513-514.
80. Hasson, D., Bramson, D., Limoni-Relis, B., and Semiat, R., *Influence of the flow system on the inhibitory action of $CaCO_3$ scale prevention additives.* Desalination, 1997. 108(1–3): p. 67-79.
81. Johnson, K.L., *Mechanics of adhesion.* Tribology International, 1998. 31(8): p. 413-418.
82. Packham, D.E., *Hand Book of Adhesion*, S. Edition, Editor 2005, John wiley & Son Ltd. p. 15-200.

83. Packham, D.E. and Johnston, C., *Mechanical adhesion: were McBain and Hopkins right? An empirical study.* International Journal of Adhesion and Adhesives, 1994. 14(2): p. 131-135.
84. Hidema, R., Toyoda, T., Suzuki, H., Komoda, Y., and Shibata, Y., *Adhesive behavior of a calcium carbonate particle to solid walls having different hydrophilic characteristics.* International Journal of Heat and Mass Transfer, 2016. 92: p. 603-609.
85. M.Arif Butt, A.C., Javaid Ahmad, Rafig Ahmad, Usman Majeed, I.H.Khan, *Theory of Adhesion its Practical Implications.* Journal of Faculty of Engineering & Technology, 2008: p. 21-45.
86. Collins, I.R., *A New Model for Mineral Scale Adhesion*, Society of Petroleum Engineers.
87. Hermansson, M., *The DLVO theory in microbial adhesion.* Colloids and Surfaces B: Biointerfaces, 1999. 14(1–4): p. 105-119.
88. Hoss, D.J., Knepper, R., Hotchkiss, P.J., Tappan, A.S., Boudouris, B.W., and Beaudoin, S.P., *An evaluation of complementary approaches to elucidate fundamental interfacial phenomena driving adhesion of energetic materials.* Journal of Colloid and Interface Science, 2016. 473: p. 28-33.
89. Antony, A., Low, J.H., Gray, S., Childrss, A.E., Le-Clech, P., and Lesile, G., *Scale formation and control in high pressure membrane water treatment systems: A review* Membrane science, 2011: p. 1-16.
90. Gomez-Morales, J., Torrent-Burgues, J., and Rodrigues-Clemente, R., *Nucleation of calcium carbonate at different initial pH conditions.* Journal of Crystal growth, 1996.
91. Andritsos, N. and Karabelas, A.J., *Calcium carbonate scaling in a plate heat exchanger in the presence of particles.* International Journal of Heat and Mass Transfer, 2003. 46(24): p. 4613-4627.
92. Macadam, J. and Parsons, S.A., *Calcium carbonate scale formation and control.* Re/Views in Environmental Science & Bio/Technology, 2004. 3(2): p. 159-169.
93. Troup, D.H. and Richardson, J.A., *Scale nucleation on a heat transfer surface and its prevention.* Chemical Engineering communication 1978. 2: p. 167-180.

94. Kitamura, M., *Controlling factor of polymorphism in crystallization process.* Journal of Crystal growth, 2002. 237–239, Part 3: p. 2205-2214.
95. Han, Y.S., Hadiko, G., Fuji, M., and Takahashi, M., *Factors affecting the phase and morphology of $CaCO_3$ prepared by a bubbling method.* Journal of the European Ceramic Society, 2006. 26(4–5): p. 843-847.
96. Feng, B., Yong, A.K., and An, H., *Effect of various factors on the particle size of calcium carbonate formed in a precipitation process.* Materials Science and Engineering: A, 2007. 445–446: p. 170-179.
97. Muryanto, S., Bayuseno, A.P., Ma'mun, H., Usamah, M., and Jotho, *Calcium Carbonate Scale Formation in Pipes: Effect of Flow Rates, Temperature, and Malic Acid as Additives on the Mass and Morphology of the Scale.* Procedia Chemistry, 2014. 9: p. 69-76.
98. Dyer, S.J. and Graham, G.M., *The effect of temperature and pressure on oilfield scale formation.* Journal of Petroleum Science and Engineering, 2002. 35(1–2): p. 95-107.
99. Wang, Z., Neville, A., and Meredith, A., *How and Why Does Scale Stick—Can the Surface Be Engineered To Decrease Scale Formation and Adhesion?*, in *SPE International Symposium on Oilfield Scale*2005, Society of Petroleum Engineers: Aberdeen, United Kingdom.
100. Merdhah, A.B.B. and Yassin, A.a.M., *Laboratory Study on Precipitation of Barium Sulphate in Malaysia Sandstone Cores.* The Open Petroleum Engineering, 2009. 2: p. 1-11.
101. Chen, T., Sorbie, K.S., Neville, A., and Zhong, Z., *Using Synchrotron Radiation Wide Angle X Ray Scattering (WAXS) to Study the Inhibiting Effect of Polyphosphonocarboxylic Acid (PPCA) on CaCO3 Scale Formation*, 2006, NACE International.
102. Beck, R., Seiersten, M., and Andreassen, J.P., *The constant composition method for crystallization of calcium carbonate at constant supersaturation.* Journal of Crystal growth, 2013. 380(0): p. 187-196.
103. Moghadasi, J., Jamialahmadi, M., Müller-Steinhagen, H., and Sharif, A., *Scale Formation in Oil Reservoir and Production Equipment during Water Injection (Kinetics of $CaSO_4$ and $CaCO_3$ Crystal Growth and Effect on Formation Damage)*, in *SPE European Formation Damage*

*Conference*2003, Society of Petroleum Engineers: The Hague, Netherlands.

104. Alsaiari, H.A., Kan, A.T., and Tomson, M.B., *Molar Ratio of Ca^{2+} to Fe^{2+} in the Supersaturated Solution of Iron Carbonate and Calcium Carbonate and in the Precipitate: Relation and Interpretation*, in *SPE International Symposium on Oilfield Chemistry*2009, Society of Petroleum Engineers: The Woodlands. Texas.
105. Hasson, D. and Cornel, A., *Kinetics Of $CaCO_3$ Precipitation In The Presence Of Shmp*, 2007, NACE International.
106. Zhu, G., Li, H., Li, S., Hou, X., Xu, D., Lin, R., and Tang, Q., *Crystallization behavior and kinetics of calcium carbonate in highly alkaline and supersaturated system.* Journal of Crystal growth, 2015. 428: p. 16-23.
107. Chen, T., Neville, A., Sorbie, K., and Zhong, Z., *Following the formation of $CaCO_3$ scale formation by in-situ WAXS.* Journal of Optoelectronics and Advanced materials, 2007. 9(No. 5): p. 1250 - 1253.
108. Setta, F.-A., Neville, P.A., and Chen, H.J., *A Surface Kinetic Scaling Model For $CaCO_3$ On a Stainless Steel Surface (316 L)*, 2012, NACE International.
109. Amjad, Z. and Zuhl, R.W., *Effect Of Heat Treatment On The Performance Of Deposit Control Polymers As Calcium Carbonate Inhibitors*, 2007, NACE International.
110. Chaussemier, M., Pourmohtasham, E., Gelus, D., Pécoul, N., Perrot, H., Lédion, J., Cheap-Charpentier, H., and Horner, O., *State of art of natural inhibitors of calcium carbonate scaling. A review article.* Desalination, 2015. 356: p. 47-55.
111. Bezerra, M.C.M., Rosario, F.F., and Rocha, A.A., *Scale Prediction and Remediation for Deep Water Fields*, in *International Symposium on Oilfield Scale*2003, Society of Petroleum Engineers Inc.: Aberdeen, United Kingdom.
112. Shen, D., Shcolnik, D., Steiner, W.H., Horstmann, D.G., Taylor, G.N., and Brown, M., *Evaluation of Scale Inhibitors in Marcellus Waters Containing High Levels of Dissolved Iron*, in *SPE International Symposium on Oilfield Chemistry*2011, Society of Petroleum Engineers: The Woodlands, Texas, USA.

113. Benslimane, S., Perrot, H., Bennezar, R., and Bouhidel, K.-E., *Thermodynamic study of Zn2 + inhibition properties and mechanism on calcium carbonate precipitation by chemical and electrochemical methods.* Desalination, 2016. 398: p. 114-120.
114. Karabelas, A.J., *Scale formation in tubular heat exchangers- research priorities.* Internation Journal of Thermal Sciences, 2002. 41: p. 682-692.
115. Chen, T., Yuan, M., and Neville, A., *Influence of Mg^{2+} on the kinetics and crystal morphology of $CaCO_3$ scale formation on the metal surface and in bulk solution*, 2004, NACE International.
116. Nancollas, G.H. and Sawada, K., *Formation of Scales of Calcium Carbonate Polymorphs: The Influence of Magnesium Ion and Inhibitors.* Journal of Petroleum Technology, 1982. 34(3): p. 645-652.
117. Nancollas, G.H., Zachowicz, W., and Gerard, D., *Calcium Carbonate Scaling. A Kinetics And Surface Energy Approach*, 2004, NACE International.
118. Cheong, W.C., Neville, A., Gaskell, P., and Abbott, S., *Using Nature to Provide Solutions to Calcareous Scale Deposition*, in *SPE International Oilfield Scale Conference* 2008, Society of Petroleum Engineers: Aberdeen, UK.
119. Eroini, V., Kapur, N., Neville, A., and Euvrard, M., *Preventing Scale Formation Using Modified Surfaces*, 2011, NACE International.
120. Gunn, D.J., *Effect of surface roughness on the nucleation and growth of calcium sulphate on metal surfaces.* Journal of Crystal growth, 1980. 50(2): p. 533-537.
121. Shipley, H.J., Kan, A.T., Fu, G., Shen, D., and Tomson, M.B., *Effect of Hydrate Inhibitors on Calcite, Sulfates, and Halite Scale Formation*, in *SPE International Oilfield Scale Symposium*2006, Society of Petroleum Engineers: Aberdeen, UK.
122. Bahadori, A., Vuthaluru, H., and Ang, M., *Predictive Tool for Estimation of Potential Precipitation From an Equilibrated Calcium Carbonate Aqueous Phase*, in *Trinidad and Tobago Energy Resources Conference*2010, Society of Petroleum Engineers: Port of Spain, Trinidad.
123. Eseosa, A. and Atubokiki, A.J., *Prediction and Monitoring of Oilfield Carbonate Scales Using Scale Check*, in *Nigeria Annual International*

*Conference and Exhibition*2011, Society of Petroleum Engineers: Abuja, Nigeria.

124. Langelier, W.F., *Chemical Equilibrium in water.* AMJ Water Works Association, 1946. 38: p. 169 -178.
125. Stiff Jr, H.A. and Davis, L.E., *A Method for predicting the Tendency of Oilfield Water to Deposit Calcium Carbonate.* Petroleum Transactions, AIME, 1952. 195: p. 213-216.
126. Stiff Jr, H.A. and Davis, L.E., *A method for predicting the tendency of oil field waters to deposit calcium sulfate.* 1952(195): p. 25-28.
127. Vetter, O.J.G., *How Barium Sulfate Is Formed: An Interpretation.* Journal of Petroleum Technology, 1975. 27(12): p. 1515-1524.
128. Carageorgos, T., Marotti, M., and Bedrikovetsky, P., *A New Laboratory Method for Evaluation of Sulphate Scaling Parameters From Pressure Measurements.* SPE Reservoir Evaluation & Engineering, 2010. 13(3): p. pp. 438-448.
129. Shuler, P.J., Burton, L., Chen, H.-J., and Daniels, E.J., *Modeling of Scale Deposition in Gas Wells with Very Saline Produced Water*, 2000, NACE International.
130. Wright, R.J. and Hall, J.R.F., *Scale Prediction, Measurement, and Control in a Subsea Satellite Field*, in *European Production Operations Conference and Exhibition*1994, Society of Petroleum Engineers, Inc.: Aberdeen, United Kingdom.
131. Mazzolini, E.I., Bertero, L., and Truefitt, C.S., *Scale Prediction and Laboratory Evaluation of $BaSO_4$ Scale Inhibitors for Seawater Flood in a High-Barium Environment.* SPE Production Engineering, 1992. 7(2): p. 186-192.
132. Akbarzadeh, K., Eskin, D., Ratulowski, J., and Taylor, S.D., *Asphaltene Deposition Measurement and Modeling for Flow Assurance of Subsea Tubings and Pipelines*, in *OTC Brasil*2011: Rio de Janeiro, Brazil.
133. Kurup, A.S., Buckley, J.S., Wang, J., Subramani, H.J., Creek, J.L., and Chapman, W.G., *Asphaltene Deposition Tool: Field Case Application Protocol*, in *Offshore Technology Conference*2012: Houston, Texas, USA.

134. Creek, J.L., Wang, J., and Buckley, J.S., *Verification of Asphaltene-Instability-Trend (ASIST) Predictions for Low-Molecular-Weight Alkanes.* SPE Production & Operations, 2009. 24(2): p. pp. 360-368.
135. Hsu, J.J.C. and Brubaker, J.P., *Wax Deposition Measurement and Scale-Up Modeling for Waxy Live Crudes under Turbulent Flow Conditions*, in *International Meeting on Petroleum Engineering*1995, 1995 Copyright 1995, Society of Petroleum Engineers, Inc.: Beijing, China.
136. Hsu, J.J.C., Santamaria, M.M., and Brubaker, J.P., *Wax Deposition of Waxy Live Crudes Under Turbulent Flow Conditions*, in *SPE Annual Technical Conference and Exhibition*1994, Society of Petroleum Engineers: New Orleans, Louisiana.
137. Bird, R.B., Stewart, W.E., and Lightfoot, E.N., *Transport Phenomena*, 2007.
138. Nakayama, Y. and Boucher, R.F., *Introduction to fluid mechanics.* Bulterworth Heineman, 1999.
139. Halvorsen, E.N., Halvorsen, A.M.K., Andersen, T.R., Reiersolmoen, K., and Biornstad, C., *New Method for Scale Inhibitor Testing*, in *SPE International Symposium on Oilfield Chemistry*2009, Society of Petroleum Engineers: The Woodlands. Texas.
140. Graham, G.M., Williams, H.L., Wat, R., Tau, L.A., and Wennberg, K.E., *Design and Application of a Novel HT/HP " Stirred Reactor" Test Rig to Study Scale Formation and Control*, in *SPE International Symposium on Oilfield Chemistry*2005, Society of Petroleum Engineers Inc.: The Woodlands, Texas.
141. Johnson, J.D., Schoppa, D., Garza, J.L., Zamora, F., Kakadjian, S., and Fitzgerald, E., *Enhancing Gas and Oil Production With Zeta Potential Altering System*, in *SPE International Symposium and Exhibiton on Formation Damage Control*2010, Society of Petroleum Engineers: Lafayette, Louisiana, USA.
142. Lopez, T.H., Yuan, M., Williamson, D.A., and Przybylinski, J.L., *Comparing Efficacy of Scale Inhibitors for Inhibition of Zinc Sulfide and Lead Sulfide Scales*, in *SPE International Symposium on Oilfield Scale*2005, Society of Petroleum Engineers: Aberdeen, United Kingdom.

143. Liu, X., Chen, T., Chen, P., Montgomerie, H., Hagen, T.H., Wang, B., and Yang, X., *Understanding Mechanisms of Scale inhibition Using Newly Developed Test Method and Developing Synergistic Combined Scale Inhibitors*, in *SPE International Conference on Oilfield Scale*2012, Society of Petroleum Engineers: Aberdeen, UK.
144. Graham, G.M., Stalker, R., and Mcintosh, R., *The Impact of Dissolved Iron on the Performance of Scale Inhibitors Under Carbonate Scaling Conditions*, in *International Symposium on Oilfield Chemistry*2003, Society of Petroleum Engineers: Houston, Texas.
145. Graham, G.M. and Mcmahon, C.P., *The Effect of Scale Inhibitor Performance Against Bulk (Homogeneous) and Surface (Heterogeneous) Scale Nucleation and Growth by the Addition of Film Forming Corrosion Inhibitors*, 2002, NACE International.
146. Liu, Y., Kan, A., Zhang, Z., Yan, C., Yan, F., Zhang, F., Bhandari, N., Dai, Z., Ruan, G., Wang, L., Greenberg, J., and Tomson, M., *An assay method to determine mineral scale inhibitor efficiency in produced water.* Journal of Petroleum Science and Engineering, 2016. 143: p. 103-112.
147. Al-Roomi, Y.M., Hussain, K.F., and Al-Rifaie, M., *Performance of inhibitors on $CaCO_3$ scale deposition in stainless steel & copper pipe surface.* Desalination, 2015. 375: p. 138-148.
148. Zidovec, D., *Dynamic Method to Measure Calcium Carbonate Scaling*, NACE International.
149. Anand, K.D., *Fully Developed pipe and Channel flows.* 2006: p. 5-9.
150. Kestin, J., Sokolov, M., and A.Wakeham, W., *Viscosity of Liquid water in Range -8^{o}C to 150^{o}C.* J.Phys. Chem, 1978. 7(3).
151. Boyer, H.E. and Gall, T.L., *Metals hand Book* D.E. Ed, Editor 1997, ASM Intl.
152. Tomson, *"Accomplishments," Rice University Brine Chemistry Consortium.* 2006.
153. Tomson, M.B. and Kan, T.A., *ScaleSoftPitzer Version 4.0*, 2009, Rice University Brine Chemistry Consortium.
154. Lewis, G.N. and Randall, M., *Thermodynamics*, D.N. Hume, King, E.L., Pople, J.A., Stork, G., and Williams, H.H., Editors. 1961, Mc Graw-Hill Book Company, INC: New York, Toronto, London. p. 242 - 332.

155. Wolf, R.E. *What is Inductively Coupled Plasma Mass Spectrometer* March 2005.
156. Oceaniques-Umr6538, L.D. *ULTIMA Horiba Jobin YVON*. Available from: http://www-iuem.univ-brest.fr/ldo/fr/Equipements/geochimie/ultima-2.
157. Lawler, D.M., *Turbidity, Turbidimetry, and Nephelometry*, in *Reference Module in Chemistry, Molecular Sciences and Chemical Engineering*. 2016, Elsevier.
158. Hach, *DR/890Portable Colorimeter* in *HACH website*.
159. Gmbh, C.Z.M. *Zeiss Microscopy EVO MA15*. Available from: http://www.zeiss.com/microscopy/en_de/home.html.
160. Alytical, P., *Philip Pan Alytical X'PRO MPD*, in *Images for philips pan analytical x'pert*.
161. Skoog, D.A., Holler, F.J., and Crouch, S.R., *Principle of Instrumental Analysis*, T. Brooks/Cole, Editor 2007.
162. Gmbh, L.M.I., *Leica Dm for materials sciences* 2012.
163. Chen, T., Neville, A., and Yuan, M., *Assessing the effect of Mg^{2+} on $CaCO_3$ Scale formation-bulk precipitation and surface deposition.* Joural of crystal growth, 2004. 275(2005).
164. Pytkowicz, R.M., *Rates of Inorganic Calcium Carbonate Nucleation.* The Journal of Geology, 1965. 73(1): p. 196-199.
165. Waly, T., Kennedy, M.D., Witkamp, G.-J., Amy, G., and Schippers, J.C., *The role of inorganic ions in the calcium carbonate scaling of seawater reverse osmosis systems.* Desalination, 2012. 284: p. 279-287.
166. Chen, C.Y.T.a.P.-C., *Nucleation, Agglomeration and Crystal Morphology of Calcium Carbonate.* AIChE journal, 1995. 14.
167. Al-Hamzah, A.A., East, C.P., Doherty, W.O.S., and Fellows, C.M., *Inhibition of homogenous formation of calcium carbonate by poly (acrylic acid). The effect of molar mass and end-group functionality.* Desalination, 2014. 338(0): p. 93-105.
168. Song, K., Kim, W., Bang, J.-H., Park, S., and Jeon, C.W., *Polymorphs of pure calcium carbonate prepared by the mineral carbonation of flue gas desulfurization gypsum.* Materials & Design, 2015. 83: p. 308-313.

169. Jung, W.M., Kang, S.H., Kim, W.-S., and Choi, C.K., *Particle morphology of calcium carbonate precipitated by gas–liquid reaction in a Couette–Taylor reactor.* Chemical Engineering Science, 2000. 55(4): p. 733-747.
170. Morteza Saffari, M.a.a.A., Ph.D., *Nucleation Kinetics of Calcium Carbonate in Gas Field Brine Containing Methanol.* The Pacific Journal of Science and Technology, 2011. 12(2): p. 348.
171. Chen, T., Neville, A., and Yuan, M., *Calcium carbonate scale formation—assessing the initial stages of precipitation and deposition.* Journal of Petroleum Science and Engineering, 2005. 46(3): p. 185-194.
172. Chen, J. and Xiang, L., *Controllable synthesis of calcium carbonate polymorphs at different temperatures.* Powder Technology, 2009. 189(1): p. 64-69.
173. Tolaieb, B., Bingham, R., and Neville, A., *Barium Sulfate Kinetics on Steel Surfaces at Different Supersaturation Ratios*, NACE International.
174. Pedrosa, J., Gamelas, J.a.F., Lourenço, A.F., and Ferreira, P.J., *Surface properties of calcium carbonate modified with silica by sol-gel method.* Colloids and Surfaces A: Physicochemical and Engineering Aspects, 2016. 497: p. 1-7.
175. Cheong, W.C., Gaskell, P.H., and Neville, A., *Substrate effect on surface adhesion/crystallisation of calcium carbonate.* Journal of Crystal growth, 2013. 363: p. 7-21.
176. Holysz, L., Chibowski, E., Wójcik, W., Busch, K.W., and Busch, M.A., *Parameters determining the deposition of calcium carbonate into a glass capillary.* Journal of Adhesion Science and Technology, 1994. 8(2): p. 181-193.
177. Wang, H., Alfredsson, V., Tropsch, J., Ettl, R., and Nylander, T., *Formation of $CaCO_3$ Deposits on Hard Surfaces—Effect of Bulk Solution Conditions and Surface Properties.* ACS Applied Materials & Interfaces, 2013. 5(10): p. 4035-4045.
178. Israelachvili, J.N., *Intermolecular and Surface Forces*, 1985: Academic Press, London.
179. Chien, W.-C., Lee, C.-C., and Tai, C.Y., *Heterogeneous Nucleation Rate of Calcium Carbonate Derived from Induction Period.* Industrial & Engineering Chemistry Research, 2007. 46(20): p. 6435-6441.

180. Bedrikovetsky, P., Mackay, E.J., Moraes, G.P., Rosario, F.F., and Monteiro, R.P., *Laboratory and Field Prediction of Sulfate Scaling Damage*, in *SPE International Oilfield Scale Symposium*2006, Society of Petroleum Engineers: Aberdeen, UK.
181. Haarberg, T., Selm, I., Granbakken, D.B., Østvold, T., Read, P., and Schmidt, T., *Scale Formation in Reservoir and Production Equipment During Oil Recovery: An Equilibrium Model.* SPE Production Engineering, 1992. 7(1): p. 75-84.
182. Spanos, N. and Koutsoukos, P.G., *Kinetics of Precipitation of Calcium Carbonate in Alkaline pH at Constant Supersaturation. Spontaneous and Seeded Growth.* The Journal of Physical Chemistry B, 1998. 102(34): p. 6679-6684.
183. Lioliou, M.G., Paraskeva, C.A., Koutsoukos, P.G., and Payatakes, A.C., *Heterogeneous nucleation and growth of calcium carbonate on calcite and quartz.* Journal of Colloid and Interface Science, 2007. 308(2): p. 421-428.
184. Zhang, Y. and Farquhar, R., *Laboratory Determination of Calcium Carbonate Scaling Rates for Oilfield Wellbore Environments*, in *International Symposium on Oilfield Scale*2001, Society of Petroleum Engineers Inc.: Aberdeen, United Kingdom.
185. Quddus, A. and Al-Hadhrami, L.M., *Hydrodynamically deposited $CaCO_3$ and $CaSO_4$ scales.* Desalination, 2009. 246(1–3): p. 526-533.
186. Quddus, A. and Allam, I.M., *$BaSO_4$ scale deposition on stainless steel.* Desalination, 2000. 127(3): p. 219-224.
187. Chen, P.-C., Tai, C.Y., and Lee, K.C., *Morphology and growth rate of calcium carbonate crystals in a gas-liquid-solid reactive crystallizer.* Chemical Engineering Science, 1997. 52(21–22): p. 4171-4177.
188. Clifford Y.Tai, J.-H.L., And Jyh-Kau Wu, *Crystal Growth Rate of Calcite in a Constant-Composition Environment.* J.Chin. inst. Chem Engrs, 2005. 36: p. 443-450.
189. Van Der Weijden, R.D., Van Der Heijden, A.E., Witkamp, G.J., and Van Rosmalen, G.M., *The influence of total calcium and total carbonate on the growth rate of calcite.* Journal of Crystal growth, 1997. 171(1): p. 190-196.
190. Nancollas, G.H., *Kinetics of crystal growth from solution.* Journal of Crystal growth, 1968. 3: p. 335-339.

191. Kurup, A.S., Wang, J., Subramani, H.J., Buckley, J., Creek, J.L., and Chapman, W.G., *Revisiting Asphaltene Deposition Tool (ADEPT): Field Application.* Energy & Fuels, 2012. 26(9): p. 5702-5710.
192. Berthoud, A., *Theorie de la formation des faces d' un crystal.* Journal de Chimique Physique, 1912. 10: p. 624-635.

Appendix A: The effect of saturation ratio on calcium carbonate scale deposition

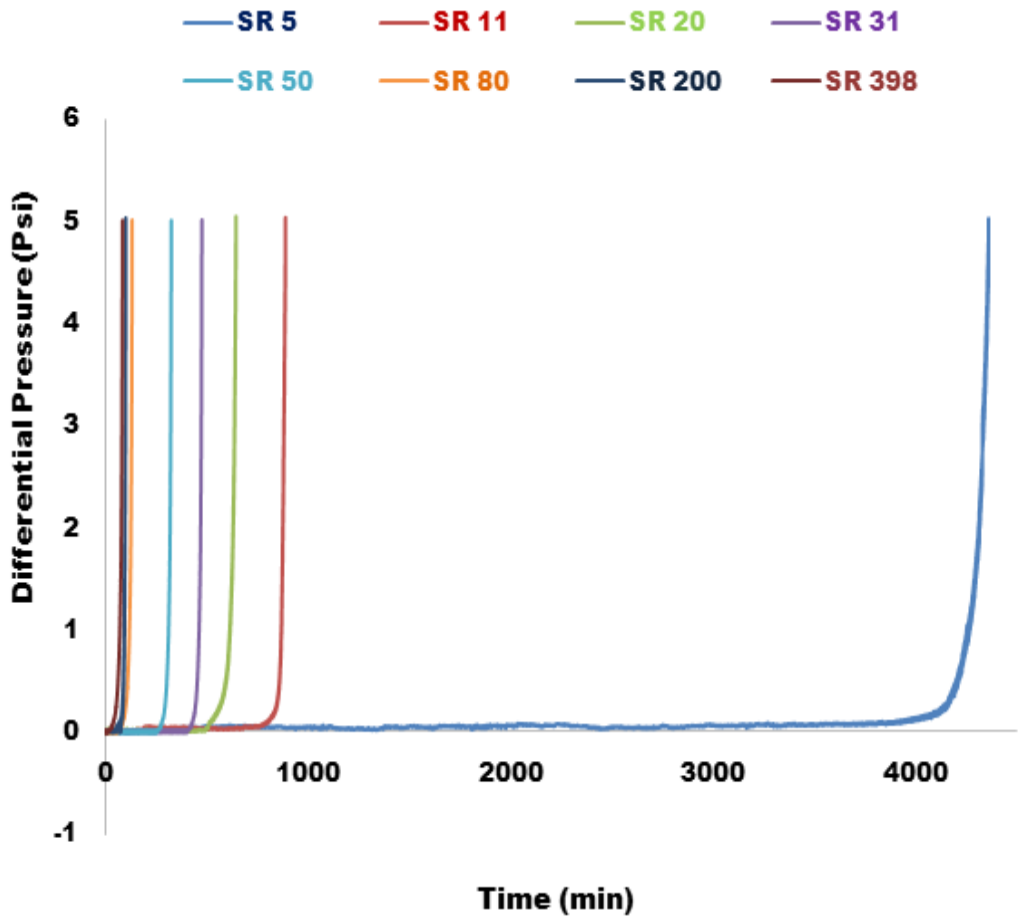

Figure 9-1: Differential pressure as a function time for 25ºC and 5ml/min at different saturation ratio

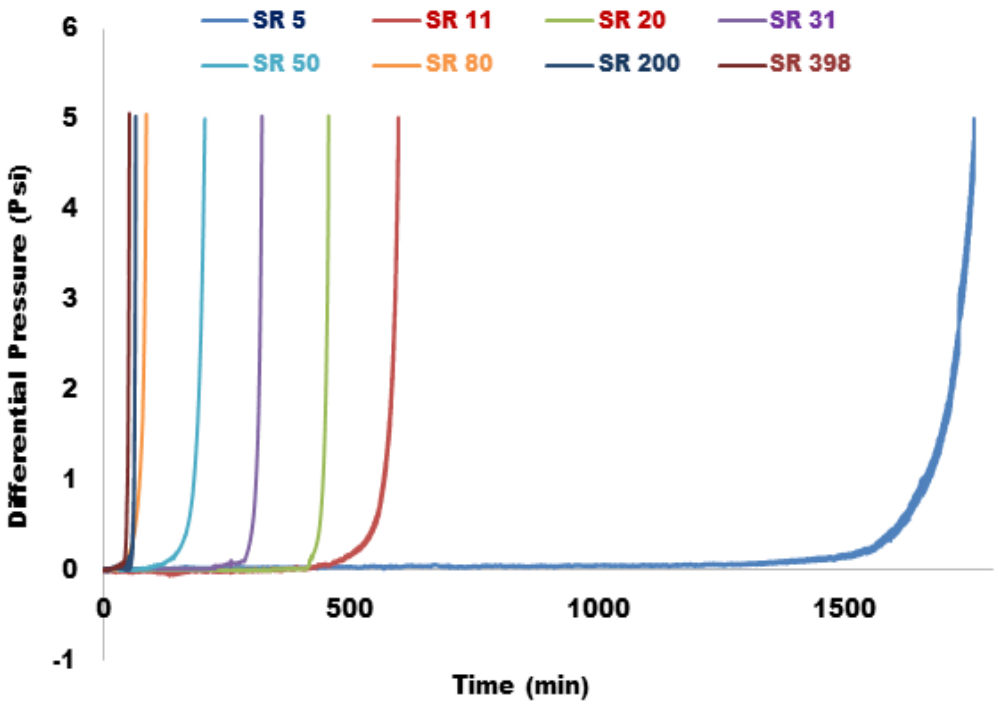

Figure 9-2: Differential pressure as a function time for 25ºC and 10ml/min at different saturation ratio

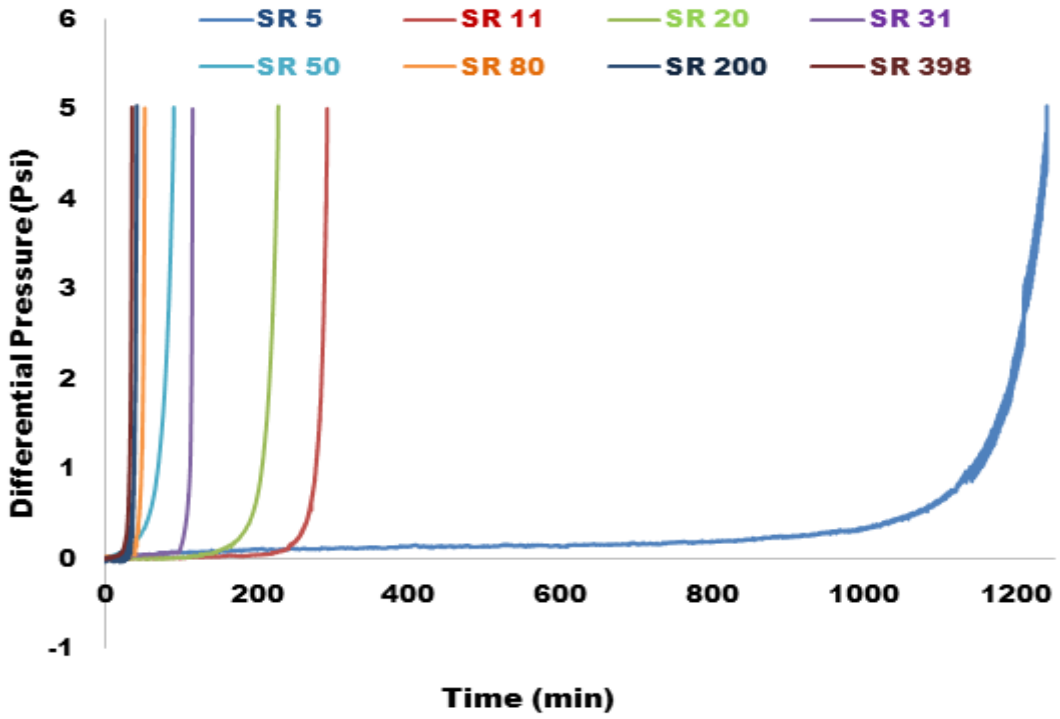

Figure 9-3: Differential pressure as a function time for 25ºC and 15ml/min at different saturation ratio

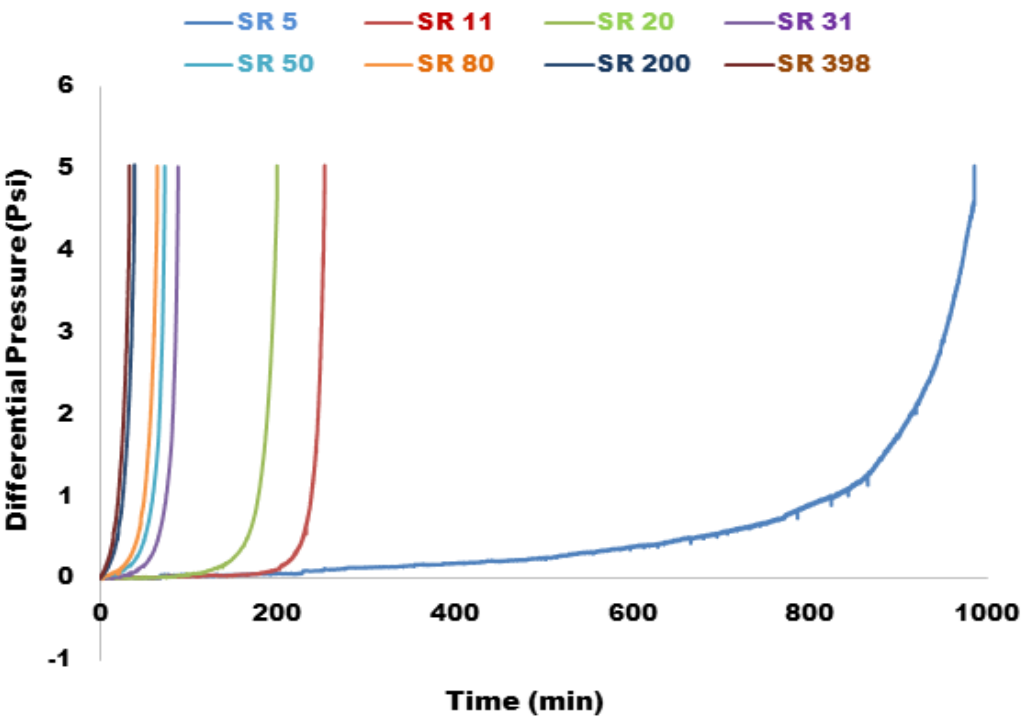

Figure 9-4: Differential pressure as a function of time for 25ºC and 20ml/min at different saturation ratio

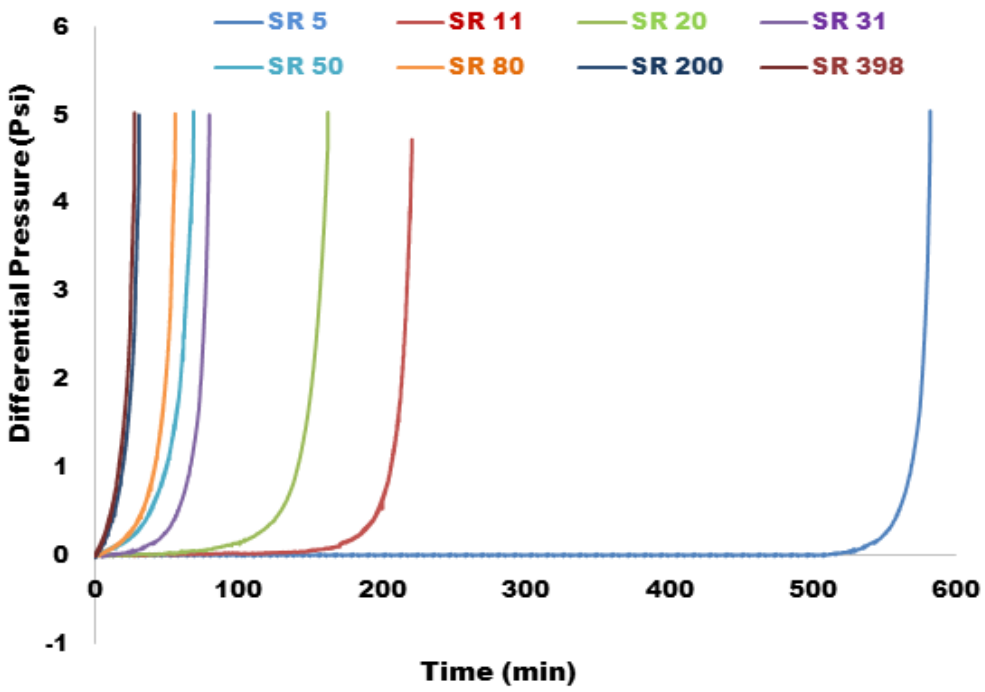

Figure 9-5: Differential pressure as a function time for 25ºC and 30ml/min at different saturation ratio

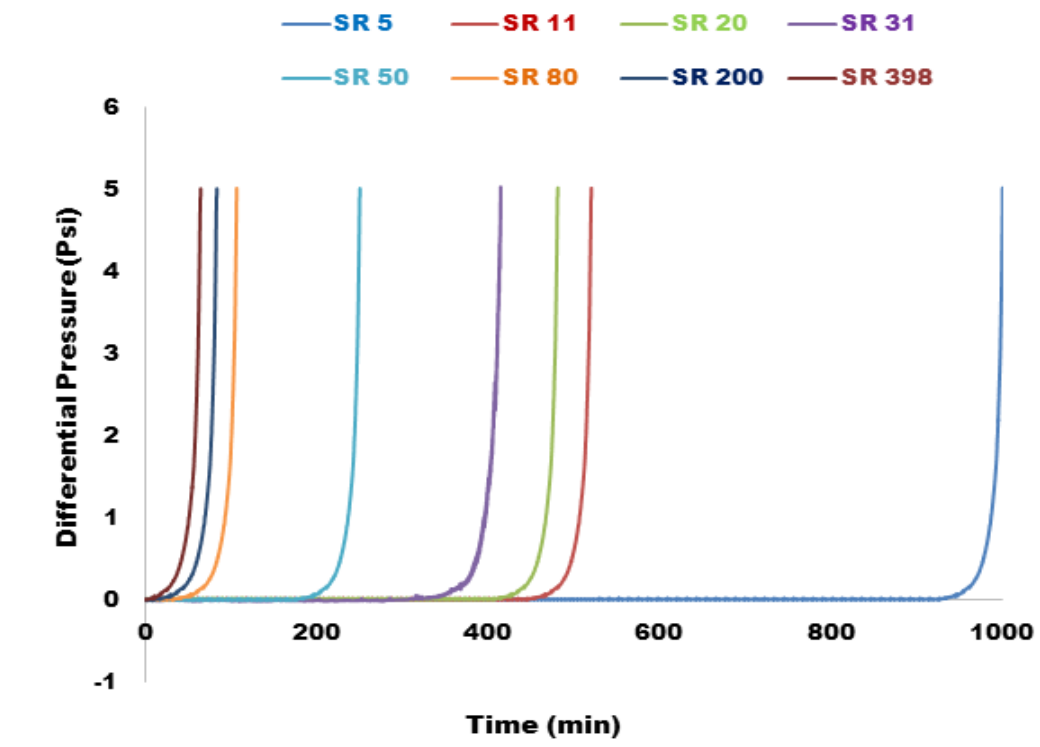

Figure 9-6: Differential pressure as a function time for 70°C and 5ml/min at different saturation ratio

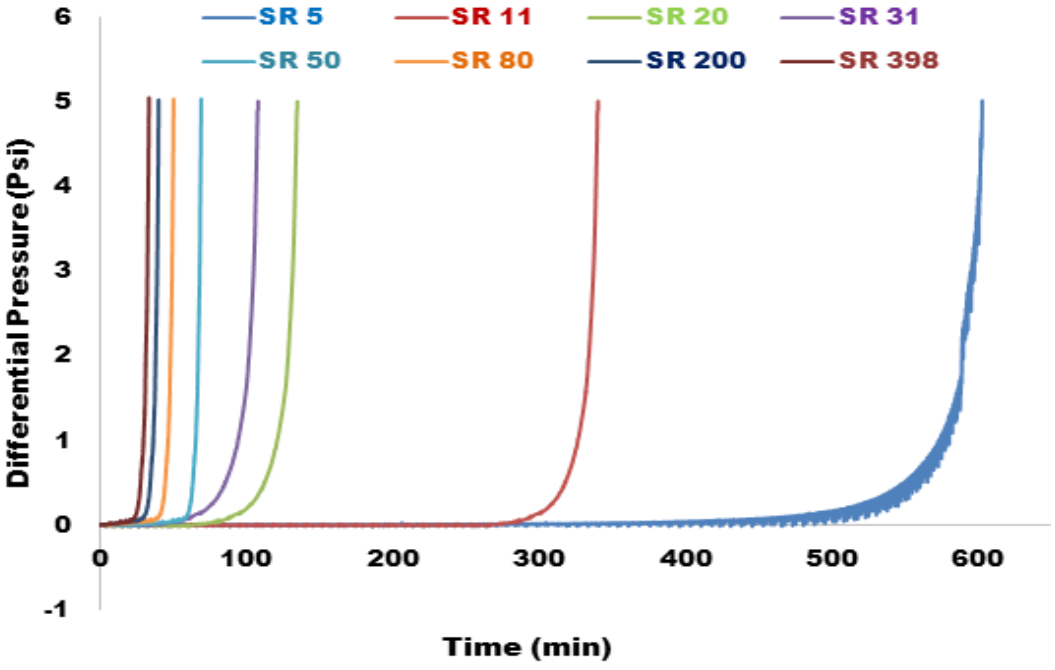

Figure 9-7: Differential pressure as a function time for 70°C and 10ml/min at different saturation ratio

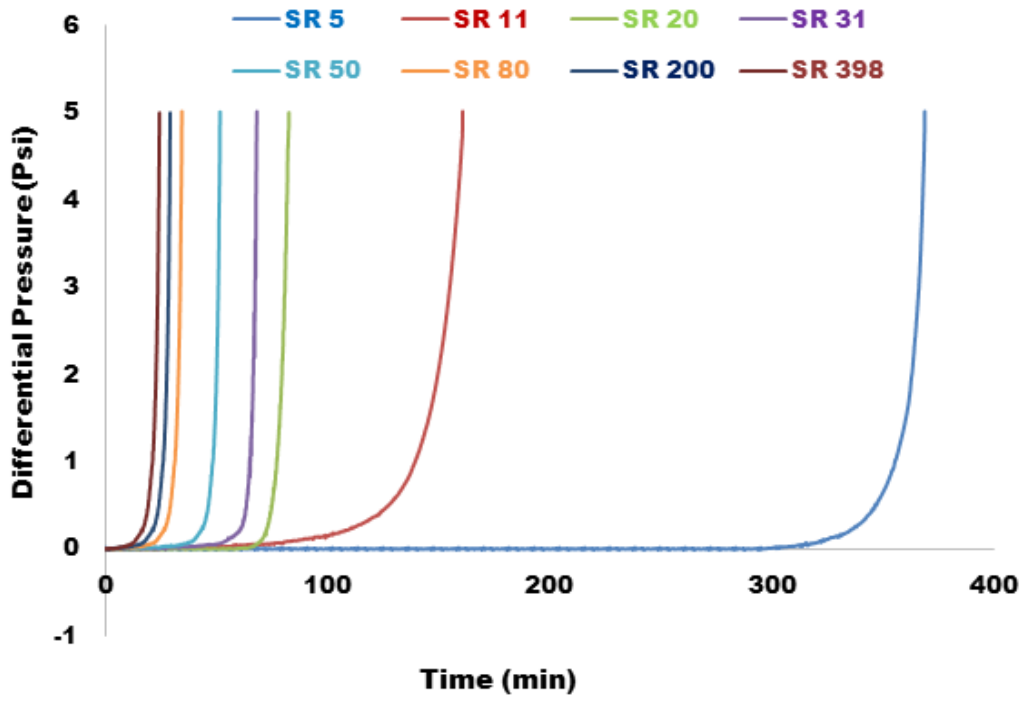

Figure 9-8: Differential pressure as a function time for 70ºC and 15ml/min at different saturation ratio

Appendix B: The effect of temperature on calcium carbonate scale deposition

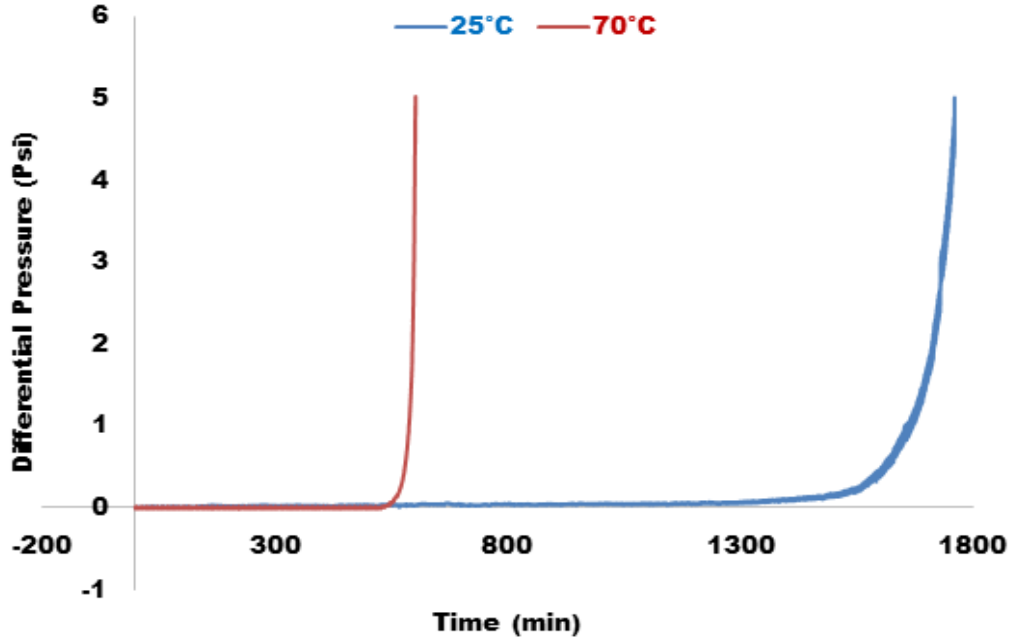

Figure 9-9: Differential pressure as a function of time for saturation ratio 5 at 10ml/min

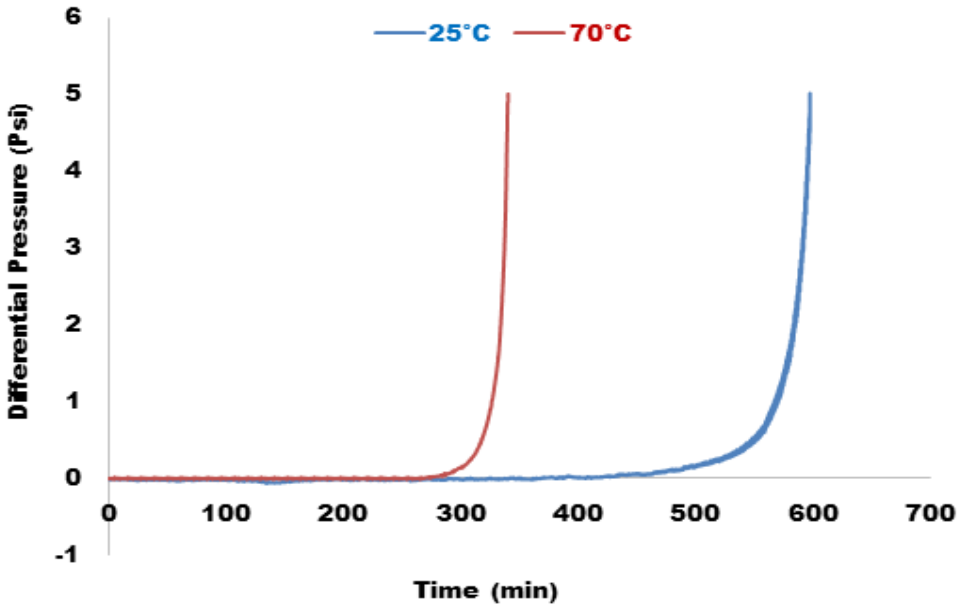

Figure 9-10: Differential pressure as a function of time for saturation ratio 11 at 10ml/min

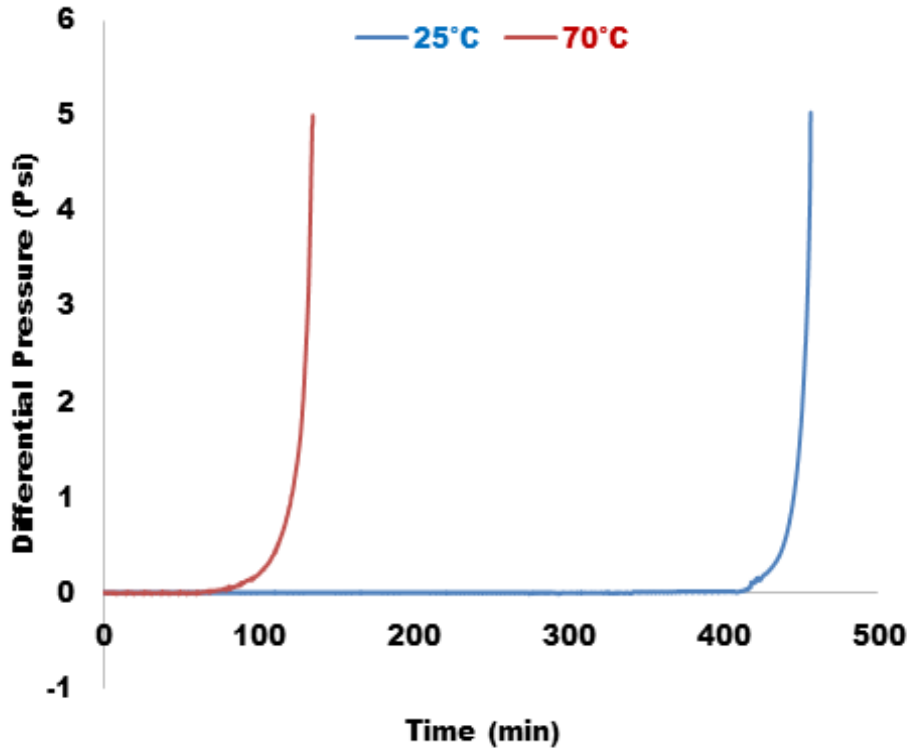

Figure 9-11: Differential pressure as a function of time for saturation ratio 20 at 10ml/min

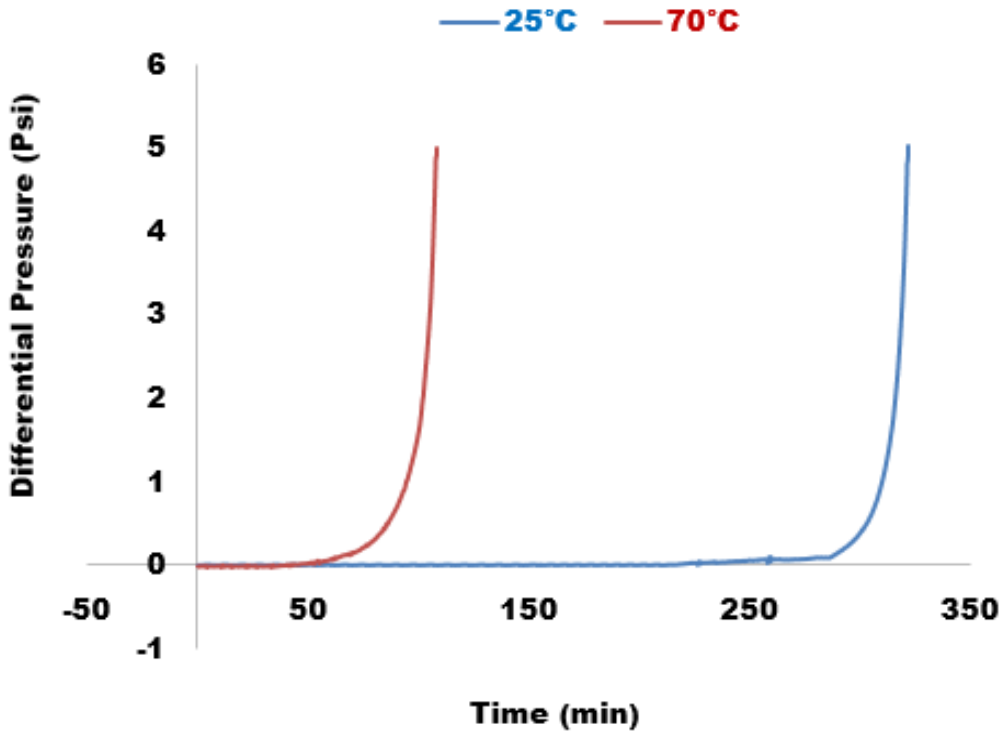

Figure 9-12: Differential pressure as a function of time for saturation ratio 31 at 10ml/min

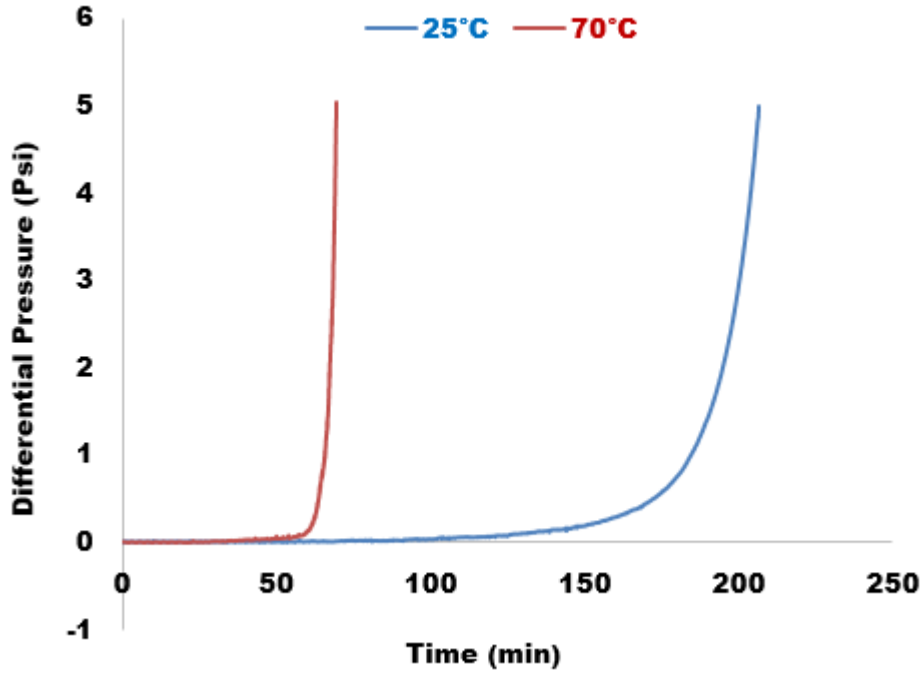

Figure 9-13: Differential pressure as a function of time for saturation ratio 50 at 10ml/min

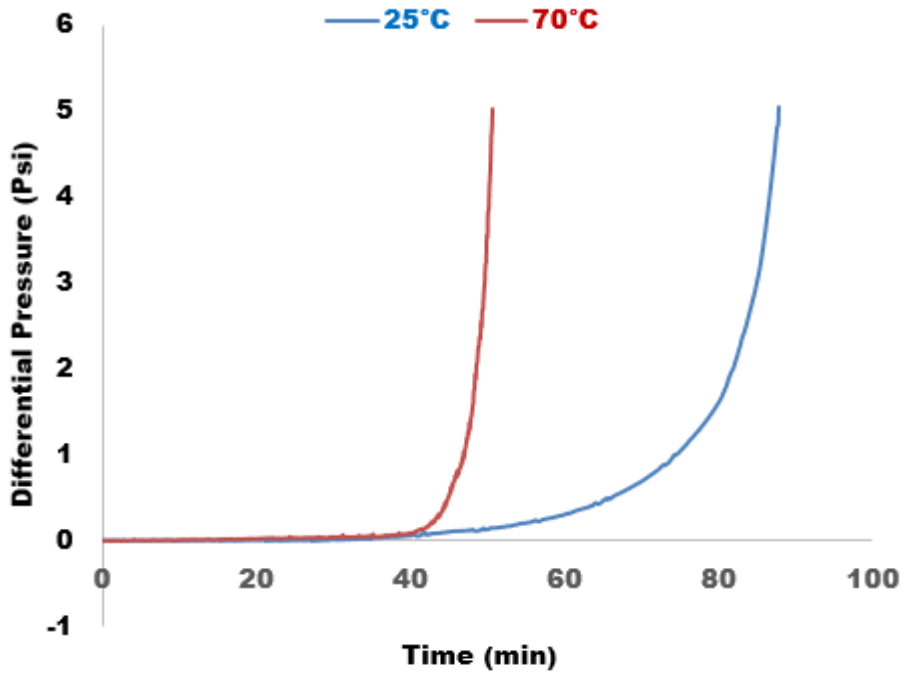

Figure 9-14: Differential pressure as a function of time for saturation ratio 80 at 10ml/min

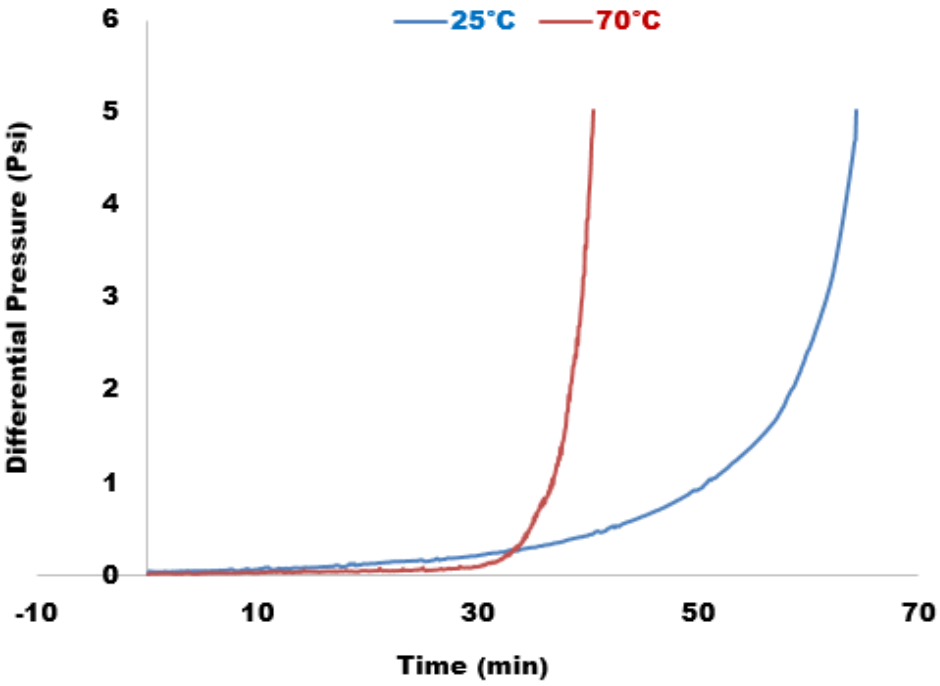

Figure 9-15: Differential pressure as a function of time for saturation ratio 200 at 10ml/min

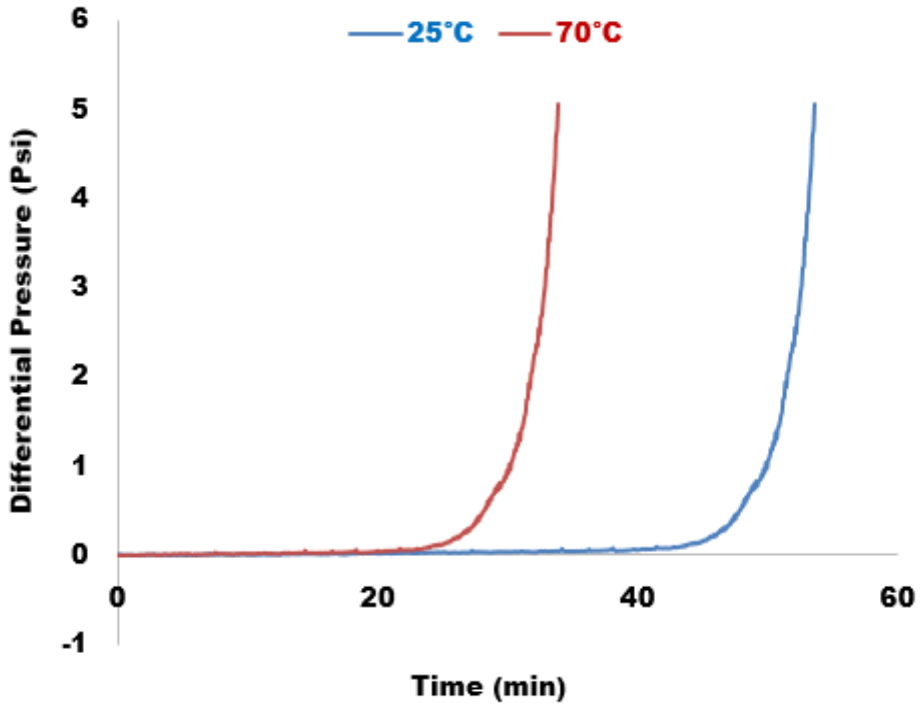

Figure 9-16: Differential pressure as a function of time for saturation ratio 398 at 10ml/min

Appendix C: Calcium carbonate scale thickness growth rate from Hagen Poiseuille and ICP

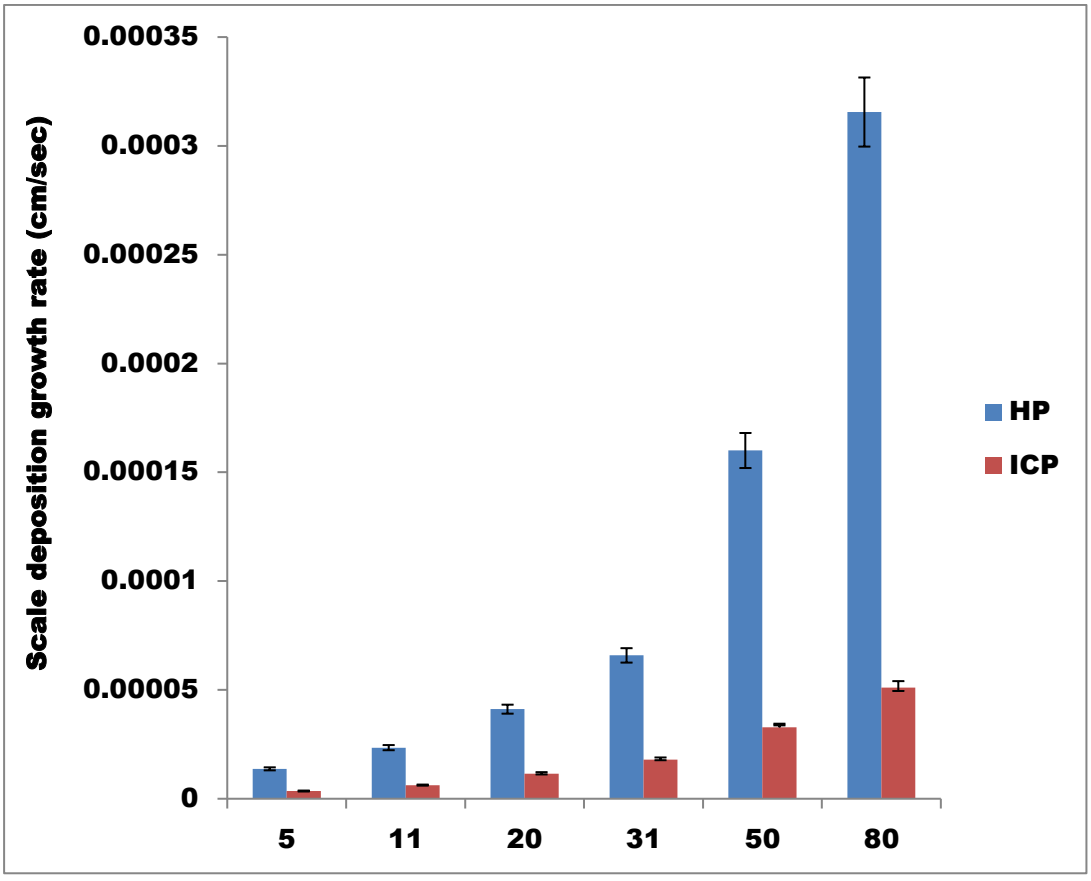

Figure 9-17: Scale deposition growth rate as a function of saturation ratio at 10ml/min and 25ºC

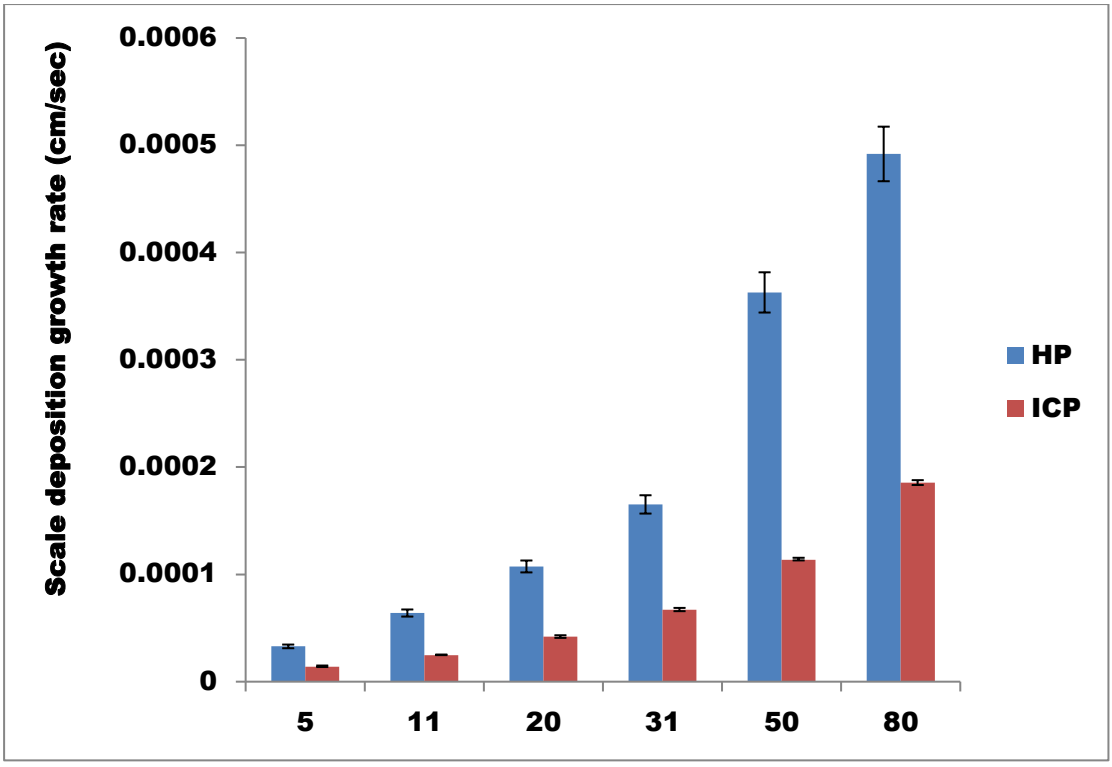

Figure 9-18: Scale deposition growth rate as a function of saturation ratio at 15ml/min and 25°C

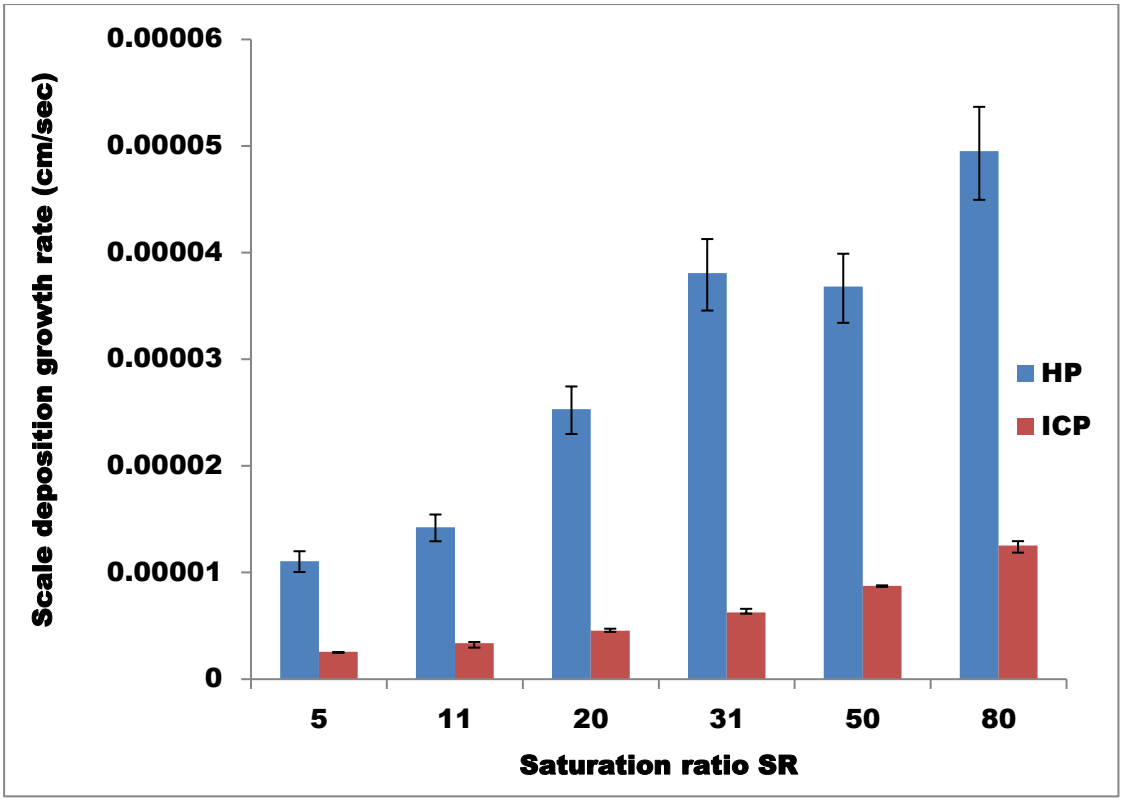

Figure 9-19 : Scale deposition growth rate as a function of saturation ratio at 10ml/min and 70°C

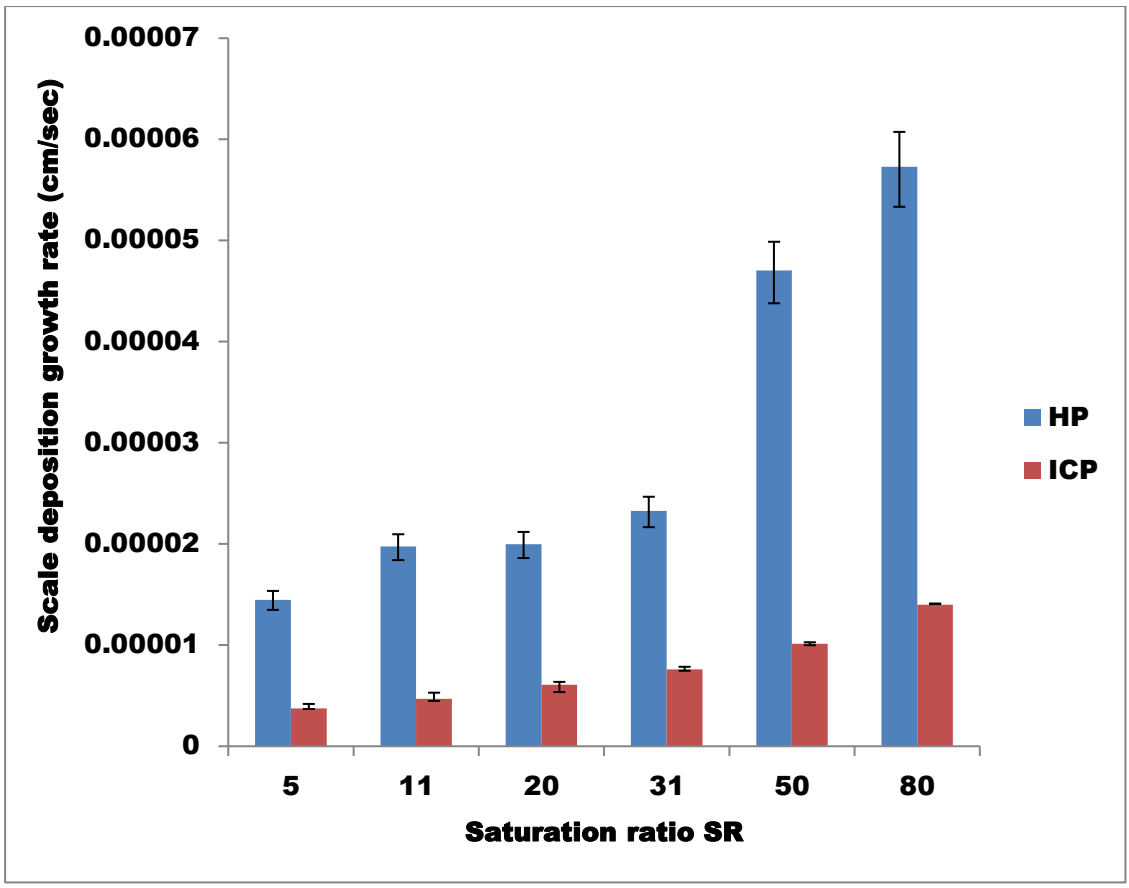

Figure 9-20: Scale deposition growth rate as a function of saturation ratio at 15ml/min and 70°C

Appendix D: Empirical relationship between average growth rate and deposition flux at different temperature

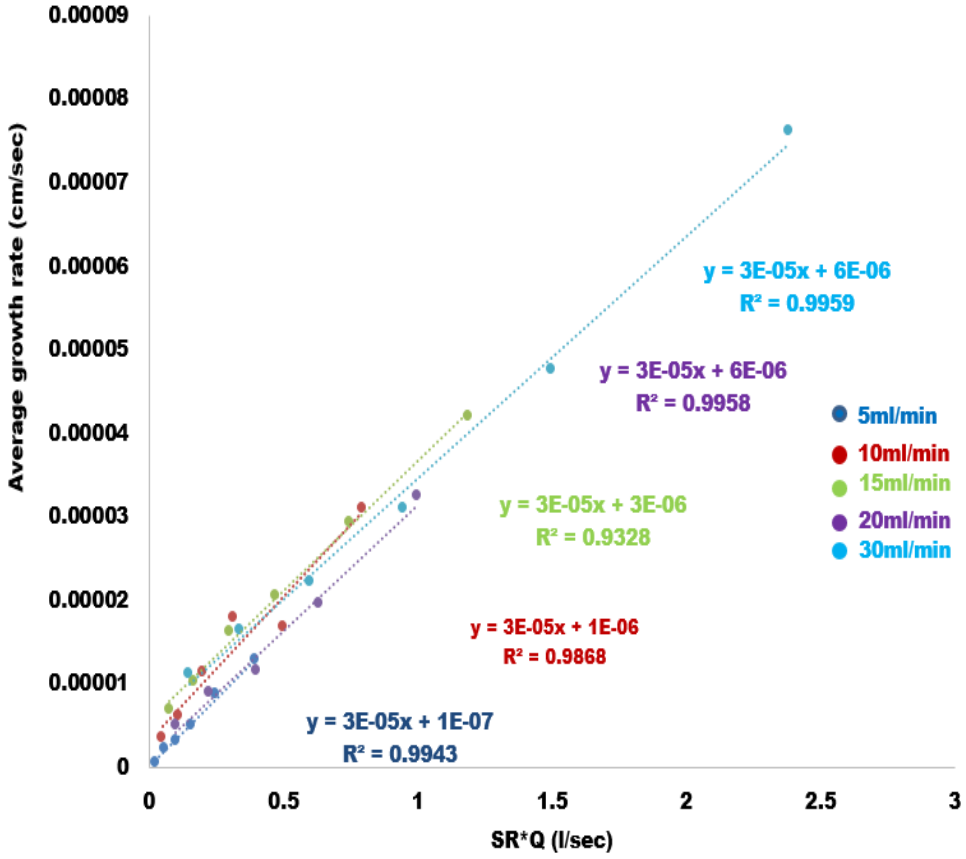

Figure 9-21: The average growth rate as a function of deposition flux at 25ºC

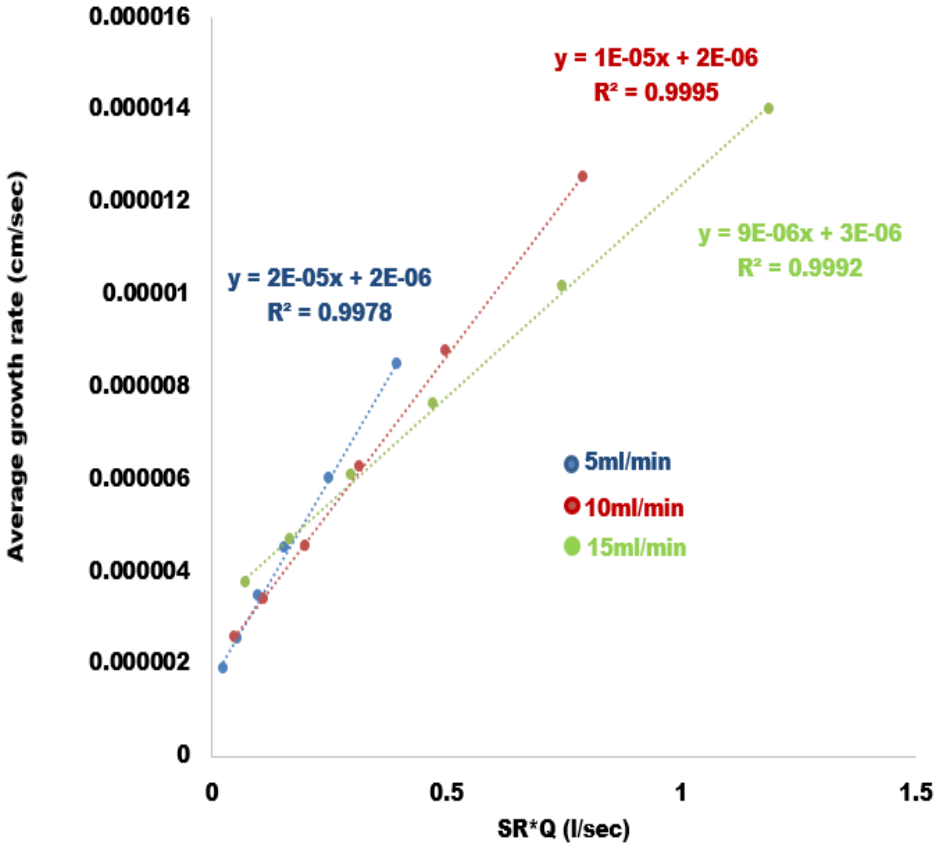

Figure 9-22: The average growth rate as a function of deposition flux at 70°C